STRUCTURAL ANALYSIS OF WOOL YARNS

A thesis
submitted in partial fulfilment of the requirements
for the Degree of
Doctor of Philosophy in Civil Engineering
at the University of Canterbury
by

Cornelis Jan van Luijk

University of Canterbury,
Christchurch, New Zealand
1981

ABSTRACT

In this report the behaviour of textile yarns under tensile loading is studied with the aid of finite-element techniques, with particular emphasis on wool yarns. Both continuous filament- and staple fibre- yarn models are developed and evaluated.

The continuous-filament yarn model is based on an earlier model developed by Carnaby, which is adapted to comply with the rigorous rules of finite-element theory. Because of the large displacements and strains which occur and the non-linear material properties the analysis utilises non-linear continuum mechanics to describe the governing equations, which are based on the principle of virtual work. An alternative analysis is also developed in which the governing equations are directly derived from the equilibrium conditions for the internal stresses. Both analyses yield results which compare favourably with those obtained by Carnaby, but use only a fraction of the previously required computing time which inhibited extensive evaluation of his model.

In order to model the long-gauge behaviour of wool yarns a staple-fibre yarn model is presented, based on earlier work by Hearle, which incorporates fibre migration and slippage. Extensive changes have been made to Hearle's original model, reflecting the advances made in the continuous-filament yarn analyses. Major additional features are the incorporation of changes in yarn configuration due to slippage, non-linear material behaviour, and a more realistic modelling of the lateral contraction of a yarn. The alternative finite-element analysis is used because it simplifies the application to non-conservative problems.

A number of specially spun yarns were used to evaluate both the continuous filament- and the staple fibre- yarn analyses.

ACKNOWLEDGEMENTS

The author wishes to express his appreciation for the support and guidance provided in the course of this work by his supervisors, Dr Garth A. Carnaby and Dr Athol J. Carr, members of the staffs of the Department of Civil Engineering, University of Canterbury, and the Wool Research Organisation of New Zealand (Inc.), and fellow students.

He also thanks Dr L. F. Story of WRONZ for checking and typing this report.

The work reported in this thesis was carried out while the author was the holder of a Post-graduate Fellowship from the Wool Research Organisation of New Zealand (Inc.).

CONTENTS

LIST OF FIGURES

LIST OF TABLES

CHAPTER 1

INTRODUCTION

1.1 SCOPE OF WORK

The work presented here is primarily concerned with the application of advanced structural analysis methods to the tensile behaviour of yarns, and in particular to wool yarns. This is the single most important property of yarns and is consequently one of the principal theoretical problems in textile physics and textile mechanics (1). The importance of the problem is reflected in the large amount of work published on this subject over the years.

The ultimate goal of this work is to be able to predict the strength of a yarn theoretically, given the fibre properties and the manufacturing parameters. This is not a single problem but a series of inter-connected problems, of which the main ones are:

- prediction of yarn structure from the manufacturing parameters and material properties;
- prediction of yarn tensile behaviour, given the yarn structure and material properties; and
- prediction of failure mechanisms and hence the breaking strength and behaviour.

In the work presented here the emphasis is on the yarn tensile behaviour up to breaking. The yarn structure used is a mixture of assumed and measured features.

For various reasons, the development of yarn mechanics in general has not kept up with the enormous advances made in computer-aided structural analysis methods which are extensively used in engineering and in other fields. One of the reasons for this stagnation as far as continuous filament yarns* are concerned is that a relatively simple semi-analytical theory as developed by Treloar and Riding (2) has been proved to be quite effective for producing a satisfactory theoretical prediction of the tensile behaviour of such yarns. The relatively simple nature of the continuous-filament yarn analysis is mainly due to the assumption that the radial contraction of the yarn is proportional to its elongation and that it is uniform throughout the yarn.

The analysis of staple-fibre yarns is more complex because of the presence of fibre discontinuities which lead to partial slipping of the

---

* A brief review of textile terms and definitions is given in Section 1.2.

fibres in the yarn. Carnaby and Grosberg (3) have tested staple-fibre (wool) yarns at short gauge lengths to evaluate the applicability of a uniform radial contraction in the case of such yarns without having to account for the added complexities due to the fibre discontinuities. Because the majority of the staple fibres are continuous throughout the short-gauge specimens it is implied that the staple-fibre yarn should effectively behave as a continuous-filament yarn. However, theoretical results obtained from Treloar's analysis with uniform radial contraction were, even if allowance was made for some inevitable slipping, considerably higher than the experimental short-gauge results (see Fig. 1.1). Carnaby (4) argued that the reason for this discrepancy was that the assumed uniform radial contraction of the yarn was not applicable to staple-fibre yarns which, in general, have a much more loosely packed and non-uniform structure than continuous-filament yarns.

A method was devised to predict the radial contraction of the yarn by applying a relationship derived by van Wyk (5) between the lateral pressure in the yarn and the specific volume. Treloar's analysis was adapted to incorporate this relationship together with a more realistic fibre distribution. The theoretical predictions of the tensile behaviour of the short-gauge wool yarns were found to be much better, especially for the lower range of yarn extension, as can be seen in Figure 1.1. Owing to the introduction of non-uniformity in the radial direction the radial displacements in the yarn could not anymore be determined as a continuous function. This necessitated a discretisation of the problem and the technique used by Carnaby can be considered as an informal application of the finite element method. Although it is effectively a continuous-filament yarn analysis it is as yet the most effective analysis for both short-gauge and long-gauge wool yarns. However, one particular disadvantage is the excessive computational effort required.

The first part of the work presented here is concerned with the reformulation of Carnaby's analysis so that it follows the more formal rules for the finite element method. This is to ensure a faster convergence of the analysis towards the correct solution of the problem within the modelling limitations. The results obtained with this new analysis, which is here called the continuous-filament yarn analysis, are not significantly different from Carnaby's results but a very considerable reduction in the computational effort required is achieved.

Alongside this formal finite element analysis a more informal analysis is introduced in Section 4.4; this utilises classical stress-analysis instead of an energy theorem to determine the governing equations. This

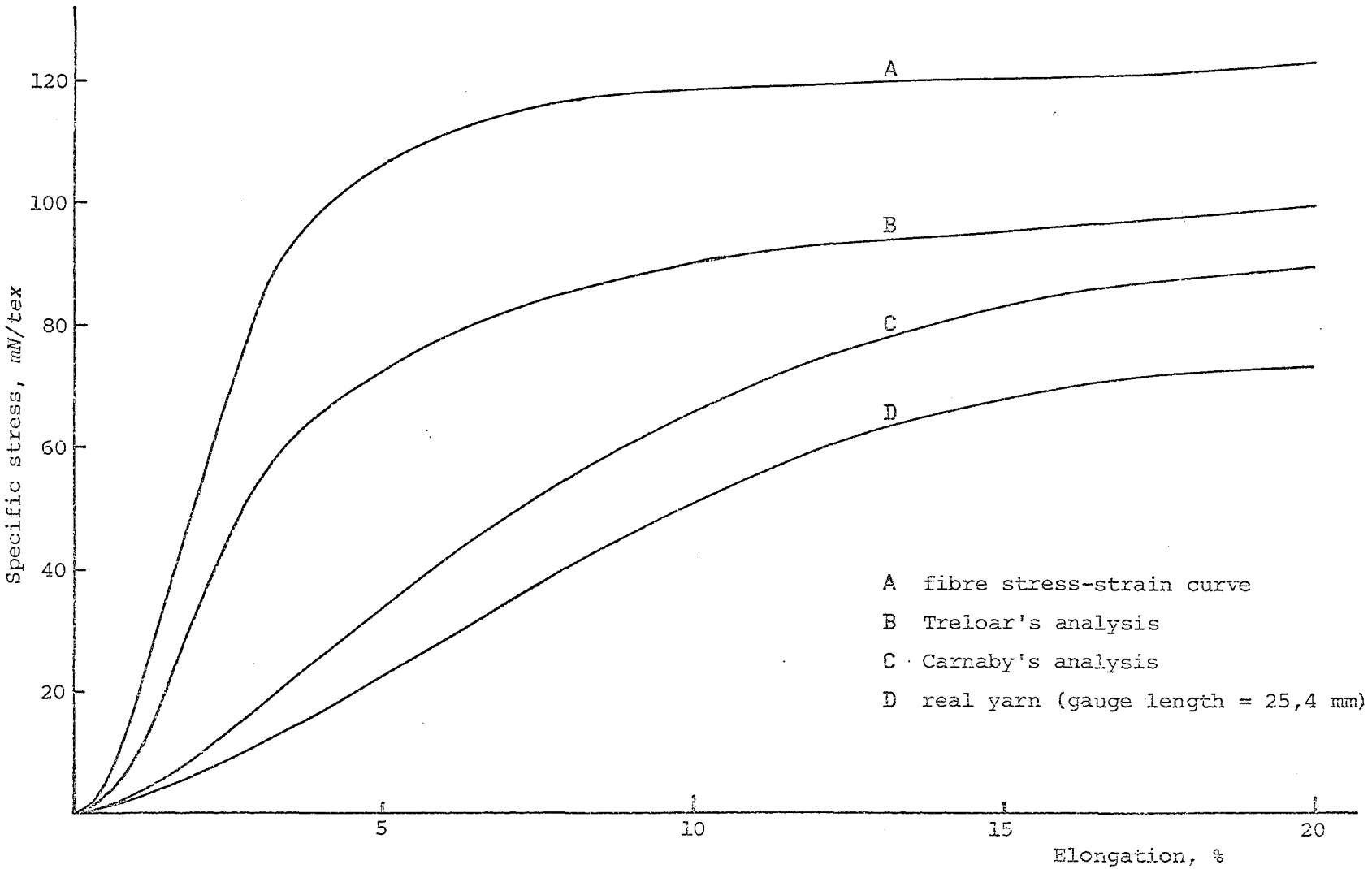

Fig. 1.1. Comparison of theoretical and experimental yarn stress-strain curves

particular analysis, which is designated 'stress analysis', was developed because it is more convenient to use with inter-fibre friction and slipping, although both features are not yet incorporated here. Comparison between the results of the stress analysis and the more formal energy analysis showed negligible differences between the two if the appropriate formulation for the governing equation was chosen for the stress analysis.

Although there still remain discrepancies between the theoretical results of the continuous-filament yarn analysis and the experimental results for the short-gauge wool yarns, it was decided to allocate the remaining time to the development of a more comprehensive staple-fibre yarn analysis. The reasons for this decision are discussed in Chapter 7.

The staple-fibre yarn analysis, which is discussed in Chapter 5, is an extensively altered version of the 'stress analysis' and it incorporates fibre migration, fibre discontinuities, and fibre slippage. Some aspects of the analysis are derived from Hearle's staple-fibre yarn analysis (6) but the present analysis has become quite different because of the many extra features added.

A number of wool yarns have been specially spun at WRONZ to enable the newly developed staple-fibre analysis to be evaluated. The testing and evaluation, which also includes the continuous-filament yarn analysis, is described in Chapter 6.

The rigorous testing of the model has revealed a number of limitations in the currently used assumptions and data, and made it clear that the problem is of a very complex physical nature. In general, the model has been found to give quite accurate predictions over the whole range of the highly non-linear stress-strain curves for a variety of wool yarns of different geometry. This is a significant advance as the previously available models are rather crude and they only incorporate an assumed but clearly unrealistic initial linear part of the yarn stress-strain curve. More importantly the steps involved in formulating the model and in obtaining the solution have led to a much clearer, and also more complex, picture of the key mechanism by which staple-fibre structures lock together when subjected to an axial tensile load. This stress-transfer mechanism consists essentially of a frictional locking together of the fibres under the transverse pressure as the structure contracts markedly in the lateral dimension.

It is also essential in this context to incorporate the interlacing effects arising from fibre migration and the mechanical state of the fibres in the geometry of the undeformed yarn. To the author's

knowledge no analysis has previously been published which combines in a more or less satisfactory way all these main features.

Reviews of yarn mechanics and the finite element method are given in Chapters 2 and 3 respectively to provide a base for the work presented in Chapters 4, 5 and 6.

1.2 TEXTILE TERMS AND DEFINITIONS

1.2.1 General

A brief review is given of textile terms and definitions as used in this work. An excellent review of textile structures and mechanics for those who are not textile specialists is given by Hearle (7). The following description is relevant to the yarn types which are explicitly or implicitly discussed in this work. Although the description covers a considerable proportion of all textile yarns there are other yarn types which are quite different in one or more aspects.

1.2.2 Fibres

The constituents of textile yarns are fibres which, generally speaking, are slender flexible rods. Fibres are subdivided into two main groups according to their length, viz., staple fibres and continuous fibres or filaments. The latter can for all practical purposes be regarded as possessing an infinite length and, with the single exception of silk, they are all of man-made origin. Staple fibres are of finite length, in general between 10 and 300 mm long. All natural fibres except silk are staple fibres, whereas all man-made fibres are initially continuous filaments though these can be simply changed to staple fibres by cutting or breaking.

1.2.3 Yarns

Yarns are long twisted structures made up of fibres. In general a central axis can be defined which runs along the length of a yarn and is called the 'yarn axis'. Because yarns are often cylindrical it is convenient to describe them in terms of a cylindrical co-ordinate system. The Z-axis of the co-ordinate system is taken so as to coincide with the yarn axis and hence the R- and θ-axes are normal to the yarn axis. The fibres generally follow a helical path of varying radius around the yarn axis, hence the twisted appearance of a yarn. The angle between a fibre and the yarn axis is called the twist- or helix-angle (α) and it varies throughout the yarn. The usual procedure for deriving the average level of twist is to count the number of turns needed to untwist a given length

of the yarn. The twist is expressed either as the number of turns of twist per metre, tpm, or as the length along the Z-axis over which a fibre completes a revolution around the yarn axis, i.e., the length of one turn of twist (TT).

Yarns are subdivided into two main groups — staple-fibre yarns and continuous-filament yarns — according to the length of the constituent fibres. Occasionally yarns may contain both staple fibres and continuous filaments, the latter usually forming a 'core' round which the staple fibres are spun. Staple-fibre yarns are commonly spun from blends of fibres of the same or different types, for example, woollen yarns are often made from a blend of different wool types, natural fibres such as wool and cotton may be blended, and natural and man-made fibres are often blended, e.g., cotton/polyester, wool/nylon, wool/rayon/acrylic. Continuous-filament yarns normally have only one component.

In some senses continuous-filament yarns and staple-fibre yarns are rather similar, because they both usually have a twisted structure. But from the point of view of tensile strength the two types are very different. In a continuous-filament yarn each individual filament extends from one end of the yarn to the other. If such a yarn has no twist it is a bundle of parallel continuous fibres and it will have a tensile strength approximately equal to the sum of the tensile strengths of the individual fibres. If a twist is given to this yarn the tensile strength will actually be reduced relative to the amount of twist inserted. This would seem to be undesirable but the twist is essential to achieve a compact yarn with satisfactory resistance to abrasion, fatigue, and other types of damage associated with stresses other than a simple tensile stress.

Twist is also needed for staple-fibre yarns for the same reasons, though these are actually of secondary importance in this case. Without twist a staple-fibre yarn longer than its longest fibre would be very weak as it would be held together only by entanglement, such as occurs in felted yarns. The insertion of twist is of primary importance because it causes the fibres to follow helical paths which are necessary to provide a strong self-locking structure. A staple-fibre yarn is only held together by friction between the fibres and this is dependent on the transverse pressures developed by the tensioned, helically wound fibres.

1.2.4 Manufacture of Yarns

The manufacture of twisted continuous-filament yarns is in principle very simple, the continuous filaments being brought together in a

parallel arrangement and then twisted into a yarn. The manufacturing process for a staple-fibre yarn is basically the same but the processing necessary to arrange the fibres prior to spinning and twisting is much more complicated because staple fibres are usually supplied in a random mass. The product of the preparatory processes is a sliver or roving, which is a long continuous strand of more or less parallel fibres. The tensile strength of a sliver is usually very low as it is essentially a thick twistless staple-fibre yarn.

The initial twisting process as above converts fibres into 'singles' yarns. For reasons of strength and texture, or colour effect, it is often necessary to twist two or more singles yarns together. The resulting yarns are called folded or plied yarns.

1.2.5 Textile Units

Perhaps the most widely accepted unit to express the linear density of fibres or fibre assemblies (slivers, yarns) is the 'tex', which is the mass in grams of 1000 m of the fibres or yarns. To circumvent the difficulties which arise in comparing yarns if the strength of a yarn is expressed in the conventional units of force per unit area of cross-section, the specific stress is used, which is expressed as the force per unit of linear density. The specific stress is also used for fibres and is here expressed in $mN.tex^{-1}$. Using the specific stress it is also easier to compare directly the structural efficiency of yarns of different linear densities.

1.2.6 Wool and Wool Yarns

The dimensions of new wool fibres are generally in the ranges of 50 - 300 mm for the length and 15 - 50 µm for the diameter (8). Because the finest wools are generally the shortest the length/diameter ratio is usually well above 1000. An additional important feature of most wool types is fibre crimp, which can be observed as a regular or random wave form of the fibres. The internal structure and chemical composition of wool are very complicated and have an important influence on the mechanical properties of wool fibres in varying physical and chemical environments. The most important physical factors affecting the normal testing of wool fibres and wool fibre assemblies are the air temperature and relative humidity and the rate of extension or compression. These factors must be closely controlled to produce comparable results, because the fibres are very sensitive to certain changes in environment. It is usual to conduct tests in a 'standard atmosphere' at $20 \pm 2^{\circ}C$ and $65 \pm 2\%$ RH.

There are two basic types of wool yarns, the rough and bulky woollen yarns and the smoother and more compact worsted yarns. In making the latter type of yarns the slivers are subjected to a thorough 'combing' process which gives a good alignment of the fibres in the slivers. In the case of woollen yarns the arrangement of the fibres in the slivers is more irregular, leading to a greater degree of entanglement and bulk in the yarns.

A third, intermediate, type is semi-worsted yarns, in which partial alignment of the fibres in the slivers is achieved by 'gilling' only and is not followed by rigorous combing. The result is a slightly more bulky yarn than a worsted yarn. The yarns used for the evaluation of the analyses presented here were all semi-worsted yarns.

CHAPTER 2

YARN STRUCTURE AND ANALYSIS

2.1 INTRODUCTION

In this chapter a review is given of the literature relevant to the mechanics of wool yarns. Although wool yarns are made of staple fibres a considerable proportion of the work on continuous-filament yarns is also of interest because most aspects of the analysis of the latter also apply in the analysis of staple-fibre yarns. Another important factor is that, for various reasons, research on continuous-filament yarns is in general in a more advanced state than that on staple-fibre yarns.

In the first part of this chapter research on the internal structure of yarns is discussed and this is followed by a review of the development of yarn analysis. The discussion is restricted to what, in the author's opinion, is the most important and relevant work. An excellent and complete review of the literature on the structure and mechanics of yarns up to 1969 is the work by Hearle *et al.* (1).

In the third part of the chapter two important factors in the behaviour of wool yarns are discussed, namely the compressibility of fibre assemblies and inter-fibre friction in fibre assemblies.

2.2 YARN STRUCTURE

2.2.1 Idealised Helical Yarn Structure

As there was no satisfactory method for observing the internal structure of a yarn at that time, the first idealised models of yarn structure leaned heavily on assumptions derived from external observation and from what was known about the spinning process. The main features of this 'idealised' structure were:

- the yarn has a circular cross-section and is approximately uniform along its length;
- the distribution of the fibres over the cross-section is approximately axisymmetric with respect to the centre of the cross-section; and
- each fibre follows a helical path around the yarn axis, so that its distance from the yarn axis remains constant for the whole length of the fibre; also every helical fibre path has the same pitch.

It must be noted that because an idealised structure is only a

tool to promote understanding of the behaviour of yarns it is not exactly quantified.

Models derived from this idealised helical yarn structure have been used widely and with success in the case of continuous-filament yarns (see Section 2.3.1). However, it was found that when using this particular structure it could not be explained why a piece of staple-fibre yarn, longer than the staple fibres, can exhibit considerable resistance to tensile forces. The basic reason for this phenomenon is the frictional forces which transmit the tensile forces from fibre to fibre throughout the yarn. These frictional forces are dependent on the transverse pressures which develop when helically wound fibres are tensioned. But the fibres on the surface of a staple-fibre yarn with the idealised helical structure would not be able to develop tension because there are no frictional forces present, due to the lack of pressure on the surface. So the surface fibres, owing to the lack of tension, would not exert any pressure on the underlying fibres which in turn could not develop any tension, and so on. The result would be a yarn which was very weak and furthermore there would be nothing to stop the fibres on the surface from peeling off so that the whole yarn could easily be destroyed.

2.2.2 Fibre Migration

To get around this defect the fibres must be assumed to vary their radial position, i.e., if they are at the surface of the yarn at one point along their path they must be tucked inside the yarn at other places. In this way the fibres could grip one another and the yarn could develop strength and cohesion. In 1947 Peirce (9) suggested that the fibres would follow random paths so that a staple-fibre yarn would actually be a random tangle of fibres. To find out the actual paths of the fibres it is necessary to look inside the yarn. This can be done by using the tracer-fibre method first described by Morton and Yen (10) in 1952.

In this method a small percentage of coloured fibres is added to a batch of uncoloured but otherwise identical fibres which is then processed into a yarn. When the finished yarn is immersed in a liquid which has the same (or a closely similar) refractive index as the uncoloured fibres the yarn will become almost transparent. Because of the different optical properties of the few coloured fibres these will still be clearly visible and their paths in the yarn can be easily distinguished. By rotating the yarn around its axis and making measurements in two projection planes at right-angles, the paths of the coloured fibres can be exactly defined (11).

On the basis of research on staple-fibre yarns with the tracer-fibre method, Morton (12) suggested that the fibres would change position between the inside and the outside of the yarn in a more regular fashion than that suggested by Peirce (9). The gradual change in radius of the helical fibre path was called 'migration'. Later research with the tracer-fibre method by Riding (13), who adapted the method to continuous-filament yarns, showed that these also exhibit migration. Morton postulated that the basic reason for the occurrence of this phenomenon is closely linked with another shortcoming associated with the idealised helical yarn structure and which is concerned with the formation of the yarn during the spinning process. All the fibres are supplied to the forming yarn at an identical rate but according to the idealised helical yarn theory the length of fibre needed for different radial positions in the yarn would vary. This would therefore cause high strains in the peripheral fibres which is of course undesirable. What actually happens according to Morton is that when the outer fibres develop a higher tension than those on the inside they will tend to interchange positions in the yarn. There will be a continuous process of interchange and in this way each fibre will oscillate between the centre and the surface of the yarn and so the lengths of the fibre paths will be approximately equal.

In 1962 Hearle and Merchant (14) gave a more sophisticated explanation of migration based on Morton's theory. The most important point raised was that migration does not occur when the fibres in the centre of the yarn are under tension. This implies that migration can be prevented by increasing the twisting tension.

Later, in 1965, Hearle and Bose (15) proposed a second mechanism based on the assumption that yarns are formed by the twisting of a flat ribbon of fibres (as they commonly emerge from the front rollers of a spinning machine after being drafted). The peculiar way in which a ribbon twists into a yarn automatically leads to migration if there is any twist in the ribbon. Hearle *et al.* (16) discussed the occurrence of both mechanisms at the same time, which is often referred to as the third mechanism.

Since then there has been intensive research into the causes and the pattern of migration, mainly on continuous-filament yarns and synthetic staple-fibre yarns. In general this work has confirmed the earlier theories of Morton and Hearle *et al.* In one of the very few publications concerned with wool yarns (worsted) Hickie and Chaikin (17) suggested that the tension mechanism as described by Morton is the most important.

An important aspect of fibre migration is the radial position of the fibre ends. Morton (12) suggested that most of the trailing ends of the fibres would be found at the yarn surface and the leading ends would be more evenly distributed throughout the yarn. However, for certain types of wool yarn Carnaby (4) found that the majority of both trailing and leading ends were present at the surface of the yarn.

Generally it was found that migration has both regular and random features which can be seen in Figure 2.1. It was also found that the radial position of the helical fibre path changes only slowly so that over a short length the geometry of an actual yarn is still similar to the idealised helical geometry. In the Figure the change seems more rapid because the dimensions are compressed in the direction of the yarn axis.

Hearle *et al.* (18) and Treloar (19) developed a modified idealised helical yarn structure which incorporates an ideal migration pattern. In this idealised structure the fibres migrate regularly and uniformly from the surface to the centre of the yarn and back. Each fibre path is identical except for a displacement along and a rotation about the yarn axis. This assumption together with the assumptions already made for the idealised helical yarn structure completely defines the path of the fibre.

2.2.3 Packing Density

Another aspect of yarn structure is the radial distribution of the fibres which is usually determined with the aid of the cross-section method. This involves the immersion of the yarn in a liquid which sets without shrinking and allows the cutting of thin cross-sectional slices without disturbing the configuration. The slices can be examined with a microscope.

It has been found that in continuous-filament yarns the fibres are closely packed over the cross-section (20) and have approximately uniform packing densities. Staple-fibre yarns, however, especially those made from crimpy fibres, are sparsely packed and the packing density varies considerably with radial position (4). The packing density also changes considerably during deformation. Most of the theoretical work on packing density is concerned with ideal close packing which is not relevant to staple-fibre yarns.

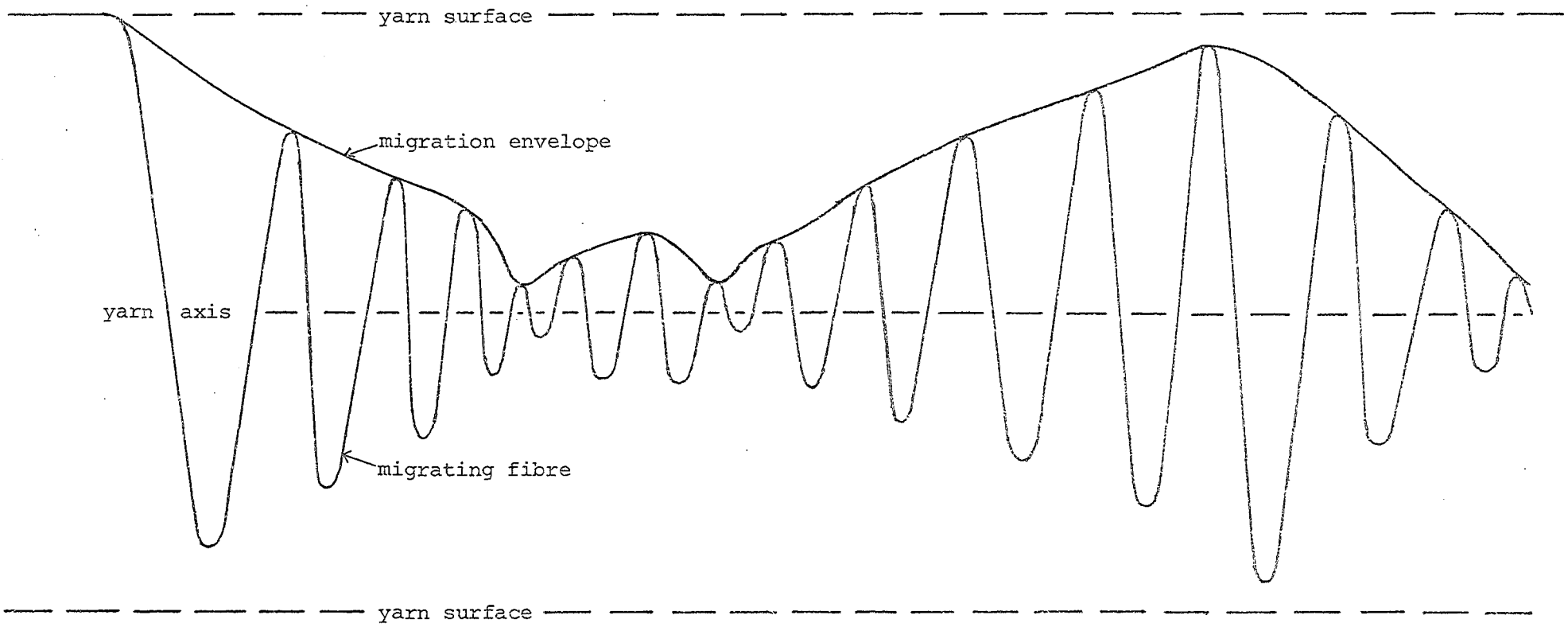

Fig. 2.1 Projection of the path of a fibre migrating over the yarn cross-section

2.3 YARN ANALYSIS

2.3.1 Continuous-filament Yarn Analysis

The first proper analyses of the tensile behaviour of yarns were made by Gegauff (21) in 1907. They were repeated independently several decades later in 1950 by Platt (22). In name Gegauff's work is concerned with staple-fibre (cotton) yarns but by assuming no fibre slippage at all his analysis is actually that of a continuous-filament yarn, as is that of Platt. As both analyses are very similar they will be dealt with together.

The main assumptions are as follows:

(a) the yarn is a continuous-filament yarn, uniform along its length, and its cross-sectional outline is circular;

(b) all the fibres within a yarn possess the same properties; they are circular in cross-section and obey Hooke's Law;

(c) the fibres are assumed to lie on perfect helices, of constant radius and constant angle; all these helices, throughout the cross-section, have the same number of turns per unit length of yarn; the axis of the helices is identical with the yarn axis;

(d) the fibres are uniformly and closely packed in the yarn;

(e) the fibre diameter is very small compared with the yarn diameter;

(f) no lateral contraction of the yarn occurs during extension of the yarn;

(g) no change in helix angle occurs during deformation;

(h) the yarn is subject to small strains; and

(i) only fibre tensile forces contribute to the yarn tensile force; i.e., no shear, torsion, bending, or lateral forces apply.

These assumptions lead to the following expression:

$$S_y = S_f . \cos^2\alpha$$

where S_y = specific stress of the yarn (N/tex);

S_f = specific stress of a fibre which has the same extension as the yarn; and

α = helix angle at the surface of the yarn.

Platt also considered non-Hookean fibre stress-strain behaviour but a closed analytical expression could only be derived for some special cases.

A major defect in these analyses is the neglect of the lateral forces in the yarn which act in a direction which is normal to that of the fibres. It is impossible to analyse a staple-fibre yarn properly without taking account of these forces.

The next step was to incorporate the lateral forces which was done by Hearle (23) in 1958. His assumptions are stated clearly and systematically and are otherwise much the same as for the previous work by Gegauff and Platt. The lateral forces are assumed to be constant in all directions normal to the fibre axis. A transverse elastic modulus (E_2), an axial Poisson's ratio (σ_1), and a transverse Poisson's ratio (σ_2) are introduced to describe the behaviour of the fibre material under the more complicated stress pattern. All of these parameters are assumed to be constant. The actual analysis is done by taking a small element of the yarn, with sides parallel and perpendicular to the fibre axis, and equating the forces acting on it. This method is called force-analysis or stress-analysis. The expression obtained for the stresses in the yarn and the yarn specific stress are relatively simple and can be evaluated numerically.

In 1961 Hearle *et al.* (24) published an extension of Hearle's previous work. A critical discussion is given of the assumptions used and two alternative analyses are presented. The first analysis is essentially the same as the previous one except that it incorporates lateral contraction of the yarn. The changes in yarn diameter are taken into account by introducing a term σ_y which is the axial Poisson's ratio of the yarn. The second analysis takes account of large yarn strains, restricted non-linear fibre tensile behaviour, and lateral contraction of the yarn, but to make the analysis tractable the transverse forces are neglected. A combination of both analyses is desirable but at that time seemed difficult to achieve with stress-analysis.

To overcome these difficulties Treloar and Riding (2) introduced a new 'energy analysis'. In this the internal elastic energy of the yarn is expressed as a function of the yarn extension (ΔL_y) and is then differentiated with respect to ΔL_y, which yields the yarn tensile force. Although not actually mentioned this is essentially the well-known virtual-work method.

The main advantage of the energy method is that it can cope quite simply with large yarn strains, any kind of non-linear fibre tensile behaviour, lateral contraction, and lateral forces. By assuming incompressibility of the fibre material, which is quite reasonable, the energy can be expressed solely in terms of the axial extension of the fibres. The yarn itself is also assumed to extend without change in volume. The assumptions about the yarn structure are the same as in the previous analyses. The predictions of the theory for the stress-strain curve of continuous-filament yarns agree very well with results from experiments.

In 1965 Treloar (19) incorporated migration in his earlier theory in order to check the assumption that if the rate of migration is not too great its influence would be very small on the tensile behaviour of a continuous-filament yarn. A method is presented to calculate the fibre paths in the case of regular migration between the centre and the surface of the yarn. The key assumption is that frictional forces will prevent the 'flowing' of tensile stress from one part of a fibre to another. From this assumption it follows that the tensile stress in a certain part of a fibre is only dependent on the local yarn deformation. The final results show that the difference in tensile strength between the idealised helical yarn model and the migration model are minimal.

In 1976 Carnaby and Grosberg (3) used Treloar and Riding's energy method to analyse staple-fibre yarn behaviour. To separate the effect of slippage near the ends of the fibres from other factors they tested the staple-fibre yarns at short gauge lengths (25 mm) so that the yarn would essentially behave as if it were composed of continuous fibres. The difference between the results of the analysis and the experiments is considerable even when allowing for some unavoidable slippage. These authors suggested that some of the assumptions used by Treloar and Riding, although reasonable for continuous-filament yarns, are too restrictive for staple-fibre yarns.

In the case of semi-worsted yarns (and the majority of wool yarns) the packing density is both low and radially dependent in the unstrained state. Also by studying the cross-sections of unstrained and strained yarns it seemed unrealistic to assume constant volume deformation or any other uniform lateral contraction. The basic solution to this problem is to let the yarn model somehow sort its geometry out during the deformation instead of imposing an arbitrary geometry by insisting on a radially independent Poisson's ratio.

To make this feasible it was necessary to define the mechanism which controls the lateral movements of the fibres. On one side this is the pressure exerted by the helically wound fibres under tension, which is already taken into account in the earlier analyses. On the other side the lateral movements are restricted by the resistance of the fibres to close packing. Carnaby and Grosberg incorporate this in their analysis by using a van Wyk-type relationship (see Section 2.4.1) which defines the pressure within a fibre assembly as a function of its specific volume.

As the variable packing density and the non-uniform lateral contraction will cause highly non-linear distributions of stresses and

strains in the radial direction the model is subdivided into concentric cylindrical zones. Aspects of the idealised helical yarn geometry are retained so that each fibre stays within a certain zone over its whole length and during the whole deformation. The energy in each zone due to tensile deformation and close packing can be expressed as a function of the material parameters, yarn extension and the inner and outer radii of each cylinder, the latter becoming the unknown parameters of the problem. The equilibrium state of the yarn at a certain extension is found by minimising the energy content with respect to the unknown parameters. The yarn tensile force is then found from the principle of virtual work.

At low yarn strains of up to 12%, the results of the analysis agree favourably with experimental data obtained by testing wool yarns at short gauge lengths. Study of the deforming geometry of the yarn model shows the non-uniform lateral movements of the fibres as a function both of radial position and of yarn extension.

A more detailed discussion of Carnaby's yarn analysis is given in Chapter 4.

2.3.2 Staple-fibre Yarn Analyses

Although the theories in the previous section are of considerable relevance to the analysis of wool yarns and staple-fibre yarns in general, they do not consider the consequences of the discontinuous nature of staple fibres on the behaviour of a yarn. This is of the utmost importance if a realistic analysis of staple-fibre yarns is to be achieved. However, probably due to the complicated nature of this problem, there have been very few publications on this subject.

The most realistic of these is an analysis incorporating fibre migration by Hearle (6) in 1965, which is briefly discussed below. As discussed earlier, fibre migration is essential in a staple-fibre yarn otherwise such a yarn would simply slip apart. Other analyses by Sullivan (25) and Holdaway (26) do not incorporate migration but use an imaginary external pressure on the yarn in order to start the build-up of the internal transverse pressure.

Hearle's staple-fibre yarn analysis is based on his continuous-filament yarn analyses (23, 24) discussed earlier but incorporating migration and fibre discontinuities in this case. The sole cause of the axial tension in the fibres is inter-fibre friction. The axial tension is zero at the fibre ends but there is a gradual build-up of frictional resistance along the fibre and hence of the tension which can be maintained. The frictional resistance is caused by the 'grip' of neighbour-

ing fibres which is a function of the transverse pressures in the yarn. At a certain distance from the end of the fibre the frictional resistance built up allows the fibre to maintain the tension as determined by the extension of the yarn. From this point on the axial tension in the fibre is governed by the extension of the yarn. The problem in solving the yarn equations is that the transverse pressure is dependent on the axial tension in the fibres which is in turn, along a certain distance from the ends, dependent on the transverse pressure. Because of this the solution must be obtained by an iterative process. Hearle gives the equations and a basic procedure for producing a solution for these equations, but no analyses were attempted.

2.4 PROPERTIES OF WOOL FIBRE ASSEMBLIES

2.4.1 Compressive Behaviour of Fibre Assemblies

The compressive properties of fibre assemblies have been extensively researched and a review on the subject has recently been published by Carnaby (27). Here only the factors directly relevant to the present analyses will be discussed.

The vast majority of the work on the compressibility of fibre assemblies is based on a paper by van Wyk (5), published in 1947. Van Wyk derived a theoretical relationship between the applied pressure on an assembly of randomly oriented wool fibres and the specific volume of the assembly:

$$p = K \left(V_{sp}^{-3} - V_{sp_0}^{-3} \right) \qquad . . . . . (2.1)$$

where p = applied pressure on the assembly;

K = a constant, to be called the van Wyk constant, which is dependent on certain fibre parameters;

V_{sp} = the current specific volume of the assembly; and

V_{sp_0} = the specific volume when $p = 0$.

The specific volume of a fibre assembly, V_{sp}, is defined by

$$V_{sp} = V.M^{-1} \qquad . . . . . (2.2)$$

where V = total volume of the assembly; and

M = mass of fibres in the assembly.

A comparison between the theoretically derived relationship and experimental results by van Wyk and later workers showed a reasonable agreement.

The most important aspect of van Wyk's theory is that the resistance of the fibre assembly to compression is solely attributed to the

energy necessary to bend the fibres into certain configurations so that the assembly as a whole takes up less volume. The bending energy is calculated by considering the assembly of fibres as a system of bending units. These bending units are the segemnts of fibre between adjacent fibre-to-fibre contacts. The unknown parameter in the ensuing equations is b, the mean distance between contact points, which is found to be a linear function of the specific volume of the fibre assembly:

$$b = a.V_{sp} \quad . \quad . \quad . \quad . \quad . \quad . \quad . \quad . \quad . \quad . \quad (2.3)$$

where a is a constant.

In the case of slivers and yarns the fibres are in general not randomly oriented but roughly aligned. In a yarn as a whole the difference in orientation between fibres on the surface and at the centre can be considerable but because the change is gradual the local situation in a yarn can be considered to be approximately the same as in a sliver (28). Several authors (29 - 33) have derived expressions for the mean distance between fibre contact points, b, in a sliver where the fibres are roughly aligned. The form of the expressions is quite different but they can all be written as:

$$b = a.V_{sp}.f(\theta) \quad . \quad . \quad . \quad . \quad . \quad . \quad . \quad . \quad . \quad . \quad (2.4)$$

where $f(\theta)$ is a correction factor, θ being the average angle of deviation of the fibres from their general direction.

As b is still a linear function of V_{sp} the relationship between the applied pressure on a roughly aligned fibre assembly and the specific volume is of the same form as the relationship derived by van Wyk for randomly oriented fibre assemblies (Equation 2.1):

$$p = K(\theta).(V_{sp}^{-3} - V_{sp_0}^{-3}) \quad . \quad . \quad . \quad . \quad . \quad . \quad . \quad . \quad . \quad (2.5)$$

As is indicated in the equation the van Wyk constant, K, will be dependent on the orientation of the fibres.

It must be emphasised that the above theory is only valid for a certain range of the specific volume of the fibre assembly. If the assembly is compressed so much that the specific volume approaches that of the fibres, which is 0,76 for wool, the compressive behaviour of the assembly will be governed mainly by the compressive properties of the fibre material. In that case the van Wyk relationship will be invalid as it is based solely on fibre bending. However, it was found that the smallest values for V_{sp} which occur in the yarn analyses are still within the limits of the van Wyk bending theory. These limits cannot be defined exactly but the results of experiments carried out at WRONZ on the compressibility of wool slivers, see Appendix F, have shown a well-defined

region where the experimentally obtained curve deviates from the theoretical curve. A typical result is shown in Figure 2.2.

There is as yet no theoretical method for determining a value for K. However, it can be determined experimentally by a simple method described in Appendix F.

The greatest merit of the van Wyk theory for yarn mechanics lies not so much in the expression derived for the compressibility of fibre assemblies, although this is convenient, but in the insight it gives into the causes of the resistance of slivers and yarns to close packing.

2.4.2 Inter-fibre Frictional Forces in Yarns and Slivers

One of the most important factors governing the behaviour of a staple-fibre yarn is the frictional forces exerted between the fibres in the yarn. Before attempting a proper analysis of a staple-fibre yarn which incorporates the effects of the fibre discontinuities and fibre slippage it is necessary to have an expression for the inter-fibre frictional forces. There are no theories or experiments on this subject in relation to actual yarns but, as in the case of the compressive behaviour, research on the subject in relation to slivers can be used as the local situation in a yarn resembles that in a sliver.

The aspect of the research on inter-fibre friction in slivers which is most relevant to staple-fibre yarn analyses concerns the withdrawal force of a single fibre from a sliver, WF, and which is defined as

$$WF = F.L^{-1}$$

where F is the force necessary to keep the fibre moving, and

L is the length of fibre present in the sliver, see Figure 2.3.

In 1952 Postle *et al.* (34) derived a theoretical relationship between WF, the sliver porosity, E, and the lateral pressure on the sliver, p:

$$WF = \frac{p}{(1 - E)}.\mu_{WF} + WF_0 \qquad (2.6)$$

where $E = V_{air} \cdot V_{total}^{-1}$;

V_{air} = volume of air in the sliver;

V_{total} = total volume of the sliver;

μ_{WF} = friction constant; and

WF_0 = withdrawal force when $p = 0$.

This relationship was confirmed by the results of experiments carried out by Postle *et al.* and later by Anderson *et al.* (32). The withdrawal force is essentially derived by considering the number of contacts

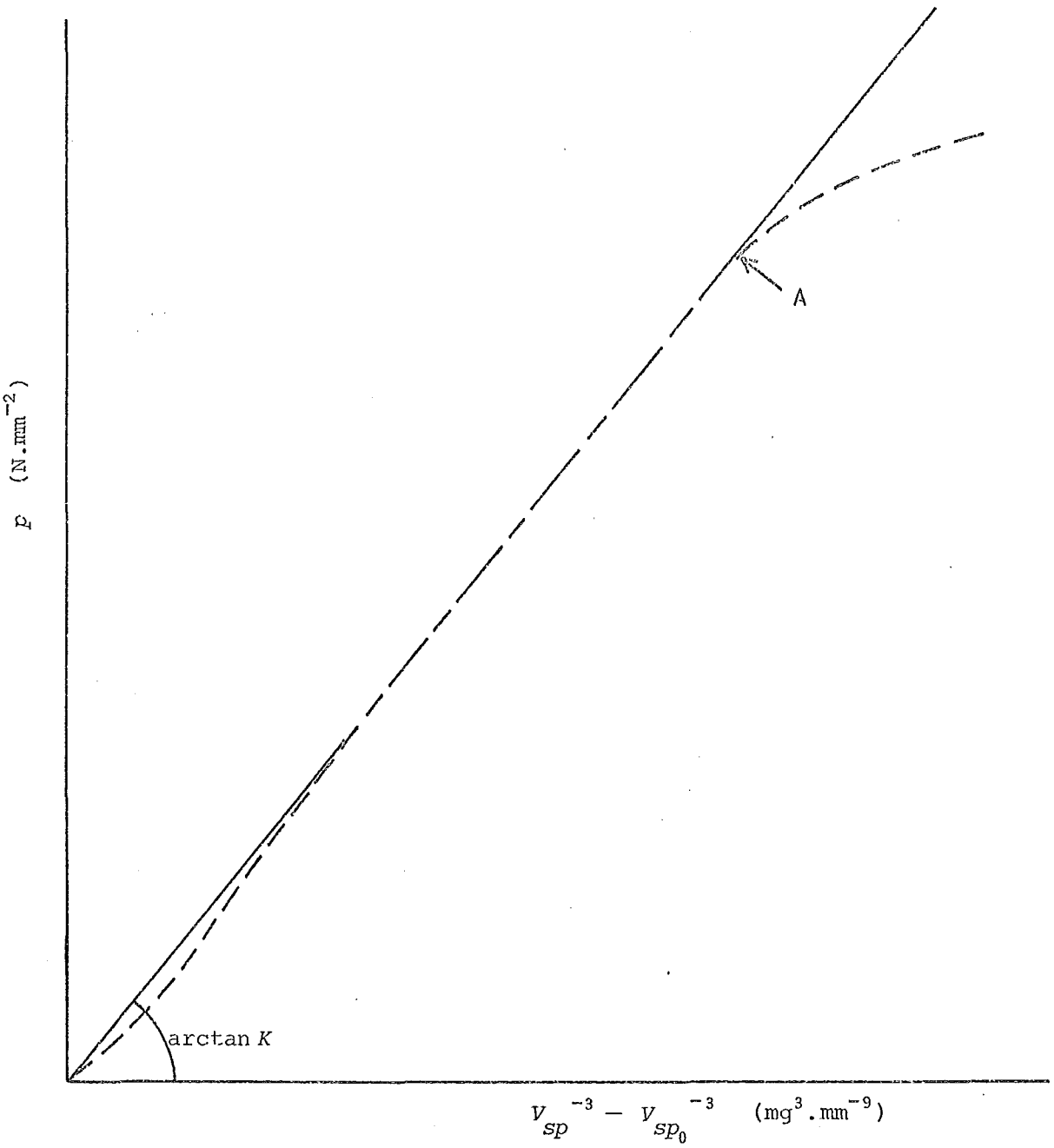

Fig. 2.2. Lateral compressibility of a wool sliver

———— theoretical curve (van Wyk)

– – – – experimental curve

A approximate upper limit for validity of the van Wyk theory

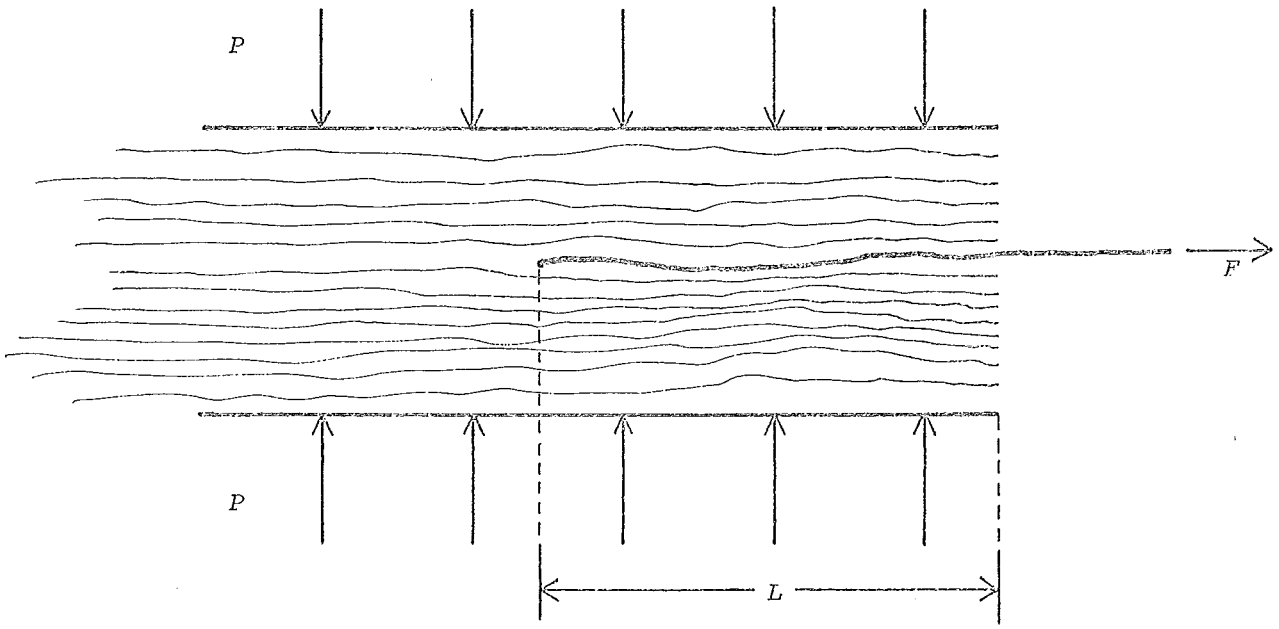

Fig. 2.3. Single fibre withdrawal from a sliver

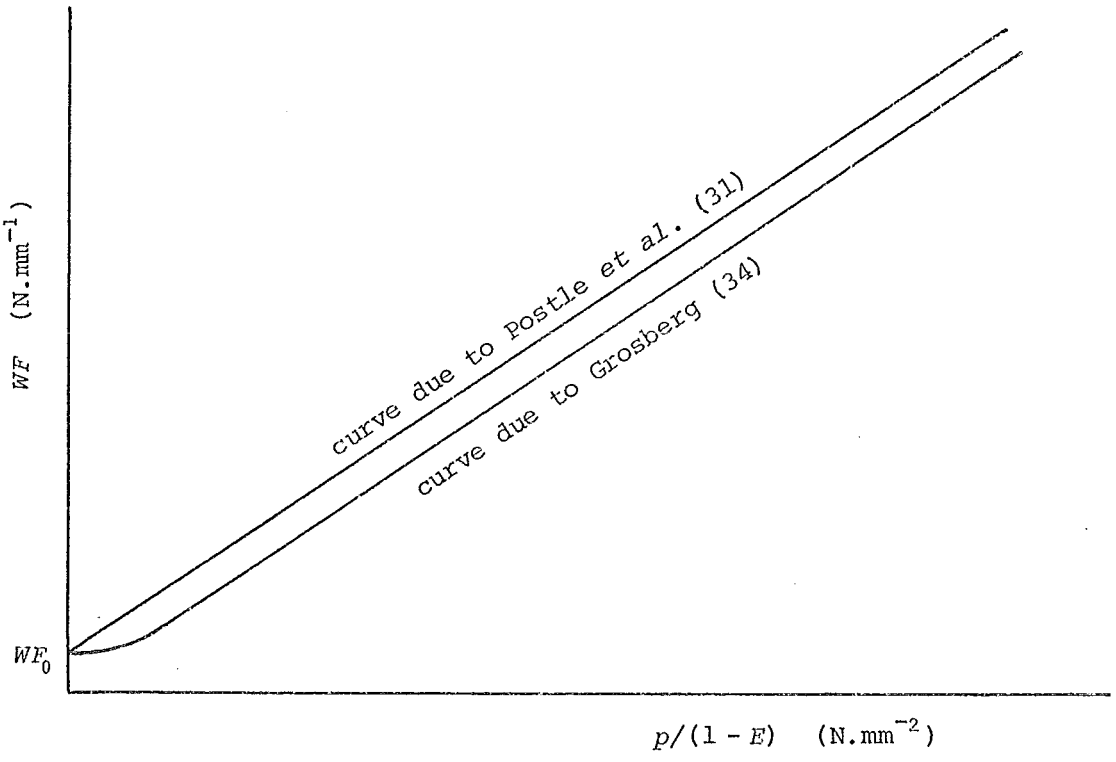

Fig. 2.4. Theoretical curves for single fibre withdrawal from a sliver

made by the withdrawn fibre with surrounding fibres in the sliver and the frictional force per contact, FF. The expression used for FF is:

$$FF = \mu . F_N + FF_0 \qquad (2.7)$$

where μ = coefficient of friction (constant);

F_N = normal force at a contact; and

FF_0 = value of FF when $F_N = 0$.

In the analysis a relationship between the normal force at a contact, F_N, and the external pressure, p, is derived from which follows:

$$p = 0 \Rightarrow F_N = 0 .$$

Together with Equation (2.7) this implies that WF_0, which is definitely not zero, is solely due to the factor FF_0. This is the most controversial point in the analysis because in the case of pure friction FF_0 is non-existent. However, it was supposed to represent an adhesional force, which was backed by some experimental evidence (33).

Grosberg (31), however, supported by other experimental evidence, denied the existence of FF_0 and developed a theory which explained non-zero values of WF_0 without having to resort to the ambiguous factor, FF_0. Essentially his explanation is that although the external pressure on an uncompressed sliver is zero ($p = 0$) the normal forces at the fibre contacts (F_N) do not vanish. Grosberg suggested that an uncompressed sliver contains stored elastic energy which cannot be released due to the friction between the fibres. This 'locked-in' energy will cause non-zero normal forces at the fibre contacts even when $p = 0$. The theoretically derived values of WF_0 agree reasonably well with experimentally found values from uncompressed slivers. For large values of the external pressure on the sliver, p, Grosberg's expression for WF becomes identical to Equation (2.6) but without the factor WF_0. In Figure 2.4 both theoretical curves are shown for equal values of WF_0.

The theoretical evaluation of the parameters involved in the expression for WF is quite complicated and is also dependent on fibre- and sliver properties which are difficult to determine. A direct experimental determination of the parameters requires specialised equipment; WF_0 is especially difficult to determine accurately.

CHAPTER 3

THE FINITE-ELEMENT METHOD

3.1 INTRODUCTION

The finite-element method, which has been used successfully to solve a wide variety of problems, originated in structural engineering in the 1950s. In the 1940s several applied mathematicians such as Courant (35) and Prager and Synge (36) had developed techniques which are now recognised as basic finite-element methods. However, the first formal applications, which are generally attributed to Argyris (37) and Turner *et al.* (38), appeared independently from the earlier mathematical approaches a decade later in aircraft structural engineering. With the increasing availability of high-speed digital computers a rapid development of the finite-element method to cover a wide range of problems in structural engineering and solid mechanics followed. In the early 1960s the method was extended to cover non-structural fields such as fluid mechanics and heat conduction (39).

In the early years the development was largely based on 'common sense' and engineering 'intuition' but slowly a more formal and rigorous mathematical description of the method was developed. Later on mathematics was not only used to support the less formal engineering approaches but to lay the basis for new techniques which have widened the scope of the finite-element method considerably.

The method is now well documented by thousands of publications (40), the majority being specialised papers. More general textbooks (41 - 47) have appeared during the past decade.

To provide a basis for the work in this thesis the concepts of the finite-element method and its application to solid mechanics will be discussed briefly.

Although the formulation can differ significantly from problem to problem a finite-element method can be distinguished by the following principal features (43):

(a) the physical region of the problem is sub-divided by a mesh of imaginary lines or surfaces into sub-regions, the so-called finite elements;

(b) one or more of the dependent variables is approximated in functional form over each element; the parameters of these trial or shape functions become the unknowns of the problem; and

(c) substitution of the above approximations in the governing equation(s) of the problem yields a set of equations in the unknown parameters, which can then be solved to give the approximate solution to the problem.

To ensure that the finite-element idealisation provides an accurate representation of the problem certain conditions must be met by the trial functions. These conditions for the solids mechanics case will be discussed in Section 3.2.2.

To give a more detailed account of the finite-element method it is helpful to choose an example from a particular field and because of its relevance to the wool yarn analysis a simple axisymmetric solid mechanics example is chosen.

3.2 APPLICATION TO SOLID MECHANICS

The problem outlined below is the analysis of a cylindrical rod under axisymmetric loading and of which the displacements are confined to the R (radial) and Z (axial) directions, see Figure 3.1. The rod is assumed to consist of a linear elastic isotropic material and it is also assumed that the configuration does not change significantly after loading.

There are several finite-element methods available for analysing solid continua, the difference between them being in the choice of the variable to be approximated and the governing equation. Here the most common method will be used, based on assumed displacement fields and using the principle of virtual work (or minimum potential energy) to develop the governing equations. Other methods are based on assumed stress- and displacement fields and use different governing equations such as the principle of minimum complementary energy or Reissner's variational principle (48).

3.2.1 Finite Element Sub-division

The rod is sub-divided by a mesh of imaginary lines into finite elements which are interconnected at certain points on the boundaries, the so-called nodes. In axisymmetric analyses the elements are rings of constant cross-section in the R-Z plane, as can be seen in Figure 3.2. As the displacements of all points with the same R and Z co-ordinates are identical the deformation of an axisymmetric element can be represented by a single cross-section in the R-Z plane. In this case the cross-sections are taken as rectangular and the nodes are situated at the corners, so there are four nodes per element. In Figure 3.2 a simple sub-division of the rod is shown with the element numbers which are

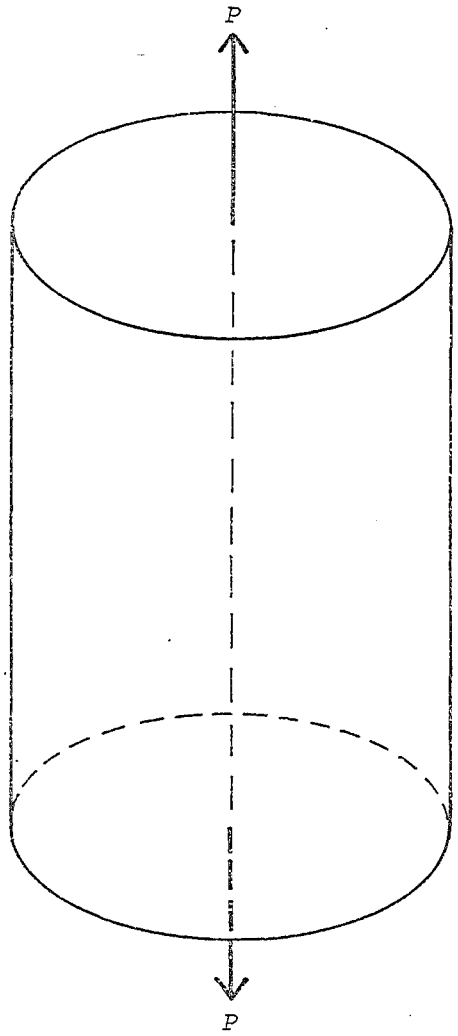

Fig. 3.1. Cylindrical rod with axisymmetrical loading

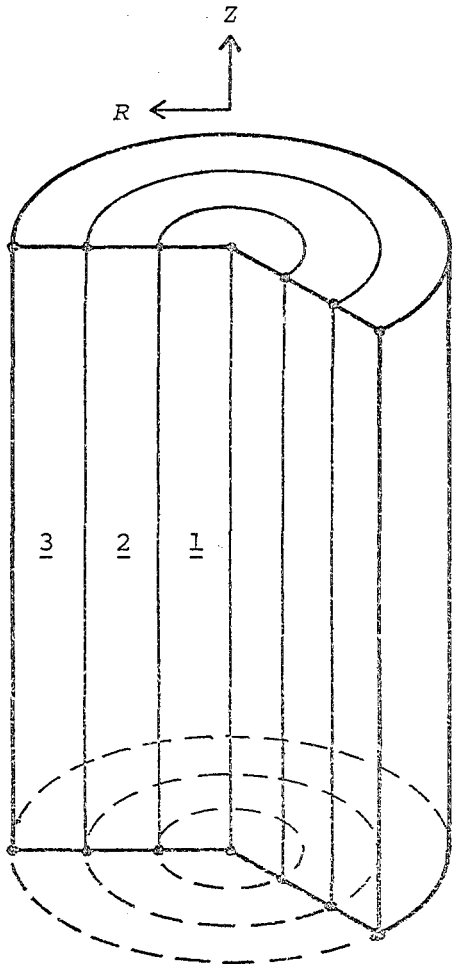

Fig. 3.2. Finite element sub-division into axisymmetric elements, with element numbers

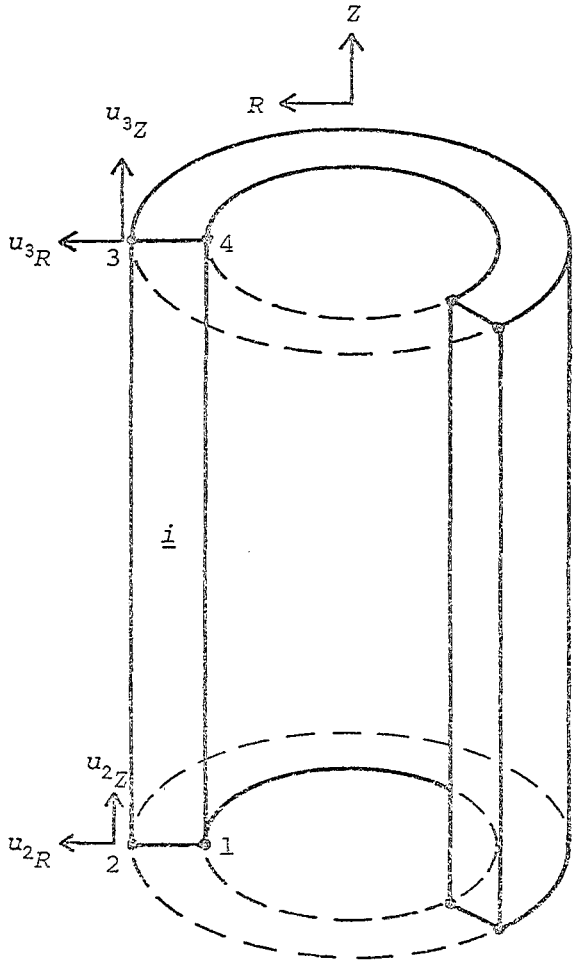

Fig. 3.3. Axisymmetric element with element nodal numbering

underlined.

An important feature of the finite-element method is that the equations derived for a typical element are valid for all the elements if they are all of the same type. In Figure 3.3 a typical element, i, is illustrated with the node numbering which is the so-called local- or element node numbering. As the problem is essentially two-dimensional the displacements of the nodes are broken down into components in the R and Z directions, the so-called degrees of freedom of a node. The element as a whole has eight degrees of freedom and the corresponding displacements are contained in the element nodal displacement vector $\{u\}$ where $\{u\}^T = < u_{1R}, \ldots, u_{4R}, u_{1Z}, \ldots, u_{4Z} >$ in which the first subscript denotes the node number and the second the direction.

3.2.2 Displacement Field

An important step in the analysis is the selection of a displacement function that uniquely defines the displacement of every point within an element as a function of the nodal displacements. In general the displacement field $\{\bar{u}\}$ over an element can be written in the form:

$$\{\bar{u}(R,Z)\} = \left[N(R, Z, R_i, Z_i) \right] . \{u\} \qquad \ldots\ldots\ldots\ldots \quad (3.1)$$

where R, Z are the co-ordinates of an arbitrary point;

R_i, Z_i are the co-ordinates of the nodes;

$\{u\}$ is the nodal displacement vector; and

$\{\bar{u}\}^T = < \bar{u}_R, \bar{u}_Z >$.

The functions contained in the matrix $[N]$ are generally referred to as the shape- or trial functions.

To ensure a proper description of the problem which is characterised by monotonic convergence to the correct solution with mesh refinement the displacement field must satisfy certain criteria (42, 44, 46):

(i) if the element is subjected to a rigid body motion the internal strain energy and the nodal forces must remain zero;

(ii) if the element nodal displacements are given values corresponding to a state of constant strain the displacement field must produce a state of constant strain within the element; and

(iii) the displacement field must possess continuity within the element and across the element boundaries, of the type required by the variational basis of the formulation.

In particular, continuity of all derivatives up to one order less than the maximum order appearing in the governing equation is mandatory.

The derivation of the shape functions, which lead to an admissible displacement field, can be accomplished in two different ways. The first method is to describe the displacement field $\{\bar{u}\}$ in terms of a polynomial expression in the appropriate co-ordinates. As the problem is two-dimensional this leads to

$$\bar{u}_R(R,Z) = < p(R,Z) > . \{a\}_R \quad . . . . . (3.2a)$$

$$\bar{u}_Z(R,Z) = < p(R,Z) > . \{a\}_Z \quad . . . . . (3.2b)$$

where $\{a\}_R$ and $\{a\}_Z$ are sets of generalised displacement parameters, and

$< p >$ is a set of functions of R and Z as defined by the Pascal triangle

$$p_1 = 1 \qquad p_2 = R \qquad p_3 = Z \qquad p_4 = R^2 \text{ etc.}$$

Expressions for $\{a\}_R$ and $\{a\}_Z$ are found by substituting the values of the displacements at the nodes into Equations (3.2).

$$\bar{u}_R(R_i,Z_i) = u_{i_R} = < p(R_i,Z_i) > . \{a\}_R \quad . . . . . (3.3a)$$

$$\bar{u}_Z(R_i,Z_i) = u_{i_Z} = < p(R_i,Z_i) > . \{a\}_Z \quad . . . . . (3.3b)$$

Repeating this for all four nodes of the rectangular element leads to

$$\{u\}_R = \begin{bmatrix} < p(R_1, Z_1) > \\ < p(R_2, Z_2) > \\ < p(R_3, Z_3) > \\ < p(R_4, Z_4) > \end{bmatrix} . \{a\}_R = [P] . \{a\}_R \quad . . . . . (3.4a)$$

$$\{u\}_Z = [P] . \{a\}_Z \quad . . . . . (3.4b)$$

where $\{u\}_R^T = < u_{1_R}, u_{2_R}, u_{3_R}, u_{4_R} >$

$\{u\}_Z^T = < u_{1_Z}, u_{2_Z}, u_{3_Z}, u_{4_Z} >$

$< \{u\}_R^T, \{u\}_Z^T > = \{u\}^T$.

It is clear that the polynomial in Equations (3.2) must contain four terms otherwise Equation (3.4) cannot be solved for $\{a\}$. A polynomial with four terms is incomplete because outside the three lower order terms (1, R and Z) it can only contain one of the three quadratic terms (R^2, RZ and Z^2). The choice is not difficult because only the term RZ will satisfy the condition that the displacement field is linear along any element boundary. In any case it is undesirable to include terms which make the displacement function asymmetric with respect to the co-ordinate axes. The resulting expression for $< p >$ is:

$$< p > = < 1 \; R \; Z \; RZ > \quad . . . . . (3.5)$$

and the displacement functions become:

$$\{\bar{u}(R,Z)\}_R = <1\ R\ Z\ RZ>\{a\}_R \qquad \ldots\ldots\ldots\ldots\ (3.6a)$$

$$\{\bar{u}(R,Z)\}_Z = <1\ R\ Z\ RZ>\{a\}_Z \qquad \ldots\ldots\ldots\ldots\ (3.6b)$$

These satisfy the conditions stated before.

The generalised displacement parameters $\{a\}_R$ and $\{a\}_Z$ can now be solved from Equations (3.4) by inverting $[P]$:

$$\{a\}_R = [P]^{-1}.\{u\}_R \qquad \ldots\ldots\ldots\ldots\ (3.7a)$$

$$\{a\}_Z = [P]^{-1}.\{u\}_Z \qquad \ldots\ldots\ldots\ldots\ (3.7b)$$

where
$$[P] = \begin{bmatrix} 1 & R_1 & Z_1 & R_1Z_1 \\ 1 & R_2 & Z_2 & R_2Z_2 \\ 1 & R_3 & Z_3 & R_3Z_3 \\ 1 & R_4 & Z_4 & R_4Z_4 \end{bmatrix} .$$

Using Equations (3.7) and (3.2), Equation (3.1) can now be written as:

$$\{\bar{u}\} = \begin{Bmatrix} \bar{u}_R \\ \bar{u}_Z \end{Bmatrix} = \begin{bmatrix} <N> & <O> \\ <O> & <N> \end{bmatrix} \{u\} \qquad \ldots\ldots\ldots\ldots\ (3.8)$$

where $<N> = <p>.[P]^{-1} = <N_1\ N_2\ N_3\ N_4>$

$<O> = <0\ 0\ 0\ 0>$.

The shape functions N_i contain permutations of the nodal co-ordinates R_i and Z_i, and the functions R, Z and RZ.

The shape functions found in this way are in fact Lagrangian interpolation functions based on the displacements at the nodes. These interpolation functions can be derived directly which is often more convenient than using the indirect method which involves a matrix inversion. This is especially true when a convenient co-ordinate system is used as shown in Figure 3.3 where the axes are parallel with the sides of the elements. The shape functions as derived by the direct method are (43):

$$\begin{aligned} N_1 &= (RZ - RZ_4 - R_2Z + R_2Z_4)/ab \\ N_2 &= (-RZ + RZ_4 + R_1Z - R_1Z_4)/ab \\ N_3 &= (-RZ + RZ_1 + R_2Z - R_2Z_1)/ab \\ N_4 &= (RZ - RZ_1 - R_1Z + R_1Z_1)/ab \end{aligned} \qquad \ldots\ldots\ldots\ldots\ (3.9)$$

where $a = R_2 - R_1$

$b = Z_3 - Z_2$.

Proper application of both methods leads to identical shape functions.

3.2.3 Governing Equation

The governing equation in this case is the principle of virtual work. Given a certain configuration of an object which is in static equilibrium, the principle of virtual work states that when the displacement field of the object, $\bar{u}$, is augmented by a kinematically admissible virtual displacement field, $\delta\bar{u}$, the following relationship holds (50):

$$\delta W_{ext} = \int_V \delta \{E\}^T \{\sigma\} \, dV \qquad \ldots\ldots\ldots\ldots (3.10)$$

where δW_{ext} = work done by forces acting on the object;

$\delta \{E\}$ = virtual increment in strain due to $\delta\bar{u}$;

$\{\sigma\}$ = stress at the given configuration; and

$\int_V$ = integration over the volume of the object.

The external work δW_{ext} is due to the external forces which are in equilibrium with the internal stress-field caused by $\bar{u}$. Applying the principle of virtual work to a single finite element and assuming that the external forces are concentrated at the nodes the external work δW_{ext} can be expressed as:

$$\delta W_{ext} = \{\delta u\}^T . \{f\} \qquad \ldots\ldots\ldots\ldots (3.11)$$

where $\{\delta u\}^T = < \delta u_{1_R} , \delta u_{2_R} , \ldots \delta u_{4_Z} >$

virtual element nodal displacement vector;

$\{f\} = < f_{1_R} , f_{2_R} , \ldots f_{4_R} , f_{1_Z} , \ldots f_{4_Z} >$

element nodal force vector.

The virtual increment in strain $\delta\{E\}$ due to $\{\delta u\}$ is

$$\delta\{E\} = \frac{\partial\{E\}}{\partial\{u\}^T} . \{\delta u\} \qquad \ldots\ldots\ldots\ldots (3.12)$$

Substituting Equations (3.11) and (3.12) into Equation (3.10) yields

$$\{\delta u\}^T . \{f\} = \{\delta u\}^T \int_V \frac{\partial\{E\}^T}{\partial\{u\}} . \{\sigma\} . dV \qquad \ldots\ldots\ldots (3.13)$$

For any set of non-zero values for $\{\delta u\}$ Equation 3.13 becomes

$$\{f\} = \int_V \frac{\partial\{E\}^T}{\partial\{u\}} . \{\sigma\} . dV \qquad \ldots\ldots\ldots\ldots (3.14)$$

where $\{f\}$, the nodal force vector, is in equilibrium with the internal stress field, $\{\sigma\}$. By expressing the stresses and strains in terms of $\{u\}$, $\{f\}$ can be written as a function of $\{u\}$:

$$\{f\} = \{f(\{u\})\} .$$

3.2.4 Stresses and Strains

To express the element nodal forces as functions of $\{u\}$ it is necessary to express the strains and stresses in terms of $\{u\}$. In the axisymmetric case the strain vector is defined as

$$\{E\} = \begin{Bmatrix} E_{RR} \\ E_{\theta\theta} \\ E_{ZZ} \\ E_{RZ} \end{Bmatrix} = \begin{Bmatrix} \bar{u}_{R,R} \\ \bar{u}_{R}(R^{-1}) \\ \bar{u}_{Z,Z} \\ \bar{u}_{R,Z} + \bar{u}_{Z,R} \end{Bmatrix} \quad \ldots\ldots\ldots (3.15)$$

where $\bar{u}_{R,Z}$ is $\bar{u}_R$ differentiated with respect to Z etc; and

E_{RR}, $E_{\theta\theta}$, E_{ZZ} and E_{RZ} are the radial strain, the hoop strain, the axial strain, and the shear strain respectively.

Using the expressions for $\bar{u}_R$ and $\bar{u}_Z$ from Equation (3.8) and differentiating with respect to the appropriate co-ordinates yields the strains as functions of $\{u\}$:

$$\{E\} = \begin{bmatrix} <N,R> & < & O & > \\ <N/R> & < & O & > \\ < & O & > & <N,Z> \\ <N,Z> & <N,R> & & \end{bmatrix} . \{u\} = [B].\{u\} \quad \ldots\ldots (3.16)$$

where $<N,R> = < Z - Z_4 , -Z + Z_4 , -Z + Z_1 , Z - Z_1 > /ab$

$<N,Z> = < R - R_2 , -R + R_1 , -R + R_2 , R - R_1 > /ab$

$<N/R> = < N > /R$.

These are derived from Equation (3.9).

Because the shape functions N_i are independent of $\{u\}$ the matrix $[B]$ will also be independent of $\{u\}$.

For an axisymmetric problem with linear elastic isotropic material the stress can be expressed as a function of the strains by:

$$\begin{Bmatrix} \sigma_{RR} \\ \sigma_{\theta\theta} \\ \sigma_{ZZ} \\ \sigma_{RZ} \end{Bmatrix} = [D] \begin{Bmatrix} E_{RR} \\ E_{\theta\theta} \\ E_{ZZ} \\ E_{RZ} \end{Bmatrix} = [D].\{E\} \quad \ldots\ldots\ldots (3.17)$$

where (46)

$$[D] = \frac{\varepsilon}{(1+\nu)(1-2\nu)} \begin{bmatrix} 1-\nu & \nu & \nu & 0 \\ \nu & 1-\nu & \nu & 0 \\ \nu & \nu & 1-\nu & 0 \\ 0 & 0 & 0 & \frac{(1-2\nu)}{2} \end{bmatrix} \quad \ldots\ldots (3.18)$$

and ε = the elastic modulus of the material;

ν = Poisson's ratio.

With linear elastic material the elastic constants ε and ν are independent of the strain level and therefore of the displacements. The stresses can be written as functions of $\{u\}$ by substituting Equation (3.16) into (3.17) which yields:

$$\{\sigma\} = [D].[B].\{u\} \qquad \ldots\ldots\ldots\ldots \quad (3.19)$$

3.2.5 Stiffness Matrix

Substituting Equations (3.16) and (3.19) into Equation (3.14) gives the element nodal force vector as a function of $\{u\}$:

$$\{f\} = \int_V \frac{\partial(\{u\}^T.[B]^T)}{\partial\{u\}}.[D].[B].\{u\}.dV \qquad \ldots\ldots \quad (3.20)$$

Because of axial symmetry the volume integral can be transformed into an area integral in the R-Z plane. Doing this and differentiating, Equation (3.20) becomes:

$$\{f\} = \left(2\pi.\int_A [B]^T.[D].[B].R.dA\right).\{u\} \qquad \ldots\ldots \quad (3.21)$$

where A is the area of the cross-section of the element.

The term on the right-hand side of Equation (3.21) is by definition the stiffness matrix of an element because it links the nodal displacements with the nodal forces.

$$\{f\} = [k].\{u\} \qquad \ldots\ldots\ldots\ldots \quad (3.22)$$

where $[k]$, the element stiffness matrix, is an 8×8 matrix in this case.

As both matrices $[B]$ and $[D]$ are independent of $\{u\}$ the stiffness matrix will also be independent of $\{u\}$. In the axisymmetric case, because of the R^{-1} terms contained in $[B]$, the integral in Equation (3.21) cannot be evaluated analytically and numerical integration techniques are necessary.

Repeating the procedures outlined above for each element, the nodal forces which are in equilibrium with the individual stress-fields of each element can be determined as a function of the element nodal displacements:

$$\{f\}_i = [k]_i.\{u\}_i \qquad \ldots\ldots\ldots\ldots \quad (3.23)$$

3.2.6 Assembly and Solution

To determine the equilibrium equations of the model, the elements, which are analysed separately in the previous section, are assembled into the finite-element model. Because of the continuity of the model certain nodes of adjacent elements must be identical to each other as

can be seen in Figure 3.4. For example node 4 of element 2 is identical to node 3 of element 1, etc. In Figure 3.5 the nodes of the assembled model are numbered according to the whole model, often referred to as the system nodal numbering.

For the assembly it is convenient to change the subscripts of the element nodal displacement- and force vectors. In the previous section two subscripts were used, one for the node and one for the direction; these are replaced by a single subscript. The R-displacements and R-forces are numbered 1 to 4 and the Z-displacements and Z-forces are numbered from 5 to 8.

Thus for $i = 1 \rightarrow 4$, $u_i = u_{i_R}$, $f_i = f_{i_R}$

$= 5 \rightarrow 8$, $u_i = u_{(i-4)_Z}$, $f_i = f_{(i-4)_Z}$.

This has no influence on the values or the arrangement of the terms within the vectors.

The displacements of the nodes as numbered according to the system are collected in the system nodal displacement vector $\{U\}$ and the subscripts are numbered in the same fashion as above.

$$\{U\}^T = < U_1, U_2, U_3, \ldots U_{NOD}, U_{NOD+1}, \ldots U_{NOD2} >$$

where $_{NOD}$ is the total number of nodes in the system;

$NOD2 = 2 \times NOD$.

Thus for $i = 1 \rightarrow NOD$, $U_i = U_{i_R}$

$i = (NOD + 1) \rightarrow NOD2$, $U_i = U_{(i-NOD)_Z}$

The individual terms of $\{U\}$ are equal to certain element nodal displacements, for example:

$$U_3 = (u_1)_{\underline{2}} = (u_2)_{\underline{1}}$$

$$U_{(NOD+6)} = (u_7)_{\underline{2}} = (u_8)_{\underline{3}} \quad \text{etc.}$$

Note that the parameters which are defined with respect to an element are written with lower-case letters and those defined with respect to the system are written with upper-case letters.

The nodal forces acting on the system nodes and which are in equilibrium with all the stress-fields in the model are contained in the system nodal force vector $\{F\}$:

$$\{F\}^T = < F_1, F_2, \ldots, F_{NOD}, F_{(NOD+1)}, \ldots, F_{NOD2} >$$

The same subscript numbering is used as with $\{U\}$.

To determine the terms in $\{F\}$ the principle of virtual work is

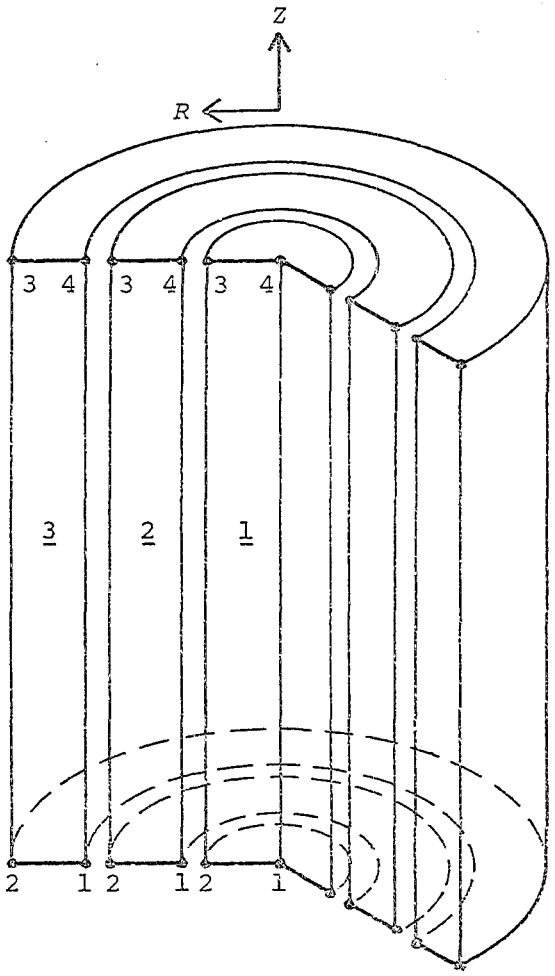

Fig. 3.4. Finite-element model with element nodal numbering

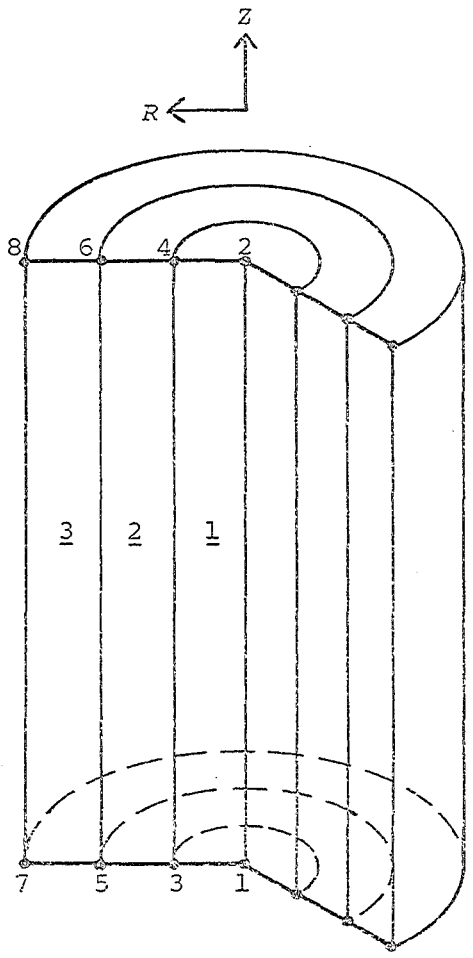

Fig. 3.5. Finite-element model with system nodal numbering

applied to the model as a whole. As discussed in Section 3.2.5 this leads to the following relationship:

$$F_i = \sum_{j=1}^{NEL} \int_{V_j} \frac{\partial \{E\}^T}{\partial U_i} . \{\sigma\} . dV_j \qquad . . . . . (3.24)$$

where NEL is the total number of elements in the model.

For most elements the first term under the integral sign in Equation (3.24) will be zero because the strains in those particular elements are not functions of U_i. For example, taking F_3, only the elements adjacent to system node 3, i.e., 1 and 2, will contribute to the right-hand side of Equation (3.24), and writing U_3 as $(u_2)_1$ and $(u_1)_2$ respectively, F_3 can be written as:

$$F_3 = \int_{V_1} \frac{\partial \{E\}^T}{\partial u_2} . \{\sigma\} . dV_1 + \int_{V_2} \frac{\partial \{E\}^T}{\partial u_1} . \{\sigma\} . dV_2$$

With the aid of Equation (3.14) the above equation becomes:

$$F_3 = (f_2)_1 + (f_1)_2 .$$

This result implies that the system nodal force acting on a system node i, F_i, is the sum of the element nodal forces of the element surrounding i, which act on the element nodes equivalent to i. The elements which do not surround i do not have an equivalent node to i and therefore they will not contribute to F_i.

Using Equation (3.22) the above equation can be expanded:

$$F_3 = (k_{21} . u_1 + k_{22} . u_2 + . . . k_{28} . u_8)_1 + (k_{11} . u_1 + k_{12} . u_2 + . . . k_{18} . u_8)_2 .$$

Switching to system nodal numbering for the nodal displacements and rearranging yields:

$$F_3 = U_1 . ((k_{21})_1) + U_2 . ((k_{24})_1) + U_3 . ((k_{22})_1 + (k_{11})_2) + U_6 . ((k_{13})_2) + U_{(NOD+1)} . ((k_{25})_1) + . . U_{(NOD+6)} . ((k_{17})_2) .$$

Finally this can be written using system stiffness terms:

$$F_3 = U_1 . K_1 + U_2 . K_2 + . . U_6 . K_6 + U_{NOD+1} . K_{NOD+1} + . . . + U_{NOD+6} . K_{NOD+6}$$

where $K_1 = (k_{21})_1$ $\qquad K_2 = (k_{24})_1$

$K_3 = (k_{22})_1 + (k_{11})_2$ etc.

Repeating this procedure for all system nodal forces yields the

system nodal force vector expressed in terms of the system nodal displacements:

$$\{F\} = [K].\{U\} \qquad \ldots\ldots\ldots\ldots (3.25)$$

where $[K]$ is the system stiffness matrix.

Because all the element stiffness matrix terms are independent of $\{U\}$, the system stiffness matrix will also be independent of $\{U\}$.

To keep the model in equilibrium the external loads, P, must be identical with the system nodal forces, F. The external loads are applied at the nodes and are contained in the nodal load vector, $\{P\}$. The equilibrium equations of the model are

$$\{P\} = \{F\} = [K].\{U\} \qquad \ldots\ldots\ldots\ldots (3.26)$$

The nodal displacements $\{U\}$ which cause stress fields which are in equilibrium with the load vector $\{P\}$ can be solved from Equation (3.26). Because $[K]$ is independent of $\{U\}$ Equation (3.26) is a set of linear equations in $\{U\}$ which can be readily solved by well-known techniques (59). When the desired displacement vector $\{U\}$ is found the stresses and strains for each element can be determined by substituting the appropriate terms of $\{U\}$ into Equations (3.16) and (3.19).

3.3 NON-LINEAR BEHAVIOUR

The problem discussed in the previous section led to a linear relationship between the unknown displacements and the loads acting on the object. This can only be the case when there are linear relationships between displacement and strain (Equation 3.16) and between strain and stress (Equation 3.17). However, many problems exist in which such linearity cannot be assumed without causing significant errors in the solution. These so-called non-linear problems are usually sub-divided into three categories reflecting the causes of non-linearity (49).

(a) Material non-linearity, which is caused by phenomena such as non-linear elasticity, plasticity, visco-elasticity, or other types of complex constitutive relationships.

(b) Geometric non-linearity, which is related to significant changes in the geometry of the object during the loading process.

(c) Combined material- and geometric non-linearity.

In all these cases the outcome is a non-linear relationship between the displacements and the loads.

$$\{P\} = \{F(\{U\})\} \qquad \ldots\ldots\ldots\ldots \quad (3.27)$$

where $\{F\}$ is a non-linear function of $\{U\}$.

Although the non-linearities in the equilibrium Equation (3.27) can have different causes the solution methods are basically the same for all cases, some examples being given in Section 3.3.5. The formulation of the equilibrium equations varies with the cause and degree of non-linearity. Relatively simple are problems with well-defined non-linear elastic materials and small displacements or problems with large displacements but small strains and linear elastic material. The setting up of the equilibrium equations in these cases is similar to the linear case. At the other end of the scale are problems which exhibit large strains and highly non-linear elasto-plastic material behaviour. The formulation here is often tedious and sometimes ambiguous, mostly because of the complexity of the non-linear continuum mechanics which must be used to describe the problem. Because of its relevance to the finite-element analysis of wool yarns a formulation with large strains and highly non-linear elastic material behaviour will be discussed.

3.3.1 Non-linear Continuum Mechanics

Large strains occurring during the deformation require the use of non-linear continuum mechanics to describe the problem. This can be done in two different ways (50):

the material or Lagrangian description, or
the spatial or Eulerian description.

In the Lagrangian description the problem is formulated in terms of the original configuration of the object before deformation in contrast to the Eulerian description where everything is referred to the deformed state. The latter is popular in fluid mechanics while in solid mechanics the Lagrangian formulation has been used extensively. In recent years a modified description has been used in some finite-element analyses where the solution was obtained by the incremental loading technique (Section 3.3.5). Essentially the Lagrangian formulation is used where the reference state is not the original state before any loading has occurred but the state calculated in the increment before. This method is usually called the updated Lagrangian description in contrast to the classical total Lagrangian description. Each method has its advantages and disadvantages, but whatever type of description is used extreme care must be taken to use parameters which refer to the appropriate configuration otherwise the governing equations will be invalid. All these formulations have been used for large-strain finite-element

analyses (51-55). Owing to the scarcity of literature providing an objective review of the advantages and disadvantages of the various formulations in relation to finite-element analyses, it is difficult to decide which method to use. In the author's opinion the total Lagrangian formulation is the clearest and the proven choice, hence it will be used here. Moore (56) has pointed out the limitations of the total Lagrangian formulation with respect to the transformation of rotational degrees of freedom for large displacements. However, the elements used here do not have these rotational degrees of freedom so this difficulty does not arise.

3.3.2 Governing Equation

As in the linear problem the principle of virtual work can be used as the governing equation (Equation 3.10). However, it must be put into a form suitable for non-linear continuum mechanics. The expression for the Lagrangian formulation (50) is:

$$\delta W_{ext} = \int_{V_0} \delta\{E\}^T . \{S\} . dV_0 \qquad . . . . . (3.28)$$

where δW_{ext} = work done by external loads due to $\delta\bar{u}$;

$\delta\{E\}^T$ = virtual increment in the non-linear Lagrangian strain due to $\delta\bar{u}$;

$\{S\}$ = Lagrangian stress; and

$\int_{V_0} dV_0$ = integration over the original configuration.

The assembly of the system nodal force vectors from the element nodal force vectors is the same as in the linear case but the formulation of the element nodal force vectors is different.

3.3.3 Strains and Stresses

The finite strain- and stress vectors in the Lagrangian formulation are known under a variety of names (Green-Lagrange strains, 2nd Piola-Kirchhoff stresses, etc.) but here they will be called Lagrangian strains and stresses.

The complete non-linear Lagrangian strain vector in the axisymmetric case is (57):

$$\begin{aligned} E_{RR} &= \bar{u}_{R,R} + 0{,}5(\bar{u}_{R,R}^{\,2} + \bar{u}_{Z,R}^{\,2}) \\ E_{\theta\theta} &= \bar{u}_R/R + 0{,}5(\bar{u}_R/R)^2 \\ E_{ZZ} &= \bar{u}_{Z,Z} + 0{,}5(\bar{u}_{R,Z}^{\,2} + \bar{u}_{Z,Z}^{\,2}) \end{aligned} \qquad . . . . . (3.29)$$

$$E_{ZR} = \bar{u}_{R,Z} + \bar{u}_{Z,R} + \bar{u}_{R,R}.\bar{u}_{R,Z} + \bar{u}_{Z,R}.\bar{u}_{Z,Z} \qquad \text{(continued}$$

$$E_{R\theta} = E_{\theta Z} = 0$$

The displacement field within an element is defined by Equation (3.8):

$$\bar{u} = \begin{Bmatrix} u_R \\ u_Z \end{Bmatrix} = \begin{bmatrix} <N><O> \\ <O><N> \end{bmatrix} \quad . . . . . (3.30)$$

In the Lagrangian formulation the shape functions, N_i contain the original co-ordinates of the nodes and of the arbitrary point of which the displacement is required. Differentiating Equations (3.30) with respect to the appropriate co-ordinates and substituting into Equations (3.29) yields the strains as functions of $\{u\}$:

$$\{E\} = \{E(\{u\})\} \quad . . . . . (3.31)$$

However, Equation (3.31) is a non-linear function of $\{u\}$ owing to the quadratic terms in Equations (3.29).

As with linear elastic material the stresses in certain non-linear elastic materials can be expressed as Equation (3.17):

$$\{S\} = [D(\{E\})].\{E\} \quad . . . . . (3.32)$$

However, in the non-linear case $[D]$ is a function of $\{E\}$ (or $\{S\}$) as indicated in the above equation. Also, with large strains the matrix $[D]$ must be defined so that it links the Lagrangian strain with the Lagrangian stress.

The Lagrangian stresses are not the actual measured stresses, which are the Eulerian or Cauchy stresses $\{T\}$, but pseudo-stresses related to $\{T\}$ by (57) (in tensor notation):

$$S_{ij} = J \frac{\partial X_i}{\partial X'_m} T_{mn} \frac{\partial X_j}{\partial X'_n} \quad . . . . . (3.33)$$

where $$J = e_{mnp} \frac{\partial X'_m}{X_1} \frac{\partial X'_n}{X_2} \frac{\partial X'_p}{X_3} = \frac{V}{V_0}$$

and $\dfrac{\partial X_i}{\partial X'_m}$ are the deformation gradients.

In some cases it can be difficult to write $\{S\}$ in the form of Equation (3.32) and it is more convenient to define $\{S\}$ as:

$$\{S\} = \{S(\{E\})\}$$

or $$\{S\} = \{S(\{u\})\} .$$

Sometimes it is only possible to define $\{S\}$ by:

$$\{\delta S\} = [D]_T . \{\delta E\}$$

where $[D]_T$ is the tangential elasticity matrix

$$D_{T_{ij}} = \partial S_i / \partial E_j \ .$$

It is mandatory to use an incremental loading technique in this case.

3.3.4 Stiffness Matrix

Substituting the expressions for $\{E\}$ and $\{S\}$ into Equation (3.14) yields the element nodal force vector $\{f\}$ as a non-linear function of $\{u\}$

$$\{f\} = \{ f (\{ u\}) \} \qquad . . . . . (3.34)$$

This can then be assembled into the system equilibrium equations:

$$\{P\} = \{F (\{u\}) \} \qquad . . . . . (3.35)$$

where $\{F\}$ is a non-linear function of $\{u\}$.

Where possible $\{f\}$ will be written as:

$$\{f\} = [k (\{u\})] . \{u\} \qquad . . . . . (3.36)$$

The stiffness matrix $[k]$ as shown above is the secant stiffness matrix $[k_S]$ in non-linear problems, in contrast to the tangent stiffness matrix $[k_T]$ which is defined by:

$$[k_T] = \partial \{f\} / \partial \{u\}^T \qquad . . . . . (3.37)$$

with $k_{T_{ij}} = \partial f_i / \partial u_j$.

Note that in the linear case $[k] = [k_S] = [k_T]$.

In many non-linear cases it is possible that the secant stiffness matrix is non-unique, though fortunately most of the popular solution methods (Section 3.3.5) do not require a secant stiffness but use the tangent stiffness instead and this can be defined uniquely.

3.3.5 Methods of Solution of Non-linear Equations

There are a large number of methods available (58) for solving the non-linear equilibrium Equations (3.27). To illustrate some of these methods a one degree of freedom structure will be used for which the equilibrium equation is:

$$F(U) - P = 0$$

where $F(U)$ is a non-linear function of U.

In Figure 3.6 the function is given in graph form where P is the load for which a solution U is desired.

In all the methods discussed below the solution of a non-linear equation involves the solution of a series of linear equations in U which, in the case of a single unknown, are solved by inversion:

$$A.U = B \quad \Rightarrow \quad U = B.A^{-1} \ .$$

In some methods the parameter A is held constant for a number of cycles and only B changes. This has the advantage that A only has to be inverted once while it is kept constant.

In the case of more than one unknown, where the inner equations to be solved are written in matrix form, $[A].\{U\} = \{B\}$, solution techniques such as Gauss elimination or Crout (Choleski) reduction (59) are preferred above inversion because of greater computational efficiency. Here also the same advantage holds when $[A]$ is kept constant for a number of cycles because the reduction of $[A]$, which is the most laborious part of the solution, only needs to be performed once for that particular number of cycles.

The simplest group of methods is that of the iterative methods which use the secant stiffness K_S:

$$F(U) = K_S\ (U).U \ .$$

Two of these methods are the functional iteration and the chord method which are shown in Figures 3.6a and 3.6b respectively. Functional iteration is of the form:

$$U^{\ell} = (K_S\ (U^{\ell-1}))^{-1}.P \qquad \ldots\ldots\ldots\ldots\ldots\ldots \quad (3.38)$$

where U^{ℓ} is the value of U calculated in the ℓ-th iteration. The main advantage of this method is its simplicity but it converges slowly (first order) if it converges at all. Also K_S needs to be recalculated and inverted (or reduced) at each iteration. The chord method does not have this disadvantage:

$$U^{\ell} = R^{\ell-1}.(K_S\ (U^0))^{-1} \qquad \ldots\ldots\ldots\ldots\ldots\ldots \quad (3.39)$$

where $\quad R^{\ell} = P - F(U^{\ell}) + R^{\ell-1} \ .$

R^{ℓ} is an 'out of balance' term which is added to the structure. The disadvantages are an even slower convergence and in some cases the recalculation of $F(U^{\ell})$ can be almost as tedious as inverting K_S. These two methods can be combined by updating K_S only when the convergence has slowed down significantly.

Newton-Raphson iteration methods which use the tangent stiffness K_T are also very popular: $\quad K_T = F'(U) \ .$

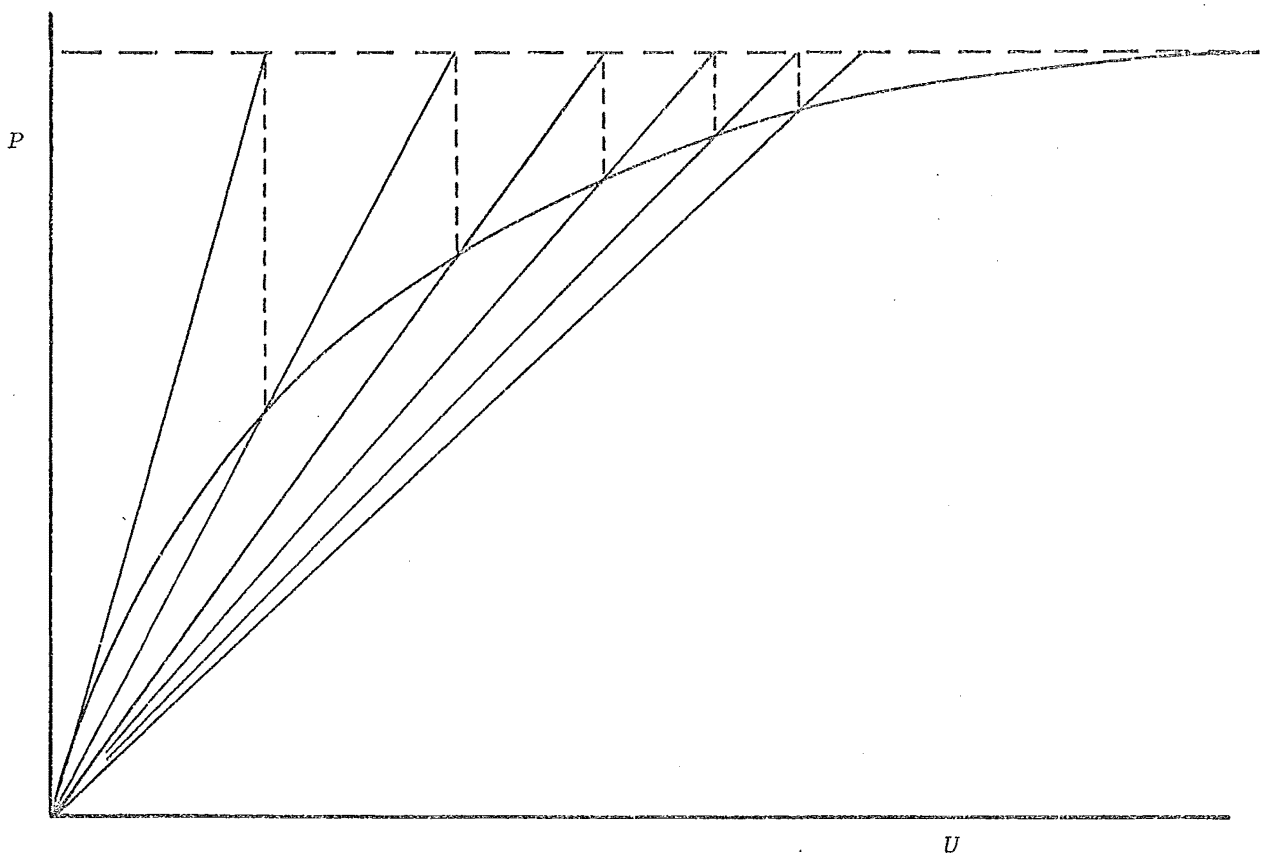

Fig. 3.6a. Functional iteration

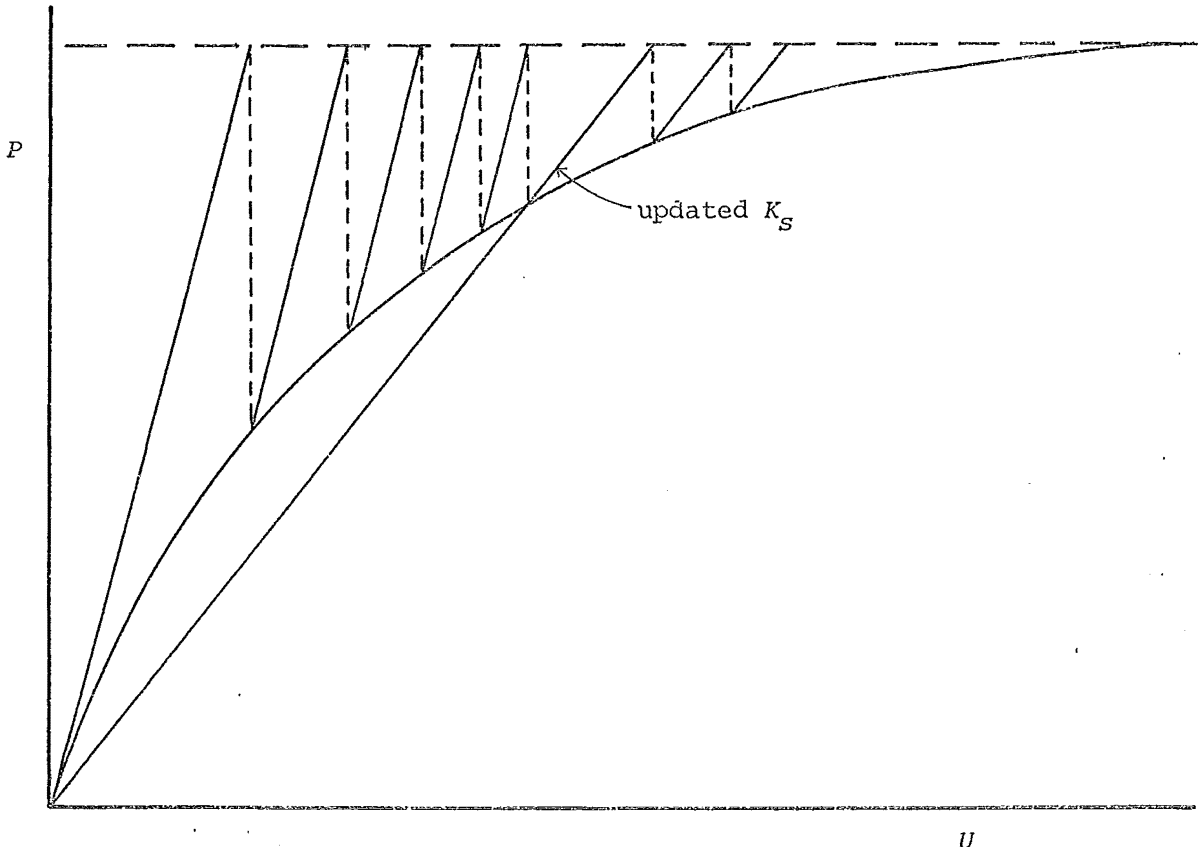

Fig. 3.6b. Chord method

Fig. 3.6. Solution methods for non-linear equations

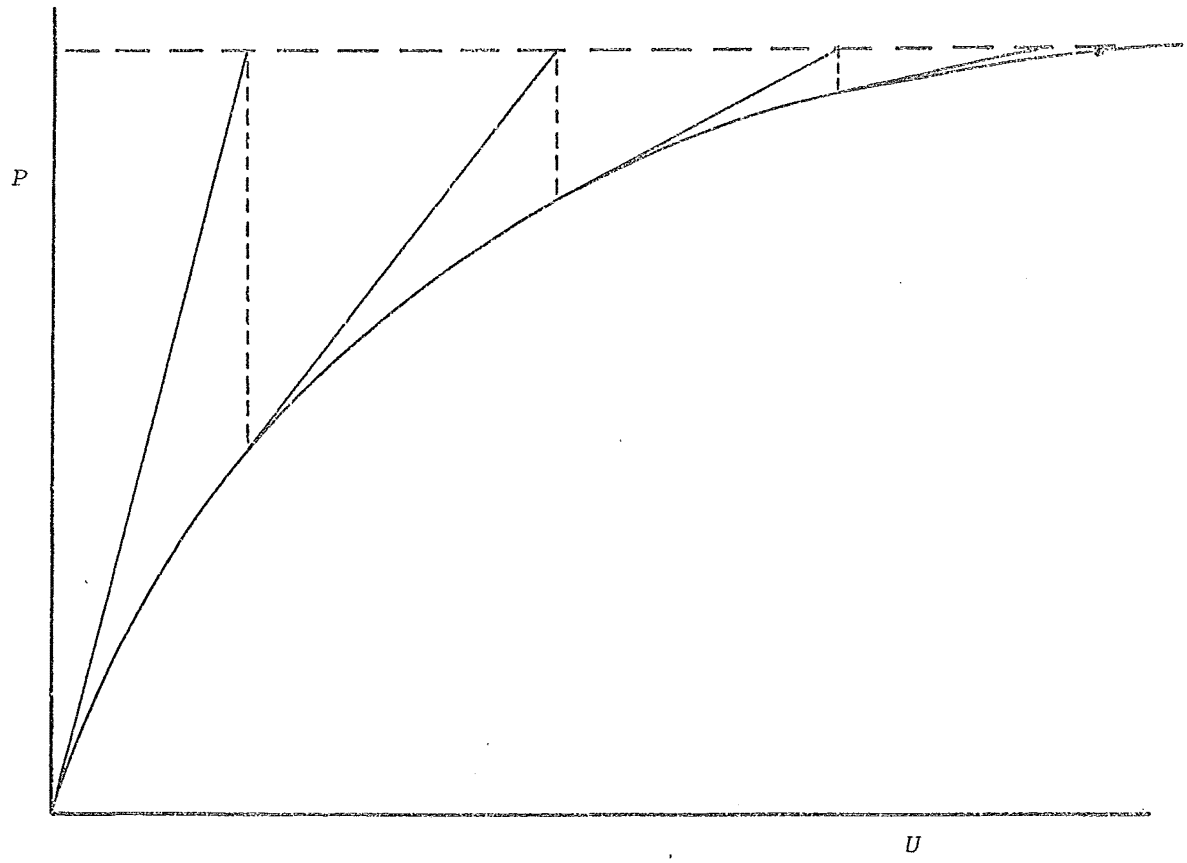

Fig. 3.6c. Newton-Raphson iteration

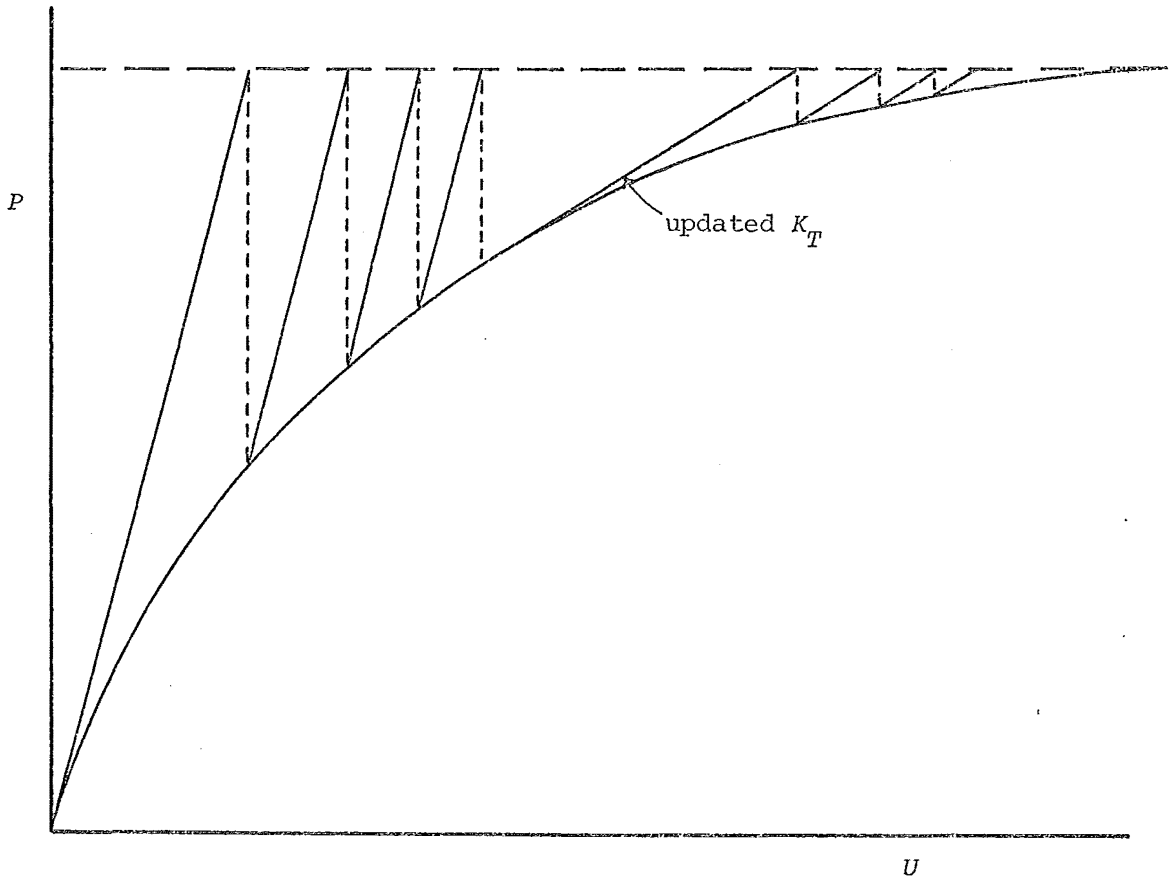

Fig. 3.6d. Modified Newton-Raphson iteration

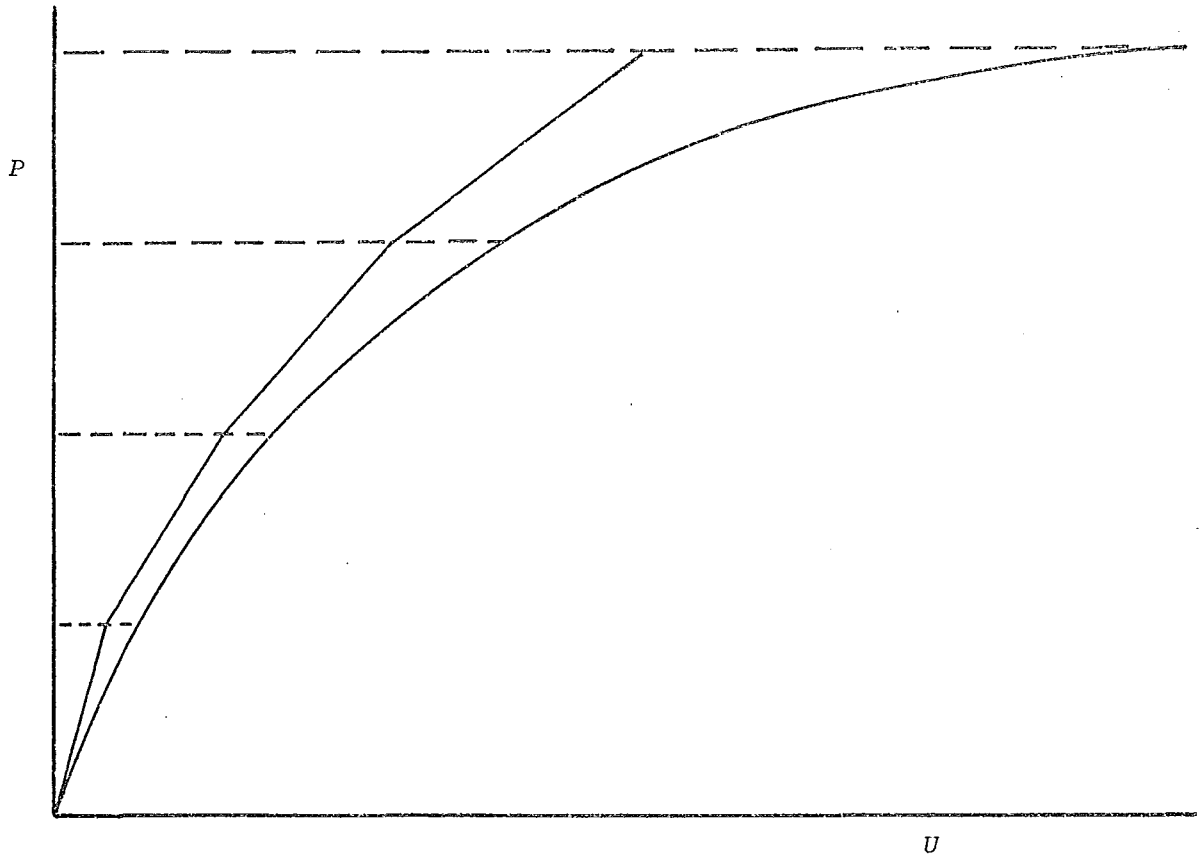

Fig. 3.6e. Incremental method

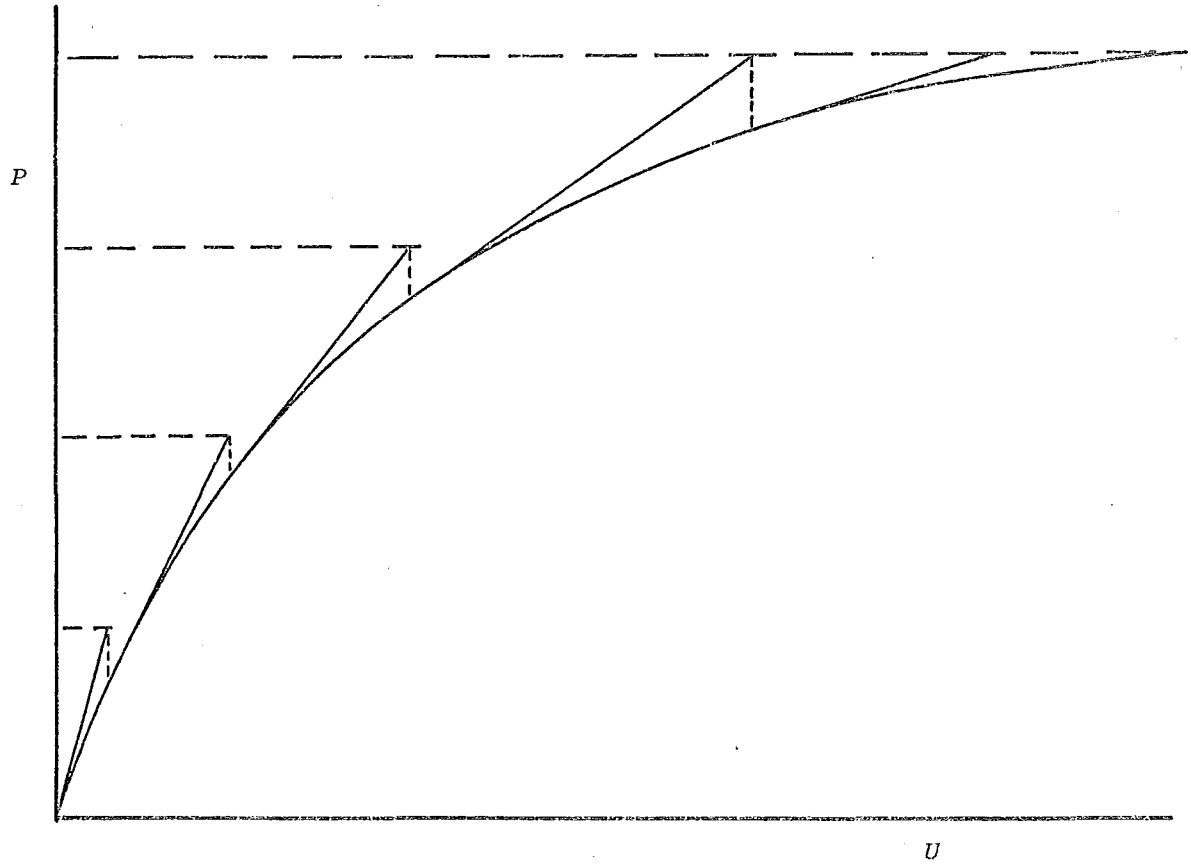

Fig. 3.6f. Self-correcting incremental method

The pure Newton-Raphson method (see Fig. 3.6c) is defined by:

$$\Delta U^{\ell} = (P - F(U^{\ell-1})).(K_T(U^{\ell-1}))^{-1} \quad \ldots\ldots (3.40)$$

where $U^{\ell} = U^{\ell-1} + \Delta U^{\ell}$.

The convergence is faster (second order) than the simple iteration methods but K_T must be recalculated and inverted at each iteration. This disadvantage can be limited by only updating K_T when the convergence rate drops below a predetermined level:

$$\Delta U^{\ell} = (P - F(U^{\ell-1})).(K_T(U^{0}))^{-1} \quad \ldots\ldots (3.41)$$

This is the modified Newton-Raphson method (see Fig. 3.6d) which, however, converges more slowly than the original method and is more difficult to programme.

The above-mentioned methods all attempt to solve the problem in one load step which can be impossible in certain cases, such as path-dependent problems, or undesirable when intermediate solutions are required. The methods which solve the problem for a sequence of load steps are called incremental methods. The formulation of these methods can be found by using a Taylor series expansion.

It is assumed that a solution U^{k-1} is known for load P^{k-1} and that a solution $U^{k} = (U^{k} + \Delta U^{k})$ is desired at load $P^{k} = (P^{k-1} + \Delta P^{k})$.

$$F(U^{k-1}) = P^{k-1} \quad \ldots\ldots (3.42)$$

$$F(U^{k-1} + \Delta U^{k}) = P^{k-1} + \Delta P^{k} \quad \ldots\ldots (3.43)$$

Using the first-order Taylor series expansion on the left-hand side of Equation (3.42) yields:

$$F(U^{k-1}) + F'(U^{k-1}).\Delta U^{k} = \Delta P^{k} + P^{k-1} .$$

Rearranging, and using Equations (3.42) and 3.43):

$$K^{T}(U^{k-1}).\Delta U^{k} = \Delta P^{k} \quad \ldots\ldots (3.44)$$

This is the formulation for the ordinary incremental method which is illustrated in Figure 3.6e. It can be seen that there is a tendency to accumulate errors as it goes through the increments. This is because total equilibrium (Equation 3.42) is not satisfied exactly, which can only be the case for a linear $F(u)$. To correct the deviations of Equation (3.44), the out-of-balance force, $P^{k-1} - F(U^{k-1})$, is added to the incremental load vector, ΔP^{k}:

$$K^{T}(U^{k-1}).\Delta U^{k} = \Delta P^{k} + P^{k-1} - F(U^{k-1}) \quad \ldots\ldots (3.45)$$

This is the so-called self-correcting incremental method (see Fig.

3.6f) which gives much better results.

To find a more accurate solution at each increment, iteration can be applied to Equation (3.45), with or without updating the tangent stiffness, K_T:

$$K_T\,(U^{k,0}).\Delta U^{k,\ell} = \Delta P^k + P^{k-1} - F(U^{k,\ell-1}) \quad . \quad . \quad . \quad . \quad . \quad . \quad (3.46)$$

$$K_T\,(U^{k,\ell-1}).\Delta U^{k,\ell} = \Delta P^k + P^{k-1} - F(U^{k,\ell-1}) \quad . \quad . \quad . \quad . \quad . \quad (3.47)$$

where k = increment number;

ℓ = iteration number; and

$U^{k,\ell} = U^{k,\ell-1} + \Delta U^{k,\ell}$.

These methods are called incremental methods with (modified) Newton-Raphson iteration.

There are many other methods described in the literature (58), most of them being variations of the basic techniques discussed here.

Because of the specific demands of each problem regarding convergence, stability, computational efficiency, etc., a general approach suitable for all classes of problems cannot be prescribed.

CHAPTER 4

CONTINUOUS-FILAMENT YARN ANALYSIS

4.1 INTRODUCTION

As discussed earlier the analysis developed by Carnaby (3, 4) was superior to previous attempts with respect to the results obtained for staple-fibre yarns, especially when tested at short gauge lengths. However, a major drawback of the analysis is the excessive computational effort required to obtain results of sufficient detail and accuracy. This is not as much caused by the model as by the formulation of the governing equation, the principle of minimum potential energy.

In Carnaby's analysis the total potential energy is expressed in terms of a set of generalised displacement parameters, γ_i. The expression obtained is then minimised directly for γ_i. An alternative approach, which will be used in the analysis described here, is to rewrite the governing equation with the aid of variational techniques so that the unknown parameters, γ_i, can be directly solved from a set of simultaneous equations. This method is the well-known principle of virtual work which can be written as:

$$\delta U(\gamma_i) = 0 \quad ,$$

where δU is the variation of the energy, U, due to the virtual displacements, $\delta\gamma_i$.

The two methods give the same answers but in general the latter method is more efficient with respect to computational effort. In the second part of this chapter a significantly modified version of Carnaby's analysis, utilising the principle of virtual work, is presented. A considerable saving in computational effort is achieved which encourages further use of the model. Also the *ad hoc* discretisation technique used by Carnaby is modified to comply as much as possible with the rigorous requirements of the extensively developed finite-element method. The implementation of these rules ensures a correct solution to the problem within the limitations of the modelling assumptions.

In the third part of the chapter an alternative finite-element approach is presented, also based on Carnaby's yarn model. This approach utilises classical stress analysis to define the equilibrium equations of the model and has some affinity with the earlier yarn analyses by Hearle (23, 24). To distinguish between the two approaches they will be named energy analysis and stress analysis respectively (60).

The stress analysis is developed because it is more convenient to use in the migration model, presented in the next chapter, which incorporates friction and slippage. However, it is in effect an *ad hoc* method and does not comply completely with the rigorous rules of the finite-element theory as set for the energy-analysis approach. This is apparent in the difficulty of defining appropriate equilibrium equations of which a number of possible forms are investigated. Here the value of the energy analysis can be appreciated because it can be used as a yardstick in the evaluation of the various alternative forms of the stress-analysis approach.

Because the yarn model developed by Carnaby is used as a basis for both the finite-element analyses a detailed discussion of its appropriate aspects will be presented first.

4.2 CARNABY'S MODEL AND ANALYSIS

4.2.1 Model

Carnaby's ideal helical yarn model is best described in a cylindrical co-ordinate system, R, θ, Z, and it is illustrated in Figure 4.1. The Z-axis coincides with the axis of the yarn model, the fixed end (bottom) being at $Z = 0$ and the other end (top) at $Z = L$. All the fibres are assumed to be identical, all being continuous and uniform along their lengths. The following assumptions are used for the geometry of the undeformed yarn:

(a) each fibre follows a path described by

R = constant;

$\theta = \theta_0 + Z.2\pi.TT^{-1}$; and (TT is defined on page 6)

$\theta = \theta_0$ at $Z = 0$.

R and θ_0 differ from fibre to fibre.

(b) TT is equal for all fibres.

(c) the values for θ_0 are such that the distribution of the fibres over the cross-section of the yarn model (Z = constant) is axisymmetric.

(d) the distances of the fibres from the yarn axis are such that a given yarn cross-section density is satisfied.

When the model is subjected to an axisymmetrical load, P, in the Z-direction, which ensures an even elongation over the cross-section, L becomes L' and the deformed configuration is described by:

(e) $TT' = TT.L'.L^{-1}$.

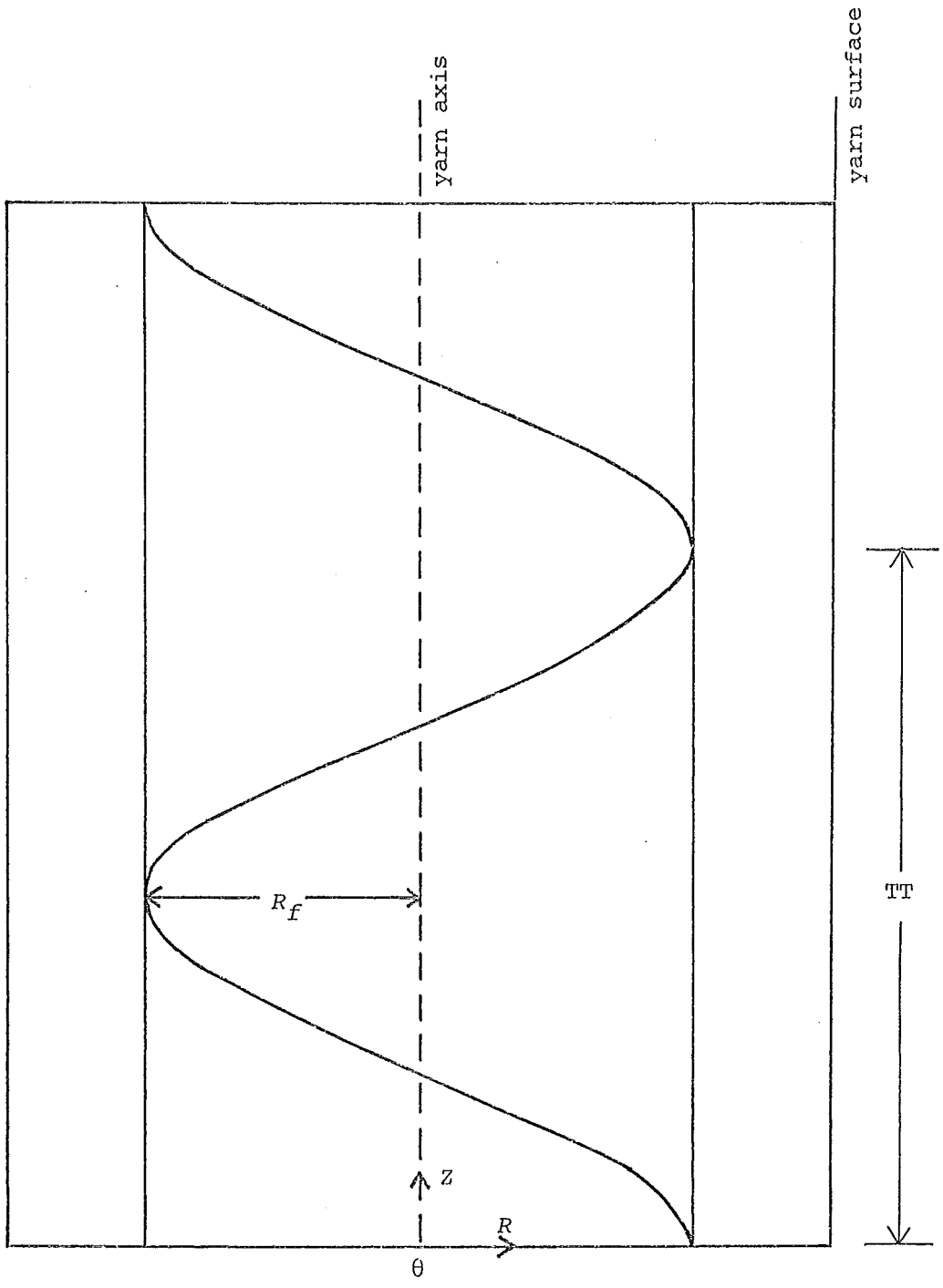

Fig. 4.1. Ideal helical yarn model

(f) the ends of the model are fixed in the θ-direction so that $\theta'_0 = \theta_0$.

(g) the deformed path of a fibre originally described by

$$R = \text{constant}; \quad \theta = \theta_0 + 2\pi.TT^{-1}.Z$$

becomes

$$R' = \text{constant}; \quad \theta' = \theta'_0 + 2\pi.TT^{-1}.Z' \ ,$$

where $Z' = Z.L'.L^{-1}$

$$\theta' = \theta_0 + 2\pi.TT^{-1}.Z \ .$$

From this it follows that $\theta' = \theta$.

(h) the radii of the helical paths of the fibres change so that

if $R_A > R_B$ then $R'_A > R'_B$

if $R_A = R_B$ then $R'_A = R'_B$.

From this it follows that if N is the number of fibres traversing a cross-section between R_A and R_B then the number of fibres between R'_A and R'_B is also N.

If the deformed length of the yarn, L', is given there is only one independent variable left to describe the geometry of the deformed fibre — this is the continuous function:

$$R' = R'(R, L, L') \ .$$

4.2.2 Radial Contraction of Yarn

In the previous yarn analyses the radial contraction of the yarn was directly linked to the yarn elongation. The link was a yarn Poisson's ratio which was taken as being independent of both the yarn elongation and the radial position within the yarn. As has been discussed earlier on page 16, this is an unrealistic assumption for a wool yarn and will lead to erroneous results.

In Carnaby's yarn analysis the relationship between the radial movement of the fibres and the yarn elongation is established via the resistance of the fibres in the yarn to close packing. In the ideal helical yarn model where the fibres are all perfectly aligned there is only resistance to close packing when the yarn has contracted so much that the fibres are jammed against one another. The compressive behaviour of the ideal helical yarn model is therefore only governed by the compressibility of the fibre material. However, in a real yarn the fibres are only roughly aligned and this will cause considerable resistance to yarn contraction long before the fibres are completely jammed against one another. The resistance is mainly due to the energy necessary to bend the fibres into configurations such that they can accommodate the paths of neigh-

bouring fibres.

In Figure 4.2 the difference in compressive behaviour between perfectly aligned and roughly aligned fibre assemblies is shown. The two parameters which are related in the graphs are p, the pressure exerted lateral to the fibres, and the inverse of V_{sp}, which is the specific volume of the fibre assembly defined by:

$$V_{sp} = V/M_f$$

where V = total volume of the assembly, and

M_f = fibre mass in the assembly.

Eventually under very high lateral pressures the compressive behaviour of the roughly aligned assembly will also be governed by the compressibility of the fibre material and there will be no significant difference between the configurations of the two assemblies. However, in the analysis of the yarn model this extreme situation is never reached and it is a reasonable assumption that the resistance of the fibres in a yarn to close packing is solely due to fibre bending.

In the case where fibre bending governs the compressive behaviour of the yarn the relationship between p and V_{sp} can be expressed by a van Wyk-type equation (Section 2.4.1):

$$p = K(V_{sp}^{-3} - V_{sp_0}^{-3}) \qquad \ldots\ldots\ldots\ldots \quad (4.1)$$

where V_{sp_0} is the specific volume when the external pressure is zero.

The lateral pressure, p, is assumed as in previous analyses to be equal in all directions normal to the fibre axis.

The simultaneous use of Equation (4.1) and the ideal helical yarn model is contradictory as perfectly aligned fibres do not possess compressive properties which can be described by a van Wyk-type relationship. However, if the fibres in the ideal helical yarn model were allowed to deviate a very small amount from their ideal paths the number of inter-fibre contacts would increase enormously and because the deviations would be very small the idealised geometry could still be used in the analysis.

To illustrate this a simple example is described. In Figure 4.3 a fibre is shown (by a full line) as it will occur in the idealised geometry (for convenience it is drawn 'straightened out'). Superimposed on the ideal line are cyclic deviations with an amplitude, A, equal to five fibre diameters and the length of one complete wave, L_w, is 10 mm. If the fibre diameter is taken as 0,035 mm (e.g., Romney wool) the length of the fibre path with the deviations is only 0,06% greater than the ideal

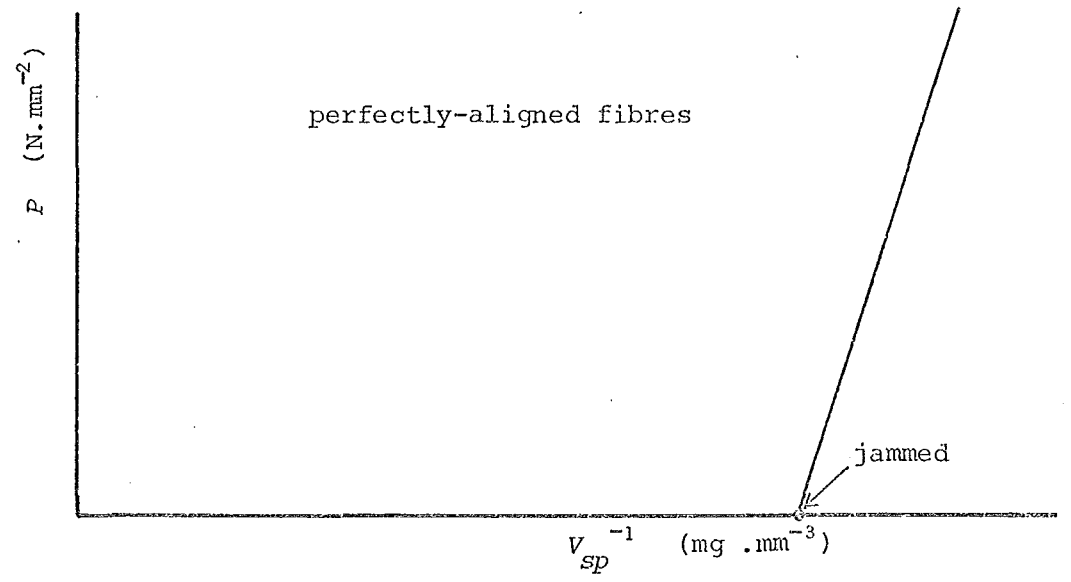

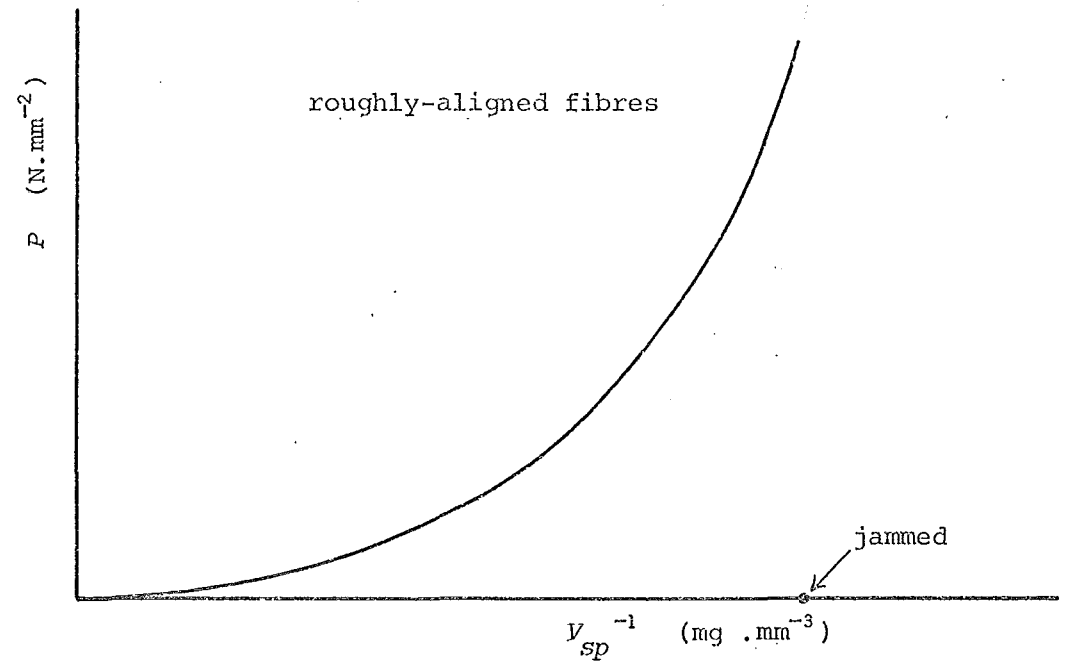

Fig. 4.2 Lateral compressibility of a fibre assembly

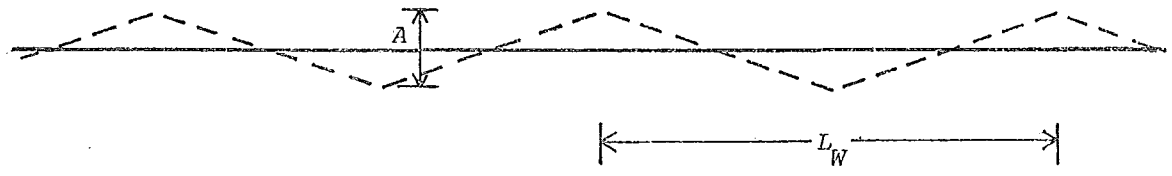

Fig. 4.3 Deviations of fibre from ideal path

path, which is of course negligible, and the angle of the deviations with respect to the ideal line is 2^{o}. If all the fibres in the idealised helical yarn model deviate in the same manner it is clear that there will be a large number of inter-fibre contacts. For these deviations to be maintained after extension of the yarn it is necessary that the fibres be entangled otherwise the deviations would be immediately straightened out if the fibre became tensioned. In the case of entanglement the deviations would have to be in different planes but this does not affect the extra length involved. The situation in a real yarn is of course much more complex but the above example does indicate that the ideal helical yarn model can still be used.

4.2.3 Strain Energy

To determine the unknown function, R', the strain energy content of the model is expressed as a function of R':

$$U = U(R, L, R', L') \quad .$$

According to the principle of minimum potential energy the function, R', which gives the minimum value for U is the correct radial configuration for the equilibrium state of the deformed yarn model with length L'.

To minimise the potential energy, U, with respect to $R'(R, L, L')$ it is necessary to describe R' in terms of a finite number of parameters. The values of γ_i ($\gamma_i = R'_i . R_i^{-1}$) at n points, R_i, are chosen as the unknown parameters with respect to which U must be minimised. An important requirement is that the parameters, γ_i, are chosen so that they are kinematically indeterminate. The points, R_i, which may be selected arbitrarily, are chosen to be evenly spaced with $R_1 = 0$ and $R_n = R_{\text{yarn surface}}$. The regions in the model between the cylindrical surfaces with radii, R_i and R_{i+1} are called zones. Each zone contains a certain number of fibres to simulate the actual distribution throughout a real yarn. The strain energy of the whole model is simply the sum of the energies in each zone.

In the energy calculations the following types of fibre deformation are taken into account:

(a) axial elongation due to elongation of the fibre path;

(b) torsion due to changes in the helical curvature of the fibre path;

(c) bending due to changes in the helical curvature of the fibre path;

(d) bending due to close packing.

It is assumed that the first three types of deformation can be determined from the configuration of an ideal helical fibre path, neglect-

ing the influence of the unknown local deviations. The fourth term is, however, solely dependent on the local deviations and can therefore not be directly quantified.

The tensile energy, U_T, which is due to the axial elongation of the fibres, can be found with the aid of an experimentally determined fibre stress-strain curve. To simplify the calculations a piecewise linear approximation is used. The fibre elongation is assumed to be constant throughout a zone and is taken as the average of the elongations of two hypothetical fibres, one on the inner periphery and one on the outer periphery of a zone.

The determination of the shear energy, U_S, due to the torsion of the fibres, is simple and straightforward and the zonal contributions are calculated in the same fashion as for the tensile energy.

The determination of the bending energy, U_B, is quite complicated as the contributions due to the two separate bending terms cannot be added linearly. This is caused by the presence in the bending-energy equation of a term in which the total change in curvature is squared. The change of curvature due to the close packing effects is not known explicitly. However, the energy spent on close packing of fibres can be determined with the aid of the van Wyk equation (Equation 4.1) and by working backwards an average change in curvature due to close packing can be calculated. This is added vectorially to the helical change in curvature and the subsequent calculation of U_B is straightforward.

4.2.4 Energy Minimisation and Solution

All the energy contributions are determined as functions of γ_i and the total energy of the yarn is found by adding the zonal contributions together:

$$U = U(\gamma_i, R, L, L') \quad .$$

U is minimised with respect to γ_i with the aid of numerical minimisation techniques (61). Because of the non-linear form of the energy terms the validity of a solution obtained must be checked by solving from alternative starting points to avoid local minima. The configuration and internal stresses at a given value of L' can now be easily obtained by back-substituting γ_i in the appropriate equations. The load, P, necessary to sustain the configuration obtained is found with the aid of the principle of virtual work as described by Treloar and Riding (2).

It must be noted that in subsequent analyses using the above theory it was found that the contributions due to fibre torsion and

fibre bending caused by the change in helical curvature are negligible. In the following analysis developed by the author advantage is taken of these findings by neglecting the above terms.

4.3 FINITE-ELEMENT ENERGY ANALYSIS

4.3.1 Continuum approximation

In the finite-element analysis presented here the yarn is assumed to consist of an equivalent continuous material. The stresses within this material form a continuous stress-field as opposed to the discontinuous stress-fields present in a real yarn. Of the two important stresses in Carnaby's model the lateral pressure can be directly adopted in these analyses because it is defined by the van Wyk equation as a continuous stress. But the axial stresses in the fibres are of a discontinuous nature because they only exist in the fibres and not in the voids between them. To obtain a continuous stress-field the fibre stresses are averaged over the area around the fibre. The stress, T_A, acting in the direction of the fibre axis at a certain point is defined by:

$$T_A = \Sigma F_A . dA^{-1} \qquad \ldots\ldots\ldots\ldots \quad (4.2)$$

where dA = infinitesimal cross-section around the point, normal to the fibre axis, and

ΣF_A = sum of the axial forces in the fibres passing through dA.

4.3.2 Finite-element Model

In the finite-element yarn model concentric cylindrical elements are used which are much the same as the zones used by Carnaby. The longitudinal cross-section of these elements is rectangular as can be seen in Figure 4.4. It is not necessary to employ more than one layer of elements in the Z-direction as the model may be regarded as uniform in this direction. In Section 3.2 the same type of element is discussed with four ring-shaped nodes at the corners (see Fig. 3.3), each node having two degrees of freedom. When the deformation pattern of the model is considered it will be clear that the radial displacements of the nodes 1 and 4 are identical and this also applies to nodes 2 and 3. The same is true of the axial displacements of the nodes 3 and 4 and the nodes 1 and 2. This is usually dealt with by 'slaving' these degrees of freedom. A simpler alternative is to use an element in which the axial displacements of the top and bottom annular surfaces and the radial displacements of the inner and outer cylindrical surfaces are the degrees of freedom of the element. In effect these surfaces are the nodes which are numbered as shown in Figure 4.5.

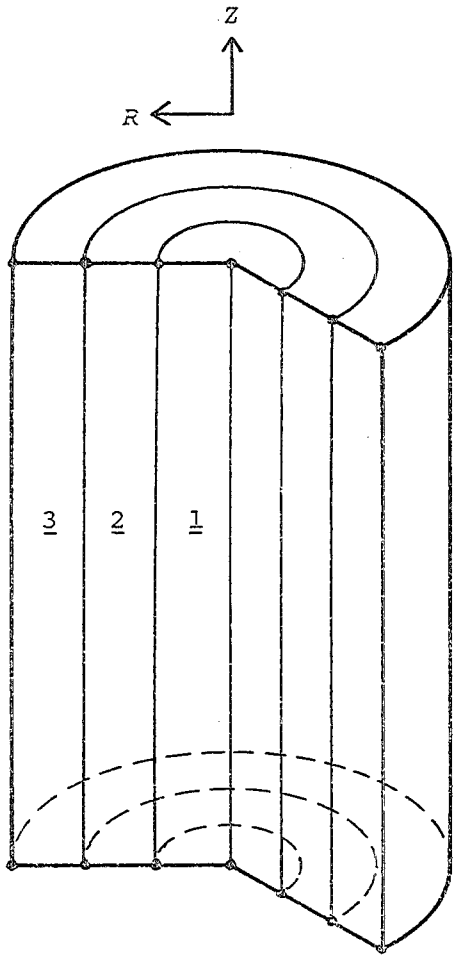

Fig. 4.4. Finite-element sub-division of yarn model

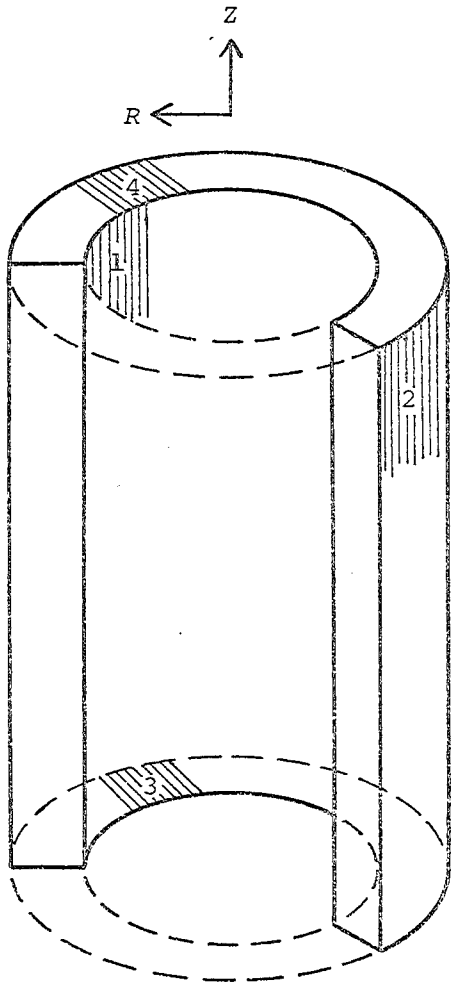

Fig. 4.5. Element, with element-nodal numbering

As node 1 of a certain element must be identical to node 2 of the inner-lying element the axial displacements of the nodes 3 and 4 of both elements must also be identical. Extending this to all elements it follows that the axial displacements of nodes 3 and 4 of all elements must be identical. This is compatible with the deformation of the model but these degrees of freedom must be slaved together as will be discussed later.

The element nodal displacement vector, $\{u\}$, is defined as:

$$\{u\}^T = \langle u_{1R} \quad u_{2R} \quad u_{3Z} \quad u_{4Z} \rangle \qquad (4.3)$$

As each node has only one displacement component the R and Z indices can conveniently be omitted. The co-ordinates of the nodes are designated by R_1, R_2, Z_3 and Z_4 in the undeformed configuration and R_1', R_2', Z_3' Z_4' in the deformed configuration, where

$$R_1' = R_1 + u_1$$
$$Z_3' = Z_3 + u_3 \quad \text{etc.}$$

Within each element the displacements are defined by a linear displacement field, $\{\bar{u}\}$:

$$\{\bar{u}\} = \begin{Bmatrix} \bar{u}_R \\ \bar{u}_Z \end{Bmatrix} = \begin{bmatrix} N_1 & N_2 & O & O \\ O & O & N_3 & N_4 \end{bmatrix} . \{u\} \qquad (4.4)$$

where
$$N_1 = (-R + R_2).dR^{-1}$$
$$N_2 = (R - R_1).dR^{-1}$$
$$N_3 = (-Z + Z_4).dZ^{-1}$$
$$N_4 = (Z - Z_3).dZ^{-1}$$

the shape functions

$$dR = R_2 - R_1$$

the 'width' of the element

$$dZ = Z_4 - Z_3$$

the 'height' of the element.

The co-ordinates in the deformed configuration of an arbitrary point, R, Z, can now be written as:

$$R' = R + \bar{u}_R = R + ((R - R_1).u_2 - (R - R_2).u_1).dR^{-1}$$
$$Z' = Z + \bar{u}_Z = Z + ((Z - Z_3).u_4 - (Z - Z_4).u_3).dZ^{-1} \qquad (4.5)$$

Each element contains a certain number of fibres, N_f, to simulate the actual distribution throughout a real yarn. This distribution is found by using the cross-sectional method (Appendix A). The fibres are assumed to maintain their relative positions within each element throughout the deformation process. For convenience the fibres are also assumed to be evenly distributed over the element cross-section in any configuration. These two assumptions are contradictory to one another but the difference in packing density due to the element deformation is so small

that it can be neglected.

With the aid of Figure 4.6 some element parameters can be defined which will be needed further on in the analysis:

$$dR' = R_2' - R_1' \quad \ldots\ldots\ldots\ldots \quad (4.6a)$$

width of deformed element

$$dZ' = Z_4' - Z_3' \quad \ldots\ldots\ldots\ldots \quad (4.6b)$$

height of deformed element

$$A' = \pi.((R_2')^2 - (R_1')^2) \quad \ldots\ldots\ldots\ldots \quad (4.6c)$$

area of element cross-section

$$\alpha' = \arctan(2\pi R'.dZ.(dZ'.TT)^{-1}) \quad \ldots\ldots\ldots\ldots \quad (4.6d)$$

helix angle

$$FL' = ((2\pi R'.dZ.TT^{-1})^2 + (dZ')^2)^{0,5} \quad \ldots\ldots\ldots\ldots \quad (4.6e)$$

length of fibre in element

$$V_{sp}' = dZ'.A'.(N_f.FL.r_f^2.\pi.\rho_f)^{-1} \quad \ldots\ldots\ldots\ldots \quad (4.6f)$$

specific volume

where N_f = number of fibres in element;
r_f = fibre radius; and
ρ_f = specific weight of fibre.

These are the definitions of the parameters in the deformed configuration; their values in the undeformed state are found by simply deleting the dashes. The first three parameters are overall element parameters which are independent of position within an element. The last three parameters are dependent on the radial position, R', in the deformed configuration. Using Equation (4.5) they can be expressed as functions of radial position in the undeformed configuration, R, which is important in the Lagrangian formulation of non-linear continuum mechanics.

4.3.3 Virtual Work

To establish the element nodal force vectors, $\{f\}$, the principle of virtual work (50) is used, from which the following relationship is obtained (Equations 3.14 and 3.28):

$$\{f\} = \int_{V_0} \frac{\partial\{E\}^T}{\partial\{u\}}.\{S\}.dV_0 \quad \ldots\ldots\ldots\ldots \quad (4.7)$$

where $\{E\}$ = Lagrangian strain vector;
$\{S\}$ = Lagrangian stress vector; and
$\int_{V_0}$ = integration over the original configuration.

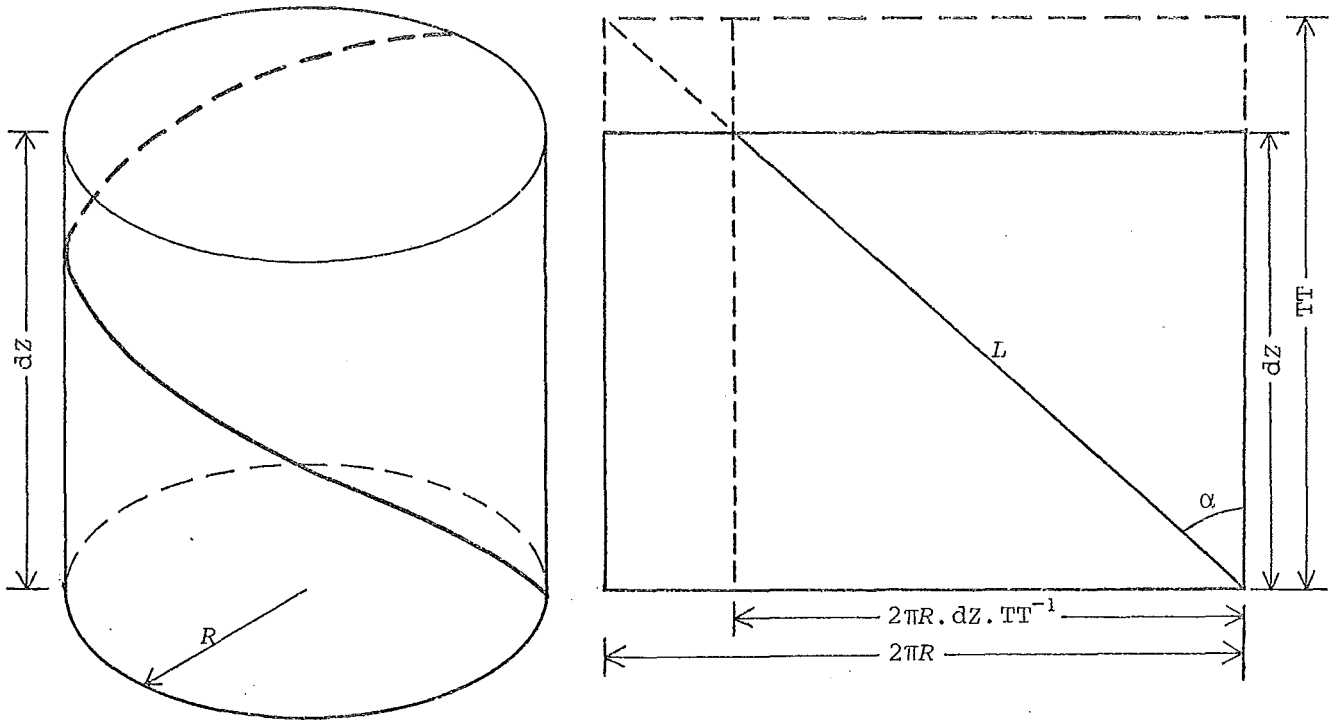

undeformed

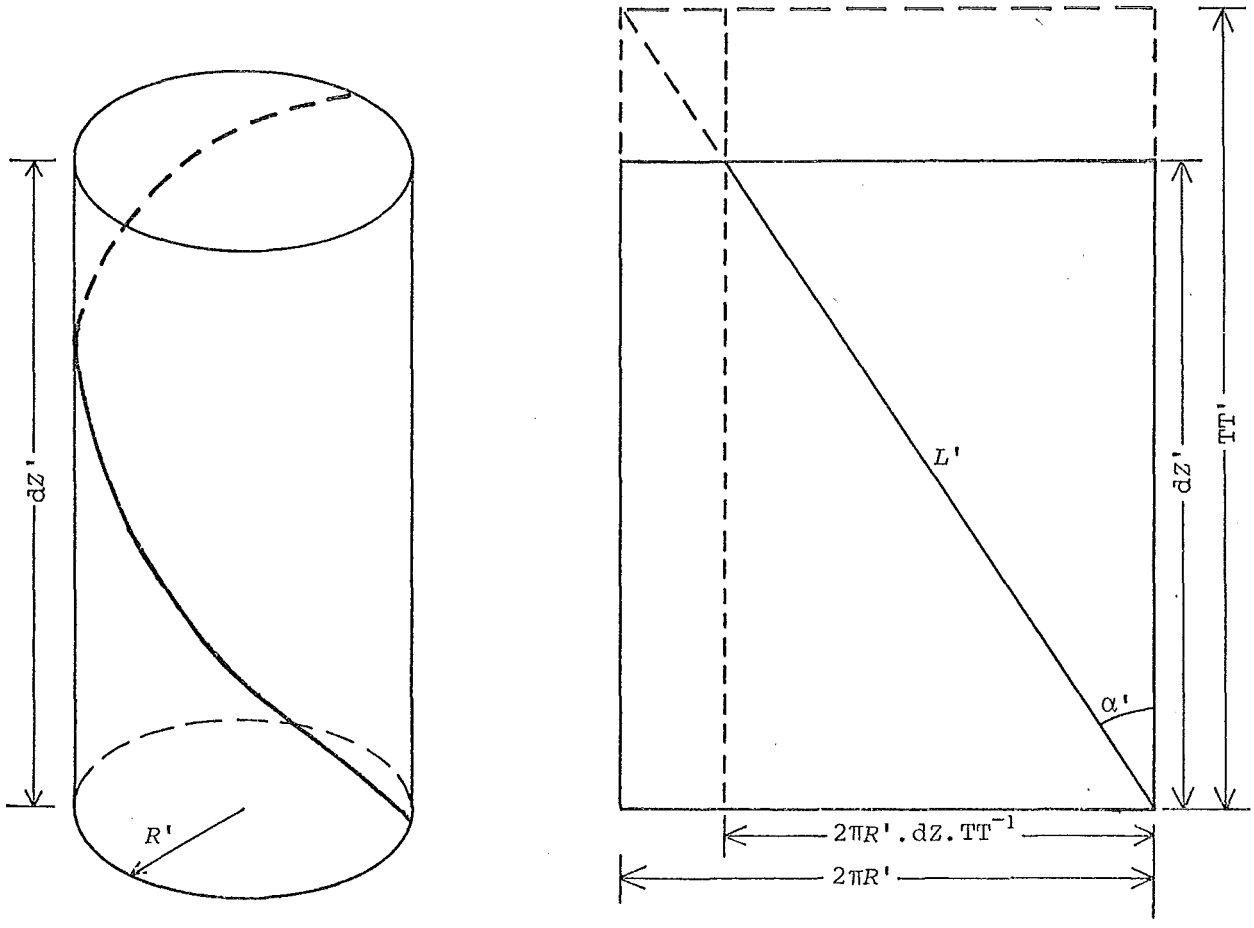

deformed

Fig. 4.6. Yarn and fibre configuration before and after deformation

The element nodal force vectors are then assembled into the system nodal force vector, $\{F\}$, which is used in the system equilibrium equations:

$$\{P\} = \{F\}$$

where $\{P\}$ = system nodal load vector.

To solve the equilibrium equations for the nodal displacements the right-hand side of the above equation must first be expressed as a function of the nodal displacements.

4.3.4 Strain-displacement Relationship

The complete non-linear Lagrangian strain vector, $\{E\}$, for the axisymmetric case is given in Equation (3.29):

$$\begin{aligned}
E_{RR} &= \bar{u}_{R,R} + 0{,}5.(\bar{u}_{R,R}^{\,2} + \bar{u}_{Z,R}^{\,2}) \\
E_{\theta\theta} &= \bar{u}_{R}.R^{-1} + 0{,}5.(\bar{u}_{R}.R^{-1})^2 \\
E_{ZZ} &= \bar{u}_{Z,Z} + 0{,}5.(\bar{u}_{R,Z}^{\,2} + \bar{u}_{Z,Z}^{\,2}) \qquad \ldots\ldots\ldots \quad (4.8) \\
E_{ZR} &= \bar{u}_{R,Z} + \bar{u}_{Z,R} + \bar{u}_{R,R}.\bar{u}_{R,Z} + \bar{u}_{Z,R}.\bar{u}_{Z,Z} \\
E_{R\theta} &= E_{\theta Z} = 0
\end{aligned}$$

Owing to the simple deformation, $u_{R,Z}$ and $u_{Z,R}$ are zero. This simplifies $\{E\}$ to:

$$\begin{aligned}
E_1 &= \bar{u}_{R,R} + 0{,}5.(\bar{u}_{R,R}^{\,2}) \\
E_2 &= \bar{u}_{R}.R^{-1} + 0{,}5.(\bar{u}_{R}.R^{-1})^2 \qquad \ldots\ldots\ldots \quad (4.9) \\
E_3 &= \bar{u}_{Z,Z} + 0{,}5.(\bar{u}_{Z,Z})^2 \\
E_4 &= E_5 = E_6 = 0 \ .
\end{aligned}$$

From the Equations (4.4) the individual terms in Equation (4.9) can be derived:

$$\begin{aligned}
\bar{u}_{R,R} &= (u_2 - u_1).dR^{-1} \\
\bar{u}_{Z,Z} &= (u_4 - u_3).dZ^{-1} \qquad \ldots\ldots \quad (4.10) \\
\bar{u}_{R}.R^{-1} &= ((R - R_1).u_2 - (R - R_2).u_1).(R.dR)^{-1}
\end{aligned}$$

The term $\partial\{E\}^T/\partial\{u\}$ in the element nodal force vector is a matrix of the form:

$$\partial\{E\}^T/\partial\{u\} = \begin{bmatrix} \partial E_1/\partial u_1 & \partial E_2/\partial u_1 \ldots & \partial E_6/\partial u_1 \\ \partial E_1/\partial u_2 & \ldots\ldots\ldots & \partial E_6/\partial u_2 \\ \partial E_1/\partial u_3 & \ldots\ldots\ldots & \partial E_6/\partial u_3 \\ \partial E_1/\partial u_4 & \ldots\ldots\ldots & \partial E_6/\partial u_4 \end{bmatrix} \qquad \ldots\ldots \quad (4.11)$$

The terms of this matrix can be found by substituting Equations (4.10) into Equations (4.9) and differentiating with respect to the terms of $\{u\}$.

4.3.5 Stress-displacement Relationship

In expressing the stresses as functions of the nodal displacements it is usual to do this indirectly by writing the stresses as functions of the element strains:

$$\{S\} = [D].\{E\} = [D].[B].\{u\}$$

This is only done because it is usually more convenient than writing the stresses directly in terms of the displacements. In this particular case, however, it is relatively easy to express the stresses directly.

As pointed out before, there are only two types of stresses present in this model; stresses acting in the direction of the fibres and stresses normal to the fibres. These stresses can be derived from relationships involving the element geometry.

The stress acting in the direction of the fibre axis (T_A) at a certain point is defined by (Equation 4.2):

$$T_A = \Sigma F_A . dA_\alpha^{-1} \quad \ldots\ldots\ldots\ldots (4.12)$$

where dA_α = an infinitesimal area around the point normal to the fibre axis, and

ΣF_A = sum of the axial forces in the fibres passing through dA.

The axial force in a fibre with centre at R is derived from the fibre elongation at that radius, $E_f(R)$, which is given by (see Fig. 4.6):

$$E_f(R) = (FL'(R') - FL_1(R)).(FL(R))^{-1} \quad \ldots\ldots (4.13)$$

Using a piece-wise linear approximation to the non-linear force-elongation curve (see Appendix C) the axial fibre force is:

$$F_A = a.E_f + b \quad \ldots\ldots\ldots\ldots (4.14)$$

With the assumption that the fibres are always evenly distributed over the cross-section, T_A can be expresed as:

$$T_A = (a.E_f + b).N_f.(A'.\cos\alpha')^{-1} \quad \ldots\ldots (4.15)$$

From Equations (4.13), (4.6), and (4.15) T_A can be completely expanded in terms of the nodal displacements.

The lateral stresses, T_L, are determined with the aid of a van Wyk relationship (*cf.* Equation 4.1):

$$T_L = K.((V_{sp}')^{-3} - (V_{sp})^{-3}) \quad \ldots\ldots (4.16)$$

Using Equations (4.6) T_L can also be completely expanded in terms of the nodal displacements.

To accommodate T_A and T_L conveniently a fibre co-ordinate system is used, namely R_α, θ_α, Z_α. The subscript, α, is used because rotating the yarn co-ordinate system by an amount α, or α' in the deformed configuration, around the R-axis will yield the fibre co-ordinate system. The Z_α-axis will coincide with the fibre axis, the R_α-axis will coincide with the yarn R-axis, and the θ-axis will be normal to the fibre axis and tangential to the cylinder on which the fibre lies. The stresses, $T_{RR\alpha}$, $T_{\theta\theta\alpha}$ and $T_{ZZ\alpha}$, will be equal to T_L, T_L and T_A respectively. All other stresses in the fibre co-ordinate system will be zero.

The stresses, $\{T\}_\alpha$, are in fact Eulerian stresses because they are the actual stresses measured in, and with respect to, the deformed configuration. For the virtual-work equation (Equation 4.7) the Lagrangian stress in the yarn-co-ordinate system, $\{S\}$, is required. To convert $\{T\}_\alpha$ into $\{S\}$ two transformations are necessary. The first one is to transform $\{T\}_\alpha$ into $\{T\}$, which is the Eulerian stress in the yarn co-ordinate system. This is done with the aid of a transformation matrix, $[TM]_\sigma$, (44), which in this case is defined as:

$$[TM]_\sigma = \begin{bmatrix} 1 & 0 & 0 & 0 & 0 & 0 \\ 0 & c^2 & s^2 & 0 & -2cs & 0 \\ 0 & s^2 & c^2 & 0 & 2cs & 0 \\ 0 & 0 & 0 & 0 & 0 & -s \\ 0 & cs & -cs & 0 & c^2-s^2 & 0 \\ 0 & 0 & 0 & s & 0 & c \end{bmatrix} \qquad \text{where} \quad \begin{aligned} c &= \cos\alpha \\ s &= \sin\alpha \end{aligned}$$

The Eulerian stress, $\{T\}$, is now found by:

$$\{T\} = [TM\ (\alpha)]_\sigma . \{T\}_\alpha \ .$$

This yields:

$$\begin{aligned} T_{RR} &= T_1 = T_{RR\alpha} \\ T_{\theta\theta} &= T_2 = T_{\theta\theta\alpha}.\cos^2\alpha' + T_{ZZ\alpha}.\sin^2\alpha' \\ T_{ZZ} &= T_3 = T_{\theta\theta\alpha}.\sin^2\alpha' + T_{ZZ\alpha}.\cos^2\alpha' \\ T_{\theta Z} &= T_5 = (T_{\theta\theta\alpha} - T_{ZZ\alpha}).\cos\alpha'.\sin\alpha' \\ T_{R\theta} &= T_4 = 0 \text{ and } T_{ZR} = T_6 = 0. \end{aligned} \qquad \ldots\ldots (4.17)$$

The Eulerian stresses, $\{T\}$, are then transformed into the Lagrangian stresses, $\{S\}$. Using tensor notation the transformation is as follows (Equation 3.33):

$$S_{ij} = J.\frac{\partial X_i}{\partial X'_m}.T_{mn}.\frac{\partial X_j}{\partial X'_n} \qquad \ldots\ldots\ldots\ldots\ldots\ldots \quad (4.18)$$

(summation convention)

where $X_1 = R \quad X_2 = \theta \quad X_3 = Z$

$X_1' = R' \quad X_2' = \theta' \quad X_3' = Z'$

$\partial X'_i/\partial X_j$ and $\partial X_i/\partial X'_j$ are the deformation gradients

J is the jacobian of the deformation gradients:

$$J = \left[\frac{\partial X'_i}{\partial X_j}\right] = \frac{V}{V_0} \quad .$$

In the simple deformation in this analysis there are only three non-zero deformation gradients of the type, $\partial X_i/\partial X'_j$, which are:

$$\frac{\partial X_1}{\partial X_1'} = \frac{\partial R}{\partial R'} = \frac{R_2 - R_1}{R_2' - R_1'} = \frac{dR}{dR'}$$

$$\frac{\partial X_2}{\partial X_2'} = \frac{\partial \theta}{\partial \theta'} = \frac{R}{R'}$$

$$\frac{\partial X_3}{\partial X_3'} = \frac{\partial Z}{\partial Z'} = \frac{Z_4 - Z_3}{Z_4' - Z_3'} = \frac{dZ}{dZ'} \quad .$$

Using the relationship (62):

$$\frac{\partial X'_i}{\partial X_j}.\frac{\partial X_j}{\partial X'_k} = \delta_{ik}$$

the deformation gradients of the type $\partial X'_i/\partial X_j$ can be derived and J can now be written as:

$$J = (dR'.R'.dZ').(dR.R.dZ)^{-1} \quad .$$

Changing from tensor notation to vector notation the end result is:

$$\begin{aligned} S_{RR} &= S_1 = T_1.J.dR^2.(dR')^{-2} \\ S_{\theta\theta} &= S_2 = T_2.J.R^2.(R')^{-2} \\ S_{ZZ} &= S_3 = T_3.J.dZ^2.(dZ')^{-2} \\ S_{\theta Z} &= S_5 = T_5.J.R.dZ.(R'.dZ')^{-1} \\ S_{R\theta} &= S_{ZR} = 0. \end{aligned} \qquad \ldots\ldots\ldots \quad (4.19)$$

The Lagrangian stress in the yarn co-ordinate system, $\{S\}$, is a function of the Eulerian stress, $\{T\}_\alpha$, in the fibre co-ordinate system, the helix angle, and the deformation gradients. As all of these can be expressed as functions of $\{u\}$, $\{S\}$ can also be expressed as a function of the nodal displacements: $\{S\} = \{S(\{u\})\}$.

Owing to the various complicated functions of $\{u\}$ which are

implied in $\{S\}$, it will also be a complicated non-linear function of $\{u\}$.

4.3.6 Evaluation of Nodal Forces

Substituting the expressions found for $\partial\{E\}^T/\partial\{u\}$ and $\{S\}$ as functions of $\{u\}$ in Equation (4.7), the element nodal force vectors are derived. These are then assembled into the global nodal force vector, $\{F\}$, which is used in the global equilibrium equation:

$$\{P\} = \{F(\{U\})\} \qquad \ldots\ldots\ldots\ldots \quad (4.20)$$

which will also be a non-linear function of the nodal displacements. As yet the deformation process is not path-dependent but the whole load-displacement curve (or at least points at frequent intervals) of the yarn is required so an incremental method with iteration will be used to solve the equilibrium equations.

In Section 3.3.5 two incremental methods with iteration are discussed, of which the one with Newton-Raphson iteration is chosen (Equation 3.47) because it is more accurate and easier to programme.

$$[K_T(\{U\}^{k,\ell-1})].\{\Delta u\}^{k,\ell} = \{P\}^k - \{F(\{U\}^{k,\ell-1})\} \qquad \ldots\ldots \quad (4.21)$$

The alternative method with modified Newton-Raphson iteration is computationally more efficient but owing to the small scale of the present analysis this is of minor importance.

The individual components of the global tangent stiffness matrix, $[K_T]$, are defined by:

$$K_{T_{ij}} = \frac{\partial F_i(\{U\})}{\partial U_j} = F_{i,j} \qquad \ldots\ldots\ldots\ldots \quad (4.22)$$

When $\{F(\{U\})\}$ is a non-linear function of $\{U\}$ then $[K_T]$ will be at least a linear function of $\{U\}$. The terms $F_{i,j}$ are assembled from the appropriate element contributions $f_{i,j}$. The i-th term in an element nodal face vector is defined by Equation (4.7):

$$f_i = \int_{V_0} \frac{\partial\{E\}^T}{\partial u_i} \cdot \{S\} \cdot dV_0 \qquad \ldots\ldots\ldots\ldots \quad (4.23)$$

Differentiating this with respect to u_j yields:

$$f_{i,j} = \int_{V_0} \left(\frac{\partial\{E\}^T}{\partial u_i . \partial u_j} . \{S\} + \frac{\partial\{E\}^T}{\partial u_i} . \frac{\partial\{S\}}{\partial u_j} \right) . dV_0 \qquad \ldots\ldots \quad (4.24)$$

The individual terms are found by differentiating the expressions for $\{E\}$ and $\{S\}$ with respect to the appropriate nodal displacements. The

integrations over the volume of each element necessary to obtain f_i and $f_{i,j}$ are carried out numerically using a Legendre-Gauss quadrature (59).

4.3.7 Assembly and Solution

A system nodal numbering must be introduced for the assembly of the elements. As the displacements of the top and bottom nodes of each element are identical they are slaved together which implies that they are regarded as a single node in the system. The system nodal numbering and the element numbering are shown in Figure 4.7. The cylindrical nodes are numbered 1→NOD and the top and bottom nodes are designated by T and B respectively. The underlined numbers are the element numbers. The relationship between the element numbers and the system nodal numbers is in this case simple, the inner and outer nodes of element $\underline{i}$ are the nodes i and $i+1$ respectively, while the node i is adjoined by element $\underline{i-1}$ on the inside and element $\underline{i}$ on the outside. This implies that node 2 of element $\underline{i-1}$ and node 1 of element $\underline{i}$ are identical to node i.

The system nodal displacement vector, $\{U\}$, is defined by:

$$\{U\}^T = \langle U_1, U_2, \ldots U_{NOD}, U_B, U_T \rangle$$

The relationship between the system nodal displacements and the element nodal displacements is also simple and is defined by:

$$\begin{aligned} U_i &= (u_2)_{\underline{i-1}} = (u_1)_{\underline{i}} \\ U_B &= (u_3)_{\underline{1}} = (u_3)_{\underline{2}} = \ldots (u_3)_{NEL} \\ U_T &= (u_4)_{\underline{1}} = (u_4)_{\underline{2}} = \ldots (u_4)_{NEL} \end{aligned} \qquad \ldots\ldots (4.25)$$

The system nodal force vector, $\{F\}$, which is defined by:

$$\{F\}^T = \langle F_1, F_2, \ldots F_{NOD}, F_B, F_T \rangle$$

is found by the element nodal forces acting on node 2 of $\underline{i-1}$ and on node 1 of i (see Section 3.2.6):

$$F_i = (f_2)_{\underline{i-1}} + (f_1)_{\underline{i}} \qquad \ldots\ldots\ldots (4.26)$$

The system nodal forces acting on the bottom and top nodes are found by adding the element nodal forces acting on the element nodes 3 and 4, respectively:

$$F_B = \sum_{k=1}^{NEL} (f_3)_k \qquad \ldots\ldots\ldots (4.27a)$$

$$F_T = \sum_{k=1}^{NEL} (f_4)_k \qquad \ldots\ldots\ldots (4.27b)$$

Each of the terms of an element nodal force vector, $\{f\}_{\underline{i}}$ is solely dependent on the element nodal displacements of that particular element:

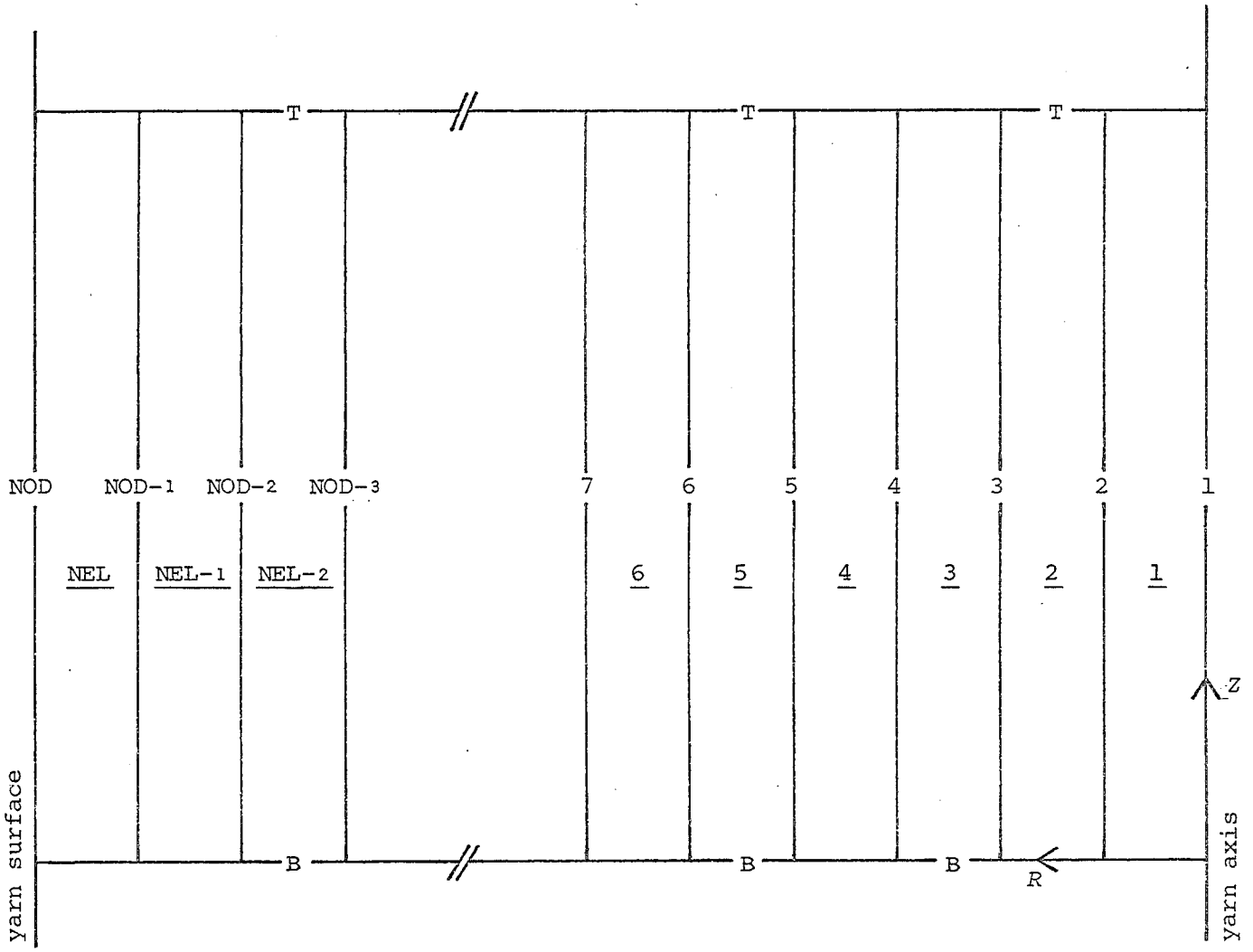

Fig. 4.7. Finite element model with element and system nodal numbering

$$\{f\}_{\underline{i}} = \left\{f(\{u\}_{\underline{i}})\right\}_{\underline{i}} = \left\{f(<u_1, u_2, u_3, u_4>_{\underline{i}})\right\}_{\underline{i}}$$

Using the relationships in Equation (4.25) the above expression can be written as:

$$\{f\}_{\underline{i}} = \left\{f\,(U_i, U_{i+1}, U_B, U_T)\right\}_{\underline{i}} .$$

Substituting the above expression into Equations (4.26) and (4.27) yields:

$$\begin{aligned} F_i &= F_i\,(U_{i-1}, U_i, U_{i+1}, U_B, U_T) \\ F_B &= F_B\,(\{U\}) \\ F_T &= F_T\,(\{U\}) . \end{aligned}$$

Because of this result the tangent stiffness matrix, $[K_T]$, the individual terms of which are defined by (Equation 4.22):

$$K_{T_{ij}} = \partial F_i / \partial U_j = F_{i,j} ,$$

will be a tridiagonal matrix with two extra rows at the bottom and two extra columns on the right-hand side:

$$[K_T] = \begin{bmatrix} F_{1,1} & F_{1,2} & 0 & 0 & \cdot & \cdot & 0 & F_{1,B} & F_{1,T} \\ F_{2,1} & F_{2,2} & F_{2,3} & 0 & \cdot & \cdot & 0 & F_{2,B} & F_{2,T} \\ 0 & F_{3,2} & F_{3,3} & F_{3,4} & \cdot & \cdot & 0 & F_{3,B} & F_{3,T} \\ \cdot & \cdot & \cdot & \cdot & \cdot & \cdot & \cdot & \cdot & \cdot \\ \cdot & \cdot & \cdot & \cdot & \cdot & \cdot & \cdot & \cdot & \cdot \\ 0 & 0 & 0 & 0 & \cdot & F_{NOD,NOD} & F_{NOD,B} & F_{NOD,T} & \\ F_{B,1} & F_{B,2} & F_{B,3} & F_{B,4} & \cdot & \cdot & F_{B,NOD} & F_{B,B} & F_{B,T} \\ F_{T,1} & F_{T,2} & F_{T,3} & F_{T,4} & \cdot & \cdot & F_{T,NOD} & F_{T,B} & F_{T,T} \end{bmatrix} .$$

Substituting this result into the basic Newton-Raphson equation (Equation 4.21) yields:

$$\left[\begin{array}{cccc|cc} F_{1,1} & F_{1,2} & \cdot & F_{1,NOD} & F_{1,B} & F_{1,T} \\ F_{2,1} & F_{2,2} & \cdot & F_{2,NOD} & F_{2,B} & F_{2,T} \\ \cdot & \cdot & \cdot & \cdot & \cdot & \cdot \\ \cdot & \cdot & \cdot & \cdot & \cdot & \cdot \\ 0 & 0 & \cdot & F_{NOD,NOD} & F_{NOD,B} & F_{NOD,T} \\ \hline F_{B,1} & F_{B,2} & \cdot & F_{B,NOD} & F_{B,B} & F_{B,T} \\ F_{T,2} & F_{T,2} & \cdot & F_{T,NOD} & F_{T,B} & F_{T,T} \end{array}\right] \left\{\begin{array}{c} \Delta U_1 \\ \Delta U_2 \\ \cdot \\ \cdot \\ \Delta U_{NOD} \\ \hline \Delta U_B \\ \Delta U_T \end{array}\right\} = \left\{\begin{array}{c} P_1 \\ P_2 \\ \cdot \\ \cdot \\ P_{NOD} \\ \hline P_B \\ P_T \end{array}\right\} - \left\{\begin{array}{c} F_1 \\ F_2 \\ \cdot \\ \cdot \\ F_{NOD} \\ \hline F_B \\ F_T \end{array}\right\}$$

. . . . . (4.28)

where $\{\Delta U\}$ is the incremental displacement vector and $\{P\}$ is the accumulated incremental load vector, both arranged in the same fashion as $\{U\}$ and $\{F\}$.

By partitioning Equation (4.28) along the broken lines shown it can be written as:

$$[K_T]^C.\{\Delta U\}^C = \{P\}^C - \{F\}^C - \{R\}^C \quad . \quad . \quad . \quad . \quad . \quad (4.29a)$$

$$\sum_{i=1}^{NOD} F_{B,i}.\Delta U_i = P_B - F_B - R_B \quad . \quad . \quad . \quad . \quad . \quad (4.29b)$$

$$\sum_{i=1}^{NOD} F_{T,i}.\Delta U_i = P_T - F_T - R_T \quad . \quad . \quad . \quad . \quad . \quad (4.29c)$$

where $R_i = F_{i,B}.\Delta U_B + F_{i,T}.\Delta U_T$

and $\{R\}^{C^T} = < R_1, R_2, \ldots . R_{NOD} >$.

The contracted matrix, $[K_T]^C$, is the upper left-hand part of $[K_T]$ as shown in Equation (4.28) and the contracted vectors, $\{\Delta U\}^C$, $\{P\}^C$ and $\{F\}^C$, are the upper parts of the appropriate vectors in the same equation.

As the bottom of the yarn model is fixed in the axial direction ΔU_B will always be zero. In this analysis ΔU_T will be given as the increment in the yarn model elongation and the yarn model axial load which is equivalent to P_T is an unknown. Because of this the set of Equations (4.29a) can be solved independently for U_{1-NOD} and P_T can be evaluated with the aid of Equation (4.29c).

4.3.8 Evaluation of the Analysis

Data on a real yarn, taken from Carnaby (4), were used to evaluate the analysis presented here. This was a semi-worsted carpet yarn spun from a blend of New Zealand Romney wools. Because the model and the associated data used here are the same as those used by Carnaby it is possible to compare the results of both analyses, which is important as there is no other way of checking this analysis.

The data are as follows:

fibre radius	r_f	$18{,}5 \times 10^{-3}$	mm
specific weight of fibre material	ρ_f	1,31	$mg.mm^{-3}$
fibre axial modulus		see Figure 4.8	
one turn of twist (length)	TT	5,42	mm
van Wyk's constant	K	3,44	$mm^7.N.mg^{-3}$
width of element (zone)	dR	$83{,}3 \times 10^{-3}$	mm
number of elements		25	
number of fibres per element starting with element no. 1	N_f	5, 15, 27, 39, 42, 40, 26, 9, 5, 3, 2, 2, 2, 1, 1, 1, 1, 1, 1, 1, 1, 1, 1, 1	

height of element	dZ	25,4	mm
specific volume of yarn	V_{sp_0}	see below	
increment of elongation	$\Delta u_T/dZ$	1	%.

One difference between the two analyses is that Carnaby used a constant (determined experimentally) value for V_{sp_0} throughout the yarn. This implies that if the actual specific volume, V_{sp}, in the undeformed yarn is smaller than V_{sp_0} there will be a lateral pressure present in the original configuration. Because this disturbs the state of equilibrium (the fibre axial forces are assumed to be zero) the model is first 'relaxed'. which leads to axial compression of the fibres in the inner elements and elongation in the outer elements. Also the yarn will shorten by a small amount.

In the present analysis V_{sp_0} is set to the actual value of V_{sp}, which can be calculated from the dimensions of the original configuration. The values of V_{sp_0} obtained by this method vary from element to element and are of course different from the experimentally determined value. However, V_{sp_0} only plays a significant role in the van Wyk equation at very low levels of lateral compression so the differences should be very small for most of the yarn stress-strain curve.

This is confirmed by comparing the results of both analyses; even at low levels of yarn-model strain the differences are insignificant. The results are shown in Figure 4.8. A major advantage of the finite-element analysis is the minimal amount of computational effort required in comparison with Carnaby's analysis, a conservative estimate being of the order of 20 to 1. It is therefore now possible to study the influence of certain parameters on the behaviour of the model without the severe computational penalties associated with Carnaby's energy-minimisation analysis.

4.3.9 Convergence and Accuracy

Two important aspects of the accuracy of a finite-element analysis are the number of integration points (if numerical integration is used) and the refinement of the element mesh.

The programme was run with a varying number of integration points per element to find the optimum. It was found that for this particular purpose the use of two integration points in the R-direction is sufficiently accurate, the difference between the results for two and five points being less than 0,2 %. The errors in using a single integration point are up to 5 % in the lower elongation range, the difference dimin-

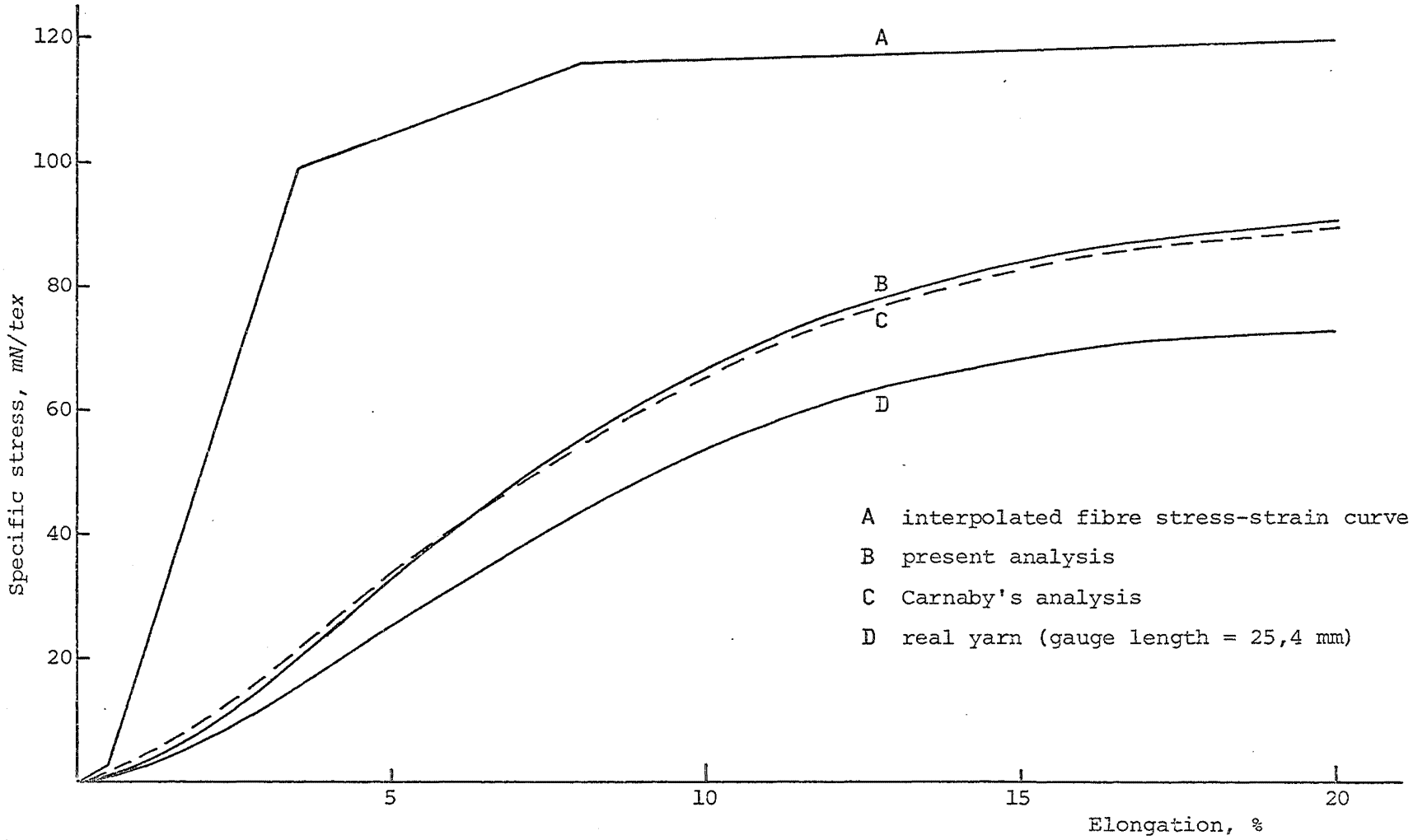

Fig. 4.8. Comparison of the present yarn analysis with Carnaby's analysis (3)

ishing with increasing elongation. As the computing costs are effectively proportional to the number of integration points the use of a single point could be tolerated in some cases.

The size of the original mesh was dictated by the fibre density function as found experimentally by Carnaby. When a finer or coarser mesh is used the number of fibres per element must be adapted to the new size of the elements. The easiest way to refine the mesh is to halve the element width and to redistribute the fibres of the original element over the two new elements which fit into its place, according to cross-sectional area. The difference in results is minimal, being less than 0,3 % at the most, and the computing costs are about trebled.

A coarser mesh was not used, but several runs were made without a certain number of the sparsely occupied outer elements. This revealed that by using only the ten inner elements the results change by less than 0,2 %. This is not only due to the small number of fibres in the outer elements but also to the fact that even at very high yarn elongations of say 30 % these fibres do not develop any tension. It must be noted that their weight cannot be neglected in the determination of the linear density of the yarn as this makes a difference of about 7 % in the specific yarn stress (mN/tex).

4.4 FINITE-ELEMENT STRESS ANALYSIS

4.4.1 Introduction

In the case of inter-fibre friction the principle of virtual work can still be used but only if the amount of slip caused by a virtual nodal displacement can be predicted. When this is not feasible, as is the case with the migration model in Chapter 5, a different method of analysis has to be applied to the yarn model.

However, stress analysis (which has been used previously by Hearle and other workers) does not have the limitations with respect to frictional forces that apply to the energy methods. This method was abandoned in the early sixties because at the time it seemed difficult to extend it to more refined yarn models. However, with the aid of modern high-speed computers a discretisised model such as a finite-element model using a form of stress analysis is shown to be feasible. In order to investigate the possibilities of such an approach the finite-element model discussed before in this chapter is adapted to stress analysis.

4.4.2 Relationship between Axial and Lateral Stresses

The key equation in the stress analysis of a twisted yarn is the relationship between the axial tension in the fibre direction (T_A) and the lateral pressure normal to the fibres (T_L):

$$\frac{\partial T_L}{\partial R} + \frac{\sin^2\alpha.(T_L - T_A)}{R} = 0 \qquad \ldots\ldots\ldots (4.30)$$

This equation has been described by Hearle and Treloar (63) and Cheng *et al.* (64). Its derivation from the Cauchy equations of motion is presented in Appendix G. Assuming that T_A and α are constant, the above differential equation can be solved for T_L (see Appendix G):

$$T_{L_1} = T_A.(1 - (R_2/R_1)^{\sin^2\alpha}) + T_{L_2}(R_2/R_1)^{\sin^2\alpha} \qquad \ldots (4.31)$$

where T_{L_1} is the lateral pressure at R_1;
T_{L_2} is the lateral pressure at R_2; and
$R_2 > R_1$.

(For small values of α an alternative solution can be obtained which takes the variation of α with R into account and can also be used for $R_1 = 0$.)

The assumption that T_A and α are constant will restrict its validity to a small range of R, i.e., one element. Although a constant T_A and α within an element was not assumed in the energy analysis the use of one integration point per element in the R-direction has the same effect and has been shown to be reasonably accurate.

4.4.3 Governing Equation

An obvious choice for the equilibrium equations is to match the lateral pressure (T_L) in each element, as found above, to the lateral pressure found by a van Wyk-type relationship (Equation 4.1):

$$F = T_{L_{V(\text{olume})}} - T_{L_{T(\text{ension})}} = 0 \qquad \ldots\ldots (4.32)$$

where T_{L_T} is the pressure normal to the fibres caused by tensioned helically wound fibres, and

T_{L_V} is the pressure normal to the fibres found by a van Wyk-type relationship.

If Equation (4.32) is evaluated for each element and expressed in terms of the unknown nodal displacement vector, $\{U\}$, this can be solved from these equations as the number of elements is equal to the number of unknown displacements.

To establish the equilibrium equations it is necessary to define one value of T_{L_V}, T_{L_T} and T_A (as a function of $\{U\}$) for each element, whether they are assumed to be constant or to vary over the element. A convenient value for T_A is determined by using Equation (4.15):

$$T_A = (a.E_f + b).N_f.(A'.\cos\alpha')^{-1} \quad . \quad . \quad . \quad . \quad . \quad . \quad . \quad (4.33)$$

and taking the mean of the values at the nodes 1 and 2 of the element.

For T_{L_V} a convenient value is found by substituting

$$V_{sp} = dZ.A.M_f^{-1}$$

and $$V_{sp}' = dZ'.A'.M_f^{-1} ,$$

where M_f is the element fibre mass,

into the van Wyk relationship, Equation (4.1):

$$T_{L_V} = -K.(V_{sp}^{-3} - V_{sp_0}^{-3}) .$$

As shown before, both T_A and T_{L_V} can be written as functions of the displacements of the adjacent nodes of the element. Using the element and node numbering of Figure 4.9:

$$\begin{aligned} T_{A_j} &= T_{A_j}.(u_i, u_{i+1}) \\ T_{L_{V_j}} &= T_{L_{V_j}}.(u_i, u_{i+1}) \end{aligned} \quad . \quad . \quad . \quad . \quad . \quad . \quad . \quad . \quad . \quad . \quad (4.34)$$

There are several possible forms which the equilibrium equations can take, depending on the way the value of T_{L_T} for an element is defined. This is illustrated with the aid of Figure 4.9. Using Equation (4.31), T_{L_T} in element j is defined as a function of R as:

$$T_{L_{T_j}}.(R) = T_{A_j}\left[1 - (R_{i+1}/R_i)^{\sin^2\alpha_j}\right] + T_{L_j}'\left[R_{i+1}/R_i\right]^{\sin^2\alpha_j} \quad (4.35)$$

The differences in the equilibrium equations are caused by the different interpretations of the lateral pressure acting on the outer periphery of the element (T_L') and the value of $\bar{T}_{L_T}$ which is to be equated with $T_{L_{V_j}}$.

Five combinations have been evaluated and are discussed below.

(i) $T_{L_j}' = T_{L_{T_{j+1}}}(R_{i+1})$. This gives the recursive equation:

$$T_{L_{T_j}}(R_i) = T_{A_j}.\left[1 - \left(\frac{R_{i+1}}{R_i}\right)^{\sin^2\alpha_j}\right] + T_{L_{T_{j+1}}}(R_{i+1}).\left[\frac{R_{i+1}}{R_i}\right]^{\sin^2\alpha_j}$$

Assuming that $\bar{T}_{L_{T_j}}$ is equal to the mean value of T_{L_T} at the adjacent nodes the equilibrium equation becomes:

$$F_j = T_{L_{V_j}} - 0{,}5.\left[T_{L_{T_{j+1}}}(R_{i+1}) + T_{L_{T_j}}(R_i)\right] \quad . \quad . \quad . \quad . \quad (4.36)$$

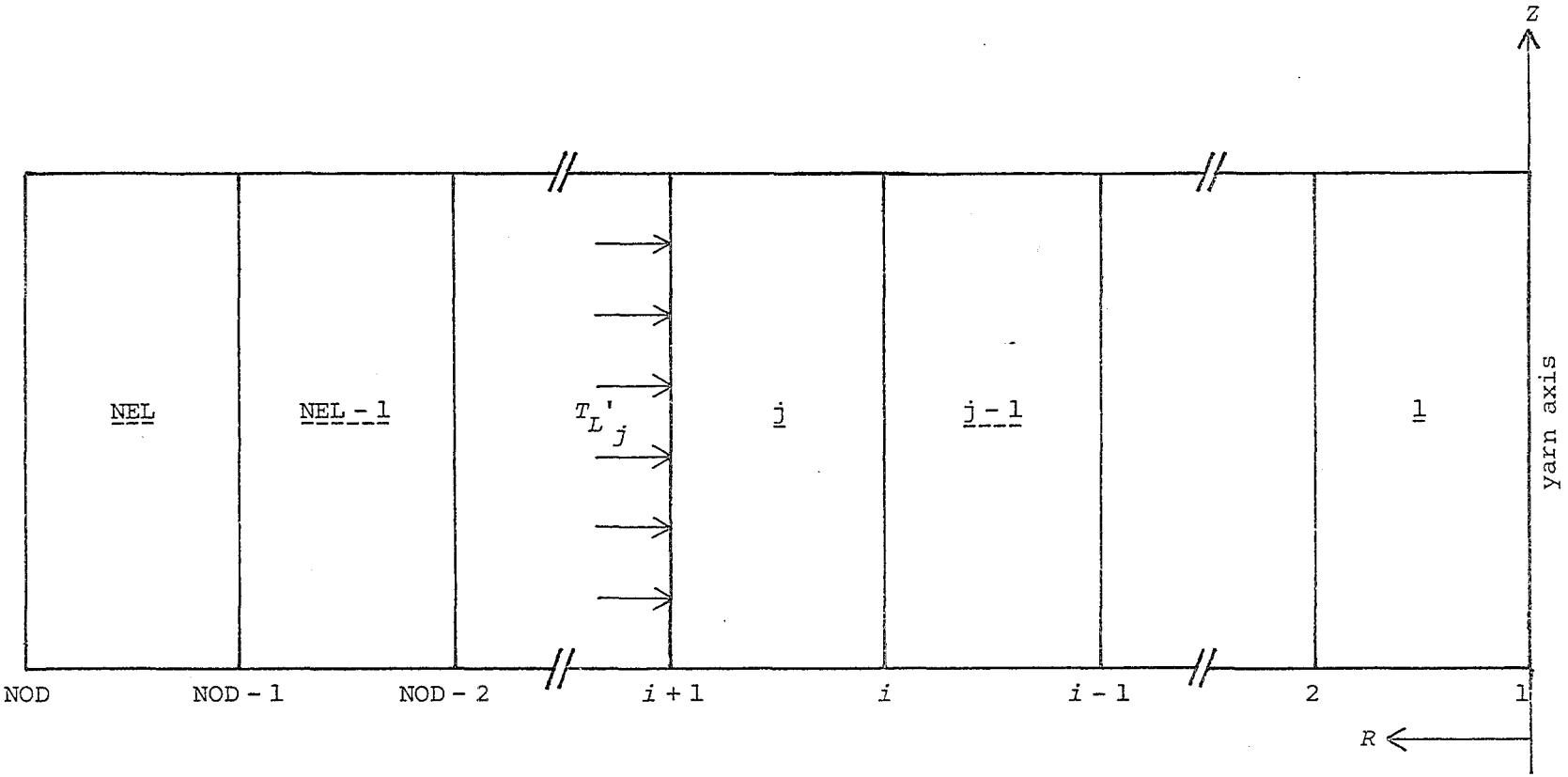

Fig. 4.9. Lateral pressure acting on an element

This implies that

$$F_j = F_j(u_{i-NOD}) \quad .$$

(ii) Setting $T_{L'_j} = T_{L_{V_j}}$ in Equation (4.35) and assuming that $\bar{T}_{L_{T_j}} = T_{L_{T_{j+1}}}(R_{i+1})$ leads to the equilibrium equation:

$$F_j = T_{L_{V_j}} - T_{A_{j+1}}\left[1 - \left(\frac{R_{i+2}}{R_{i+1}}\right)\sin^2\alpha_{j+1}\right] - T_{L_{V_{j+1}}}\left(\frac{R_{i+2}}{R_{i+1}}\right)\sin^2\alpha_{j+1} \quad . \quad . \quad . \quad . \quad . \quad (4.37)$$

from which it follows that

$$F_j = F_j(u_i, u_{i+1}, u_{i+2}) \quad .$$

(iii) Setting $T_{L'_j} = T_{L_{V_{j+}}}$ in Equation (4.35) and assuming that $\bar{T}_{L_{T_j}} = T_{L_{T_{j+1}}}(R_{i+1})$ leads to

$$F_j = T_{L_{V_j}} - T_{A_{j+1}}\left[1 - \left(\frac{R_{i+2}}{R_{i+1}}\right)\sin^2\alpha_{j+1}\right] - T_{L_{V_{j+2}}}\left(\frac{R_{i+2}}{R_{i+1}}\right)\sin^2\alpha_{j+1} \quad . \quad . \quad . \quad . \quad . \quad (4.38)$$

where $F_j = F_j(u_i, u_{i+1}, u_{i+2}, u_{i+3})$.

(iv) Setting $T_{L'_j} = 0{,}5.(T_{L_{V_j}} + T_{L_{V_{j+1}}})$ in Equation (4.35) and assuming that $\bar{T}_{L_{T_j}} = T_{L_{T_{j+1}}}(R_{i+1})$ leads to

$$F_j = T_{L_{V_j}} - T_{A_{j+1}}\left[1 - \left(\frac{R_{i+2}}{R_{i+1}}\right)\sin^2\alpha_{j+1}\right] - 0{,}5(T_{L_{V_{j+2}}} + T_{L_{V_{j+1}}})\left(\frac{R_{i+2}}{R_{i+1}}\right)\sin^2\alpha_{j+1} \quad . \quad . \quad . \quad . \quad . \quad (4.39)$$

where $F_j = F_j(u_i, u_{i+1}, u_{i+2}, u_{i+3})$.

(v) This is slightly different as $\bar{T}_{L_{T_j}}$ is calculated in two stages. Defining the value of R at the centre of element j as

$\bar{R}_j = 0{,}5.(R_{i+1} + R_i)$, $\bar{T}_{L_{T_j}}$ is assumed to be

$$\bar{T}_{L_{T_j}} = T_{A_j}\left[1 - (R_{i+1}.\bar{R}_j)^{\sin^2\alpha_j}\right] + T_{L'_j}(R_{i+1}.\bar{R}_j)^{\sin^2\alpha_j} \quad ,$$

and $T_{L'_j}$ is assumed to be

$$T_{L'_j} = T_{A_{j+1}}\left[1 - \left(\frac{\bar{R}_{j+1}}{R_{i+1}}\right)\sin^2\alpha_{j+1}\right] + \bar{T}_{L_{T_{j+1}}}\left(\frac{\bar{R}_{j+1}}{R_{i+1}}\right)\sin^2\alpha_{j+1} \quad .$$

This yields:

$$F_j = T_{L_{V_j}} - T_{A_j}\left[1 - \left(\frac{R_{i+1}}{\bar{R}_j}\right)\sin^2\alpha_j\right] - T_{A_{j+1}}\left[1 - \left(\frac{\bar{R}_{j+1}}{R_{i+1}}\right)\sin^2\alpha_{j+1}\right] \times$$
$$\left(\frac{R_{i+1}}{\bar{R}_j}\right)\sin^2\alpha_j - T_{L_{V_{j+1}}}\left(\frac{\bar{R}_{j+1}}{R_{i+1}}\right)\sin^2\alpha_{j+1} \cdot \left(\frac{R_{i+1}}{\bar{R}_j}\right)\sin^2\alpha_j \quad . \quad . \quad . \quad (4.40)$$

where $F_j = F_j(u_i, u_{i+1}, u_{i+2}, u_{i+3})$.

4.4.4 Solution and Determination of Yarn Force

As in the energy analysis the equilibrium equations are expanded into functions of the nodal displacement vector, $\{U\}$. The equations obtained will be non-linear and they are solved by the incremental method with Newton-Raphson iteration (Equation 3.47):

$$\{F(\{U\})\} = \{O\}$$
$$[K^T(\{U\}^{k,\ell-1})].\{\Delta U\}^{k,\ell} = -\{F(\{U\}^{k,\ell-1})\}$$

where k is the increment number, and

ℓ is the iteration number.

The tangent stiffness matrix, $[K_T]$, is defined by Equation (4.22):

$$K_{T_{ij}} = \partial F_i/\partial U_j \ .$$

The incremental procedure is the same as discussed in Section 4.3.6. In contrast to the energy analysis the axial yarn force, P, is not included in the equilibrium equations because these are only concerned with radial equilibrium. At the end of each increment P is obtained separately by an equilibrium check in the direction of the yarn axis over the top surface of the yarn.

At any point on the top surface there is a co-ordinate system in which there are only principle stresses. This is the fibre co-ordinate system ($R\alpha$, $\theta\alpha$, $Z\alpha$) which is obtained by rotating the yarn co-ordinate system by an amount α (the helix angle) around the R-axis (see page 55). The stresses along the $R\alpha$, $\theta\alpha$ and $Z\alpha$ axes are equal to T_L, T_L and T_A respectively. The components of these stresses acting on the top surface in the direction of the yarn axis are

$$0.T_{RR} = 0$$
$$-\sin^2\alpha.T_{\theta\theta} = -\sin^2\alpha.T_L$$
$$-\cos^2\alpha.T_{ZZ} = -\cos^2\alpha.T_A$$

where T_L and T_A are positive for tension and negative for compression.

Assuming that the helix angle α is constant throughout an element the yarn force, P, can be obtained from the equilibrium condition in the

Z-direction:

$$P = \sum_{j=1}^{NEL} (T_{L_j}.\sin^2\alpha_j + T_{A_j}.\cos^2\alpha_j).A_j \quad . \quad . \quad . \quad . \quad . \quad (4.41)$$

where A is the area of the element cross-section.

4.4.5 Evaluation

The stress-analysis approach presented here is not based on the rigorous rules of the finite-element theory as used for the energy analysis. These rules ensure a monotonic convergence to the correct answer, within the limitations of the modelling assumptions, with mesh refinement. Also the equilibrium equations are uniquely defined.

This does not imply that deviations from the correct procedures automatically lead to unacceptable results. It is perfectly possible that the answers obtained, which are theoretically incorrect, are for all practical purposes identical to the correct answers. However, this can only be found out by comparing the results of the various theories discussed in the previous section with the answers from the energy analysis.

Each of the five different approaches was evaluated using Carnaby's yarn model. The data used in the analyses are shown in Section 4.3.8. For the calculations only the twelve inner elements were used. To check convergence an element mesh twice as fine as the original mesh was also used, in this case only the 24 inner elements being used.

The results are presented in Table 4.1 in the form of the relative error (%) between the specific yarn stress as calculated by the stress-analysis theories and the specific yarn stress as found by the energy analysis, where there was no significant difference between the finer and the coarser mesh. At the foot of the table the average number of Newton-Raphson iterations per increment is shown. Also shown is the approximate average error over the whole elongation range obtained by using the root mean square method.

It can clearly be seen in the table that theory (v) is superior and that theories (iii) and (iv) must be rejected, not only because of the RMS error but mainly because of the unacceptable deviations in the lower elongation range. Because of the large number of increments required in the migration analysis due to the path-dependence of friction, computational efficiency also plays a role in the evaluation. In this case theory (ii) is vastly superior because of the small number of Newton-Raphson iterations per increment compared with theories (i) and (iv). The effort per iteration to the equations is dependent on the number and the place of the non-zero elements of the tangent stiffness matrix, $[K_T]$.

This again is in favour of theory (ii) because the associated $[K_T]$ has a tri-diagonal structure plus an adjacent lower diagonal and theory (i) has a full lower triangle plus an adjacent upper diagonal (lower Hessenburg form). Because of the marginal accuracy of the approach (i) this means that it also can be rejected. The efficiency of theory (ii) is such that with 24 elements it still only uses one-third of the computing time necessary for theory (v) with 12 elements.

The ultimate choice between theories (ii) and (v) possibly depends on other factors which may become apparent in analyses using the migration model.

Table 4.1 RELATIVE ERROR OF ALTERNATIVE GOVERNING EQUATIONS, %

Yarn elong-ation %	Yarn specific stress*	Theory (i)		Theory (ii)		Theory (iii)		Theory (iv)		Theory (v)	
		number of elements									
		12	*24*	*12*	*24*	*12*	*24*	*12*	*24*	*12*	*24*
1	2,37	-8,3	-5,4	8,9	3,2	30	29,5	19,0	17,6	0,7	-0,5
2	8,00	-9,7	-6,4	8,7	2,9	25,9	24,9	17,4	14,7	-0,4	-1,4
3	15,56	-9,3	-6,1	7,8	2,3	21,5	20,3	14,7	12,0	-0,6	-1,7
4	24,58	-8,2	-5,9	6,9	1,7	18,3	16,7	12,7	9,7	-1,2	-2,3
6	41,49	-8,0	-5,5	5,3	1,1	13,7	12,3	9,5	7,2	-1,9	-2,2
8	55,59	-6,4	-4,5	4,7	1,0	11,1	8,8	7,9	5,5	-1,6	-1,8
10	66,97	-5,0	-3,5	4,0	0,8	8,2	6,7	6,1	4,0	-1,4	-1,5
12	75,69	-2,6	-2,8	3,7	0,8	5,7	4,6	4,7	3,1	0	-1,1
14	81,82	-2,4	-1,7	3,0	0,9	4,8	3,2	4,1	2,1	-0,5	-0,6
16	86,39	-0,7	-1,7	1,8	0,7	2,5	2,0	2,1	1,4	0	-0,4
18	89,45	-1,9	-2,1	1,3	0,4	1,9	1,3	1,6	1,0	0	-0,2
20	91,78	-3,1	-1,9	1,2	0,3	1,5	1,0	1,4	0,7	0,2	-0,1
RMS ($\sqrt{\Sigma error^2/n}$)		6,2	4,3	5,4	1,64	15,3	14,4	10,3	8,5	0,95	1,3
No. of Newton-Raphson iterations per increment		23	35	5,4	6,1	5,5	6,2	5,5	6,3	24	32

* virtual-work model

CHAPTER 5

STAPLE-FIBRE YARN ANALYSIS

5.1 INTRODUCTION

As has been discussed in Chapter 4, the influence of fibre migration on the axial behaviour of a short-gauge staple-fibre yarn can conveniently be neglected, permitting the application of the ideal helical model. For longer gauge lengths, however, it is crucial to take account of the fibre migration without which a staple fibre longer than the longest fibre would be very weak. In this case the ideal helical yarn structure is inadequate as from the definition it cannot model the effects of fibre migration on the behaviour of the yarn. It must be noted, however, that in some cases where fibre slippage is minimal, as in high-twist staple-fibre yarns, the results obtained with the ideal helical yarn model will be comparable with those obtained with an equivalent migration model (Treloar, 19). When slippage is not negligible the use of a model which incorporates migration is essential. Such models have been developed by Treloar (19) and Hearle (6), in which the fibre migration pattern is idealised to make an analysis possible. Treloar's theory, which is discussed in Section 2.3.1, is, however, concerned with continuous-filament yarns and therefore the analysis does not take account of the effects of the fibre discontinuities which occur in staple-fibre yarns. Hearle's theory (Section 2.3.2) does include these effects and it is in fact the only one to date which incorporates all the basic features desirable in a model of a staple-fibre yarn. The development of the analysis, however, is based on Hearle's ideal helical yarn analysis (23, 24) which is limited by the use of some very restrictive assumptions especially with respect to the lateral contraction of the yarn. These limitations have been overcome in recent developments so the lateral contraction of a yarn can now be modelled more realistically.

In this chapter an attempt is made to combine in one model and analysis the desirable aspects of Hearle's migration model and of the recent continuous-filament yarn analyses. The resulting staple-fibre yarn analysis is in comparison with Hearle's analysis much more sophisticated, except for one particular assumption which is concerned with the path of the migrating fibres. Hearle assumed that the fibre ends are randomly distributed over the cross-section of the yarn but here it is assumed that they are all at the same radial position. With some fur-

ther development of the analysis this seemingly restrictive assumption can probably be discarded but it is maintained here to keep the description of the analysis as simple as possible. The consequences of the use of this assumption are discussed in Section 6.6.2.

The complexity of the analysis is proportional to the assumed complexity of the migration path of the fibres. Therefore the detailed discussion of the analysis is based on a simple, probably unrealistic, shape of the migration envelope. An analysis based on a more realistic, but more complex, migration envelope is discussed in less detail at the end of the chapter.

The description of the analyses is preceded by a discussion of the model and several important features to be used in the analyses.

5.2 MIGRATION PATH

Several very restrictive assumptions are made in representing the migration of the fibres, which is in reality enormously complex. These are:

(a) each fibre in the yarn follows an identical path except for a shift in position along or around the yarn axis; this implies that the fibres are of equal length and that the fibre ends are all at the same radial position;

(b) the starting points of the individual fibre paths are evenly distributed along the Z-axis; and

(c) the twist is constant throughout the yarn.

Given the elementary shape of the migration path and the distribution of the fibres over the cross-section, an analytical expression can be devised for the path of the migrating fibre (see Appendix B). The function describing the migration path is of the form: $Z = Z(R)$. In Figure 5.1 a W-shaped migration envelope (which is the projection of the fibre path onto the R-Z plane) is shown with the fibre ends at the yarn surface. The tangent of the migration envelope ($\partial R/\partial Z$) is dependent on the cross-sectional fibre density at radius R, the straight lines shown being a simplification. The distance along the Z-axis between two consecutive fibres (1 and 2) is dF, which is defined by

$$dF = L_Z/N_f \qquad \ldots\ldots\ldots\ldots \quad (5.1)$$

where L_Z = distance along the Z-axis between the ends of a single fibre, and

N_f = total number of fibres in the yarn cross-section.

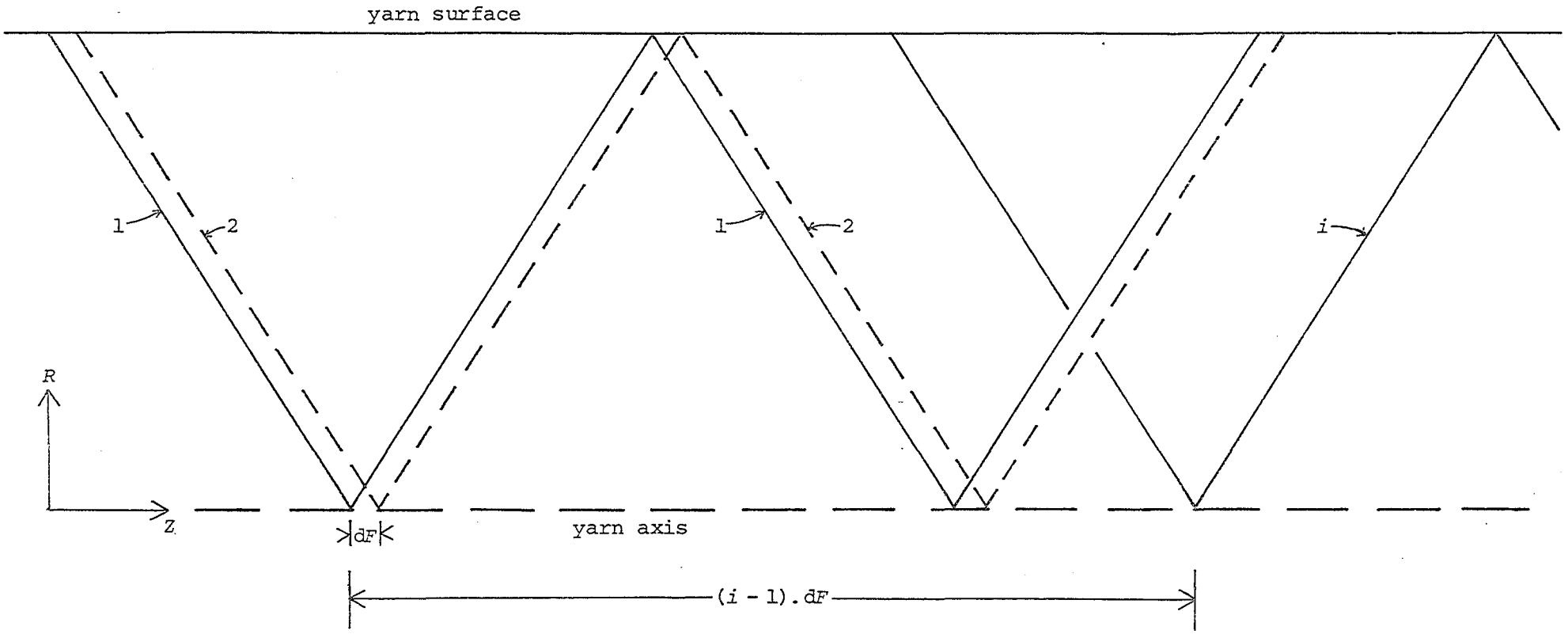

Fig. 5.1. Migration envelope

If fibre 1 starts at $Z = 0$ then fibre i starts at $(i - 1).dF$. Each fibre path is now uniquely defined except for its phase, which is defined by the θ-co-ordinate of its starting point. This is not quantified explicitly but is assumed to take such a value that the distribution of fibres over the yarn cross-section is approximately axisymmetric. If there are a reasonably large number of fibres in the yarn cross-section the above assumptions will imply that the yarn can be considered to be uniform in the θ- and Z directions. This in turn implies that the behaviour of the fibres during deformation of the yarn will be identical. This is a very important conclusion as otherwise the analysis would not be feasible.

It is possible that the mathematical form of the fibre paths will lead to a situation in which the fibres will occupy the same space at certain points in the yarn, especially near the yarn axis. This difficulty was also observed by Treloar (19) who alleviated it by assuming that the fibres do not reach the yarn axis ($R = 0$) but turn their paths at a certain finite value of R, small in comparison with the radius of the yarn.

As in the previous analyses the deformation pattern of the yarn, which is considered to consist of a continuous matter, is quite simple and is defined by:

if $\quad R_A = R_B \quad \Rightarrow \quad R'_A = R'_B$

$\quad Z_A = Z_B \quad \Rightarrow \quad Z'_A = Z'_B$

$\quad R_A > R_B \quad \Rightarrow \quad R'_A > R'_B$

$\quad Z_A > Z_B \quad \Rightarrow \quad Z'_A > Z'_B$;

if $Z_A = Z'_A$ and $Z_A \neq Z_B$,

then $\quad Z'_C = Z_C + (Z_C - Z_A).(Z'_B - Z_B).(Z_B - Z_A)^{-1}$.

The last line simply implies that the displacement field in the Z-direction is linear, i.e., the axial elongation is uniform throughout the yarn. However, the fibres do not necessarily follow the yarn deformation as is the case in a continuous-filament yarn, due to the slippage of the fibres.

For the explanation of what happens to the fibres during the deformation of the yarn it is considered that they run along cavities in the continuous yarn matter. The cavities can be compared to imaginary tubes which surround the fibres. The presence of these cavities has no influence whatsoever on the deformation of the yarn matter. After

deformation of the yarn the tubes will deform with the yarn according to the above rules but the fibres will be free, apart from the effect of frictional forces, to slide in their tubes. The tube constrains the movement of the fibre in two dimensions, the movement in the remaining dimension being governed by the frictional forces which are exerted by the walls of the tube on the fibre. In reality these forces are caused by contacts with neighbouring fibres. If the frictional forces are so large that the fibre is firmly gripped by its tube the fibre will be subjected to the same extension as the tube, i.e., the yarn. If not, the fibre will slip with respect to its tube.

5.3 YARN AND FIBRE BEHAVIOUR

5.3.1 Radial Contraction of the Yarn

If the fibres follow the ideal migration paths exactly, the same problem will arise with respect to the radial compressibility of the yarn model as is discussed in Section 4.2.2 in connection with the ideal helical yarn model. The model with the ideal migration paths will also immediately collapse into a configuration where the fibres are jammed tightly against one another when an axial force is applied to the yarn model. In even the most ideal real yarn such a sudden collapse will not occur because of the large number of crossover contacts between the fibres which will cause a considerable resistance to radial contraction of the yarn long before the jammed configuration is reached. As discussed in Section 4.2.2 this situation can also be achieved in the ideal helical yarn model, or in this case the ideal migration model, if the fibres are allowed to deviate slightly from their ideal configuration. It is assumed that the slight deviations do not cause any significant changes in the length or the general orientation of the ideal fibre paths, which implies that the determination of the fibre axial forces and their contribution to the yarn strength can still be based on the ideal geometry.

At any point within the migration model there will be two groups of fibres, distinguished by their general orientation, one migrating outwards ($\partial R/\partial Z > 0$) and the other migrating inwards ($\partial R/\partial Z < 0$). However, the migration angle is generally very small, a few degrees at the most, and because of the deviations there will be little distinct difference between the local orientation of the two groups so that the local situation in the model will resemble an untwisted sliver where the fibres are roughly aligned.

5.3.2 Inter-fibre Friction

In the case of the ideal migration model the large number of fibre contacts caused by the deviations also allows a more realistic description of the frictional forces acting between the fibres. If the fibres were to follow the ideal geometry exactly there would be very few, if any, fibre contacts in the loosely packed, undeformed yarn configuration, which implies that the fibres could not build up sufficient tension to 'lock' the helical structure and the model would simply slip apart when an axial force was applied.

Because all the fibres behave approximately identically it is sufficient to discuss the behaviour of a typical fibre.

A small segment, dA, of a typical fibre, A, is shown in Figure 5.2. Contacts with other fibres are distributed along the length of the segment. When the yarn is elongated the imaginary tubes surrounding the fibres will also be elongated, the amount being dependent on the radial position. However, the fibres will resist the elongation and they will tend to slip with respect to their tubes. For example, dA wants to slip to the left (arrow in the Figure) and some of the contacting fibres will also want to slip to the left, either more or less than dA, while the others want to slip to the right. Because the fibres are roughly aligned the slipping occurs in approximately opposed directions and the resulting frictional forces acting at the contact points will be roughly aligned with the fibres.

If all the contacting fibre segments wanted to move to the right with respect to dA then the local situation in a yarn would resemble the withdrawal of a single fibre from an untwisted sliver. This is discussed in Section 2.4.2 where the following relationship (31) is given for the withdrawal force per unit length, WF:

$$WF = \frac{p}{1 - E} \cdot \mu_{WF} + WF_0 \qquad (5.2)$$

where p = external pressure exerted on the sliver;

E = porosity of the sliver;

μ_{WF} = coefficient of friction; and

WF_0 = withdrawal force when the external pressure on the sliver is zero.

The withdrawal force per unit length is identical to the sum of the frictional forces acting on a unit length of the withdrawn fibre. Because the withdrawn fibre moves relatively more in the withdrawal direction than the contacting fibres the frictional forces all act in the

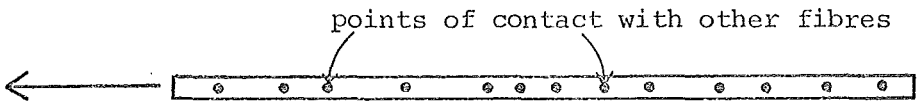

Fig. 5.2. Small segment of fibre, dA

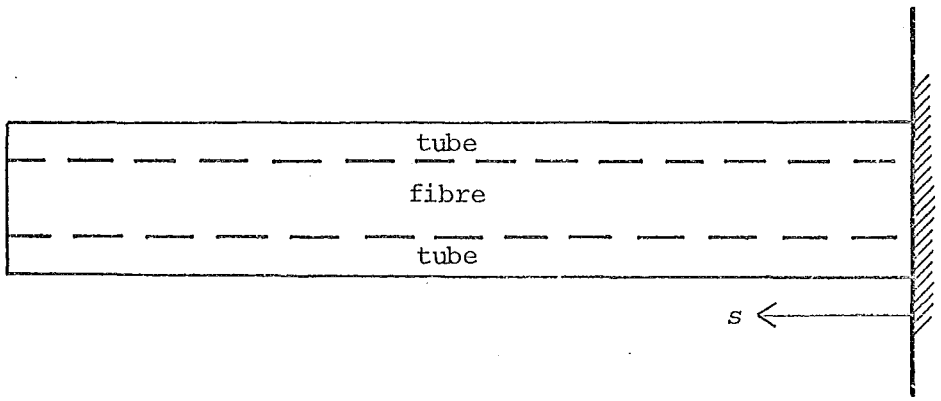

Fig. 5.3. A fibre in its tube

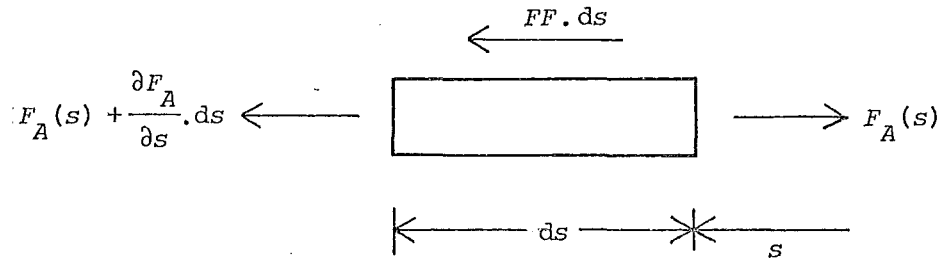

Fig. 5.4. Infinitesimal section of a fibre with axial and frictional forces

direction opposite to the withdrawal and therefore WF can be written as:

$$WF = \sum_{i=1}^{n_c} F_c \qquad \ldots\ldots\ldots\ldots \quad (5.3)$$

where n_c = the number of contacts per unit length, and

F_c = the magnitude of the frictional force acting at a contact.

However, in the migration yarn model not all of the frictional forces are opposing the movement of dA because some of the contacting fibres will move more to the left than dA, thereby aiding dA in its movement. This implies that the force per unit length resisting the movement of dA, which is defined as FR, is equal to:

$$FR = \sum_{i=1}^{n_{opp}} F_c - \sum_{i=1}^{n_{aid}} F_c \qquad \ldots\ldots\ldots\ldots \quad (5.4)$$

where n_{opp} = the number of contacts per unit length where the frictional force opposes movement of dA, and

n_{aid} = the number of contacts where the frictional force aids movement of dA.

Because the frictional force only vanishes if a contacting fibre moves exactly the same amount and in the same direction as dA the number of 'neutral' contacts can be assumed to be negligible, which yields the following relationship:

$$n_{opp} + n_{aid} = n_c \qquad \ldots\ldots\ldots\ldots \quad (5.5)$$

If it is further assumed that the contact frictional forces are all of equal magnitude the standard value of F_c can be expressed as (Equation 5.3):

$$F_c = WF/n_c \ .$$

Substituting this result into Equation (5.4) and using Equation (5.5) yields:

$$FR = n_{opp} \cdot \frac{WF}{n_c} - n_{aid} \cdot \frac{WF}{n_c} = WF.C \qquad \ldots\ldots\ldots\ldots \quad (5.6)$$

where $C = (1 - 2.n_{aid}/n_c)$.

The term C is a correction factor which is used to determine FR from WF. This is convenient as the force resisting a fibre segment in a yarn would be very difficult, if not impossible, to determine experimentally. The parameters in the equation for WF, μ_{WF} and WF_0, can be determined experimentally.

To determine C it is necessary to know the ratio of n_{aid} to n which will be different for different types of migration paths. In

Appendix D approximate values for C are derived for the two types of migration paths used in the analyses presented here.

Substituting the expression for WF (Equation 5.2) into Equation (5.6) yields:

$$FR = \left(\frac{p}{1 - E} \cdot \mu_{WF} + WF_0 \right) .C \qquad . . . . . \quad (5.7)$$

where p and E are now the local pressure in the yarn and the local porosity respectively. Because p and E are radially dependent, FR will be a function of the radial position and its value will constantly change along a migrating fibre. It must be noted that FR as derived above is the maximum possible frictional force acting on the fibre and it only occurs when the fibre segment slips or is about to slip.

5.3.3 Fibre Axial Force

The problem is to determine the axial force in the fibre, F_A, as a function of s when given both the elongation of the fibre tube and the frictional force, FR_V, as functions of s. To solve this problem an analogy with a simple model is made. If the fibre and its tube are depicted 'straightened out' the situation of the fibre in the yarn resembles the situation shown in Figure 5.3 (in which only one half is included because of symmetry). The fibre and its tube are considered to be two slender rods fixed at one end and contacting one another over their whole lengths. Deformation is only possible in the axial direction so the problem is effectively one-dimensional. After deformation of the yarn the elongation of the tube, which deforms with the yarn, is expressed by the function, $u_t(s)$. This is the displacement of a point of the tube originally at s. Between the fibre and the tube there are frictional forces, FF, also dependent on s. The axial forces developed in the fibre due to FF do not in any way influence the elongation of the tube which can be considered to have an infinite stiffness. The elongation of the tube is assumed to be small, which implies that any slippage will also be small. The elongation of the fibre is expressed by the function, $u_f(s)$, which is defined in the same way as $u_t(s)$. In Figure 5.4 an infinitesimally small section of the fibre of length ds and located in the original configuration at s is shown. For equilibrium the frictional force exerted by the tube on the fibre, $FF.ds$, must be equal in magnitude and acting in the opposite direction to the resultant axial force in the fibre:

$$\frac{\partial F_A}{\partial s} . ds + FF.ds = 0 \qquad . . . . . \quad (5.8)$$

Depending on the relationship between $u_f(s)$ and $u_t(s)$ certain conditions apply to the frictional force, *FF*. These are:

(i) $u_f(s) < u_t(s)$. This implies that the fibre slips with respect to its tube to the right. In this case, $FF = FR$.

(ii) $u_f(s) > u_t(s)$ The fibre slips with respect to its tube to the left, in which case: $FF = -FR$.

(iii) $u_f(s) = u_t(s)$. There is no slippage of the fibre with respect to its tube. In this case, $FR > FF > -FR$.

In the above equations *FR* is the maximum possible frictional force per unit length as discussed in the previous section and which is always expressed as a positive value. A further condition is that the fibre axial force, F_A, is compatible with the fibre axial strain, E_f, which is defined by:

$$E_f = \frac{\partial u_f(s)}{\partial s} \qquad \ldots\ldots\ldots\ldots \quad (5.9)$$

If a piecewise linear approximation is used for the fibre stress-strain curve (see Appendix C) F_A is related to E_f by:

$$F_A = a.E_f + b \qquad \ldots\ldots\ldots\ldots \quad (5.10)$$

Because the frictional forces, *FR*, in the yarn are also dependent on the unknown fibre axial force, F_A, the final answer must be obtained by a series of single solutions. Also because the method assumes small elongations an incremental approach must be used as the deformations of the fibre and its tube can be quite considerable. The necessary application of increments and iterations is technically no problem as they are already incorporated in the yarn analysis.

However, the main problem is to produce a single solution which in general it is impossible to do analytically. A numerical solution-method for problems involving friction has recently been published (65) and this can be simply adapted to the above problem. Unfortunately the method also involves iterations and to obtain a single solution is in itself a major computational effort. This effort multiplied by the large number of iterations and increments involved in the yarn-analysis would probably push the total computational effort required to prohibitive levels. Another problem associated with this method is that, because it is numerical, the required derivatives of F_A with respect to the element nodal displacements will have to be evaluated numerically. This would involve at least two separate solutions for F_A which will yet again raise the computational effort required.

Under certain conditions an alternative solution method can be used which is simple and computationally efficient. It has been applied previously by Hearle (6) in his staple-fibre yarn analysis. To obtain the solution two possible fibre axial forces are calculated, F_{AF} and F_{AS}. The first, F_{AF} , is the fibre axial force which could be maintained by the frictional forces and is defined by:

$$F_{AF}(s) = \int_{s}^{s_E} FR(s)\, ds \qquad \ldots\ldots\ldots\ldots (5.11)$$

where $s_E = s$ at the fibre end.

The second, F_{AS} , is the fibre axial force which would be obtained by elongating the fibre by the same amount as its tube:

$$F_{AS}(s) = a.E_t + b \qquad \ldots\ldots\ldots\ldots (5.12)$$

where $E_t(s)$ is the elongation of the tube at s which is equal to $\partial u_t(s)/\partial s$, and

a and b are parameters of the approximated fibre stress-strain function (see Appendix C).

The actual fibre axial force, F_A, at any point s is now found by taking the minimum of F_{AF} or F_{AS}.

$$F_A(s) = \text{minimum}\,\{F_{AF}(s),\ F_{AS}(s)\} \qquad \ldots\ldots\ldots\ldots (5.13)$$

This solution is shown in graphical form in Figure 5.5 in which it can be seen that the implications of the above solution are that the fibre sticks to its tube between $s = 0$ and $s = s_1$ and slips between $s = s_1$ and $s = s_E$ with respect to its tube in the negative s-direction. In the simple case illustrated the solution meets the conditions as set out before if the following is valid between $s = 0$ and $s = s_1$:

$$FR > \frac{\partial F_{AS}}{\partial s} > -FR \qquad \ldots\ldots\ldots\ldots (5.14)$$

where in this case $FR = -\dfrac{\partial F_{AF}(s)}{\partial s}$.

If this condition is not met (see Fig. 5.6a) the solution can only be obtained numerically, which will also be the case if the situation is more complicated as shown in Figure 5.6b.

In the development of the analysis in the following sections it is assumed that the simple solution method can be used, but the conditions will have to be checked when the analysis is carried out.

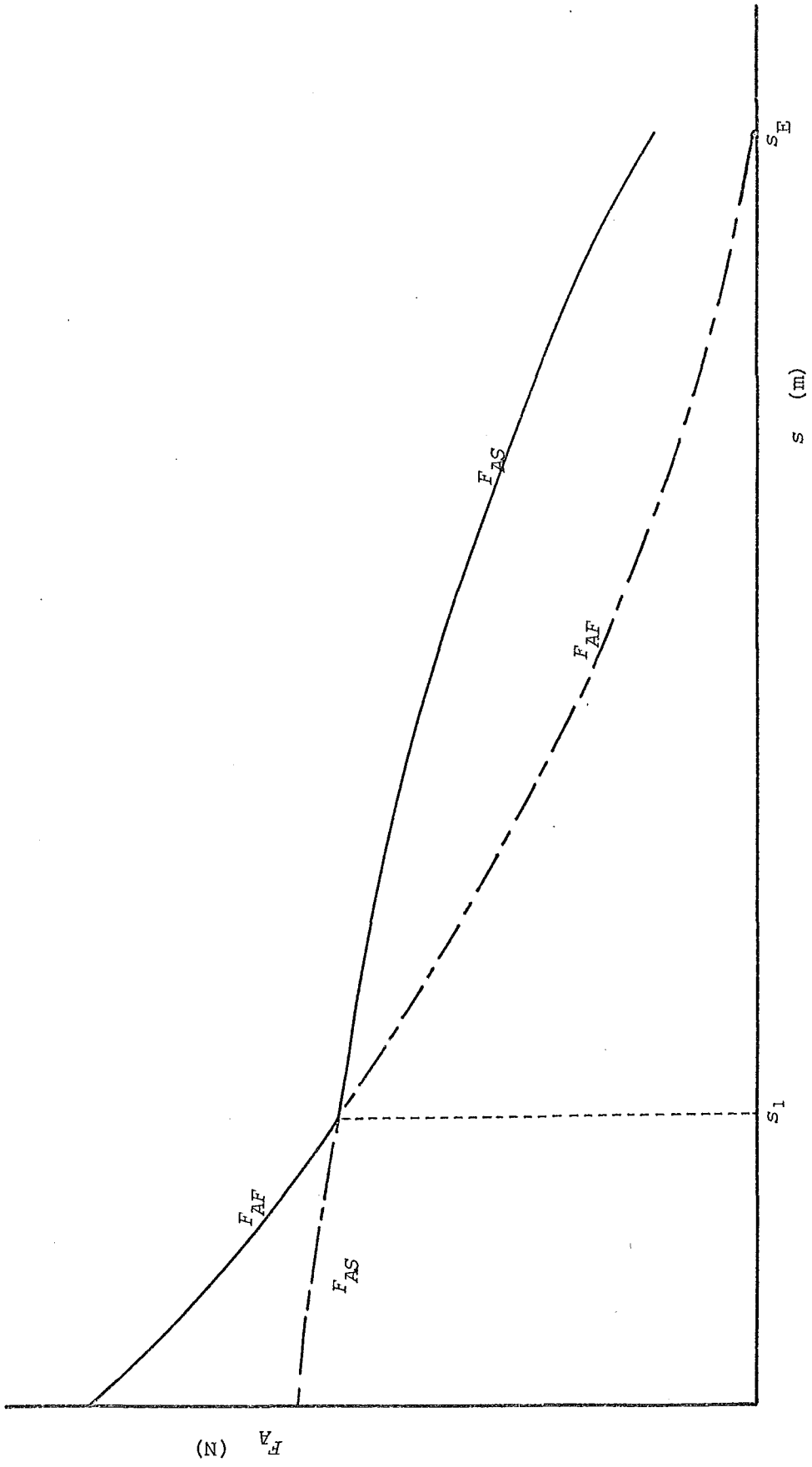

Fig. 5.5. 'Simple' solution of the friction problem

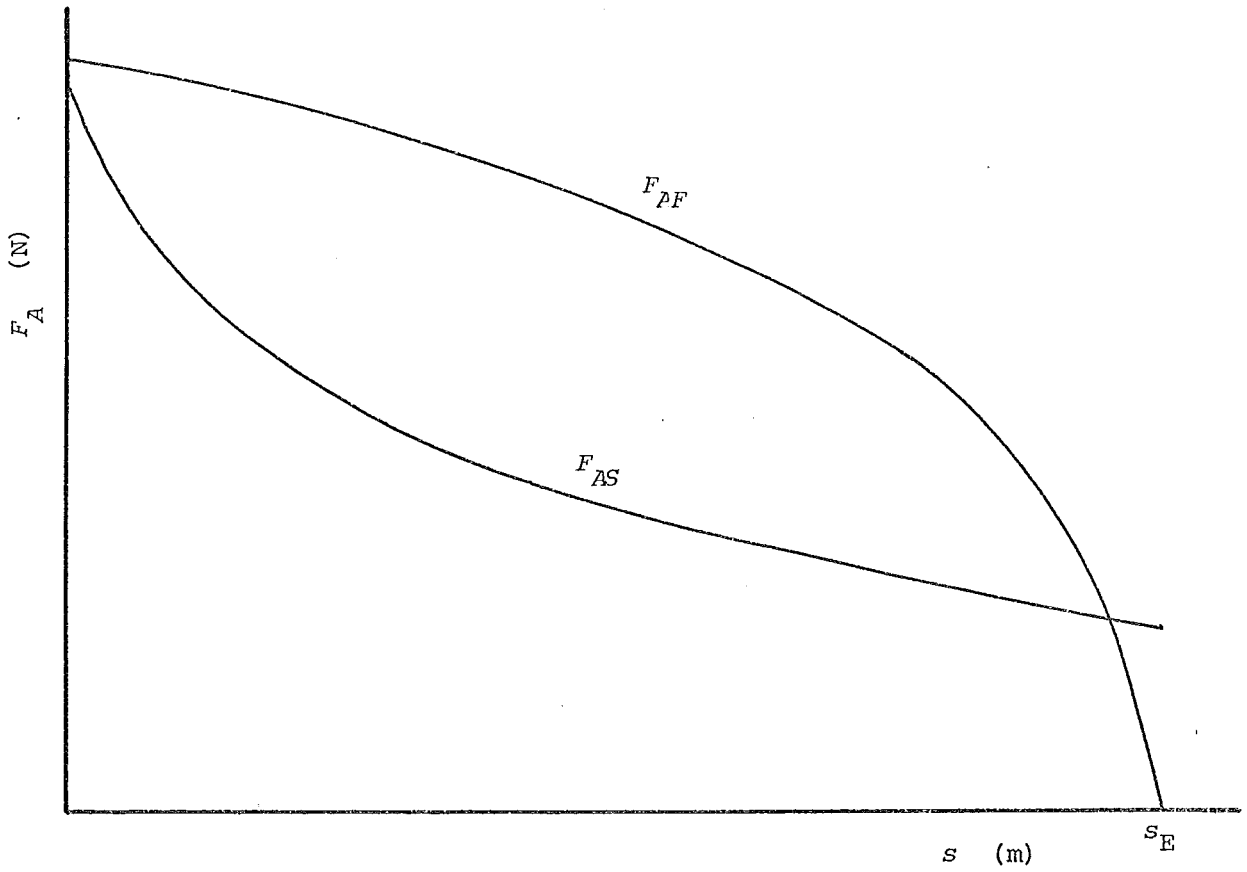

Fig. 5.6a

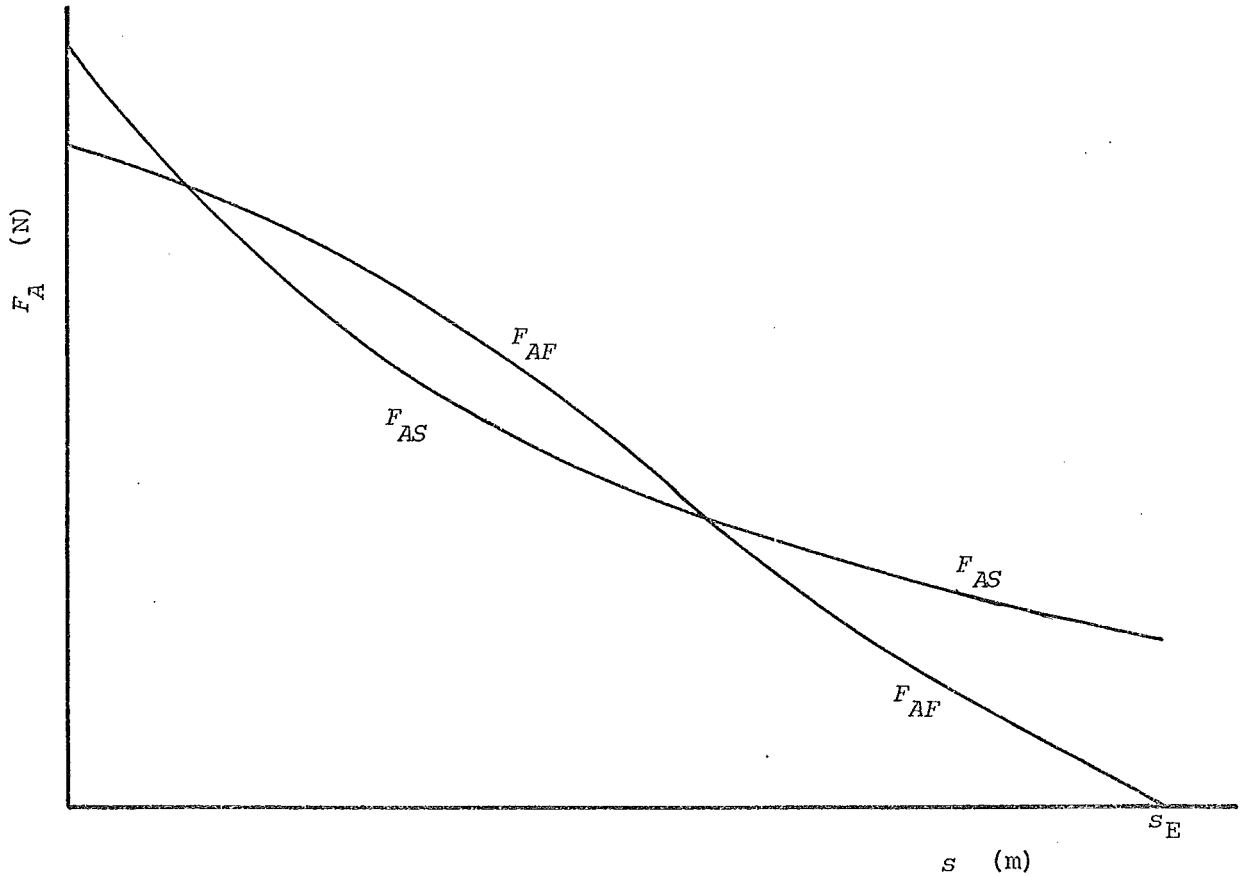

Fig. 5.6b

Fig. 5.6. Situations where the 'simple' solution of the friction problem cannot be applied

5.4 ANALYSIS OF YARN WITH A SIMPLE FIBRE-MIGRATION ENVELOPE (V-shape)

5.4.1 Introduction

The finite-element analysis of the model discussed in the previous section can not, for various reasons, be generalised to account for any type of migration path. A separate though similar analysis must be developed for each alternative path. Because the analysis is quite complicated one of the simplest possible migration paths is chosen for the initial detailed discussion. The path chosen has a symmetrical V-shaped migration envelope with the fibre ends at the yarn surface (see Fig. 5.7). This was preferred to an inverted V-shape with the fibre ends at the yarn axis because there is some evidence that the majority of the fibre ends in a semi-worsted yarn are near the yarn surface (see Section 2.2.2).

In a later section the analysis of a W-shaped migration path is discussed; this is very similar to that of a V-shaped path although it is more complicated.

As the migration path is symmetrical about its middle (M) only only one half of the fibre needs to be considered. In the analysis discussed here it is assumed that the internal stresses are zero. This assumption is commented on in Chapter 6.

5.4.2 Finite-element Model

In order to solve the problem it is discretised by sub-dividing the yarn model into concentric cylindrical elements as in the previous analyses presented here. Using the virtual-work governing equation as described in Section 4.3.3 it would be necessary to define the virtual amount of slippage between the fibres due to a virtual displacement. This would be very complicated if it were possible at all so a governing equation of the type derived for the stress-analysis approach (Section 4.4.3) is applied here. Although slipping energy must also be accounted for when using the stress-analysis approach it does not interfere with the governing equations, which remain unchanged.

A difference between this and the previous analyses presented here is that during deformation there is a transport of fibre material from one element to another due to the slipping of the fibres in their tubes. This is accounted for by correcting the fibre length, and hence the fibre mass, in the elements after the configuration for an increment has been calculated. A further difference is in the calculation of the yarn force, which must include slipping energy. This is

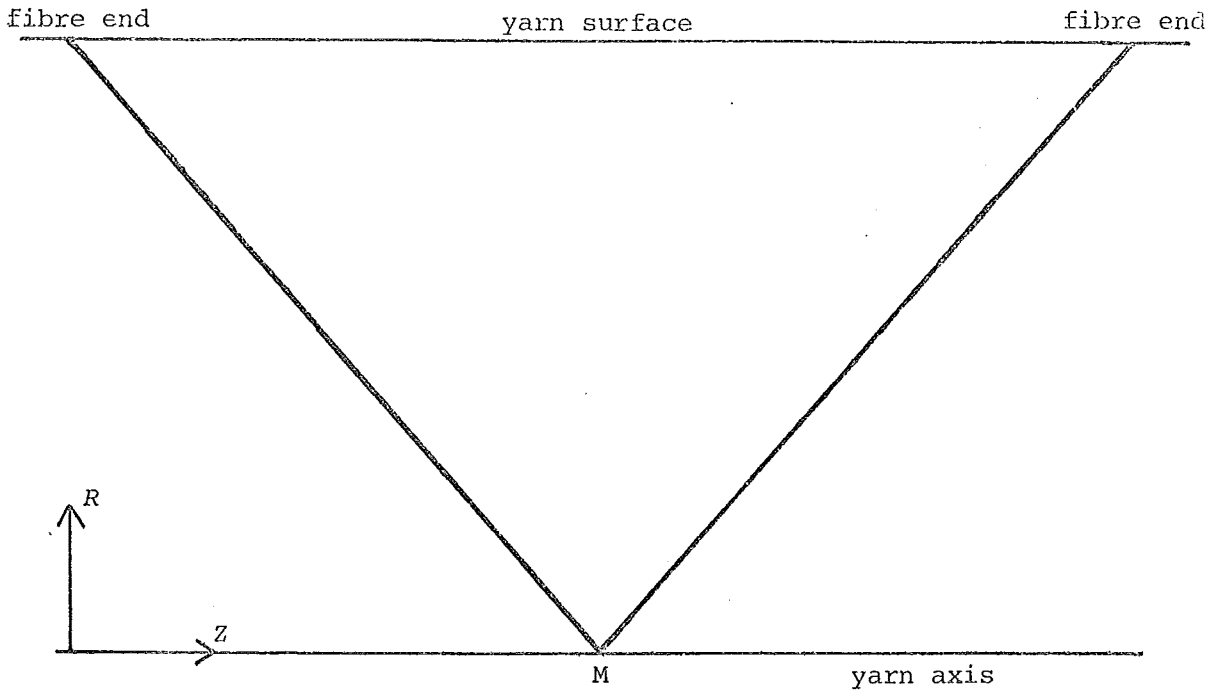

Fig. 5.7. V-shaped migration path

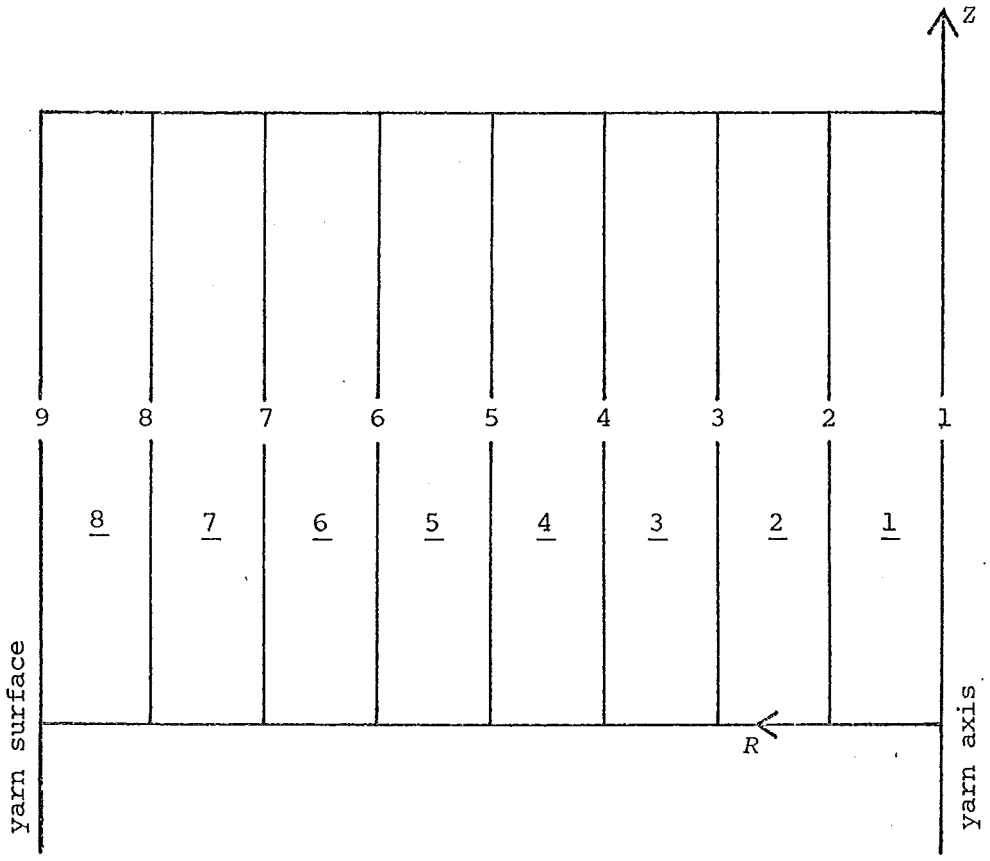

Fig. 5.8. Element and system nodal numbering of finite-element model

achieved by using the virtual-work principle with numerically calculated derivatives of the slipping energy.

As in the previous models the dimensions of the elements in the Z-direction, dZ, are identical. The value of dZ is immaterial but once a value has been chosen it must be used consistently throughout the analysis. A convenient sub-division in the radial direction is the one that is used to define the cross-sectional density of the yarn, though any other sub-division could be used. The finite-element model is shown in Figure 5.8 with the element and system node numbers. As before the element and system node numbering are arranged so that element $\underline{i}$ has nodes i and $i+1$ on either side of it. All the equations are written with the appropriate parameters already expressed in terms of the global node numbering.

5.4.3 Fibre Configuration

Attention is focused on one fibre and its imaginary tube the behaviour of which is identical to that of all other fibres. Only one half of the fibre is used because of symmetry. It is assumed that in the original configuration there are no axial stresses in the fibres and no lateral stresses in the yarn as a whole.

A V-shaped migration envelope is shown in Figure 5.9 with the radial sub-division of the model into elements. The length along the Z-axis between the entry point and exit point of the migration path in a particular element, $\underline{i}$, is defined as $\Delta Z_{\underline{i}}$. This can be calculated for each element using the equation for the migrating-fibre path (see Appendix C). When the yarn is elongated an amount, E_y (relative elongation), $\Delta Z_{\underline{i}}$ becomes:

$$\Delta Z'_{\underline{i}} = \Delta Z_{\underline{i}} (1 + E_y) \qquad \ldots\ldots\ldots\ldots (5.15)$$

The same is valid for TT (the length of one turn of twist) and dZ, the length of the model:

$$TT' = TT\,(1 + E_y) \qquad \ldots\ldots\ldots\ldots (5.16)$$

$$dZ' = dZ\,(1 + E_y) \qquad \ldots\ldots\ldots\ldots (5.17)$$

Other parameters to be used in the analysis are:

$DL_{\underline{i}}$ which is the length of the imaginary tube between the entry and exit points of the fibre in element $\underline{i}$.

$$DL'_{\underline{i}} = B' \left| \left\{ \frac{R}{2}(A' + R^2)^{0,5} + \frac{A'}{2} \ln \left| R + (A' + R^2)^{0,5} \right| \right\} \right|_{R'_i}^{R'_{i+1}} \qquad \ldots (5.18)$$

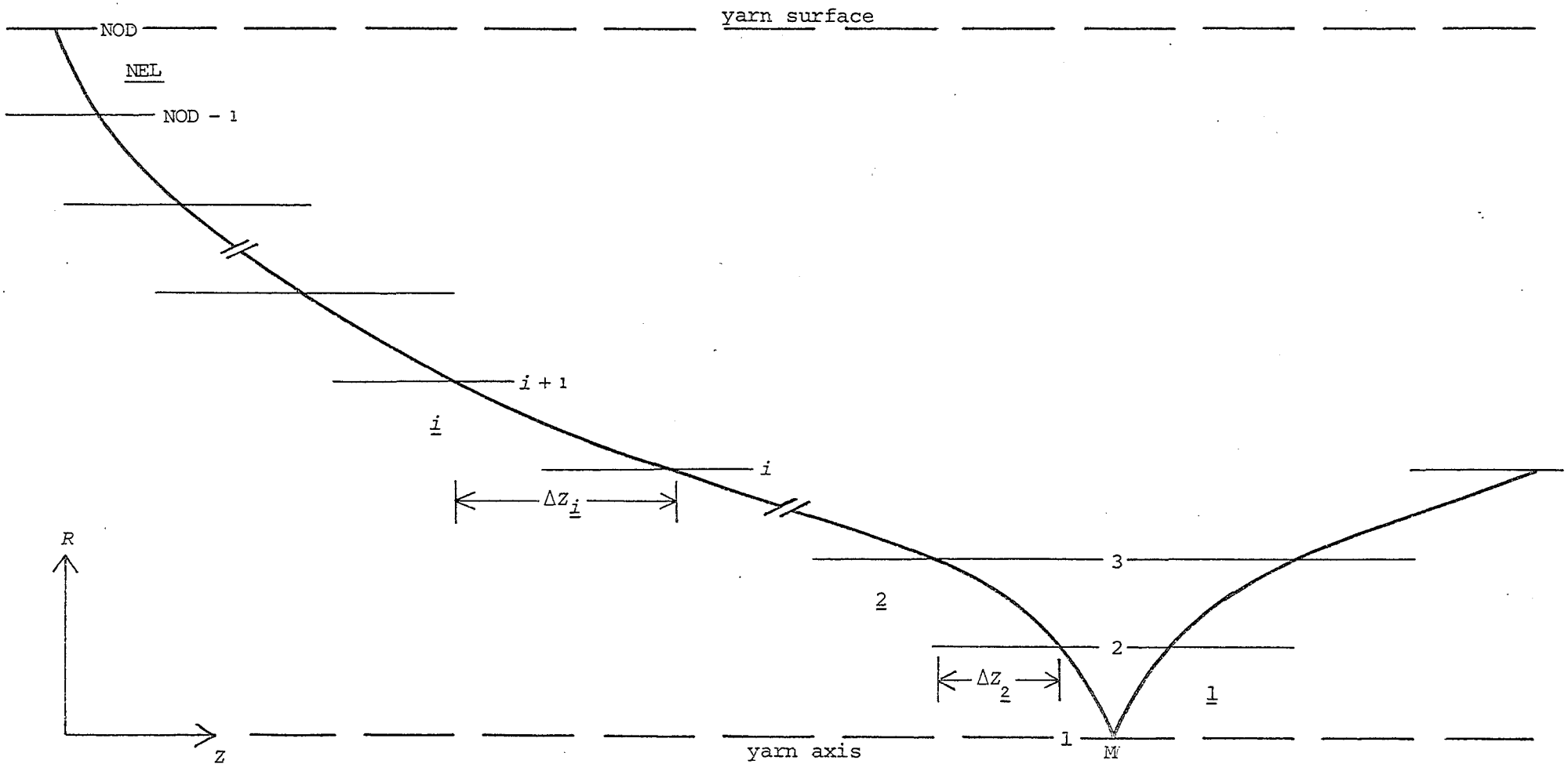

Fig. 5.9. V-shaped migration envelope with radial sub-division into elements

where $$A' = (B')^{-2}.\left\{1 + \left[\frac{(1+E_y).2\pi R.\rho_i(R).dF.(R_{i+1} - R_i)}{n_i.(R'_{i+1} - R'_i)}\right]^2\right\}$$

$$B' = \left\{\frac{(2\pi R)^2.(1+E_y).\rho_i(R).dF.(R_{i+1} - R_i)}{n_i.TT.(R'_{i+1} - R'_i)}\right\} .$$

The derivation of Equation (5.18) is given in Appendix B.

FL_i which is the original (unstressed) length of fibre present in the tube in element i. This will change during yarn deformation owing to slippage. The derivation of FL'_i will be discussed in Section 5.4.5. In the undeformed yarn FL_i is equal to DL_i.

FM_i which is the fibre mass present in element i:

$$FM'_i = FL'_i.(R_f^2.\pi.1,31).2.dZ.dF^{-1} \quad . . . . . (5.19)$$

where R_f = fibre radius;

1,31 = specific weight of the fibre material;

$2.dZ.dF^{-1}$ = number of fibre segments present in element i (same for each element); and

dF is defined in Equation (5.1).

5.4.4 Stresses

In the equilibrium equations discussed in Section 4.4.3 two stresses were used, one in the direction of the fibres (T_A) and one normal to the fibres (T_L). This was for the ideal helical yarn model. In the migration model the direction of the fibres is slightly different owing to the migration angle. This angle is, however, very small and as in Hearle's analysis it will be ignored in the calculations.

The lateral pressure in an element as determined by its geometry is found with the aid of the van Wyk relationship (Equation 2.1):

$$T_{LV_i} = K(V_{sp}^{-3} - V_{sp_0}^{-3}) \quad . . . . . (5.20)$$

where $V_{sp} = (R'^2_{i+1} - R'^2_i).\pi.dZ'.(FM'_i)^{-1}$.

As in the previous analyses, T_{LV} can be written as a function of $\{U\}$. As discussed in Section 5.3.3, the actual tensile force in a fibre at a certain point along its path is the minimum of either the tensile force as dictated by the yarn strain or the tensile force as limited by friction. In this analysis the fibre axial force (F_A) is assumed to be constant throughout an element. F_A due to yarn strain is then simply:

$$F_{AS} = a.E_f + b \quad . . . . . (5.21)$$

where $E_f = (DL_{\underline{i}} - FL_{\underline{i}}).FL_{\underline{i}}^{-1}$ . . . . . (5.22)

a and b, see Appendix C.

According to Equations (5.7 and 5.11) the tensile force in the fibre limited by friction is:

$$F_{AF} = \int_{s}^{s_E} \left\{ \left(\frac{-p}{1-E} \right) . \mu_{WF} + WF_0 \right\} . C_V \, dS \quad . . . . . (5.23)$$

where p = pressure normal to the fibres;

E = porosity

μ_{WF}, WF_0 = friction parameters for single fibre withdrawal;

C_V = correction factor for V-shaped migration path (see Appendix D); and

s = distance along the deformed fibre from its middle.

For the pressure, p, in Equation (5.23) the van Wyk pressure (T_{LV}) can be used here; it is assumed to be constant throughout an element.

The porosity E is defined as:

$$E = 1 - \frac{V_{\text{fibre}}}{V_{\text{sliver}}} \quad . . . . . (5.24)$$

In this equation V_{sliver} can be replaced by the volume of the element, which is related to V_{sp} by:

$$V_{\text{element}} = V_{sp} . FM$$

where FM is defined in Equation (5.19).

The volume of fibre within an element can be written as:

$$V_{\text{fibre}} = FM/1,31.$$

Equation (5.24) now becomes:

$$E = 1 - 1/1,31.V_{sp} \quad . . . . . (5.25)$$

Because V_{sp} is assumed to be constant throughout an element, so also will be E. As no parameter under the integral sign in Equation (5.23) is dependent on s within an element, F_{AF} at node i (see Fig. 5.10) can be written as: tensile force in the fibre

$$F_{AF_i} = \sum_{k=j}^{NEL} DL_{\underline{k}} . (-T_{LV_{\underline{k}}} . 1,31 . V_{sp_{\underline{k}}} . \mu_{WF} + WF_0) . C_V \quad . . . (5.26)$$

A representative value for F_{AF} within an element (F_{AF} is assumed to be constant throughout an element) is the average value at the adjacent nodes:

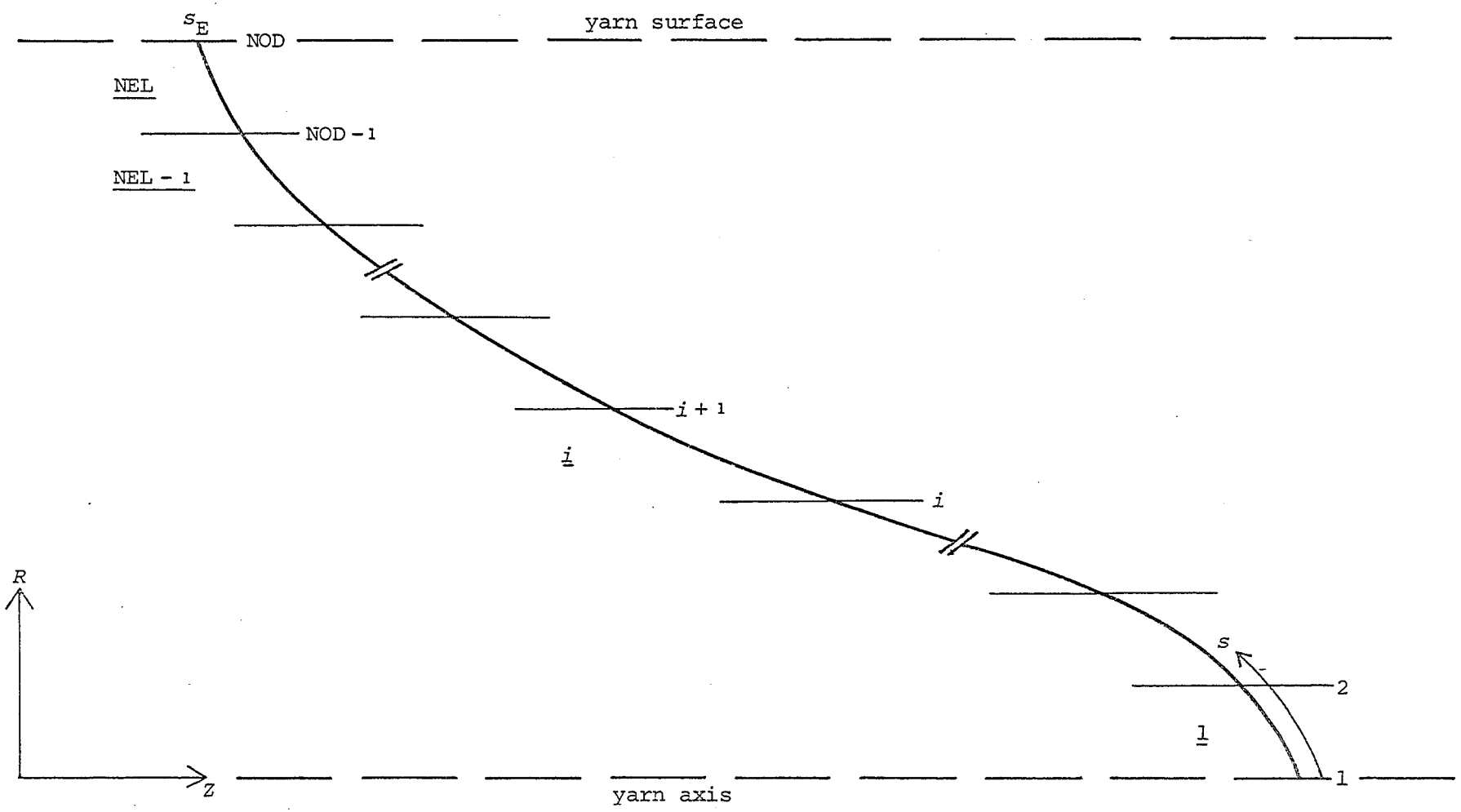

Fig. 5.10. V-shaped migration path with co-ordinate system along the fibre path

$$F_{AF_i} = \sum_{k=i+1}^{NEL} DL_k(-T_{LV_k}.1,31.V_{sp_k}.\mu_{WF} + WF_0).C_v + 0,5.DL_i(-T_{LV_i}.1,31.V_{sp_i}.\mu_{WF} + WF_0).C_v \quad . \quad . \quad . \quad (5.27)$$

This in turn leads to the recursive relationship:

$$F_{AF_i} = F_{AF_{i+1}} + 0,5.(DL_{i+1}(-T_{LV_{i+1}}.1,31.V_{sp_{i+1}}.\mu_{WF} + WF_0).C_v + DL_i(-T_{LV_i}.1,31.V_{sp_i}.\mu_{WF} + WF_0).C_v) \quad . \quad . \quad . \quad . \quad (5.28)$$

The axial stress T_A within an element is defined by (Equation 4.15):

$$T_A = F_A.N_f.(A'.\cos\alpha')^{-1} \quad . \quad . \quad . \quad . \quad . \quad . \quad . \quad . \quad . \quad . \quad (5.29)$$

where F_A is the minimum value of either F_{AF} or F_{AS} according to the theory discussed in Section 5.3.3.

5.4.5 Incremental Analysis

The governing equation discussed in Section 4.4.3, case (ii), is chosen here to formulate the equilibrium equations.

$$F_i = T_{LV_i} - T_{A_{i+1}}\left(1 - (R_{i+2}.R_{i+1}^{-1})\sin^2\alpha_{i+1}\right) - T_{LV_{i+1}}.(R_{i+2}.R_{i+1}^{-1})\sin^2\alpha_{i+1} \quad . \quad . \quad . \quad . \quad . \quad (5.30)$$

The incremental method with Newton-Raphson iteration is used (Equation 3.47) to solve the equilibrium equations:

$$\left[K_T(\{U\}^{k,\ell-1})\right].\{\Delta U\}^{k,\ell} = \{P\}^k - \{F(\{U\}^{k,\ell-i})\} \quad . \quad . \quad . \quad (5.31)$$

where k = increment number, and

ℓ = iteration number.

In this case the vector, $\{P\}$, only contains zeroes and can be deleted.

The tangent stiffness matrix is defined by Equation (3.37):

$$K_{T_{ij}} = \frac{\partial F_i(\{U\})}{\partial U_j} \quad . \quad . \quad . \quad . \quad . \quad . \quad . \quad . \quad . \quad . \quad (5.32)$$

The parameters involved in the formation of F and K_T in Equation (5.32) are all updated at each iteration by using $\{U\}^{k,\ell-1}$ for their evaluation. However, there are two basic parameters for which this is not feasible and these are only updated at each increment. These two are the original fibre length present in the element (FL) and the closely related element fibre mass (FM). As these are constant throughout

each increment their derivatives with respect to $\{U\}$ are considered to be zero. The effect on the analysis of not updating FM and FL at each iteration can be checked by running a few analyses with varying sizes of increment.

The procedure at the k-th increment is as follows. A value for $\{U\}$ is given at the start of the increment, this being the last calculated value in the previous increment. This is designated as $\{U\}^{k,0}$. Values are also given for $\{FL\}$ and $\{FM\}$ which have been calculated at the end of the previous increment and are designated by $\{FL\}^{k-1}$ and $\{FM\}^{k-1}$. In the k-th increment the yarn is given an incremental elongation of ΔE_y^k. The total yarn elongation (relative) is given by:

$$E_y^k = \sum_{m=1}^{k} \Delta E_y^m \qquad \ldots\ldots\ldots\ldots (5.33)$$

From the above equation and Equations (5.15, 5.16 and 5.17) it follows that:

$$DZ^k = DZ^0 . (1 + E_y^k) \qquad \ldots\ldots\ldots\ldots (5.34)$$

$$TT^k = TT^0 . (1 + E_y^k) \qquad \ldots\ldots\ldots\ldots (5.35)$$

$$\Delta Z_{\underline{i}}^k = \Delta Z_{\underline{i}}^0 . (1 + E_y^k) \qquad \ldots\ldots\ldots\ldots (5.36)$$

With the aid of the above-mentioned parameters, other parameters can be calculated such as $DL^{k,0}$, $V_{sp}^{k,0}$, etc., from which in turn the element stresses, $T_A^{k,0}$, $T_{LV}^{k,0}$, and their derivatives, can be calculated. For the stress T_A the minimum value of either F_{AF} or F_{AS} is used for each element and also the appropriate derivative is used.

On substituting these values in $\{F(\{U\}^{k,0})\}$ and $[K_T(\{U\}^{k,0})]$, Equation (5.31) can now be solved for $\Delta\{U\}^{k,1}$. $\{U\}^{k,1}$ is found by the equation:

$$\{U\}^{k,\ell} = \{U\}^{k,\ell-1} + \Delta\{U\}^{k,\ell} \qquad \ldots\ldots\ldots\ldots (5.37)$$

All the appropriate parameters are updated, $\{F(\{U\}^{k,1})\}$ and $[K_T(\{U\}^{k,1})]$ are found, and $\Delta\{U\}^{k,2}$ can be evaluated, etc. This process is stopped when $\Delta\{U\}^{k,\ell}$ or $\{F\}^{k,\ell}$ approaches zero. $\{FL\}$ and $\{FM\}$ are corrected at the end of the increment.

To explain the change in $FL_{\underline{i}}$ the imaginary tube which contains the fibre and the fibre itself are drawn as if they were straight lines in Figure 5.11. This is the situation at the start of increment k just before ΔE_y^k is applied. After ΔE_y^k has been applied and the new equilibrium configuration calculated the dimensions of the fibre and its tube

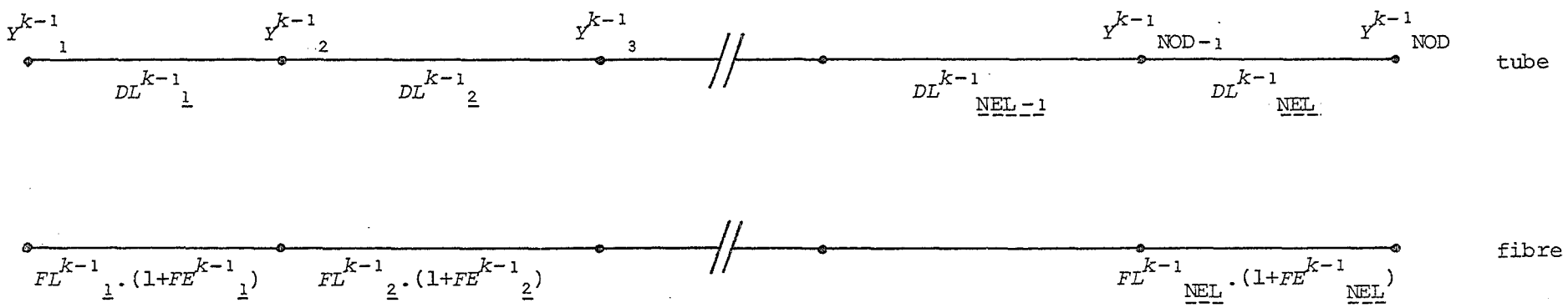

Fig. 5.11. Configuration of fibre and tube at the beginning of an increment

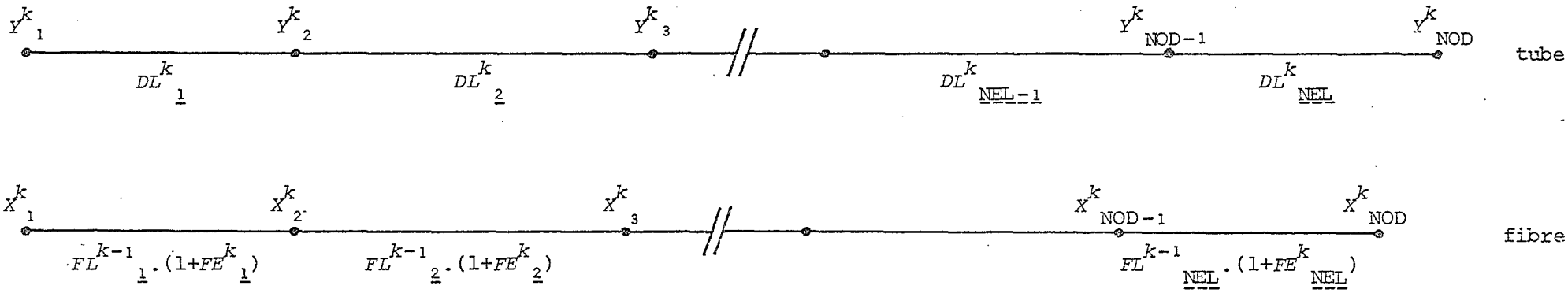

Fig. 5.12. Configuration of fibre and tube at the end of an increment

are as shown in Figure 5.12.

The vector $\{FE\}$ contains the elongations of the fibres due to either F_{AF} or F_{AS} and is defined by:

$$FE_{\underline{i}} = a' . F_{A_{\underline{i}}} + b' \qquad (5.38)$$

where a' and b' are elastic constants (see Appendix C), and

$F_{A_{\underline{i}}}$ is the minimum value of $F_{AS_{\underline{i}}}$ or $F_{AF_{\underline{i}}}$.

Two different co-ordinate systems are set up along the fibre and its tube, respectively X and Y. X_i and Y_i are defined by:

$$X^k_i = \sum_{m=1}^{i-1} \left\{ FL^{k-1}_{\underline{m}} (1 + FE^k_{\underline{m}}) \right\} \qquad (5.39)$$

$$Y^k_i = \sum_{m=1}^{i-1} DL^k_{\underline{m}} \qquad (5.40)$$

The co-ordinates Y_i correspond to the points on the tube at the element boundaries: Y_1 is at the yarn axis and Y_{NOD} at the yarn surface. The co-ordinates X_i correspond to points on the fibre which were situated at the element boundaries at the beginning of the increment before ΔE^k_y was applied. When slip has occurred at node i during the increment X_i will be smaller than Y_i. This assumes that the fibre always slips towards the middle of its tube. The amount of slip at node i during the increment k is defined as:

$$\Delta SL^k_i = Y^k_i - X^k_i \qquad (5.41)$$

A simple method is then used to correct $FL_{\underline{i}}$, see Figure 5.13. If X^k_i is equal to Y^k_i (no slip), then:

$$FL^k_{\underline{i}} = FL^{k-1}_{\underline{i}} + (Y^k_{i+1} - X^k_{i+1}) . (X^k_{i+2} - X^k_{i+1})^{-1} . FL^{k-1}_{\underline{i+1}} \qquad (5.42)$$

where left-hand side = length of unstressed fibre between Y^k_i and Y^k_{i+1};

first term of the right-hand side = length of unstressed fibre between X^k_i and X^k_{i+1}; and

second term of the right-hand side = length of unstressed fibre between X^k_{i+1} and Y^k_{i+1}.

Also:

$$FL^k_{\underline{i+1}} = (X^k_{i+2} - Y^k_{i+1}) . (X^k_{i+2} - X^k_{i+1})^{-1} . FL^{k-1}_{\underline{i+1}} + \\ + (Y^k_{i+2} - X^k_{i+2}) . (X^k_{i+3} - X^k_{i+2})^{-1} . FL^{k-1}_{\underline{i+2}} \qquad (5.43)$$

and so on.

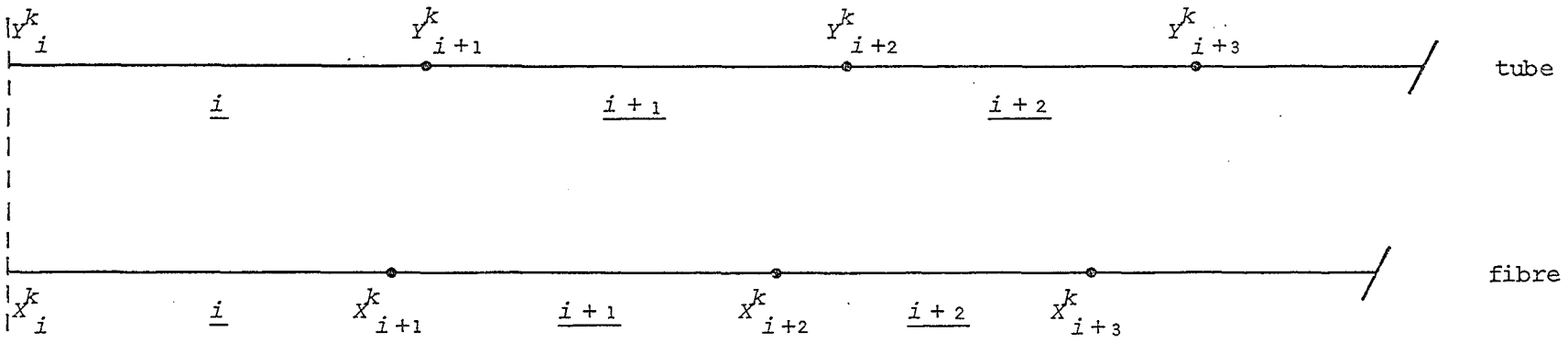

Fig. 5.13. Illustration of method for updating fibre configuration

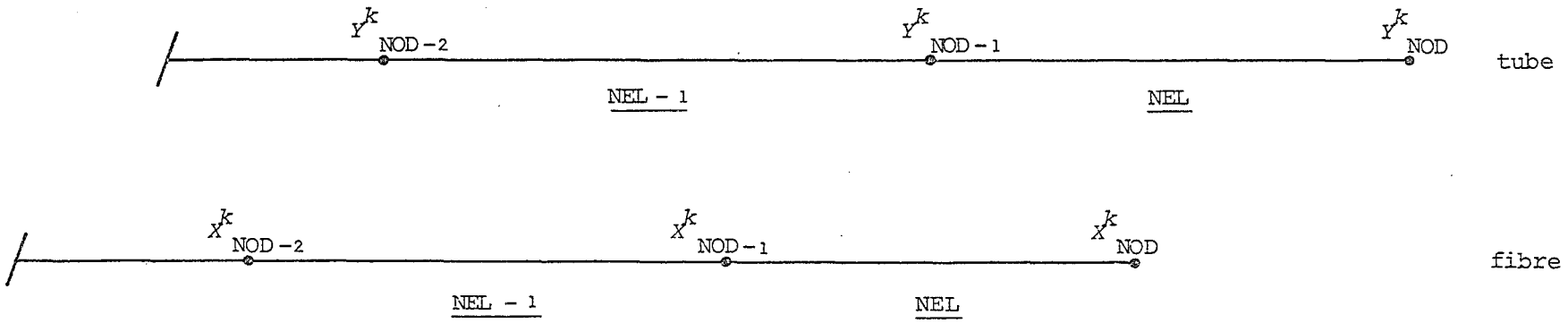

Fig. 5.14. Configuration of fibre and tube near their ends

The new value for the fibre mass present in element $\underline{j}$ can now be simply calculated by using Equation (5.19):

$$FM^{k}_{\underline{j}} = FL^{k}_{\underline{j}}.(R_f^2.\pi.1,31).2dZ.dF^{-1} \quad . \quad . \quad . \quad . \quad . \quad . \quad . \quad . \quad . \quad (5.44)$$

A problem arises in the element(s) near the yarn surface, see Figure 5.14. If $FL^{k}_{\underline{NEL}}$ is calculated according to Equation (5.42) as:

$$FL^{k}_{\underline{NEL}} = (X^{k}_{NOD} - Y^{k}_{NOD-1}).(X^{k}_{NOD} - X^{k}_{NOD-1}).FL^{k-1}_{\underline{NEL}} \quad . \quad . \quad (5.45)$$

then in the next increment $(k+1)$ the fibre elongation, E_f,

$$E_f = (DL_{\underline{i}} - FL_{\underline{i}}).FL_{\underline{i}}^{-1}$$

will be too high because $FL^{k}_{\underline{NEL}}$ obviously does not cover the whole length of the fibre tube in the outside element. Two methods are used to correct this. The first is to calculate $FL^{k}_{\underline{NEL}}$ as:

$$\begin{aligned} FL^{k}_{\underline{NEL}} &= (X^{k}_{NOD} - Y^{k}_{NOD-1}).(X^{k}_{NOD} - X^{k}_{NOD-1})^{-1}.FL^{k-1}_{\underline{NEL}} + \\ &+ (Y^{k}_{NOD} - X^{k}_{NOD}).(X^{k}_{NOD} - X^{k}_{NOD-1})^{-1}.FL^{k-1}_{\underline{NEL}} = \\ &= (Y^{k}_{NOD} - Y^{k}_{NOD-1}).(X^{k}_{NOD} - X^{k}_{NOD-1})^{-1}.FL^{k-1}_{\underline{NEL}} \quad . \quad (5.46) \end{aligned}$$

This situation corresponds with the idea that fibre material is drawn into the effective yarn zone from the ineffective 'hairy zone' (see the comment in Section 6.4).

The second method is to leave $FL^{k}_{\underline{NEL}}$ as calculated in Equation (5.45) and to correct $\Delta Z_{\underline{NEL}}$ for the next increment:

$$\Delta Z^{k+1}_{\underline{NEL}} = (X^{k}_{NOD} - Y^{k}_{NOD-1}).(\Delta Z^{k}_{\underline{NEL}})^{-1}.(1+E_y^{k+1}).(1+E_y^{k})^{-1}.$$

When the fibre has slipped out of the outer element completely, this element of course becomes ineffective and the process is repeated for the 'new' outer element. In both methods $FM^{k}_{\underline{NEL}}$ must be corrected appropriately.

5.4.6 Calculation of Yarn Forces

The simple stress-component method as described in Section 4.4.4 is used to calculate the yarn force due to the stresses T_A and T_L. However, in this case there is an extra amount necessary to pull the slipping fibres along one another. The virtual-work method is used to calculate this component of P:

$$P_{FR}.\delta U_y = \delta EN_{FR} \quad . \quad . \quad . \quad . \quad . \quad . \quad . \quad . \quad . \quad . \quad (5.47)$$

where P_{FR} = yarn force component due to friction;

δU_y = virtual elongation of the yarn (absolute); and

δEN_{FR} = energy dissipated in heat by friction due to the virtual elongation of the yarn, δU_y.

As $E_y = U_y/dZ$, dividing Equation (5.47) by dZ gives:

$$P_{FR}.\delta E_y = \delta EN_{FR}/dZ \quad \ldots\ldots\ldots\ldots \quad (5.48)$$

where δEN_{FR} is now due to δE_y.

Alternatively Equation (5.48) can be written as:

$$P_{FR} = \left(\frac{\partial EN_{FR}}{\partial E_y}\right).dZ^{-1} \quad \ldots\ldots\ldots\ldots \quad (5.49)$$

As EN_{FR} cannot be expressed as a continuous function of E_y, $\partial EN_{FR}/\partial E_y$ will have to be evaluated numerically. The simplest expression for a numerically evaluated derivative is (59):

$$f'(x) = 0,5.(f(x + \Delta x) - f(x - \Delta x)).\Delta x^{-1} \quad \ldots\ldots \quad (5.50)$$

Substituting in Equation (5.49) yields:

$$P_{FR}^{\ k} = 0,5.\{EN_{FR}.(E_y^{\ k} + \Delta E_y) - EN_{FR}.(E_y^{\ k} - \Delta E_y)\}.(\Delta E_y.dZ)^{-1} \quad (5.51)$$

As $EN_{FR}^{\ k+1} = EN_{FR}^{\ k} + \Delta EN_{FR}^{\ k+1}$,

where $\Delta EN_{FR}^{\ k+1}$ is the energy dissipated in heat due to friction during increment $(k + 1)$,

Equation (5.51) becomes:

$$P_{FR}^{\ k} = 0,5.(\Delta EN_{FR}^{\ k} + \Delta EN_{FR}^{\ k+1}).(\Delta E_y.dZ)^{-1} \quad \ldots\ldots \quad (5.52)$$

5.4.7 Energy Dissipated because of Friction

The same methodology as used in Section 5.3.2 and Appendix D is applied to explain the derivation of the energy dissipated in heat because of friction.

In the case of a symmetrical V-shaped migration path a small segment of fibre, dA will, if slip occurs, slip substantially with respect to approximately half the neighbouring fibres which are migrating in the opposite direction to dA. It will also slip with respect to the other half of the neighbouring fibres which are migrating in the same direction, but the amount of slippage will be negligible. The amount of slippage with respect to one another of neighbouring fibres migrating in opposite directions will be twice the amount which an individual fibre slips with respect to its tube.

Taking account of what is stated above and in Section 5.3.2, the amount of energy dissipated due to slippage between dA and its neighbouring fibres will be:

$$0,5.dA.\left|2\Delta SL\right|.\left(\frac{-p}{1-E}.\mu_{WF} + WF_0\right) \qquad (5.53)$$

where dA is the length of the fibre segment dA.

Over the length of the section of fibre present in element $\underline{i}$ the increment in dissipated energy will be:

$$0,5.\int_{Y_i}^{Y_{i+1}} \left|2.\Delta SL\right|.(-T_{LV_{\underline{i}}}.1,31.V_{sp_{\underline{i}}}.\mu_{WF} + WF_0)\,dY \qquad (5.54)$$

The total amount of energy dissipated due to friction in the model during increment k can now be written as:

$$\Delta EN_{FR}^{\ k} = \frac{dZ}{dF}.0,5.\sum_{i=1}^{NOD-1}\left\{\int_{Y^k_i}^{Y^k_{i+1}} \left|2.\Delta SL\right|.(-T_{LV}^{\ k}_{\underline{i}}.1,31.V_{sp}^{\ k}_{\underline{i}}.\mu_{WF} + WF_0)\,dY\right\} \qquad (5.55)$$

There are dZ/dF fibre halves which are migrating in the same direction as dA present in the model of length dZ. The other fibre halves which migrate in the opposite direction are not counted as they have already been accounted for.

In Equation (5.55) there is still one unknown, ΔSL, the incremental amount of slip of a point along the fibre with respect to its path. The amount of slip of the fibre at each node during an increment is given by Equation (5.41):

$$\Delta SL^k_{\ i} = Y^k_{\ i} - X^k_{\ i}.$$

The slip at any point between the nodes is assumed to be a linear function of Y from which follows:

$$\Delta SL^k = \Delta SL^k_{\ i} + (Y - Y^k_{\ i}).(\Delta SL^k_{\ i+1} - \Delta SL^k_{\ i}).(Y^k_{\ i+1} - Y^k_{\ i})^{-1} \qquad (5.56)$$

for $Y^k_{\ i} < Y < Y^k_{\ i+1}$.

As the assumptions now stand the fibre cannot reverse the slipping with respect to its path, so the modulus sign under the integral in Equation (5.55) can be deleted. The only parameter dependent on Y in Equation (5.55) is ΔSL and as this is linearly dependent the integration is easy and Equation (5.55) becomes:

$$\Delta EN_{FR}^{k} = \frac{dZ}{dF}.0,5.\sum_{i=1}^{NOD-1}(\Delta SL_{i}^{k} + \Delta SL_{i+1}^{k}).(-T_{LV\,\underline{i}}^{k}.1,31.V_{sp\,\underline{i}}^{k}.\mu_{WF} + WF_{0}) \times$$

$$\times (Y_{i+1}^{k} - Y_{i}^{k}) \qquad . . . . . (5.57)$$

Substituting this result into Equation (5.49) will yield the component of the total yarn force at increment k due to friction.

5.5 ANALYSIS OF A YARN WITH A COMPLEX FIBRE MIGRATION ENVELOPE (W-shape)

5.5.1 Introduction

In this Section a version of the staple-fibre yarn analysis is presented. This utilises a W-shaped migration path in which the fibre ends are also at the yarn surface. Although a W-shaped migration envelope does not resemble the irregular and complex real migration envelopes much more than a V-shaped one it is thought that a W could give a better representation of the actual yarn behaviour than a simple V. The main reason for this is the presence of a 'loop' in a W which is not present in a V-shaped migration envelope with the fibre ends at the yarn surface, see Figure 5.15. In the sense used here a loop is a section of the fibre path which extends from the yarn axis to the yarn surface and back to the yarn axis. Loops, or some form of loops, are present in most of the observed migration paths in real yarns.

The W-shaped migration envelope used here is 'double-symmetric', i.e., the envelope is symmetrical around its middle (M) and the left and right halves are also symmetrical with respect to their middles (M'), see Figure 5.15. This requirement can also be expressed as a condition for any two points A and B on the migration path:

$$\text{if} \quad R_A = R_B \quad \Rightarrow \quad |\partial R/\partial Z(R_A)| = |\partial R/\partial Z(R_B)| \ .$$

After deformation of the yarn the migration path is assumed to stay double-symmetrical.

As with the V-shaped migration envelope the behaviour of the fibre in this case is symmetrical about its middle, M, but it must be noted that the behaviour of either of the fibre halves on both sides of M will not necessarily be, and in most cases it will certainly not be, symmetrical about M'.

5.5.2 Finite-element Analysis

The model is subdivided into finite elements in the same way as in the 'V-analysis', and these are also numbered from the inside out-

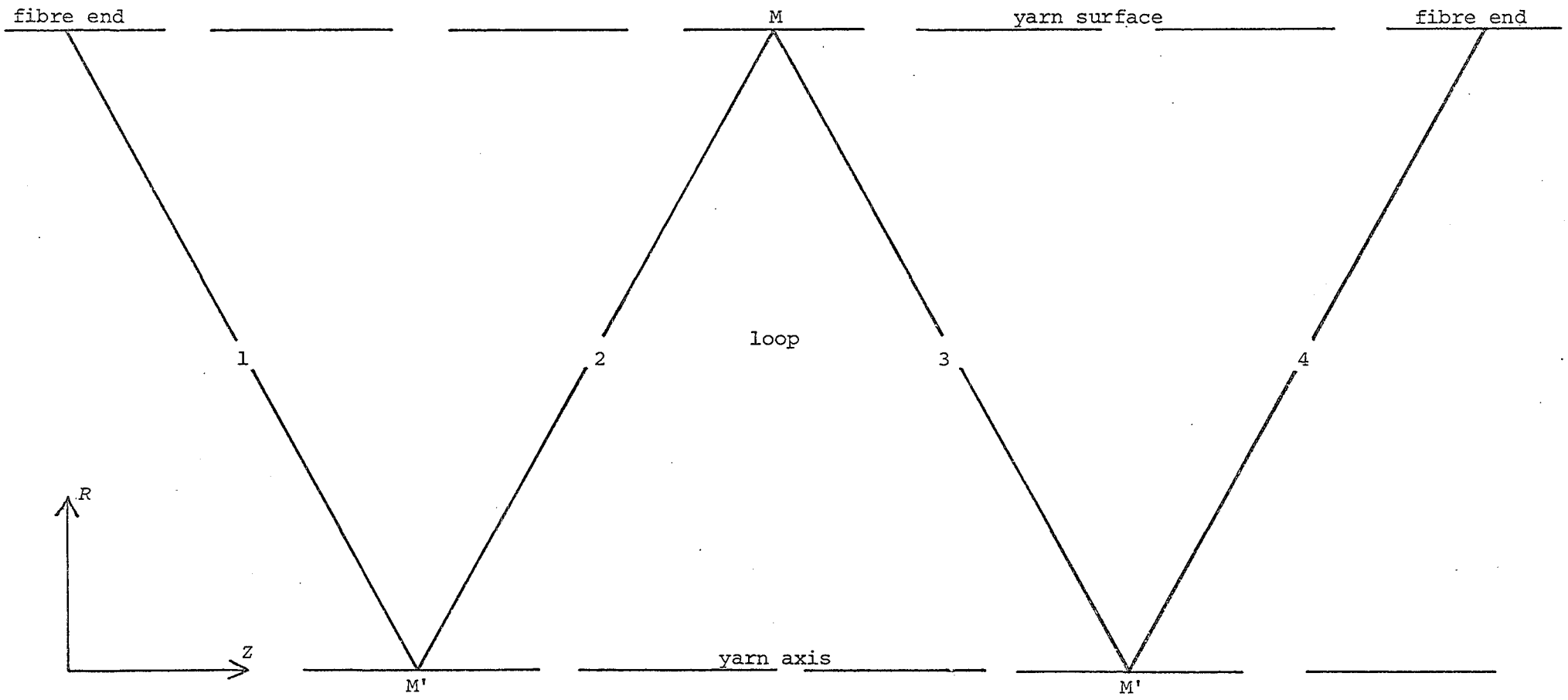

Fig. 5.15. W-shaped migration path

wards, see Figure 5.8. As mentioned before, the fibre paths are still double symmetrical after deformation, which implies that $\Delta Z_{\underline{i}}$ is equal on both sides of M'. This is also valid for $DL'_{\underline{i}}$ which is the length of tube between the entry and exit points in the element $\underline{i}$. However, the original length of fibre present in an element, $FL'_{\underline{i}}$, can be different for the inner and outer legs of the W owing to differences in slippage. The two values for $FL'_{\underline{i}}$ are distinguished by an extra superscript, I(nner) or O(uter) in front of $FL'_{\underline{i}}$. This system will also apply to other parameters which are different for the inner and outer legs. In the original configuration:

$$^{I}FL_{\underline{i}} = {}^{O}FL_{\underline{i}} = DL_{\underline{i}}.$$

The fibre mass present in element $\underline{i}$ is now defined as (Equation 5.19):

$$FM'_{\underline{i}} = 0{,}5.(^{I}FL'_{\underline{i}} + {}^{O}FL'_{\underline{i}}).(R_f^{\,2}.\pi.1{,}31).4.dZ.dF^{-1} \quad . \; . \; (5.58)$$

where the term at the end of Equation (5.19) is now $4.dZ.dF^{-1}$ because there are twice as many fibre segments present in an element with a W-shaped path.

The pressure in an element derived by a van Wyk-type relationship, $T_{LV_{\underline{i}}}$, is calculated in the same way as in Section 5.4.4, Equation (5.20).

The axial force in the fibre, F_A, is derived from the minimum of F_{AS} or F_{AF}, which are both different for the outer and inner legs of the W. Proceeding as in Section 5.4.4 we have:

$$^{I}F_{AS_{\underline{i}}} = a.{}^{I}E_{f_{\underline{i}}} + b \quad . \; . \; . \; . \; . \; . \; . \; . \; . \; . \; . \; . \; (5.59a)$$

$$^{O}F_{AS_{\underline{i}}} = a.{}^{O}E_{f_{\underline{i}}} + b \quad . \; . \; . \; . \; . \; . \; . \; . \; . \; . \; . \; . \; (5.59b)$$

where $^{I}E_{f_{\underline{i}}} = (DL'_{\underline{i}} - {}^{I}FL'_{\underline{i}}).(^{I}FL'_{\underline{i}})^{-1}$

and $^{O}E_{f_{\underline{i}}} = (DL'_{\underline{i}} - {}^{O}FL'_{\underline{i}}).(^{O}FL'_{\underline{i}})^{-1}$.

The tensile force in the fibre limited by friction, F_{AF}, is for the outer leg (Equation 5.28):

$$^{O}F_{AF_{\underline{i}}} = {}^{O}F_{AF_{\underline{i+1}}} + 0{,}5.\Big[DL'_{\underline{i+1}}(-T_{LV_{\underline{i+1}}}.1{,}31.V_{sp_{\underline{i+1}}}.\mu_{WF} + WF_0).{}^{O}C_W +$$

$$+ DL'_{\underline{i}}.(-T_{LV_{\underline{i}}}.1{,}31.V_{sp_{\underline{i}}}.\mu_{WF} + WF_0).{}^{O}C_W\Big] \quad . \; . \; . \; (5.60a)$$

$^{I}F_{AF_{\underline{1}}}$ is equal to:

$$ {}^{I}F_{AF_1} = {}^{O}F_{AF_1} + 0,5.\left[DL'_1.(-T_{LV_1}.1,31.V_{sp_1}.\mu_{WF} + WF_0).{}^{O}C_W + \right. $$

$$ \left. + DL'_1.(-T_{LV_1}.1,31.V_{sp_1}.\mu_{WF} + WF_0).{}^{I}C_W\right] \quad . \; . \; . \; (5.60b) $$

For the other elements ${}^{I}F_{AF}$ is:

$$ {}^{I}F_{AF_i} = {}^{I}F_{AF_{i-1}} + 0,5.\left[DL'_{i-1}.(-T_{LV_{i-1}}.1,31.V_{sp_{i-1}}.\mu_{WF} + WF_0).{}^{I}C_W + \right. $$

$$ \left. + DL'_i.(-T_{LV_i}.1,31.V_{sp_i}.\mu_{WF} + WF_0).{}^{I}C_W\right] \quad . \; . \; . \; (5.60c) $$

The correction factors ${}^{I}C_W$ and ${}^{O}C_W$ are derived in Appendix D. The actual tensile force in the fibre is found by:

$$ {}^{O}F_{A_i} = \text{minimum}({}^{O}F_{AS_i}, {}^{O}F_{AF_i}) \quad . \; . \; . \; . \; . \; . \; . \; . \; . \; (5.61a) $$

$$ {}^{I}F_{A_i} = \text{minimum}({}^{I}F_{AS_i}, {}^{I}F_{AF_i}) \quad . \; . \; . \; . \; . \; . \; . \; . \; . \; (5.61b) $$

The axial stress in the element, T_A, is defined by averaging the stresses in the inner and outer legs, see Equation (5.29).

$$ T_{A_i} = 0,5.({}^{O}F_{A_i} + {}^{I}F_{A_i}).N_f.(A'.\cos\alpha')^{-1} \quad . \; . \; . \; . \; . \; (5.62) $$

The incremental analysis proceeds in the same way as discussed in Section 5.4.5. The determination of ${}^{I}FL$ and ${}^{O}FL$ is along the same lines as the determination of FL, but the administration is more complex. The two co-ordinate systems, X and Y, start at M and go along both the inner and outer legs of the W. The situation at the end of increment k is illustrated in Figure 5.16. The co-ordinate Y_1 is at the yarn surface (M), Y_{NOD} is at the yarn axis (M'), and Y_{NOD2-1} is at the yarn surface. X^k_i and Y^k_i are defined by:

$$ X^k_i = \sum_{m=1}^{i-1}\left({}^{I}FL^{k-1}_{\underline{j}}.(1 + {}^{I}FE^{k}_{\underline{j}})\right) \quad \text{for } i = 1 \rightarrow NOD;\ \underline{j} = NEL - m + 1 $$

$$ X^k_i = \sum_{m=NOD}^{i-1}\left({}^{O}FL^{k-1}_{\underline{j}}.(1 + {}^{O}FE^{k}_{\underline{j}})\right) + X^k_{NOD} \quad \text{for } i = NOD + 1 \rightarrow NOD2 - 1,\ \underline{j} = m - NEL $$

$$ Y^k_i = \sum_{m=1}^{i-1} DL^k_{\underline{j}} \quad \text{for } i = 1 \rightarrow NOD;\ \underline{j} = NEL - m + 1 $$

$$ Y^k_i = \sum_{m=NOD}^{i-1} DL^k_{\underline{j}} \quad \text{for } i = NOD + 1 \rightarrow NOD2 - 1;\ \underline{j} = m - NEL $$

where NOD2 = 2.NOD.

The method for correcting ${}^{O}FL$ and ${}^{I}FL$ after each increment is further very much the same as described in Section 5.4.5.

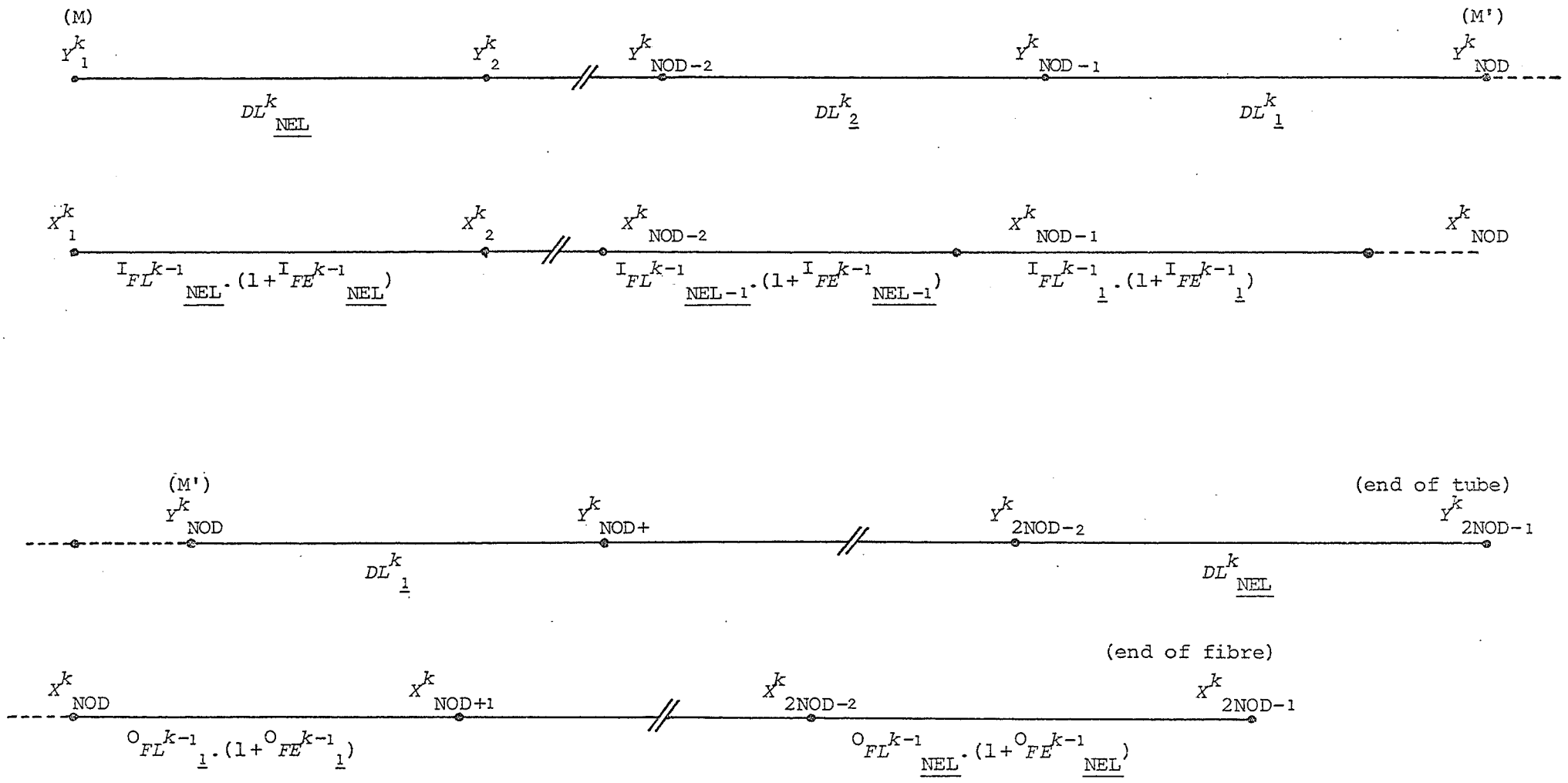

Fig. 5.16. Configuration of tube and fibre at the end of the kth increment (W)

5.5.3 Calculation of Yarn Forces

The same method is used for calculating the yarn forces as was described in Section 5.4.6. The derivation of the amount of energy dissipated into heat because of friction is also basically the same though somewhat more complex.

The increment of slippage between a fibre and its tube at the nodes is given by Equation (5.41):

$$\Delta^{I}SL^{k}_{i} = Y^{k}_{m} - X^{k}_{m} \qquad m = NOD - i + 1 \qquad (5.63a)$$

$$\Delta^{O}SL^{k}_{i} = Y^{k}_{m} - X^{k}_{m} \qquad m = NOD + i - 1 \qquad (5.63b)$$

For any point between the nodes the amount of slip is assumed to be a linear function of Y, see Equation (5.56).

In Figure 5.15 the legs of the W-shaped migration path are numbered from 1 to 4. The increment of slippage at a certain radius is designated by $\Delta^{O}SL$ and $\Delta^{I}SL$ which is illustrated in Figure 5.17. As pointed out in Appendix D, this pattern of slipping where the slippage of the fibre in its tube is always towards the middle of the W (M) and decreases with increasing distance from the fibre end follows from the conditions set out in Section 5.3.3. In the actual analyses there are some difficulties concerning this rule and these are discussed in Section 6.4.

The increment of slippage at a certain radius of the yarn between the legs of the W-shaped fibres is as follows:

between legs 1 and 2	$\Delta^{O}SL - \Delta^{I}SL$
" 1 and 3	$\Delta^{O}SL + \Delta^{I}SL$
" 1 and 4	$\Delta^{O}SL + \Delta^{O}SL$
" 2 and 3	$\Delta^{I}SL + \Delta^{I}SL$
" 2 and 4	$\Delta^{I}SL + \Delta^{O}SL$
" 3 and 4	$\Delta^{O}SL - \Delta^{I}SL$.

As discussed in Appendix D the frictional force per unit length exerted on a segment of fibre situated in leg x by all the neighbouring fibres which belong to leg y ($x \neq y$) is approximately one-quarter of the single-fibre withdrawal force.

Using the same procedures as described in Section 5.4.7 and Equations (5.56, 5.63 and 5.2) the amount of energy dissipated into heat due to friction throughout the whole yarn model is defined by:

$$\Delta EN_{FR}^{k} = \frac{dZ}{dF} \cdot \sum_{i=1}^{NOD-1} \left(0{,}75 \cdot (\Delta^{O}SL^{k}_{i} + \Delta^{O}SL^{k}_{i+1}) + 0{,}25 \cdot (\Delta^{I}SL^{k}_{i} + \Delta^{I}SL^{k}_{i+1}) \right) \times$$

$$\times \left(- T^{k}_{LV\,\underline{i}} \cdot 1{,}31 \cdot V^{k}_{sp\,\underline{i}} \cdot \mu_{WF} + WF_{0} \right) \cdot (Y^{k}_{NOD+i} - Y^{k}_{NOD+i-1}) .$$

Substituting this equation into Equation (5.49) yields the component of the total yarn force due to friction.

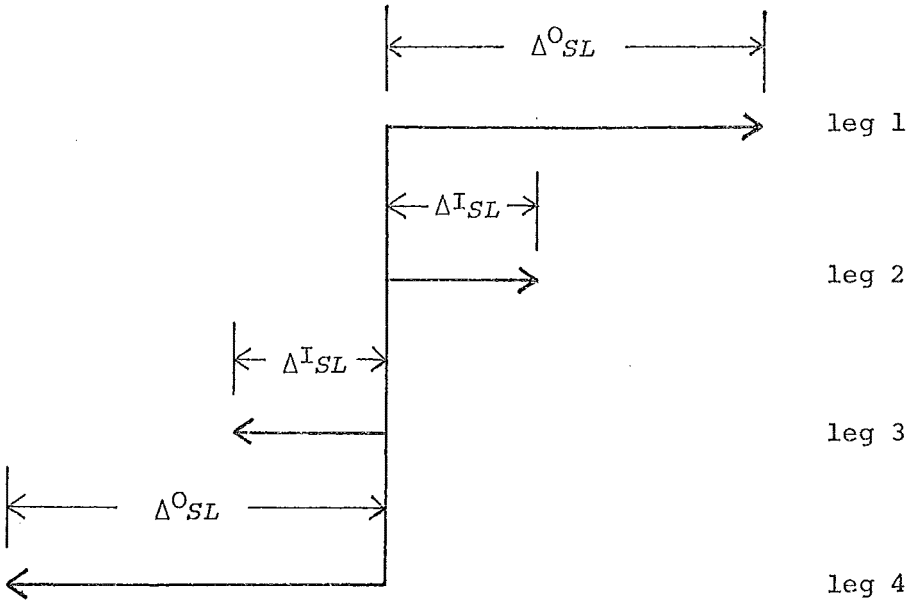

Fig. 5.17. Slippage per increment of each leg of the W

CHAPTER 6

RESULTS AND DISCUSSION

6.1 INTRODUCTION

A number of special semi-worsted yarns were spun at WRONZ to evaluate the analyses presented in the previous chapters. These yarns were made from single lines of wool, i.e., there was no blending, to reduce the fibre types in each yarn. The three wools used were Cheviot, Romney, and Lincoln/Leicester, which are respectively very crimpy, moderately crimpy, and almost straight (8). Two yarns with identical linear densities but different twist levels were manufactured from each wool type. In addition two heavier Romney yarns were spun, also at different twist levels.

Following Carnaby's method the results of the continuous-filament yarn analysis were compared with experimental results from short-gauge (25 mm) tests. The results of long-gauge yarn tests were used for the evaluation of the staple-fibre yarn analysis. The gauge length was taken sufficiently long (400 mm) to ensure that the fibres in the middle part of the segment of yarn being tested were not gripped by either of the jaws of the testing machine.

6.2 MANUFACTURING AND TESTING OF YARNS AND FIBRES

The experimental yarns were manufactured on the semi-worsted system. The only problem encountered was with the carding of the Lincoln wool as the web was extremely weak, but a sliver could be made with some care. Two different Romney slivers were made by using different draft settings on the gillbox, one of 12 ktex and the other of 6 ktex. Only one 6-ktex sliver was made from each of the Cheviot and Lincoln wools and two yarns were spun from each sliver. The nominal and measured twist levels and linear densities are given in Table 6.1.

The stress-strain curves of the yarns were determined on an Instron tensile-testing machine by elongating the yarns at a fixed rate of extension. The rate of extension was chosen so that the relative rate of elongation was the same for both gauge lengths. Fifty specimens of each yarn were tested and the average stress-strain curve was determined by the method described in Appendix E. As pointed out in (1) the stress-strain curve to be used in the comparisons with the theoretical results is not the average curve but a single experimental curve of

Table 6.1 NOMINAL AND ACTUAL YARN PARAMETERS

Wool	A B	C	D	E
Romney	300/100	111	268	272
Romney	300/180	200	285	280
Romney	600/ 80	103	595	575
Romney	600/130	145	617	596
Cheviot	300/100	113	299	283
Cheviot	300/180	199	313	302
Lincoln	300/100	106	281	279
Lincoln	300/180	194	283	287

A = nominal linear density of yarn, *tex*

B = nominal twist of yarn, *turns/m*

C = actual twist of yarn, *turns/m*

D = actual linear density of yarn, *tex*

E = linear density of yarn, calculated using the cross-sectional density, *tex*

which the initial modulus, the breaking load, and the extension at break are close to the average values. This is done because the characteristic shape of the experimental yarn stress-strain curve is often blurred by averaging.

The experimental results will be biased towards the strength of the weakest part of the tested yarn segment in contrast to the theoretical results which will be biased towards the average strength along the length of the segment. To diminish the influence of this anomaly in the model the tested yarn segment was carefully chosen so that no obvious weak spots were included. This method is of course quite arbitrary but a check between the averages of 20 selected segments and 20 random segments showed a small difference in breaking load and extension at break. The most significant difference, however, was between the standard deviations; the figure for the random segments was twice that for the selected specimens.

The results of the tests are shown in Figures 6.1 a - d. One obvious feature is the weakness of the low-twist yarns at long gauge lengths - they all exhibited moderate to extreme (Lincoln 300/100) drafting, i.e., these yarns failed after a relatively short extension due to loss of cohesion between the fibres. This was as expected, but perhaps surprising is the fact that the initial moduli of these low-twist yarns when tested at long gauge lengths were approximately identical to the short-gauge moduli of the corresponding yarns. There was also no significant difference between the initial moduli of the low-twist and high-twist yarns spun from the same sliver whether tested at a short gauge or a long gauge.

The stress-strain relationship of the fibres in the axial direction was determined and averaged in the same way as with the yarns. The gauge length used was 24 mm and 50 specimens of each wool type were taken. Because of the much lower forces involved and the method of mounting the fibres in the jaws of the testing machine (see Appendix E) it can safely be assumed that there was no significant slipping of the fibres in the jaws. For use in the analyses the stress-strain curves are approximated by a piecewise linear function (see Appendix C). These approximations are shown together with the experimental yarn curves in Figures 6.1 a - d.

Compression tests on slivers of each wool type were carried out as described in Appendix F for the determination of the parameters in the van Wyk relationship. Ten specimens of each wool type were tested;

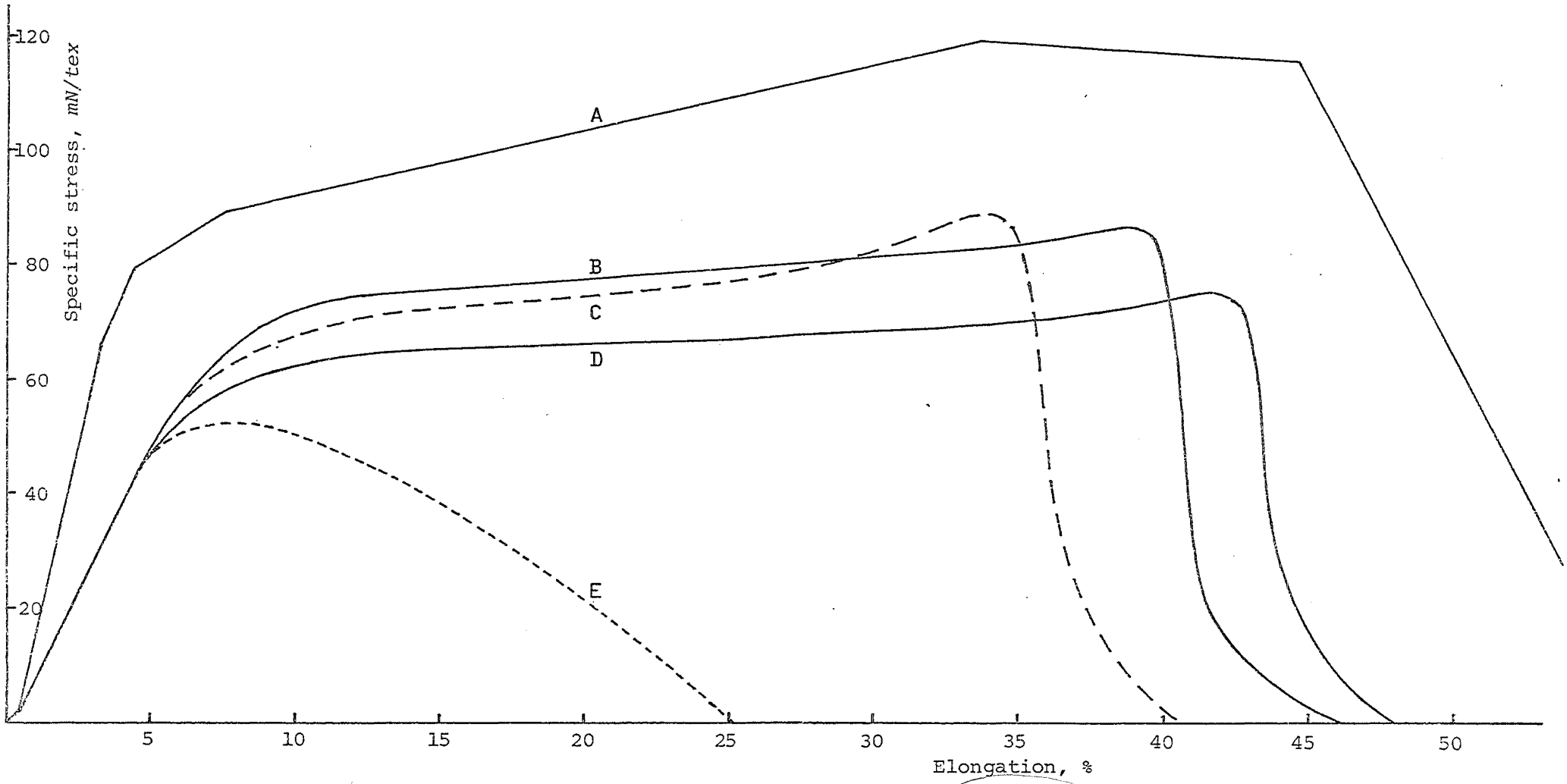

Fig. 6.1a. Romney 300 tex; experimental A = Romney fibre; B = Romney 300 tex/180, short gauge (25 mm); C = Romney 300 tex/180, long gauge (400 mm); D = Romney 300 tex/100, short gauge; E = Romney 300 tex/100, long gauge

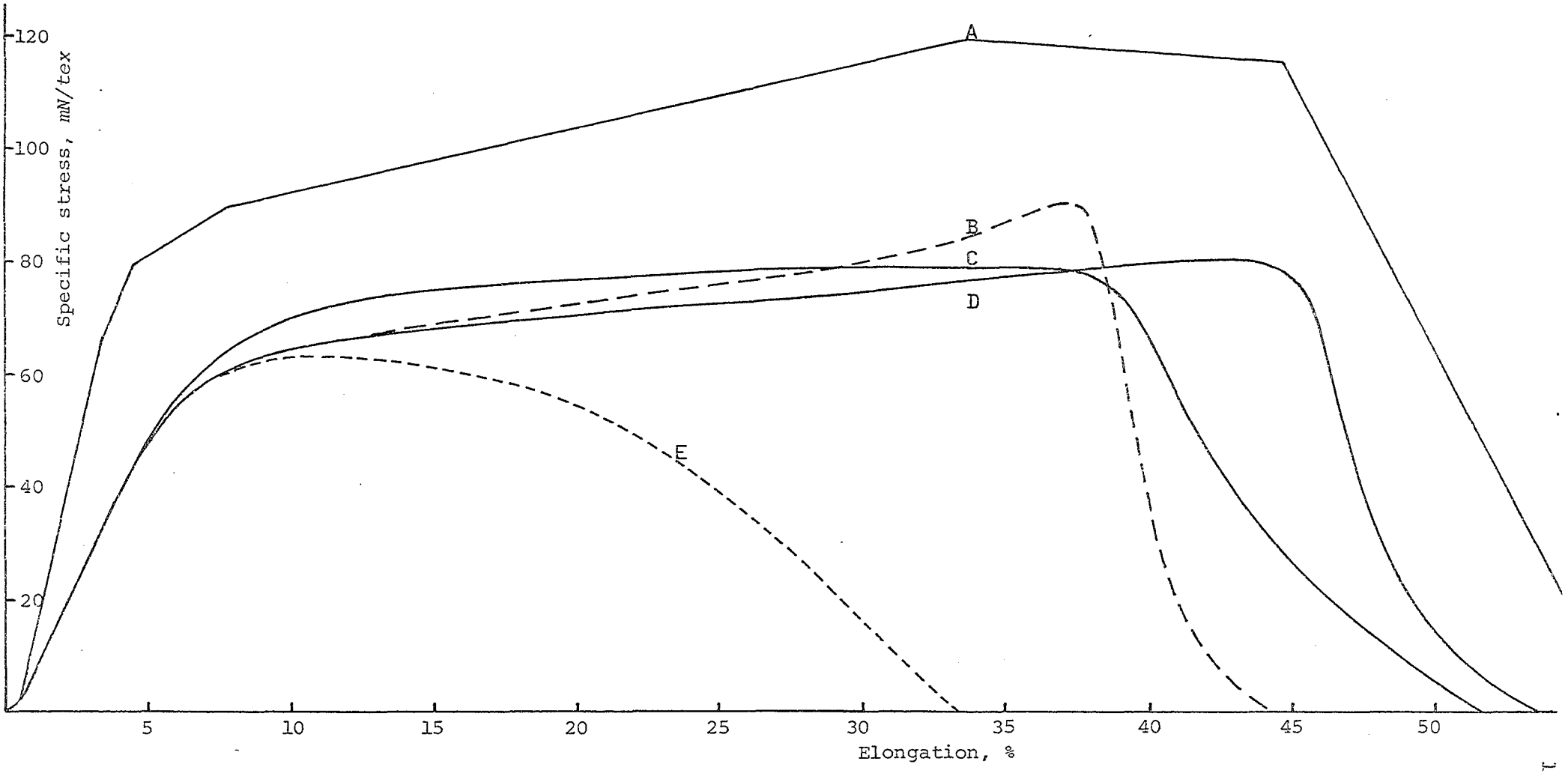

Fig. 6.1b. Romney 600 tex; experimental A = Romney fibre; B = Romney 600 tex/130, long gauge (400 mm); C = Romney 600 tex/80, short gauge (25 mm); D = Romney 600 tex/130, short gauge; E = Romney 600 tex/80, long gauge

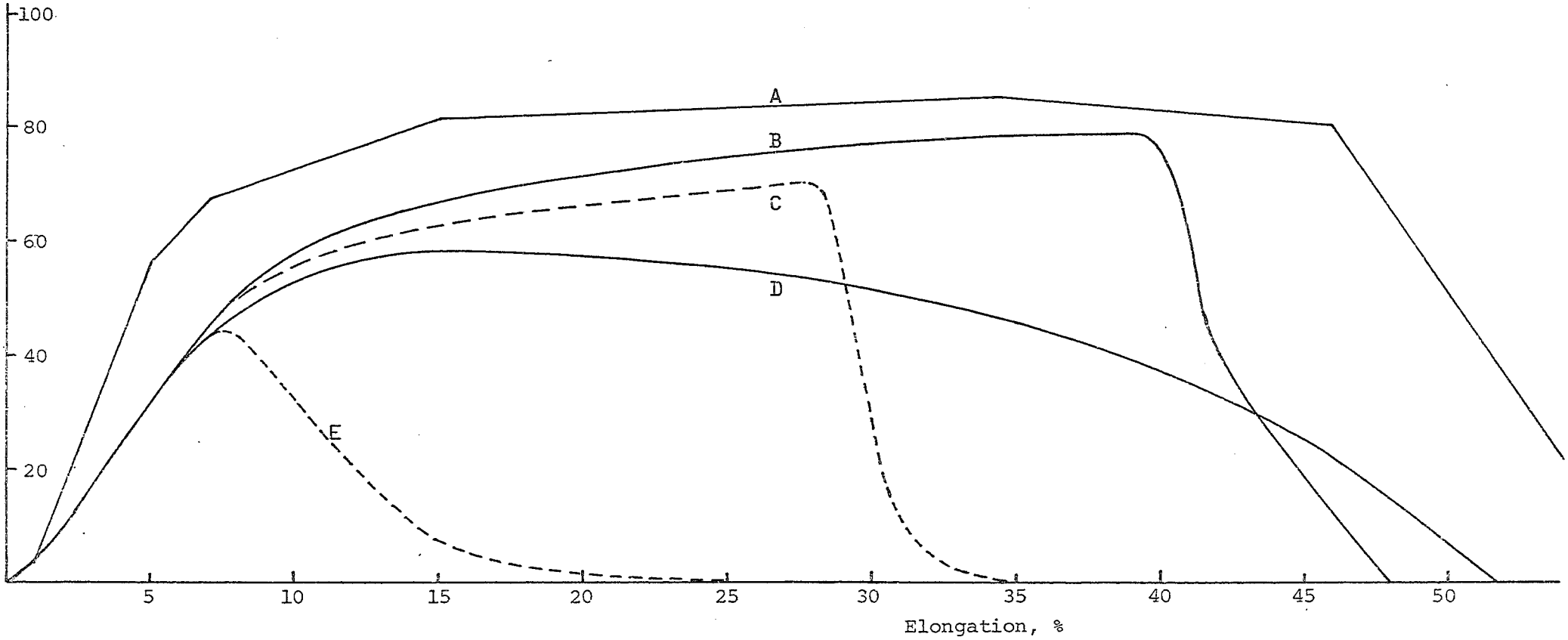

Fig. 6.1c. Cheviot 300 tex; experimental A = Cheviot fibre; B = Cheviot 300 tex/180, short gauge (25 mm); C = Cheviot 300 tex/180, long gauge (400 mm); D = Cheviot 300 tex/100, short gauge; E = Cheviot 300 tex/100, long gauge

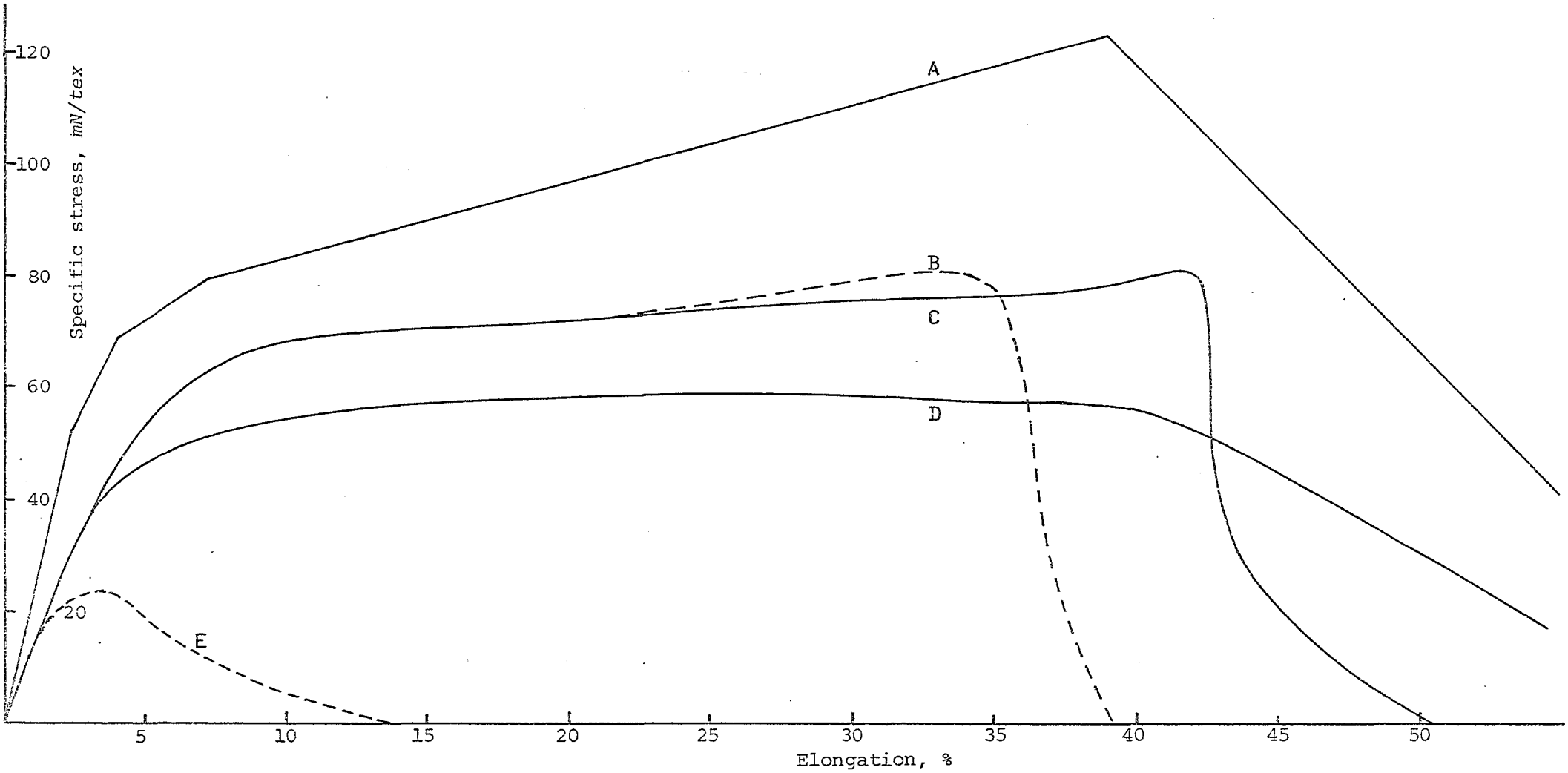

Fig. 6.1d. Lincoln 300 tex; experimental A = Lincoln fibre; B = Lincoln 300 tex/180, long gauge (400 mm); C = Lincoln 300 tex/180, short gauge (25 mm); D = Lincoln 300 tex/100, short gauge; E = Lincoln 300 tex/100, long gauge

the average values of K for each wool type are given in Appendix H together with the other data necessary for the analyses.

The cross-sectional density of the yarns was determined by the cross-section method (see Section 2.2.3). Some difficulties were encountered in trying to find a suitable resin. The recipe given by Carnaby (4) did not set for unknown reasons while others set too quickly. The most suitable of the resins tried, although not perfect for this particular application, was 'Selley's' brand polyester resin containing 33 % styrene, which is used with a hardener containing 50 % cyclohexanone peroxide (the other ingredients of both the resin and the hardener are not known). The timing of the cutting of the cross-section slices was quite critical, the best time being between about three and four hours after preparation. If the cutting was done earlier the blade of the microtome would push the fibres sideways a short distance in the resin which was still too soft, before cutting the fibres. If the resin was left to set for more than four hours the sample would be too hard and brittle and it would shatter under the force exerted by the microtome blade. The most suitable thickness of the cross-section slices both for observing and cutting was in this case 50 µm. The cross-section densities of the yarns are given in Appendix H. On the basis of these figures and the yarn twist a value for the yarn weight can be calculated. This can be used as a simple check for the correctness of the cross-section density by comparing the calculated weight with the directly measured weight. Both weights are given in Table 6.1.

6.3 CONTINUOUS-FILAMENT YARN ANALYSES

The energy-analysis version of the continuous-filament yarn analysis, which is the formal version, was used for the analyses carried out here as discussed in Section 4.3. The yarn model was subdivided into concentric elements 0,0625 mm wide, corresponding to the zones used, for the determination of the cross-section density of the yarns. As with the previous analyses it was assumed that the internal stresses in the undeformed yarn were zero. This was accomplished in the case of the lateral pressure by setting V_{sp_0} in the van Wyk relationship (Equation 4.16) to the value of V_{sp} as measured in the original configuration.

The actual analyses were straightforward and there were no problems except with the Lincoln 300/100. The results for this yarn could not be obtained because the iterative process used to obtain the solution would not converge under any circumstances. As discussed further on in

Section 6.6.1 the difference between a staple-fibre yarn analysis with high values for μ_{WF} and WF_0 and a continuous-filament yarn analysis for the same yarn is negligible. Therefore in this particular case the results of the staple-fibre yarn analysis were used and, perhaps surprisingly, did not exhibit any numerical difficulties. The data used in the analyses are collected in Appendix H.

6.4 STAPLE-FIBRE YARN ANALYSIS

The staple-fibre yarn model is subdivided into finite elements in the same way as in the previous Section and the same data are used. The extra data necessary are the average fibre length and the two parameters in the single-fibre withdrawal relationship, μ_{WF} and WF_0. The analytical expression for the migration path can be derived from the average fibre length and the cross-section density of each yarn (Appendix B). All the relevant data for the staple-fibre yarn analyses are collected in Appendix H.

The W-shaped migration path is utilised for all the analyses the results of which are compared with the experimental results. Only a few analyses were run with the V-shaped path, mainly to investigate the influence of the shape of the migration path on the results.

As the outer elements of all the yarns contained very few fibres these elements were not used in the analyses. They were, however, incorporated into the calculation of the linear density of the yarns and of the migration paths. Figure 6.2 shows how this was done. The elements where the path is shown with a broken line were not used in the analysis and they are considered to form the 'hairy region' of the yarn as defined by Carnaby (4). When the fibres slip in their tubes the extra length of fibre necessary to keep the tubes filled can come from these ineffective outer elements. It must be noted that these elements are really ineffective in contrast to the 'ineffective layer' as introduced by Holdaway (26) which actually had a significant effect on the yarn behaviour. Several analyses were run with a different number of effective elements and showed no significant difference as long as only the sparsely occupied elements were ignored.

As in the continuous-filament yarn analyses the internal stresses in the undeformed yarns were assumed to be zero. The correctness and implications of this assumption are discussed in Section 6.6.3.

The actual analyses were troubled by many numerical problems, most of which were concerned with convergence. However, the main problem

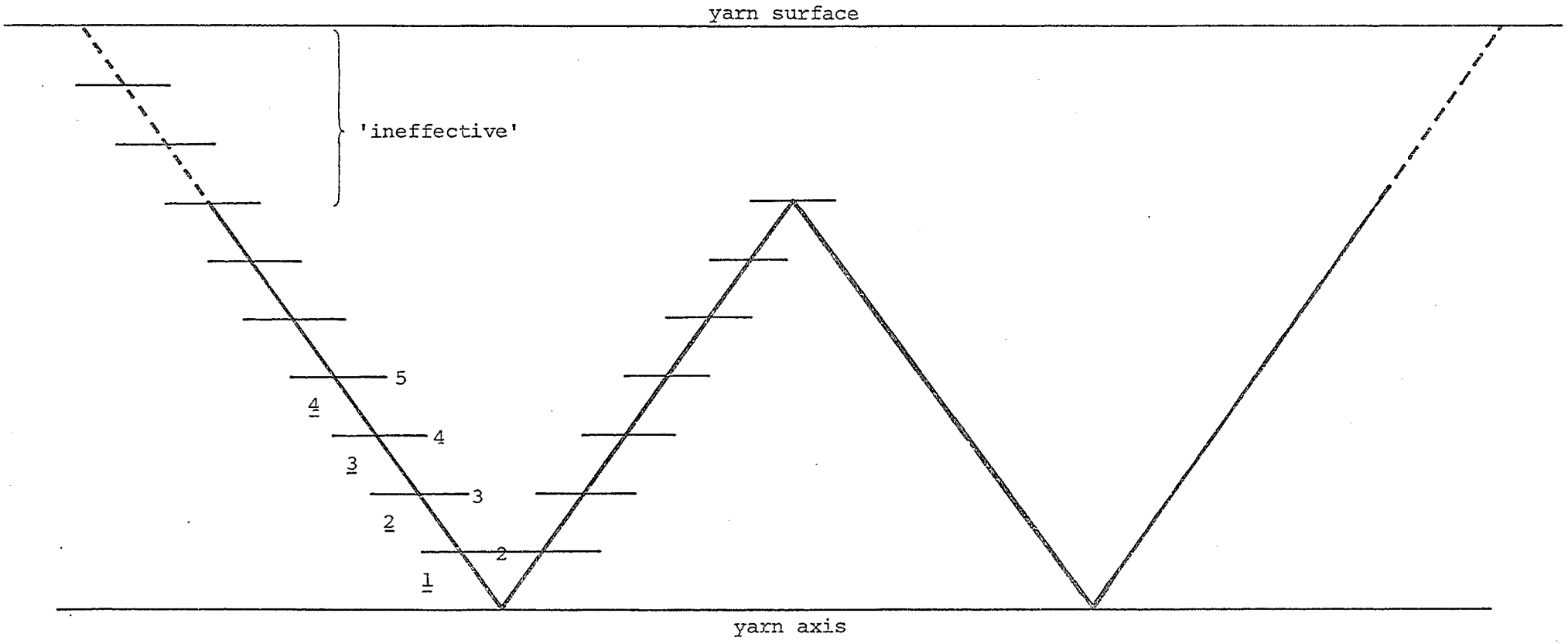

Fig. 6.2. W-shaped migration envelope with ineffective outer layer

was concerned with the determination of the fibre axial force, and is discussed in Section 5.3.3. Three typical problem situations are shown in Figures 6.3 a - c. The two curves shown in each Figure are F_{AS} and F_{AF}, the potential fibre axial force due to the yarn elongation, and the potential axial force due to friction respectively. In these situations F_A cannot be determined by the simple method of taking the minimum of F_{AF} and F_{AS} because the conditions for its use are not met. The only simple way of getting around the problems illustrated in Figures 6.3 a and b is to ignore the conditions and use the minimum method anyway. Fortunately this kind of situation only occurred in the first increment of an analysis; in later increments F_{AF} and F_{AS} would take on different forms because of slip and these caused no more problems. A typical situation for a later increment is shown in Figure 6.3d. The problem in Figure 6.3c was solved in a different way by assuming that R_1, the inner radius of the inner element, which is usually zero, has some positive non-zero value and did not change during deformation. This would take the 'dip' out of the F_{AS} curve.

6.5 EVALUATION AND DISCUSSION OF THE CONTINUOUS-FILAMENT YARN ANALYSIS

6.5.1 General

The theoretically obtained results from the continuous-filament yarn analysis are shown in Figure 6.4 together with the short-gauge experimental results. The general conclusion on looking at these Figures is that the initial part of the theoretical curves compares favourably with the curves obtained experimentally but at higher strain levels the stresses predicted theoretically are too high. Also the predicted strain level at which the yarn stress decreases is too high. One notable exception is the Cheviot 300/180, in which case the predicted curve matches the experimental curve well.

However, it must also be noted that the data for the analyses of the Cheviot yarns are the least reliable of the three wool types, especially the yarn cross-section density, as the Cheviot yarns and fibres were particularly irregular in behaviour and geometry.

One striking feature of all the comparisons, with the above exception, is the consistency of the discrepancy between theory and experiment, which can be roughly expressed in graphical form as shown in Figure 6.5. Because of the consistency of the difference between theory and experiment it is likely that there are one or more common factors causing the difference - random factors such as mistakes in the

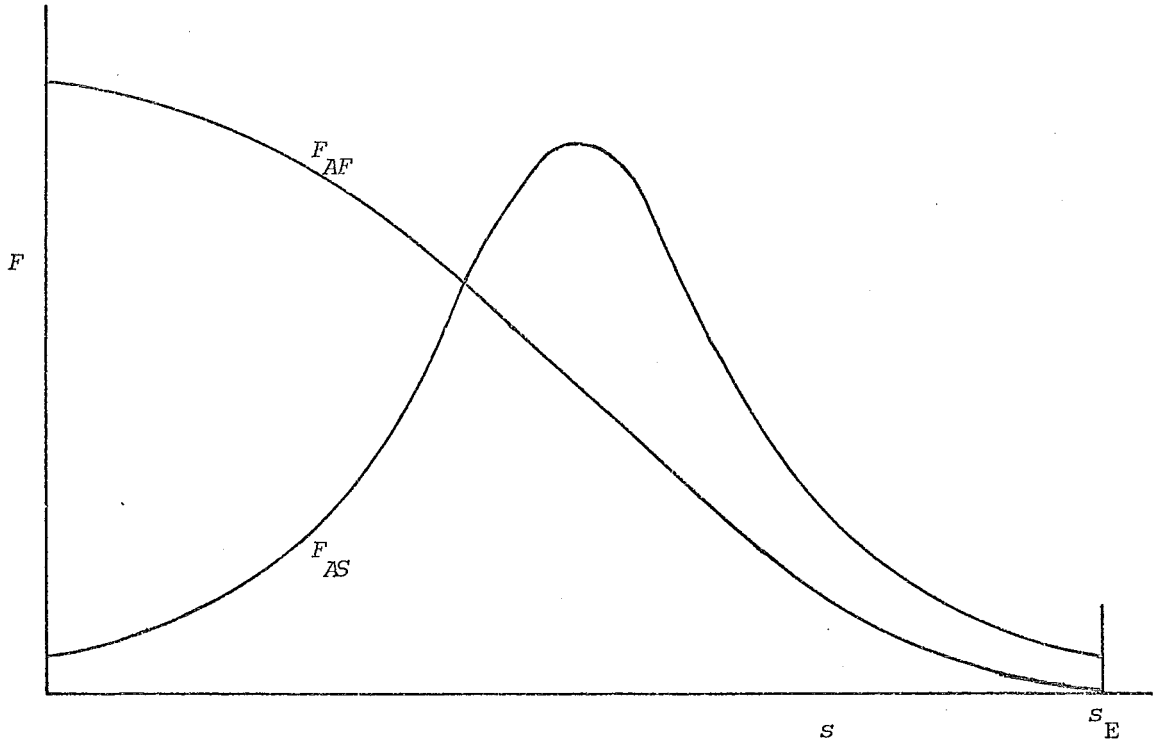

Fig. 6.3a. 'Simple' solution cannot be applied

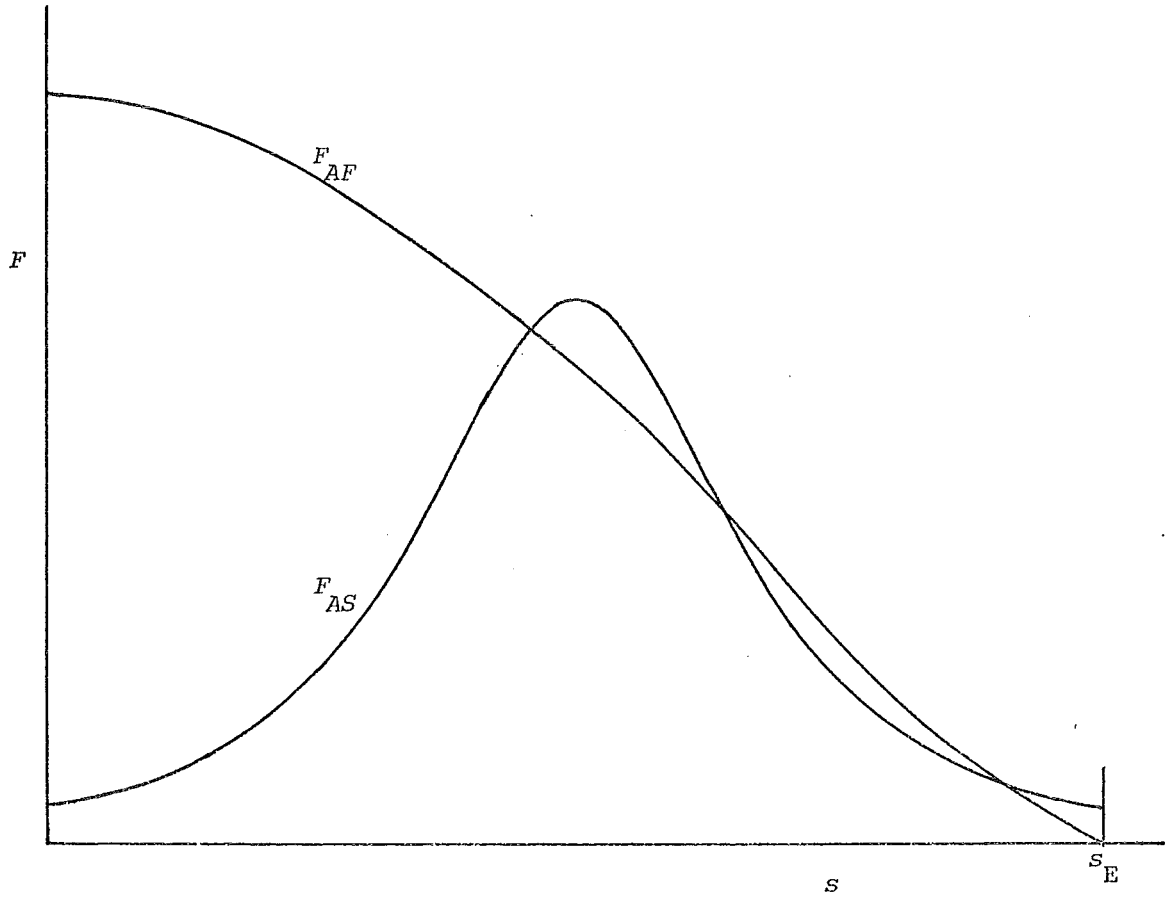

Fig. 6.3b. 'Simple' solution cannot be applied

Fig. 6.3. Configuration of the friction problem

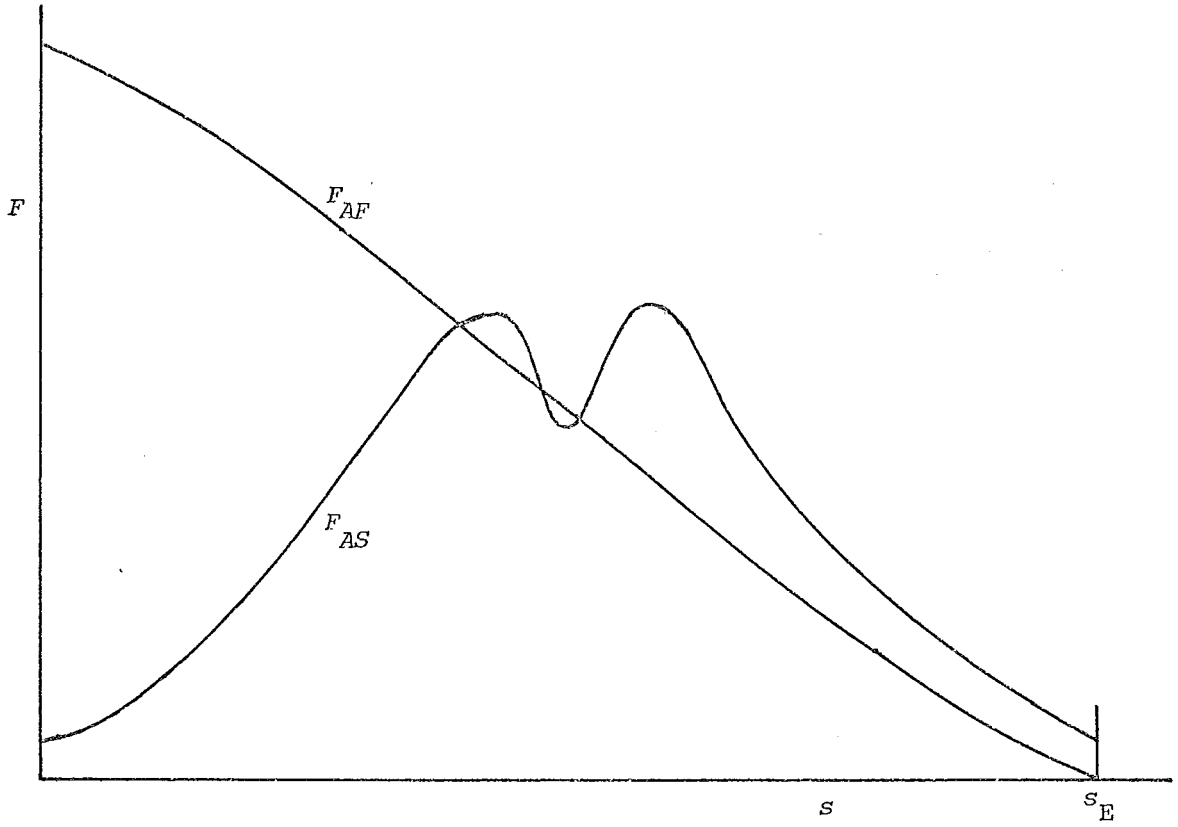

Fig. 6.3c. 'Simple' solution cannot be applied

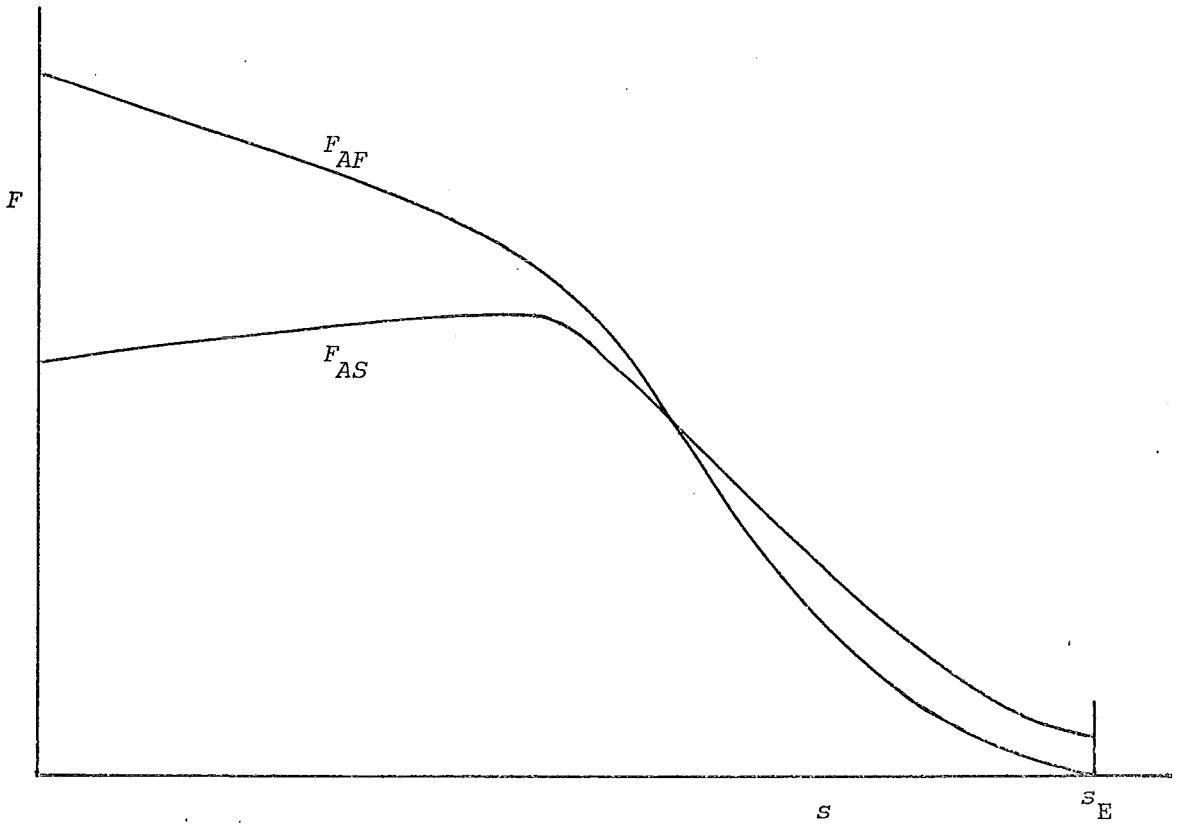

Fig. 6.3d. 'Simple' solution can be applied

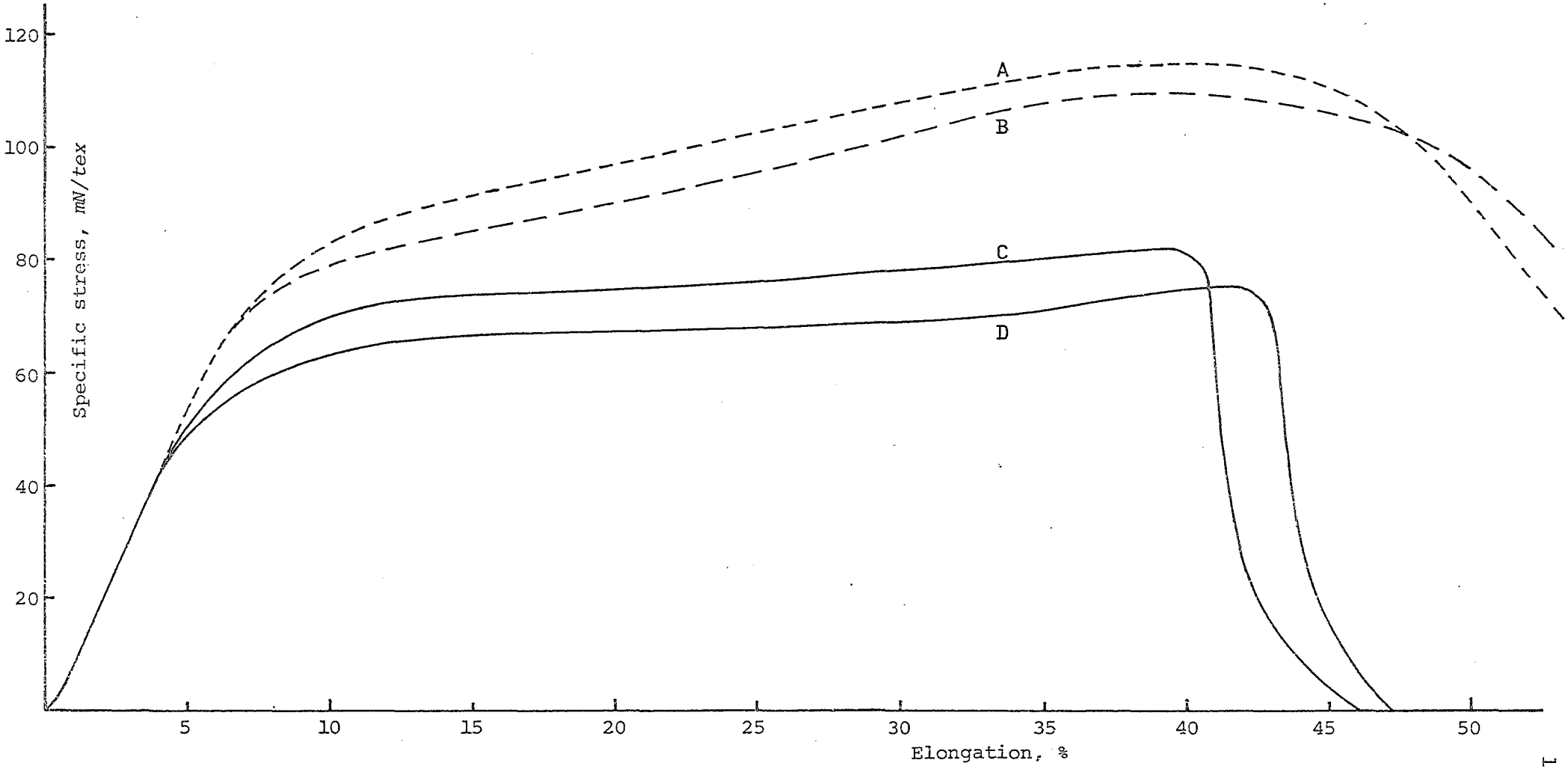

Fig. 6.4a. Romney 300 tex; short-gauge theoretical (continuous line = experimental; broken line = theoretical)
A and D = Romney 300 tex/100; B and C = Romney 300 tex/180

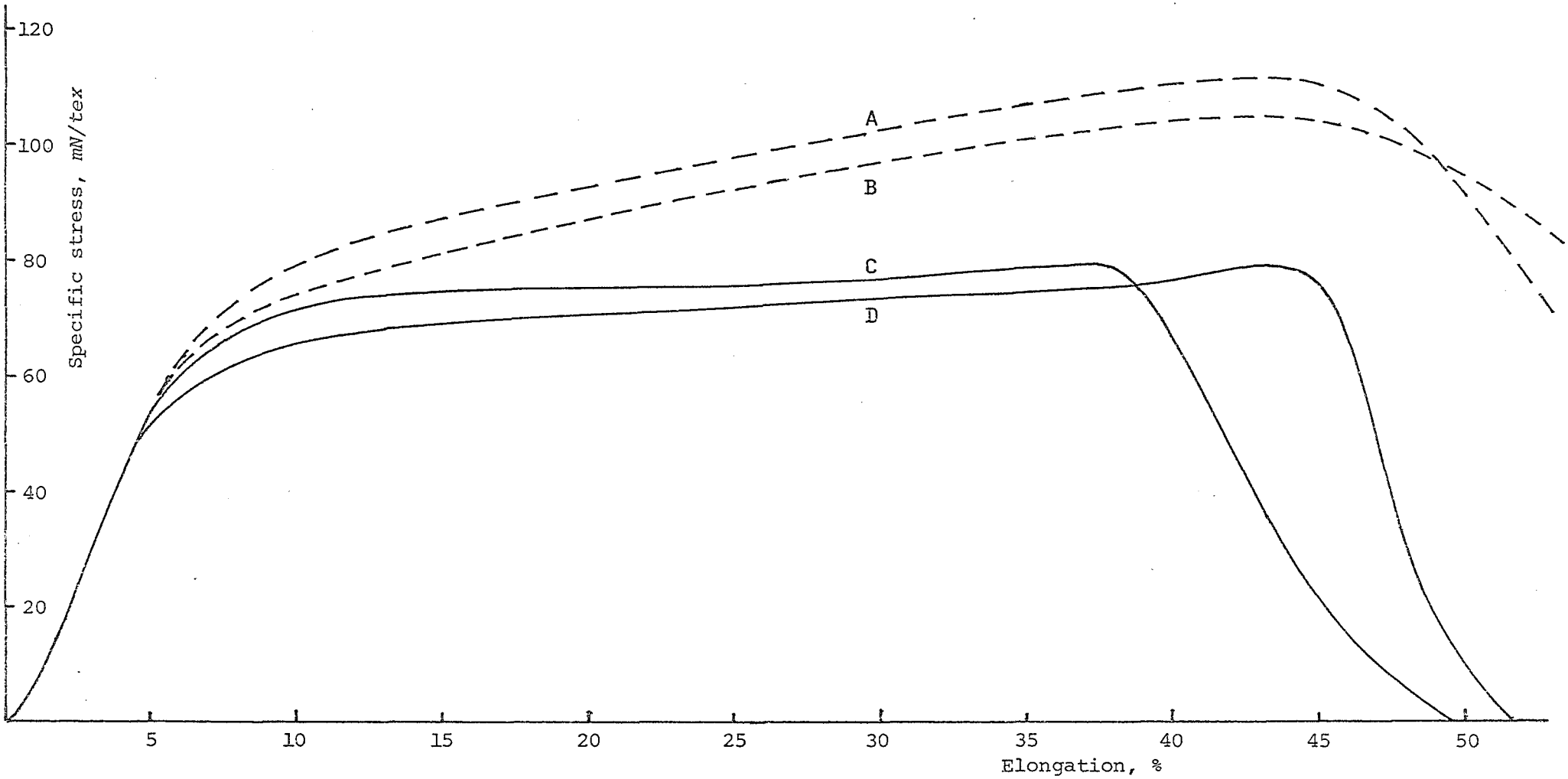

Fig. 6.4b. Romney 600 tex; short-gauge theoretical (continuous line = experimental; broken line = theoretical)
A and C = Romney 600 tex/80; B and D = Romney 600 tex/130

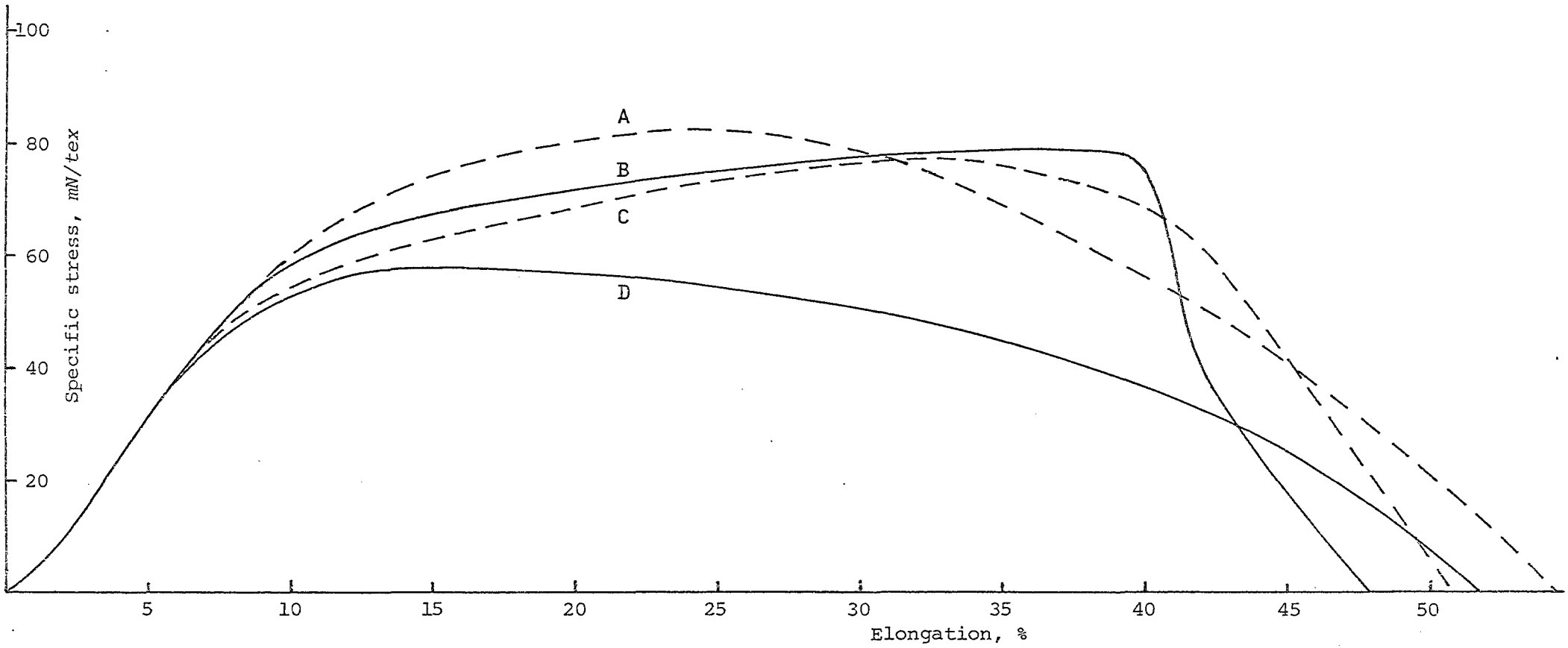

Fig. 6.4c. Cheviot 300 tex; short-gauge theoretical (continuous line = experimental; broken line = theoretical)
A and D = Cheviot 300 tex/100; B and C = Cheviot 300 tex/180

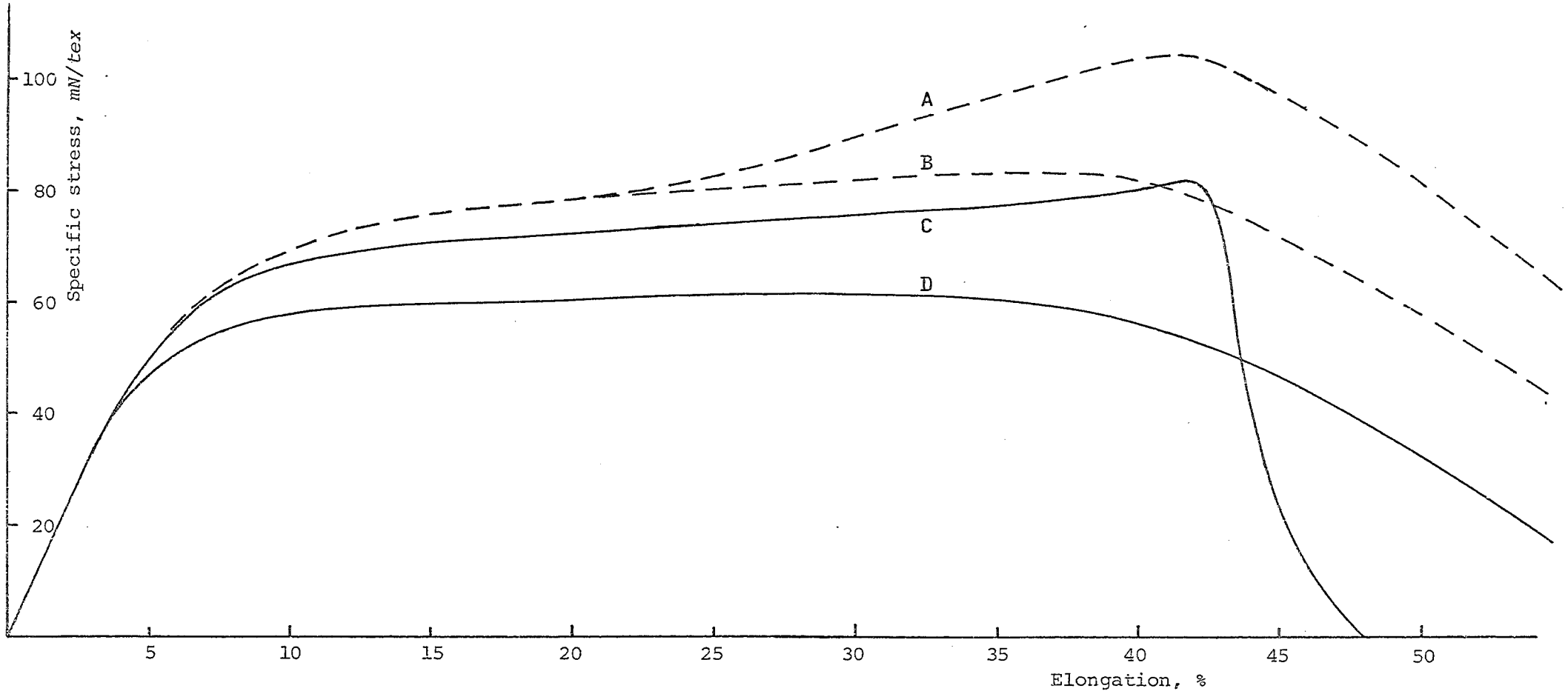

Fig. 6.4d. Lincoln 300 tex; short-gauge theoretical (continuous line = experimental; broken line = theoretical)
A and C = Lincoln 300 tex/180; B and D = Lincoln 300 tex/100

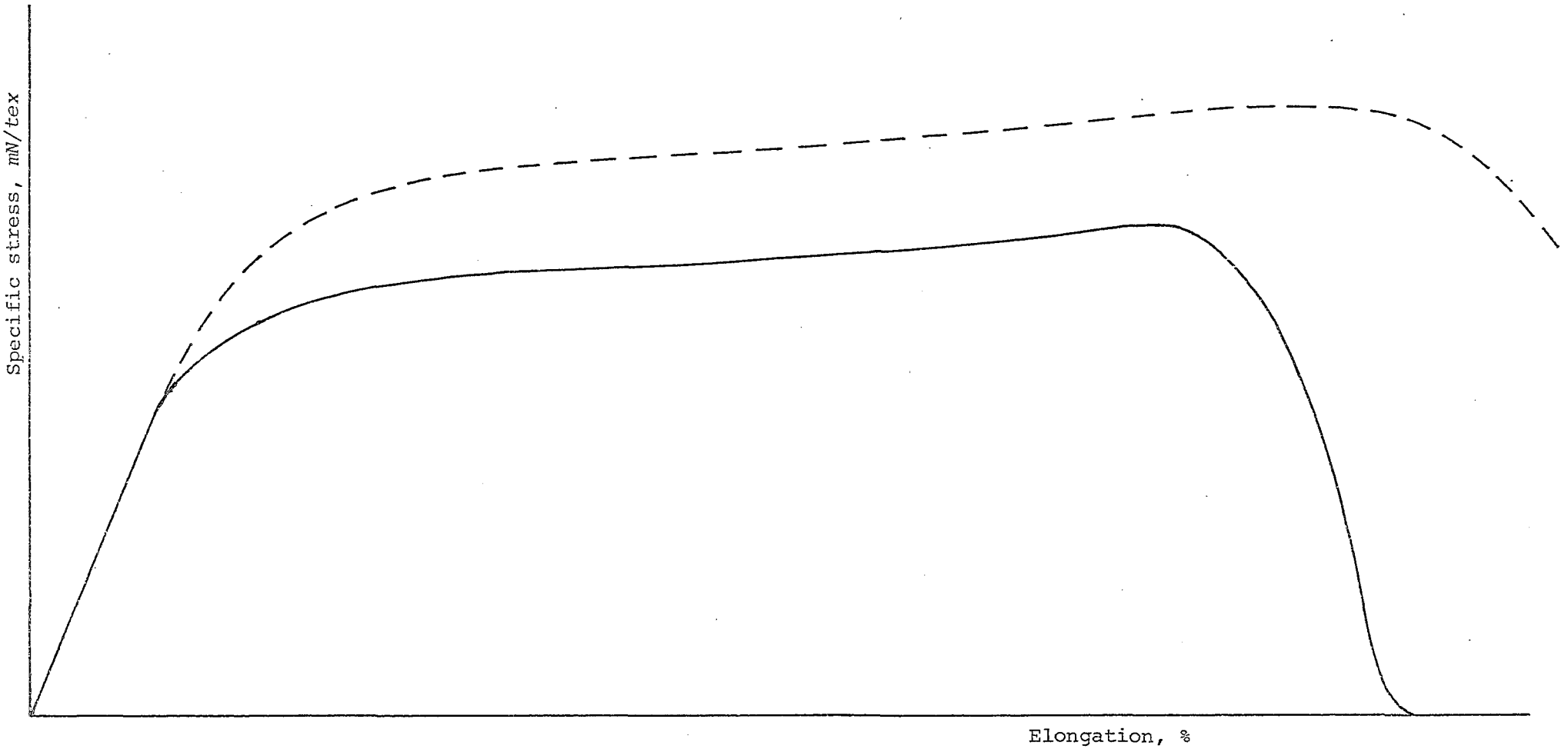

Fig. 6.5. Typical form of short-gauge experimental (continuous line) and theoretical (broken line) curves

data would produce inconsistent discrepancies. Although there probably is a common factor (3) behind the discrepancy for all the yarns the problem is to identify it. This is difficult as many of the assumptions made for the analysis could be more or less suspect. Here two assumptions will be discussed which seemed the most likely to the author.

6.5.2 Discontinuous Fibres in Short-gauge Specimens

An assumption that is particular to the short-gauge model is that all the fibres are continuous. However, this can only be the case if the gauge length is close to or equal to zero. In the experiments conducted here the gauge length used was 25 mm which implies that a significant proportion (30 - 50 %) of the fibres in the tested yarn segment would not be gripped by both jaws of the testing machine. The contribution of these discontinuous fibres to the general yarn strength is dependent on the inter-fibre friction, just as in the long-gauge yarn tests, and can be anywhere between 0 and 100 %. At present the contribution is assumed to be 100 %, i.e., a discontinuous fibre is assumed to be as strong as a continuous fibre.

The only simple alternative to the present assumption is to assume that the discontinuous fibres do not contribute at all to the axial stresses in the yarn, T_A. Their presence should still be accounted for in the determination of the specific volume and hence the lateral stress, T_L. However, this new assumption would imply that a long-gauge yarn would have no strength at all because all the fibres would be discontinuous in that case.

When the staple-fibre yarn analysis was developed later it was realised that this could be used to assess the effect of the discontinuous fibres in the short-gauge yarn tests. This was done by assuming that a certain percentage of the fibres in the staple-fibre yarn, P_C, would not slip at all. The other fibres, P_{DC} %, were treated as usual in the staple-fibre yarn model, i.e., slippage could take place. Because of the extra complications involved, this method was only used in the staple-fibre yarn analysis with the V-shaped migration path. Only one yarn was evaluated in this way, the Romney 300/180, for which the values of μ_{WF} and WF_0 were taken as 0,002 and 0,005 respectively. With 100 % discontinuous fibres these values give a good agreement with the long-gauge yarn results. The analysis was run for a series of different percentages of continuous and discontinuous fibres and the results are shown in Figure 6.6. It is evident from the results that only a small percentage of continuous fibres is necessary to keep the

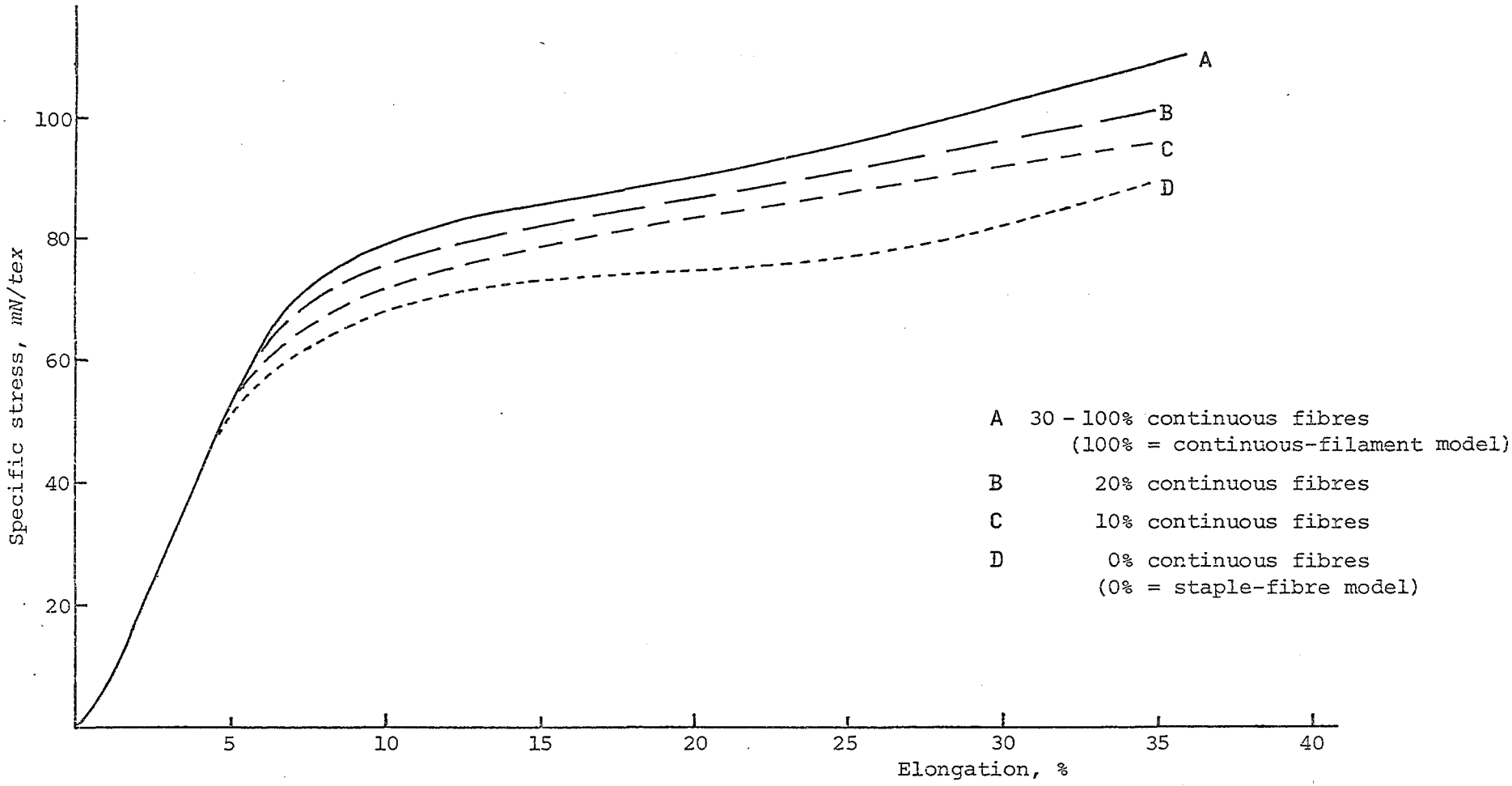

Fig. 6.6. Influence of percentage of continuous fibres on staple-fibre yarn model (Romney 300 tex/180)

yarn model at full strength. The actual percentage of continuous fibres in the short-gauge (25 mm) yarn is roughly estimated as 70, 65, and 55 % for the Lincoln, Romney, and Cheviot yarns respectively. The differences are caused by the different lengths of the fibres of the three wool types.

Because of the large margin between the actual percentage of continuous fibres and the theoretically derived percentage which is necessary to keep the yarn model at full strength, the assumption that all the fibres are continuous in a 25-mm length of yarn can be regarded as more or less valid.

6.5.3 Lateral Compressibility of Yarn under Tension

The other factor which could relate to the discrepancy between reality and theory for the short-gauge yarn tests is the assumed van Wyk relationship for the lateral pressure. As discussed in Section 2.4.1, the relationship is only evaluated for an untensioned sliver. Because of the relationship assumed the lateral pressure on the sliver remains the same if the sliver is elongated without change in volume. Owing to a certain entanglement of the fibres in the sliver it will contract considerably if it is elongated. This would mean that the lateral pressure would actually decrease on a sliver which is elongated under constant volume change. This effect implies that K will decrease if the fibres in a yarn, which are also slightly entangled, are tensioned. This is hard to verify experimentally as this would require an elaborate experimental arrangement where the sliver could be tensioned while being compressed laterally.

To check the influence on the yarn model strength of a van Wyk parameter, K, which decreases with the tension in the fibres a special relationship for K is assumed here:

$$K' = K^{1/(1+a.E_f)}$$

where K' = van Wyk parameter for tensioned sliver;

K = van Wyk parameter as determined on untensioned sliver;

E_f = fibre strain in the yarn; and

a = an arbitrary factor.

It must be noted that the above function is quite arbitrary and it has no theoretical or experimental basis. The experimental results for the Romney 300/180 yarn are used to evaluate the influence on the results of the continuous-filament yarn analysis. The results for values of a of 0, 10 and 50 are shown in Figure 6.7 together with the experimental short-gauge result for the Romney 300/180. The result for

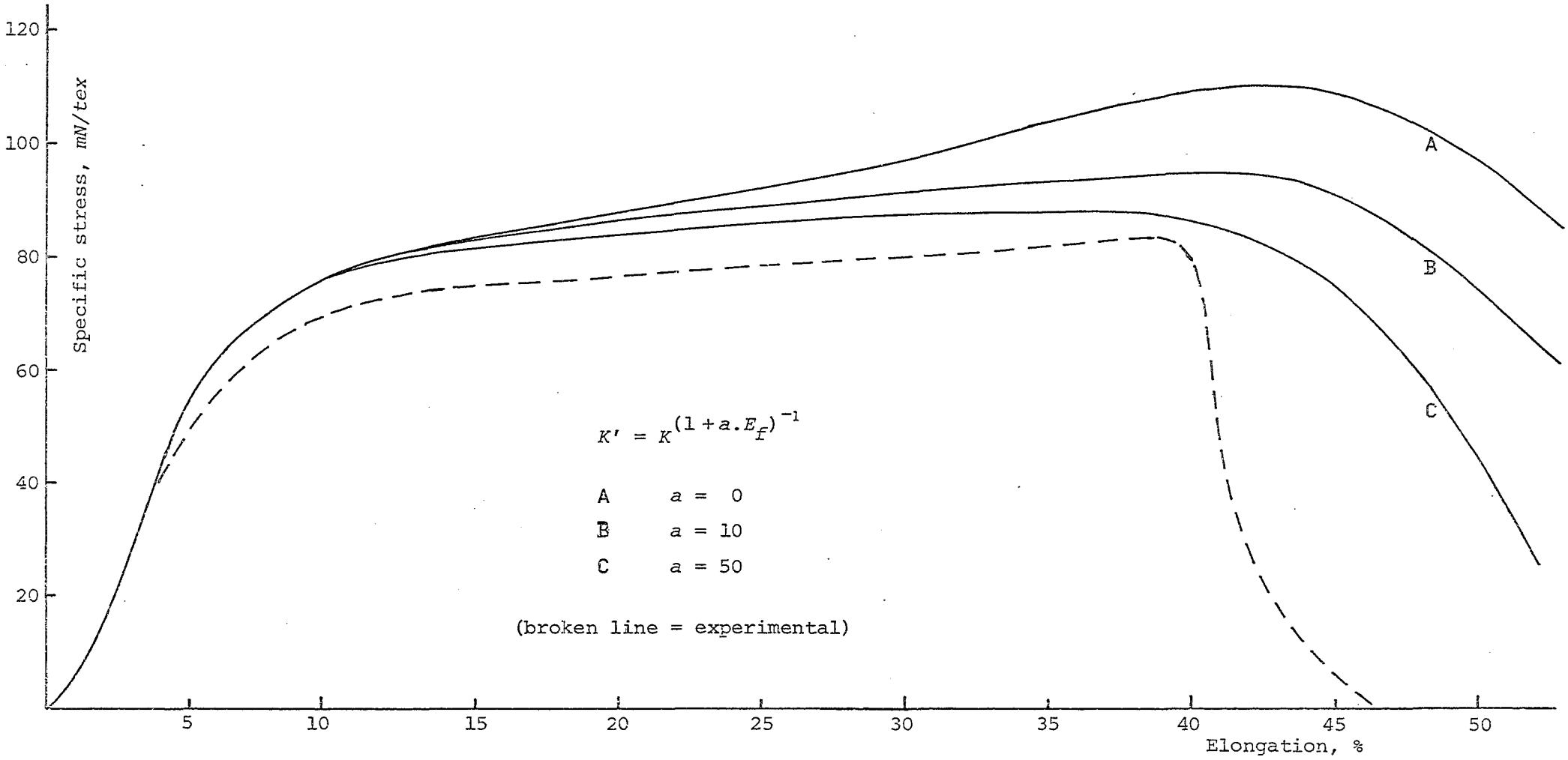

Fig. 6.7. Influence of van Wyk parameter, K, on continuous-filament yarn model (Romney 300 tex/180)

a = 0 is of course identical to that obtained with an uncorrected K. It can be seen in the Figure that the correction of K gives the theoretical curve a push in the right direction. However, it would be premature to draw any conclusions as this whole procedure is very crude and arbitrary. Nonetheless it seems worthwhile to investigate the compressive behaviour of a sliver under tension to check the hypothesis discussed above.

6.6 EVALUATION AND DISCUSSION OF THE STAPLE-FIBRE YARN ANALYSIS

6.6.1 General

A method for evaluating the general correctness of the staple-fibre yarn analysis is to compare the results of a continuous-filament yarn analysis with those of a similar staple-fibre yarn analysis in which no slip occurs. This is achieved by setting the values of μ_{WF} and WF_0 to large numbers in which case the staple-fibre yarn model will behave as if all the fibres were continuous. It is found that the difference in the results when no slip occurs in the staple-fibre yarn analysis is negligible, which is in accordance with the work of Treloar (19).

It was also found that when the values of μ_{WF} and WF_0 are sufficiently high to prevent substantial slipping the results of the V-analysis and the W-analysis are identical. However, for values of μ_{WF} and WF_0 which allow a substantial amount of slipping in the model, the V-yarn model is significantly weaker than the W-yarn model, see Figure 6.8b. This is not surprising as the inner legs of the W will act as a 'loop', maintaining the lateral pressure in the yarn even if the outer legs slip.

A problem arises when trying to compare the results of the staple-fibre yarn analysis with the experimental results of long-gauge yarn tests as two parameters necessary for the analysis, μ_{WF} and WF_0, have not been determined experimentally. The values for μ_{WF} and WF_0 given in the literature ($3{,}33 \times 10^{-3}$ mm and 1×10^{-4} N.mm^{-1} respectively (31)) give theoretical results for the yarn strength which are far too low. However, these values were obtained with Botany (Merino) wool and they may not be representative of the wool types and slivers used here.

In order to investigate this question the parameters μ_{WF} and WF_0 were treated as unknowns, the procedure used being to determine the values of these parameters which would give the best fit between the theoretical and experimental yarn-strength curves. Only the Romney

yarns were thoroughly covered because this procedure involved a large number of analyses. Some of the results are shown in Figures 6.8 a - d, only a few solutions for each yarn type being given for the sake of clarity.

A remarkable finding was that the phenomenon of drafting, where the yarn strength decreases after a short extension — as exhibited by the experimental curves for the low-twist yarns (Romney 300/100 and Romney 600/80) — could be induced for the theoretical analyses of the low-twist yarns but not for the high-twist yarns. If very low values for μ_{WF} and WF_0 are used for the high-twist yarns the theoretical curve does exhibit drafting but no decrease in yarn strength. It can also be seen that for certain values of μ_{WF} and WF_0 for which the high-twist yarns show considerable strength, the low-twist yarns exhibit drafting and loss of strength after a short extension.

Another interesting feature, which is not shown in the Figures, is that for $WF_0 = 0$ the model shows no resistance to elongation at all; i.e., the initial strength of a staple-fibre yarn is not dependent on fibre migration but on the factor, WF_0. The importance of fibre migration to the model is more significant after the initial extension as can be seen in Figure 6.8b, where the theoretically obtained curves of V- and W-models are shown. It must be noted that for analyses in which the initial increment of elongation is quite large (> 2 %) the model will sometimes develop resistance against extension even when WF_0 is zero. This anomaly is due to numerical rounding-off errors and it vanishes when either smaller increments are chosen or double precision is used.

The amount of energy which is dissipated into heat by friction is quite significant, being almost 100 % of the total energy in some cases (drafting). In the analyses which yield results comparable with the experimental results the dissipated energy is on average 10 - 20 % of the total energy expended on extending the yarn.

All in all the staple-fibre yarn analysis does simulate certain aspects of the behaviour of wool yarns quite realistically and promotes our understanding of the role of certain mechanisms in the development of the strength of staple-fibre yarns. However, there are still quite a few discrepancies between theory and experiment. Only in one case, the Romney 300/180, was a good agreement found between a theoretical curve and the long-gauge experimental curve; in this case the values of μ_{WF} and WF_0 were 2×10^{-3} mm and 5×10^{-3} N.mm^{-1} respectively. The predicted value for μ_{WF} is of the same order of magnitude as that given

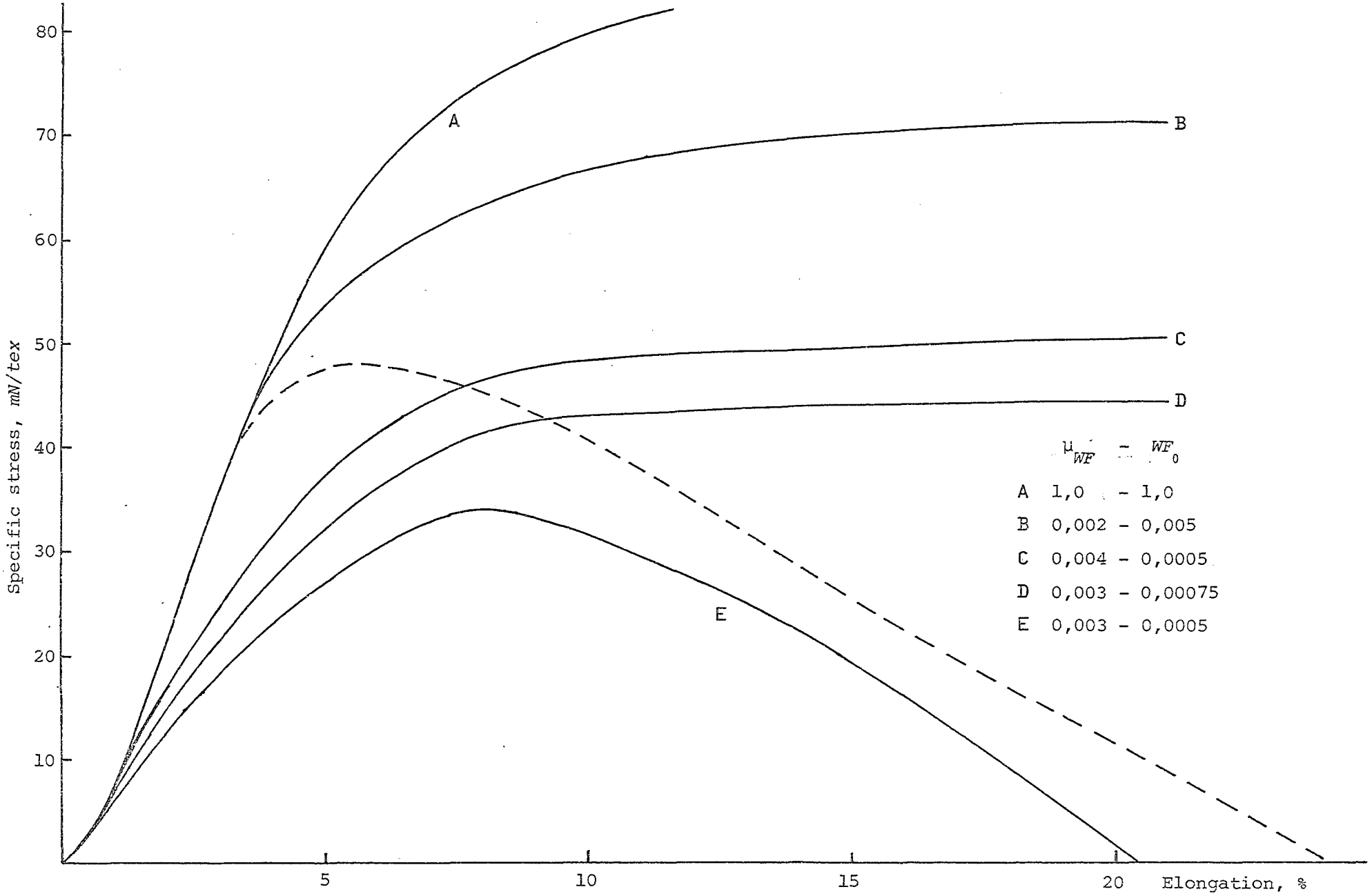

Fig. 6.8a. Romney 300 tex/100; long-gauge theoretical (broken line = experimental)

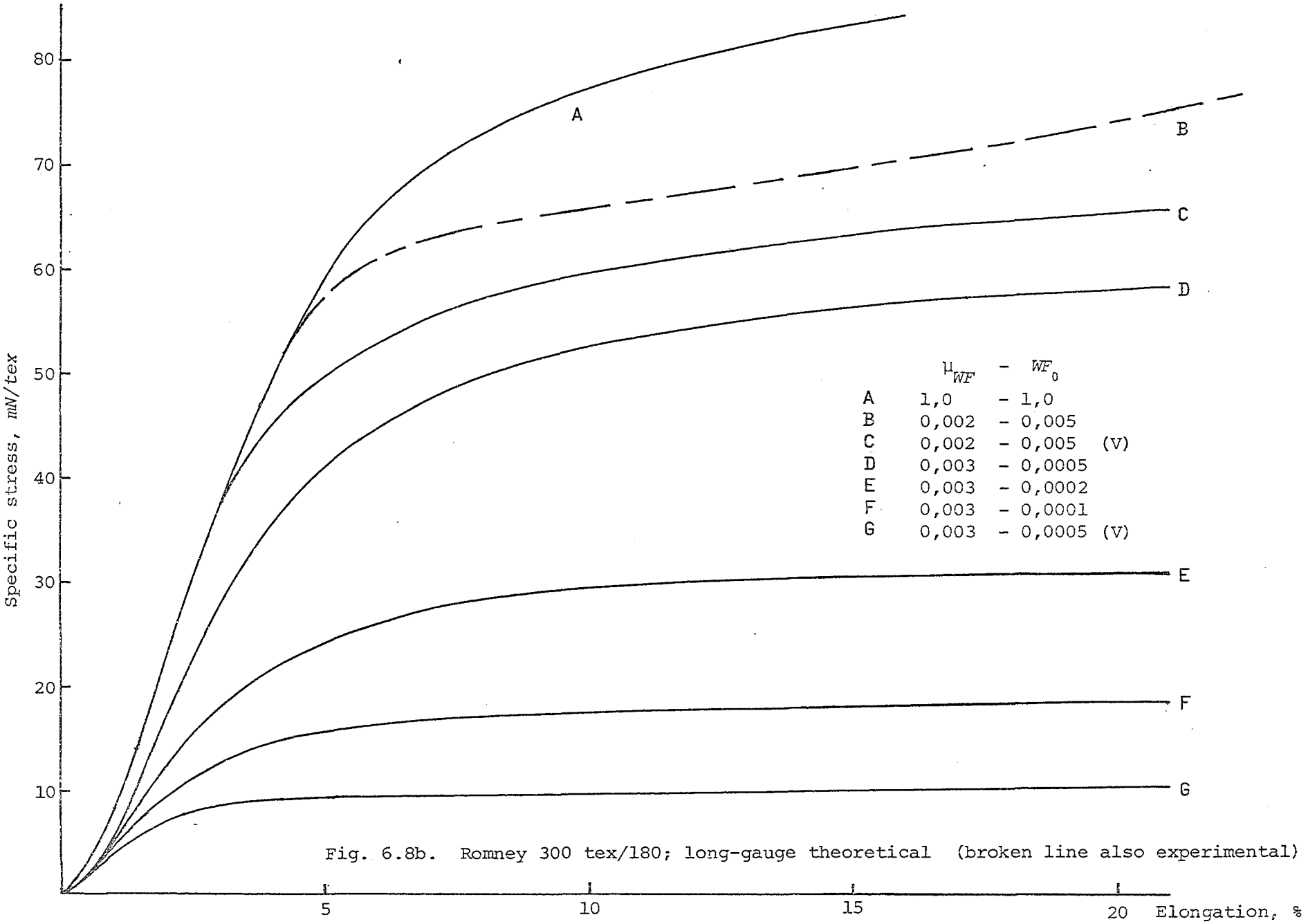

Fig. 6.8b. Romney 300 tex/180; long-gauge theoretical (broken line also experimental)

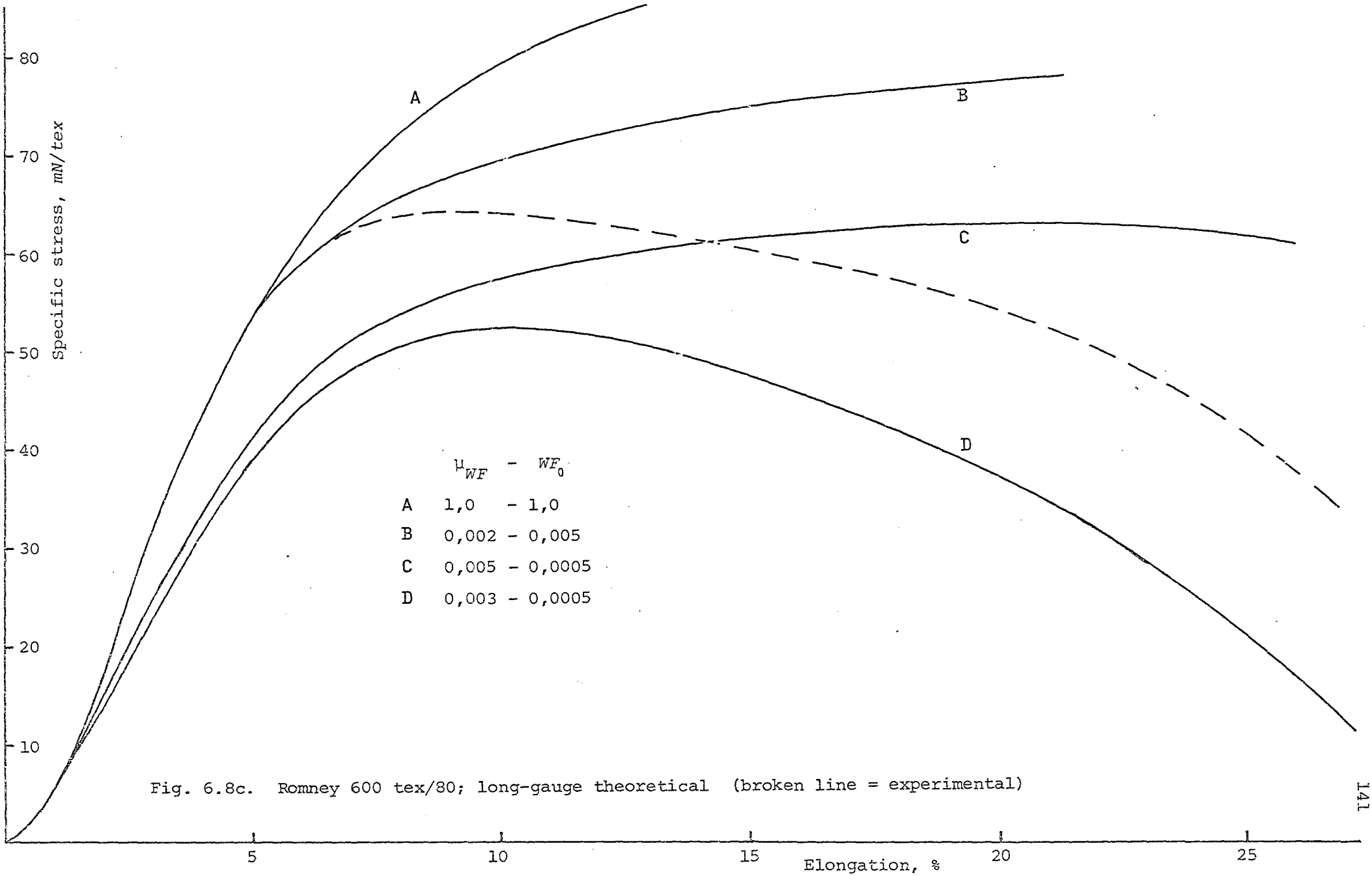

Fig. 6.8c. Romney 600 tex/80; long-gauge theoretical (broken line = experimental)

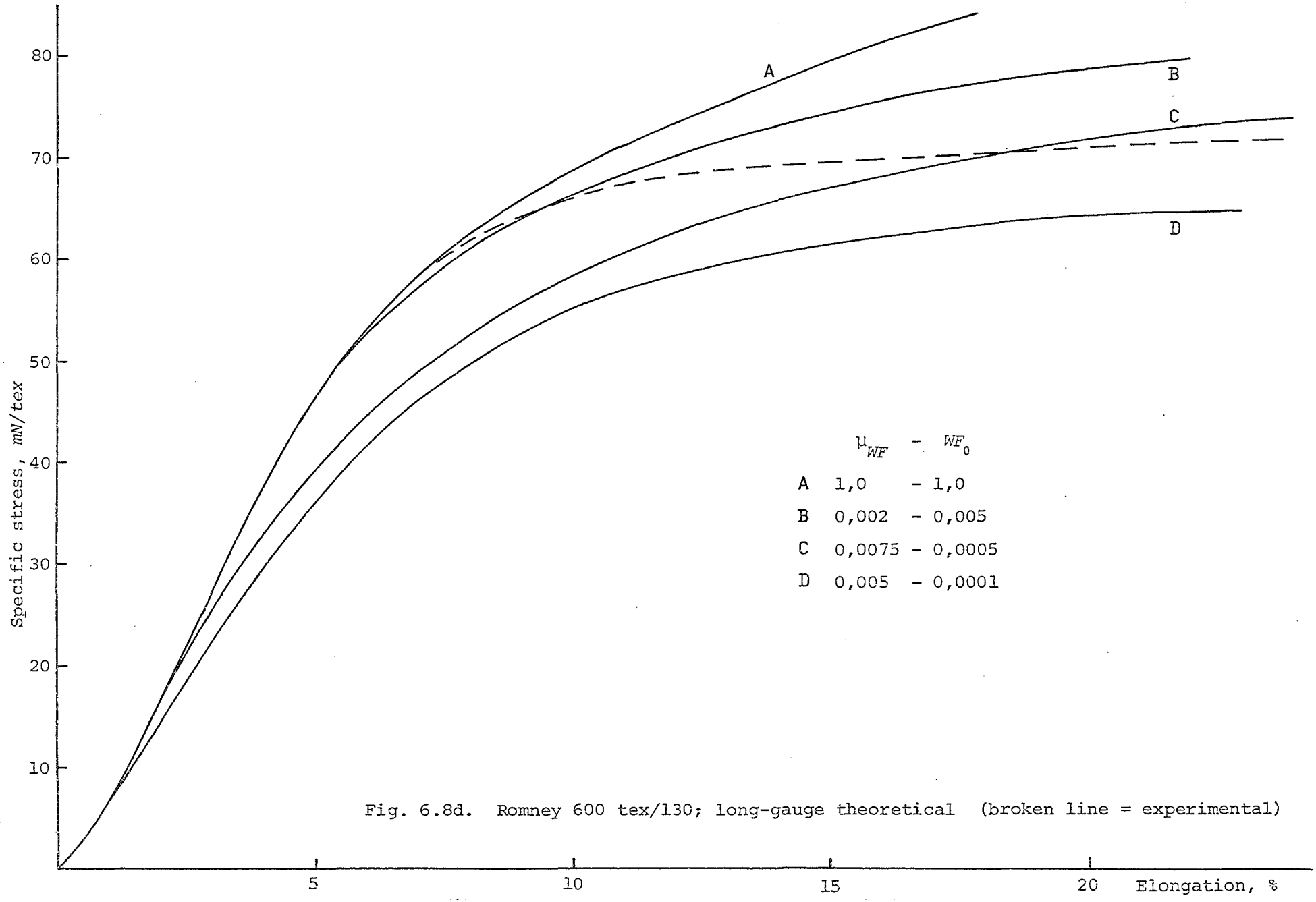

Fig. 6.8d. Romney 600 tex/130; long-gauge theoretical (broken line = experimental)

in the literature (31, 34) but the value for WF_0 is 50 times as high. This high value for WF_0 is not just an exception since the same value is necessary for all three other yarns to induce a good agreement for the initial moduli. Although as pointed out earlier the value for WF_0 given in the literature is possibly not representative of the wool types used here, the difference is so large that some other factor(s) must be involved. There are a multitude of factors which could be responsible for the discrepancy between theory and experiment. The most important of these are thoroughly discussed in the following Sections.

6.6.2 Radial Position of the Fibre Ends

One particular assumption which is quite controversial is that concerning the radial position of the fibre ends. Although there is some evidence that a fair proportion of the fibre ends are near the surface of the yarn (see Section 2.2.2) there will undoubtedly be quite a few fibre ends elsewhere in the yarn. The question is whether there would be any significant difference between the results of the present analysis and those of an analysis where the fibre ends were more realistically distributed. Extensive changes to the analysis would be necessary to account for a different distribution pattern of the fibre ends and these would make the formulation much more complicated. An alternative method would be to have all the fibre ends at the yarn axis as an inverted W, and see what would be the difference from the normal W analysis with the fibre ends at the yarn surface. If the difference was small it is possible that a yarn model with a more random distribution of fibre ends would also yield results that were much the same as those for the present model. It is comparatively simple to change the analysis so that the fibre ends are all at the yarn axis; however, owing to numerical difficulties no significant results were obtained. The analysis only gave results for very high and very low values of μ_{WF} and WF_0, which correspond to no slipping at all or extreme slipping. The results obtained for the extreme values of μ_{WF} and WF_0 were identical for both the normal W-shaped migration path and the inverted path as would be expected. Given time the numerical problems could probably be solved but it was decided to devote effort to other aspects of the work. For the time being it will be assumed that an analysis with all the fibre ends at the yarn surface is a realistic proposition.

6.6.3 Influence of the Internal State of the Undeformed Yarn on the Analysis

The internal state of an undeformed wool yarn is of much more

significance to yarn mechanics in general and possibly also to the present problem. In the present analysis it is assumed that the fibres in the undeformed yarn are unstressed and are identical to fibres taken from the sliver from which the yarn was spun. The actual situation in a real wool yarn is much more complicated, but this does not automatically imply that the assumption should lead to erroneous results. To explain this the most important factors which have an influence on the behaviour of the yarn and the fibres in the state in which they are tested are discussed below.

The procedure for yarn spinning and the experiments was as follows:

(a) manufacture of slivers followed by spinning into yarns which were immediately wound onto bobbins;

(b) the bobbins and the remaining slivers were stored under controlled conditions, the slivers being stored so that no significant external pressure was exerted on them;

(c) after six months the bobbins and slivers were taken out of storage and tested under controlled conditions; the stress-strain curves of the yarns were determined immediately after winding the yarn off the bobbins; the stress-strain curves of fibres were determined on fibres taken from the slivers; yarns were mounted under a very small tension in frames immediately after being wound off the bobbins for determination of the cross-section density, resin being poured into the frames between 2 h and 2 days after the mounting; the parameters of the van Wyk relationship were determined from the slivers.

To explain the influence of the above procedures on the behaviour and the state of the yarn and the fibres when they were tested the following factors must be taken into account;

(d) the yarn is wound onto the bobbin under a certain tension, the so-called spinning tension; this implies that immediately after winding on the fibres have non-zero axial and bending stresses, the latter being due to the lateral pressure present in the tensioned yarn; because of the situation on the bobbin the corresponding strains are not free to recover by movement of the fibres;

(e) wool fibres have complicated visco-elastic properties (66); if a wool fibre is held in a stressed configuration for a period of time the fibre stress will diminish, the extent of the stress-relief being time-dependent; the recovery of the fibre to its original state after removal of the external constraints is also time-dependent; the rate of both the stress-relief and the recov-

ery are also dependent on other factors such as temperature and the medium in which the fibre is present.

The general conclusion from the above-mentioned points is that the yarn wound off the bobbin after six months storage is not in the same state as when it was wound onto the bobbin. This was especially evident in the case of the high-twist yarns which exhibited extreme snarling just after spinning but not any more after storage. This is of course caused by the stress-relief of the fibres.

Several workers (67 - 70) have shown by experiments that fibres taken from a yarn which has been stored for a considerable time after being spun exhibit stress relief or cohesive set (as this effect is called in the textile literature) to a certain extent. Carnaby (4) found a value of about 0,5 % for the cohesively set axial strain in fibres from yarns stored for six months which were similar to those used here. Fibres taken from the corresponding slivers had no cohesively set strain which implies that the stresses (relieved or not) present in the fibres of the yarn are due to the spinning process. What cannot (yet) be measured is the strain in the fibres that is possibly still present but not cohesively set, because this will immediately be recovered either when the yarn is wound off the bobbin or when the fibre is taken out of the yarn to be tested. However, it can be safely assumed that after a long storage period the fibres will be almost completely stable in respect of both axial and bending stresses. Because the bending stresses are also relieved the lateral pressure in the yarn will be zero.

The conclusion therefore is that, at the time it is tested, the yarn has indeed zero internal stresses as was assumed. But it can also be concluded that this assumption does not specify the situation adequately, that is to say, the stress history of the fibres should also be mentioned. In the tests previously described in Section 6.2 this aspect has been neglected and the necessary data have been taken from fibres from the sliver which did not have the same stress history as the fibres present in the yarn.

The question is, what are the consequences for the results of the analyses ? Assuming that the values for the cohesively set strain as obtained by Carnaby (about 0,5 %) are also applicable to these yarns there is probably little difference between the stress-strain curve of a typical fibre taken from the sliver and one taken from the yarn after storage. Because of the chemical and physical phenomena occurring dur-

ing stress relaxation there will be very little difference in the initial part of the stress-strain curve, the main difference being in the post-yield region. However, the set strain is so low that it can be assumed that there will also be little difference in the post-yield region. The correct method would be to determine the stress-strain curve from fibres taken from the yarn. In general it can be said that a possible correction to the fibre stress-strain curves as used here would have a negligible influence on the analyses.

To determine the lateral compressibility of the fibres in the yarn the compressive behaviour of the equivalent sliver is measured. However, the sliver is still in its original undisturbed state after storage, which is characterised by a value for V_{sp_0} of about 10 $mm^3.mg^{-1}$. The fibres in the yarn have been held at a much lower specific volume for a long time and because of this the bending stresses have been relieved. This implies that the value of V_{sp} for which there is no external pressure necessary to keep the fibres in a certain configuration, V_{sp_0}, is now equal to the value of V_{sp} as present in the yarn. These values of V_{sp_0} vary throughout the yarn, increasing with the distance from the yarn axis, with a minimum of 1,2 $mm^3.mg^{-1}$ for the inner elements of the high-twist yarns.

The present analysis takes account of the changed V_{sp_0} but it is questionable whether the van Wyk parameter, K, which is determined on the undisturbed sliver, can be used for the stress-relieved fibres in the yarn. In Figure 6.9 the compression curves are given for different values of V_{sp_0} but the same values of K. It can be seen that the curves are only slightly different and then only at low external pressures. Theoretically this could be justified by the fact that at high external pressures the fibres have so many bending points that the exact original configuration of the fibre does not matter. Experimental evaluation could be performed by compressing pieces of sliver to a certain specific volume and storing them in that state. After a given period of time the compressibility of the samples could be measured and compared with that of the undisturbed slivers. This procedure would necessarily take a long time but it need not be complicated.

A factor which probably has much more influence on the analysis than any variations in the value of K is the value of WF_0. The values of WF_0 which are given in the literature were determined from slivers which had high specific volumes, e.g., in (34) V_{sp_0} was about 8 $mm^3.mg^{-1}$. The reason for the existence of WF_0 is given in (31) as the small residual forces at the inter-fibre contacts which are still present in an

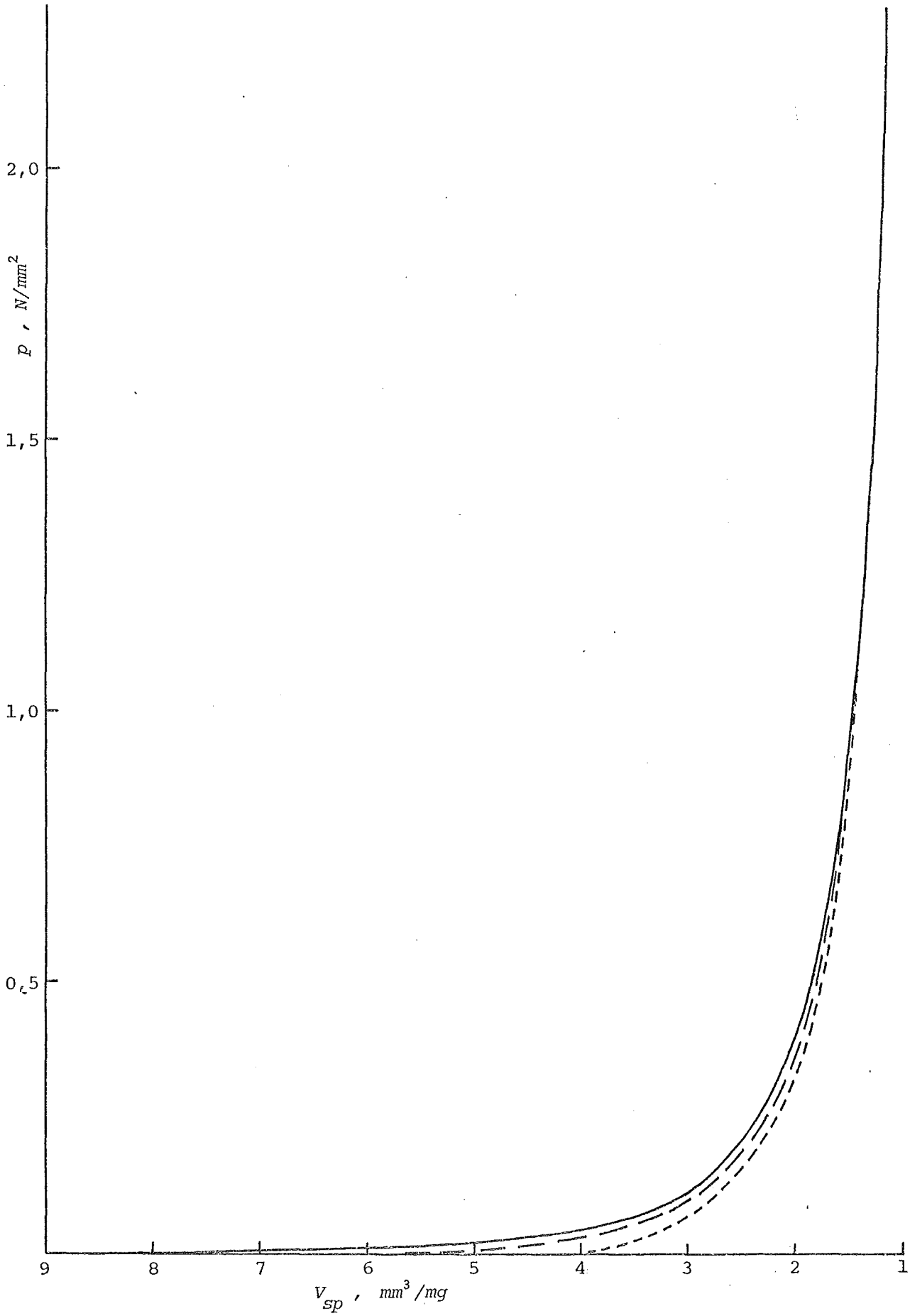

Fig. 6.9. Van Wyk relationship for different values of V_{sp_0}

——— V_{sp_0} = 10; — — V_{sp_0} = 6; - - - - - V_{sp_0} = 4

uncompressed sliver. These small residual contact forces will also exist in a sliver which has been set into a configuration which has a much lower value for V_{sp_0}. However, the number of inter-fibre contacts will be higher if V_{sp_0} is, for example, 1,2 $mm^3.mg^{-1}$ than it would be if V_{sp_0} is 8 $mm^3.mg^{-1}$. If it is assumed that the contact forces are equal in both cases and the number of contacts is inversely proportional to V_{sp} (31), the value of WF_0 for V_{sp_0} = 1,2 $mm^3.mg^{-1}$ will be 6,6 times the value of WF_0 for V_{sp_0} = 8 $mm^3.mg^{-1}$. This implies that WF_0 varies throughout the yarn. To evaluate this hypothesis an analysis was run with varying values of WF_0 for the Romney 300/180. The values for μ_{WF} and WF_0 were taken as $3,33 \times 10^{-3}$ mm and 1×10^{-4} $N.mm^{-1}$ as determined in (31). This is the value for WF_0 when V_{sp_0} is 10 $mm^3.mg^{-1}$; for the analysis it was corrected for each element by using the following relationship:

$$WF'_0 = \frac{V_{sp_0}}{V_{sp'_0}} . WF_0$$

where WF'_0 = corrected value for WF_0;

V_{sp_0} = specific volume of sliver in undisturbed state; and

$V_{sp'_0}$ = local specific volume in the undeformed yarn.

The results with this method were slightly better than those when using the uncorrected value of WF_0 but the yarn still exhibited excessive slipping, see Figure 6.10.

Another hypothesis which could explain the discrepancy between theory and experiment is concerned with the compressive behaviour of a drafting sliver which is cohesively set into a configuration with a low specific volume. Before any compression of the sliver has taken place the fibres will exhibit to a large extent their natural configuration which ranges from straight to highly crimped. There will be some distortion though not very much. When the sliver is compressed the number of inter-fibre contacts increases and fibres are forced into unnatural distortions so as to accommodate neighbouring fibres. If the sliver is held in the compressed state for a long time the resistance of the fibres to their new unnatural state decreases because the bending stresses associated with the distortions are relaxed. When the sliver has been compressed long enough the new configuration becomes the 'natural' configuration. There is a difference from the undisturbed sliver, however. The distortions of the fibres in the compressed and set sliver are to a much greater extent matched to one another locally because of the much smaller volume. If the set sliver (on which no external pressure is being exerted) is now tensioned and slipping of fibres with

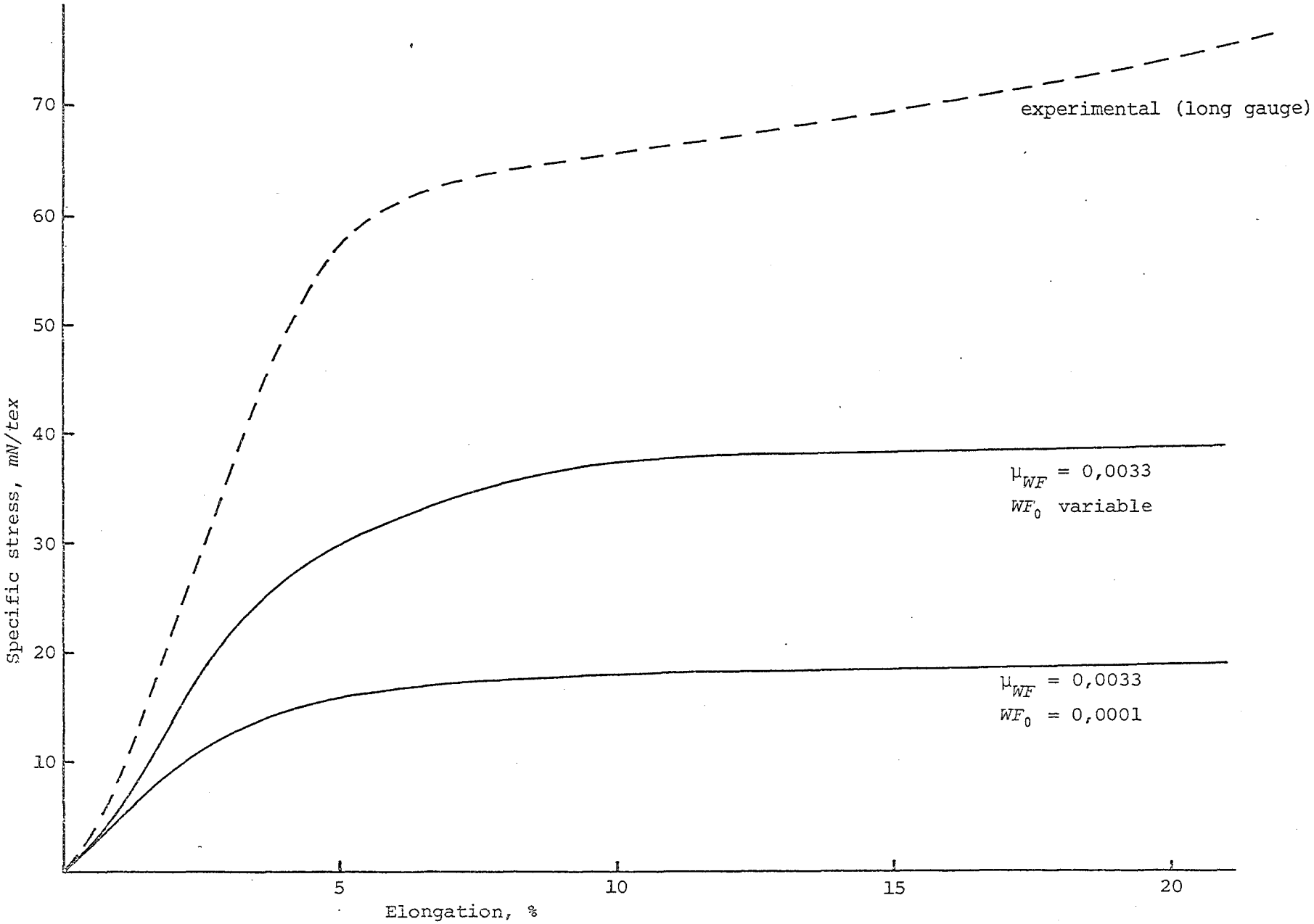

Fig. 6.10 Romney 300 tex/180; long-gauge theoretical with WF_0 dependent on V_{sp_0}

respect to one another takes place a large number of previously matching distortions will be pulled out of alignment. This would cause the fibres to distort into fresh configurations and hence create new bending stresses. If the sliver is constrained externally this implies that the lateral pressure which was first negligible will suddenly rise considerably. This process is illustrated in Figure 6.11.

The fibres need only slip a very small amount for this phenomenon to occur because the distance between the inter-fibre contacts and hence the dimension of the distortions is very small. In the van Wyk relationship this effect can be described by a change in V_{sp_0} to a higher value than $V_{sp}'_0$. What the exact value of $V_{sp}''_0$ will be is hard to estimate but it will probably be dependent on $V_{sp}'_0$. It is almost certainly lower than the original V_{sp_0} owing to a certain amount of irreversible slipping during the initial compression process.

If the hypothesis discussed above is true the potential implications for the staple-fibre yarn analysis are considerable. In general it will imply that if slip occurs somewhere in the yarn the lateral pressure will suddenly increase thereby causing an increase in the frictional force which could possibly stop the slipping. This could be realised in the analysis by first using a value for V_{sp_0} as calculated from the undeformed yarn geometry, $V_{sp}'_0$, and if slipping occurs V_{sp_0} would be changed to a higher value, $V_{sp}''_0$. This also implies that if slipping occurs in an element which has already been considerably compressed during yarn extension the change in V_{sp_0} will have a marginal influence on the lateral pressure. However, the main effect of the change in V_{sp_0} is expected to be in the initial stages of yarn extension.

To investigate the influence of the changing V_{sp_0} on the theoretical results the analysis of the Romney 300/180 yarn was used, with WF_0 dependent on $V_{sp}'_0$. The change in V_{sp_0} takes effect if a certain level of slip is reached. This 'trigger' value is arbitrarily taken as 0,1 mm. Although $V_{sp}''_0$ is probably dependent on $V_{sp}'_0$ it is conveniently taken as being constant throughout the yarn. Elements where the slip reached the trigger value and which have a value for $V_{sp}'_0$ higher than the chosen $V_{sp}''_0$ are considered not to change their V_{sp_0}. For the first analysis $V_{sp}''_0$ was taken as 8 $mm^3.mg^{-1}$. This caused the analysis to fail probably because of the large change in V_{sp_0} in several elements. The value for $V_{sp}''_0$ was reduced stepwise by 1 $mm^3.mg^{-1}$ until the numerical difficulties were resolved, which did not occur until $V_{sp}''_0$ = 2 $mm^3.mg^{-1}$ was reached. The result is shown in Figure 6.11 and is certainly better than the original result without $V_{sp}''_0$. However, a consid-

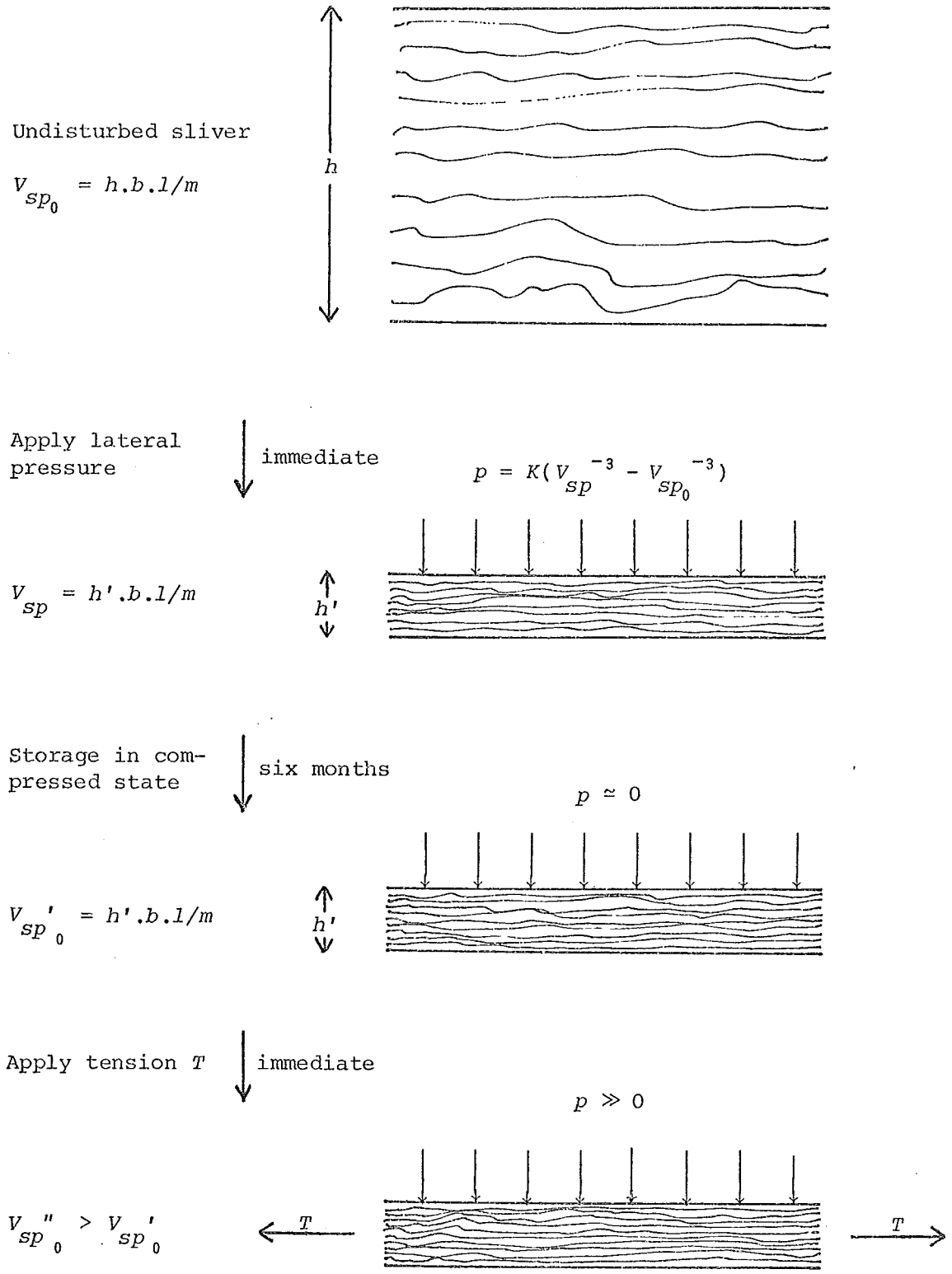

Fig. 6.11. Influence of storage and subsequent tensioning on V_{sp_0} of a sliver m = mass of sliver; b = width; l = length

erable number of elements did not benefit because their $V_{sp}{}'_0$ was larger than 2 $mm^3.mg^{-1}$. Because there are still too many arbitrary factors involved it was not considered worthwhile to spend a lot of time in solving the numerical problems.

CHAPTER 7

SUMMARY, CONCLUSIONS, AND SUGGESTIONS FOR FURTHER WORK

7.1 SUMMARY AND CONCLUSIONS

7.1.1 Introduction

The work presented here is concerned with the structural analysis of textile yarns under tension, with the emphasis on singles wool yarns. Although this subject has been extensively studied before a systematic approach to the problem using the full advantages of modern high-speed computing equipment and the associated powerful numerical techniques has been lacking. Here an attempt has been made to fill this gap, relying mainly on yarn models based on continuous filaments and staple fibres which have been described previously by Carnaby (4) and Hearle (6) respectively.

7.1.2 Continuous-filament Yarn Analysis

In the case of the continuous-filament yarn theory the model used here is essentially the same as that described by Carnaby, but a more formal mathematical development of the problem along the lines of the finite-element method is applied. The major achievement in this case is a considerable reduction in the computational effort required so that the model can be used freely to evaluate the multitude of permutations possible in yarn structures. An alternative development of Carnaby's continuous-filament yarn model is also described which can be more readily adapted to incorporate inter-fibre friction and fibre slippage, but which is less formal in the mathematical sense. Because of this care must be taken to ensure that an accurate solution to the problem is obtained.

The general conclusion in the case of the continuous-filament yarn analysis presented here is that it yields a reasonable approximation of the behaviour of wool yarns at a short-gauge length, especially in the initial range of extensions. An appreciable discrepancy between theory and experiment still exists at higher extensions but the general shape of the theoretically predicted curve agrees well with that of the experimentally obtained curves.

In Sections 6.5 and 6.6 several factors are discussed which could explain the discrepancy between theory and experiment at high levels of yarn extension. Further study is needed especially with respect to the

lateral compressibility properties of the yarns.

7.1.3 Staple-fibre Yarn Analysis

Although the short-gauge model is very useful in the development of our understanding of yarn mechanics, in practice the long-gauge strength of wool yarns, and of staple-fibre yarns in general, is of more consequence. It was therefore decided to devote the rest of the time to the development of a staple-fibre yarn analysis rather than to refine the continuous-filament yarn analysis, which would involve extensive experimental work.

To simulate the behaviour of long-gauge wool yarns a model is developed which incorporates the effects of the fibre discontinuities and fibre migration. A staple-fibre yarn model previously described by Hearle (6) is used as the basis but extensive changes are made which reflect the advances made in the modelling of the lateral contraction of wool yarns during deformation. The inter-fibre friction forces, which are so important in staple-fibre yarns, are incorporated into the model by an analogy with the withdrawal force of a single fibre from a sliver. To enable the analysis to cover the higher ranges of yarn extension where most of the fibre slippage occurs the changes in the relative position of the fibres due to slippage are accounted for. Also the energy which is dissipated into heat by the fibre slippage is taken into account for the calculation of the yarn force.

A method is presented for calculating the ideal migration paths in staple-fibre yarns of which the cross-section density is dependent on the radial position in the yarn. This method has similarities with previous methods (6, 19); however, in both of these cases a constant cross-section density throughout the yarn was assumed.

The analysis is developed for two types of migration envelopes, a simple V-shape and a more complex W-shape, both with the fibre ends at the surface. The analysis with the V-shaped fibre path was mainly used as a 'prototype', the actual evaluation of the model being done with the W-analysis. If desired it would be comparatively straightforward to incorporate other types of migration envelopes, for example, a triple-V (VVV) shape.

While the staple-fibre yarn model can not as yet be used to predict the strength of a yarn reliably, it does represent the first serious attempt at predicting the important features of the observed stress-strain curve for these yarns. There are still too many unknown factors involved, however, to be able to attribute the shortcomings of

the current analysis to either inadequacy of the model or of the data. However, the staple-fibre yarn model does simulate quite realistically certain phenomena characteristic of the behaviour of real staple-fibre yarns, see Section 6.6.1. This is quite encouraging and marks a substantial progress in the mechanics of staple-fibre yarns which has always been rather neglected, due to its additional complexity in comparison with the mechanics of continuous-filament yarns. It is felt by the author that more detailed information on factors such as lateral compressibility and inter-fibre friction will enable the staple-fibre yarn analysis to yield better results, without having to make extensive changes in the model.

7.2 SUGGESTIONS FOR FURTHER WORK

The problem discussed in this work is in fact the simplest possible combination of the many aspects concerning the tensile behaviour of textile yarns. In Table 7.1 a list is given of the most important features by which the yarn or the testing of the yarn can be described. Furthermore, two lists are given of the form in which these are incorporated into the present analysis and of the possible alternatives for future analyses.

Table 7.1 Yarn and Test Features

Features	Present	Alternative
Fibre properties	uniform	non-uniform (blends)
Number of plies in yarn	one (singles)	more than one (plied)
Yarn geometry along the yarn axis	uniform	non-uniform (weak spots)
Loading	single extension	cycling (hysterisis)
Duration of loading	independent of time	very short (dynamic effect)
		very long (creep; stress relaxation)

Some of the alternative features could possibly be incorporated into the present analyses with a few minor changes. To incorporate certain other features in an analysis would necessitate extensive changes in the present models and/or analyses or even a totally new model, as would be the case for plied yarns. Although incorporation of any of the alternative features would imply a more complex analysis than the present one the basic methodology described here, utilising the finite-element method, could be applied.

However, before proceeding to these more advanced tasks it is of the utmost importance that the problems encountered in the present

analyses, which would inevitably recur for the more complex analyses in the future, are fully understood if not overcome.

In the author's opinion further work should be concentrated on three factors which, as discussed in Chapter 6, are closely related:

internal state of the undeformed yarn;
lateral compressibility of the yarn; and
inter-fibre friction.

The last factor is not of course relevant in the case of the continuous-filament yarn analysis. The lateral compressibility and the inter-fibre friction are both modelled with the aid of theories and data which are concerned with slivers, not yarns. However, this does not have to be a problem as long as the state of the fibres in the sliver is approximately the same as the state of those in the yarn — this is where the internal state of the undeformed yarn becomes important. A thorough study of these three important factors will entail a considerable amount of elaborate experimental work but this is certainly warranted if progress is to be made in yarn mechanics.

Another important point is the numerical solution of the model equations. Many of the staple-fibre yarn analyses failed because of convergence or other related problems. It is probably worthwhile to consider other solution methods than the presently used Newton-Raphson iteration, or to devise a more elaborate computing strategy which would probably help very considerably.

A final suggestion is the development of a model which can predict the geometry of a yarn from the manufacturing parameters and material properties. This is certainly not an easy task but it is very closely related to the present problem and could possibly be solved in a similar fashion using finite-element techniques. Furthermore the solution of this problem is essential if the ideal is to be achieved of being able to predict the behaviour of textile yarns, and fabrics too for that matter, without ever having to manufacture the yarns.

REFERENCES

1. Hearle, J.W.S., Grosberg, P., and Backer, S. "Structural Mechanics of Fibers, Yarns and Fabrics", vol. 1, New York, Wiley-Interscience, 1969, 469p.

2. Treloar, L.R.G. and Riding, G. 'A theory of the stress-strain properties of continuous-filament yarns', *J. Text. Inst.* 54, T156-70, 1963.

3. Carnaby, G.A. and Grosberg, P. 'The tensile behaviour of staple-fibre yarns at small extensions', *ibid.* 67, T299-308, 1976.

4. Carnaby, G.A. 'The structure and mechanical properties of wool carpet yarns', Ph.D. Thesis, Dept of Textile Industries, University of Leeds, 1976.

5. Van Wyk, C.M. 'Note on the compressibility of wool', *J. Text. Inst.* 37, T285-92, 1946.

6. Hearle, J.W.S. 'Theoretical analysis of the mechanics of twisted staple-fibre yarns', *Text. Res. J.* 35, 1060-71, 1965.

7. Idem. 'The formation of textile structures', *in* "Mechanics of Flexible Fibre Assemblies", ed. Hearle, J.W.S., Thwaites, J.J., and Amirbayat, J., Alphen aan den Rijn, The Netherlands, Sijthoff & Noordhoff, 1980, pp. 1-33.

8. Onions, W.J. "Wool: An Introduction to its Properties, Varieties, Uses and Production", London, Benn, 1962.

9. Peirce, F.T. 'Geometrical principles applicable to the design of functional fabrics', *Text. Res. J.* 17, 123-47, 1947.

10. Morton, W.E. and Yen, K.C. 'The arrangement of fibres in Fibro yarns', *J. Text. Inst.* 43, T60-6, 1952.

11. Neckář, B. 'Internal mechanics of twisted yarn', *Text. Res. J.* 46, 545-62, 1976.

12. Morton, W.E. 'The arrangement of fibres in single yarns', *ibid.* 26, 325-31, 1956.

13. Riding, G. 'An experimental study of the geometrical structure of single yarns', *J. Text. Inst.* 50, T425-42, 1959.

14. Hearle, J.W.S. and Merchant, V.B. 'Interchange of position among the components of a seven-ply structure: mechanism of migration', *ibid.* 53, T537-52, 1962.

15. Hearle, J.W.S. and Bose, O.N. 'Migration of fibers in yarns. II. A geometrical explanation of migration', *Text. Res. J.* 35, 693-9, 1965.

16. Hearle, J.W.S., Gupta, B.S., and Goswami, B.C. 'The migration of fibers in yarns. V. The combination of mechanisms of migration', *ibid.* 35, 972-8, 1965.

17. Hickie, T.S. and Chaikin, M. 'Some aspects of worsted-yarn structure. V. A comparison of the configurations of the leading, middle, and trailing portions of single fibres in some worsted yarns', *J. Text. Inst.* 65, 546-51, 1974.

18. Hearle, J.W.S., Gupta, B.S., and Merchant, V.B. 'Migration of fibers in yarns. I. Characterization and idealization of migration behavior', *Text. Res. J.* 35, 329-34, 1965.

19. Treloar, L.R.G. 'A migrating-filament theory of yarn properties',

J. Text. Inst. 56, T359-80, 1965.

20. Hearle J.W.S. and Bose, O.N. 'The form of yarn twisting. I. Ideal cylindrical and ribbon-twisted forms', *ibid.* 57, T294-307, 1966.

21. Gegauff, C. 'Force et elasticité des files en coton', *Bull. Soc. Ind. Mulhouse*, 153-213, 1907.

22. Platt, M.M. 'Mechanics of elastic performance of textile materials. III. Some aspects of stress analysis of textile structures - continuous-filament yarns', *Text. Res. J.* 20, 1-15, 1950.

23. Hearle, J.W.S. 'The mechanics of twisted yarns: the influence of transverse forces on tensile behaviour', *J. Text. Inst.* 49, T389-407, 1958.

24. Hearle, J.W.S. and El-Behery, H.M.A.E. 'The mechanics of twisted yarns: theoretical developments', *ibid.* 52, T197-220, 1961.

25. Sullivan, R.R. 'A theoretical approach to the problem of yarn strength', *J. Appl. Phys.* 13, 157-67, 1942.

26. Holdaway, H.W. 'A theoretical model for predicting the strength of singles worsted yarns', *J. Text. Inst.* 56, T121-44, 1965.

27. Carnaby, G.A. 'The compression of fibrous assemblies, with applications to yarn mechanics', *in* "Mechanics of Flexible Fibre Assemblies", ed. Hearle, H.W.S., Thwaites, J.J., and Amirbayat, J., Alphen aan ben Rijn, The Netherlands, Sijthoff & Noordhoff, 1980, pp. 99-112.

28. Smith, P.A. 'The effect of twist on a worsted roving', *J. Text. Inst.* 53, T511-28, 1962.

29. Komori, T. and Makishima, K. 'Numbers of fiber-to-fiber contacts in general fiber assemblies', *Text. Res. J.* 47, 13-7, 1977.

30. Idem, 'Estimation of fiber orientation and length in fiber assemblies', *ibid.* 48, 309-14, 1978.

31. Grosberg, P. 'The strength of twistless slivers', *J. Text. Inst.* 54, T223-33, 1963.

32. Anderson, S.L., Cox, D.R., and Hardy, L.D. 'Some rheological properties of twistless combed wool slivers', *ibid.* 43, T362-79, 1952.

33. Medley, D.G., Stell, J.E., and McCormick, P.A. 'Basic drafting theory', *ibid.* 53, T105-43, 1962.

34. Postle, L.J., Ingham, J., and Cox, D.R. 'The measurement of interfibre friction in slivers', *ibid.* 43, T77-90, 1952.

35. Courant, R. 'Variational methods for the solution of problems of equilibrium and vibrations', *Bull. Amer. Math. Soc.* 49, 1-23, 1943.

36. Prager, W. and Synge, J.L. 'Approximations in elasticity based on the concept of junction space', *Quart. Appl. Math.* 5, 241-69, 1947.

37. Argyris, J.H. 'Energy theorems and structural analysis', *Aircraft Engrg* 26, 347-56, 383-94, 1954; 27, 42-58, 80-94, 125-34, 145-58, 1955.

38. Turner, M.J., Clough, R.W., Martin, H.C., and Topp, L.J. 'Stiffness and deflection analysis of complex structures', *J. Aeronaut. Sci.* 23, 805-24, 1956.

39. Zienkiewicz, O.C. and Cheung, Y.K. 'Finite elements in the solution of field problems', *The Engineer*, 507-10, 1965.

40. Norrie, D.H. and de Vries, G. "A Finite Element Bibliography", New York, Plenum Press, 1973.

41. Zienkiewicz, O.C. "The Finite Element Method in Engineering Science" London, McGraw-Hill, 2nd ed., 1971.

42. Norrie, D.H. and de Vries, G. "The Finite Element Method", New York, Academic Press, 1973.

43. Idem. "An Introduction to Finite Element Analysis", New York, Academic Press, 1978.

44. Cook, R.D. "Concepts and Applications of Finite Element Analysis", New York, Wiley, 1974.

45. Martin, H.C. and Carey, G.F. "Introduction to Finite Element Analysis", New York, McGraw-Hill, 1973.

46. Gallagher, R.H. "Finite Element Analysis, Fundamentals", Eaglewood Cliffs, N.J., Prentice Hall, 1973.

47. Strang, G. and Fix, G.J. "An analysis of the Finite Element Method", Eaglewood Cliffs, N.J., Prentice Hall, 1973.

48. Pian, T.H.H. and Tong, P. 'Basis of finite element methods for solid continua', *Int. J. Num. Meth. Engrg* 1, 3-28, 1969.

49. Oden, J.T. 'Finite element applications in non-linear structural analysis', "Application of Finite Element Methods in Structural Engineering", American Society of Civil Engineers (Symposium), Nashville, Tenn., 1969.

50. Malvern, L.E. "Introduction to the Mechanics of a Continuous Medium", Eaglewood Cliffs, N.J., Prentice Hall, 1969.

51. Oden, J.T. "Finite Elements of Non-linear continua", New York, McGraw-Hill, 1972.

52. Hibbit, H.D., Marcal, P.V., and Rice, J.R. 'A finite element formulation for problems of large strain and large displacement', *Int. J. Solids Struct.* 6, 1069-86, 1970.

53. Bathe, K.-J., Ramm, E., and Wilson, E.L. 'Finite element formulations for large deformation dynamic analysis', *Int. J. Num. Meth. Engrg* 9, 353-86, 1975.

54. McMeeking, R.M. and Rice, J.R. 'Finite element formulations for problems of large elasto-plastic deformation', *Int. J. Solids Struct.* 11, 601-16, 1975.

55. Horrigmoe, G. 'Non-linear finite element models in solid mechanics', *Report* No. 76-2, Univ. of Trondheim, 1976.

56. Moore, T.A. 'Finite element analysis of box-girder bridges', Ph.D. Thesis, Dept of Civil Engineering, University of Canterbury, 1975.

57. Little, R.W. "Elasticity", Eaglewood Cliffs, N.J., Prentice Hall, 1973.

58. Haisler, W.E., Stricklin, J.A., and Stebbins, F.J. 'Development and evaluation of solution procedures for geometrically non-linear structural analysis', *AIAA Journal* 10, 264-72, 1972.

59. Hildebrand, F.B. "Introduction to Numerical Analysis", New York, McGraw-Hill, 1956.

60. Huang, N.C. and Funk, G.E. 'Theory of extension of elastic continuous filament yarns', *Text. Res. J.* 45, 14-24, 1975.

61. Powell, M.J.D. 'Efficient method for finding minimum of function of several variables without calculating derivatives', *Comp. J.* 7, 155-62, 1964.

62. Eringen, A.C. "Mechanics of Continua", New York, Wiley, 1967.

63. Treloar, L. R. G. and Hearle, J. W. S. 'The mechanics of twisted yarns: a correction', *J. Text. Inst.* 53, T446-8, 1962.

64. Cheng, C. C., White, J. L., and Duckett, K. E. 'A continuum mechanics approach to twisted yarns', *Text. Res. J.* 44, 798-803, 1974.

65. Okamoto, N. and Nakazawa, M. 'Finite element incremental contact analysis with various frictional conditions', *Int. J. Num. Meth. Engrg* 14, 337-57, 1979.

66. Morton, W. E. and Hearle, J. W. S. "Physical Properties of Textile Fibres", London, Heinemann, 1962.

67. Baird, K. R. 'Relaxation shrinkage of worsted yarns. I. Some causes and some consequences', *Text. Res. J.* 45, 442-52, 1975.

68. Ingham, J. and Lawes, J. 'The effects of storage on wool products', *Wool Sci. Rev.* 40, 2-13, 1971.

69. Hickie, T. S. and Chaikin, M. 'The configuration and mechanical state of single fibres in woollen and worsted yarns', *J. Text. Inst.* 51, T1120-30, 1960.

70. Idem. 'Some aspects of worsted yarn structure. I. The single fibre mechanical state in yarns produced on high-draft spinning systems', *ibid.* 65, 421-5, 1974.

71. Abramowitz, M. and Stegun, I. A. "Handbook of Mathematical Functions", New York, Dover, 1970.

72. Anon. 'The measurement of crimp in wool', *Wool Sci. Rev.* 11, 40-50, 1953.

73. Pearson, C. E. "Handbook of Applied Mathematics", New York, Van Nostrand Reinhold, 1974.

APPENDIX A YARN CROSS-SECTION DENSITY

The number of fibres in a yarn cross-section is determined by the cross-sectional method (see Section 2.2.3). Because the distribution of fibres is in general non-uniform in the radial direction (wool yarns) the cross-section is subdivided into annular rings and the number of fibres per ring counted. The rings are taken so that they coincide with the finite element subdivision (or vice versa) and an example is shown in Figure A1.

The rings (or zones) are numbered in increasing order from the yarn axis outwards and the bordering circles of zone i lie at radii R_i and R_{i+1} respectively. The number of fibres in a zone i is designated by N_i.

The cross-section density function, $\rho(R)$, is used for the analysis of the migration path (Appendix B), and this is defined by:

$$\rho(R) = \lim_{\Delta R \to 0} \frac{N}{\Delta R} \qquad \ldots\ldots\ldots\ldots \quad (A1)$$

where N is the number of fibres present between the circles with radii $R + 0{,}5.\Delta R$ and $R - 0{,}5.\Delta R$ respectively.

This is purely a mathematical tool as in reality $\rho(R)$ would either be zero or infinity, because of the finite dimensions of fibres.

Here three possible forms of $\rho(R)$ are investigated:

(a) $\rho_i(R) = c_i \qquad \ldots\ldots\ldots\ldots \quad (A2)$

(b) $\rho_i(R) = a_i.R + b_i \qquad \ldots\ldots\ldots\ldots \quad (A3)$

(c) $\rho_i(R) = d_i.R^{-1} \qquad \ldots\ldots\ldots\ldots \quad (A4)$

In each zone $\rho_i(R)$ must satisfy the following equation:

$$\int_{R_i}^{R_{i+1}} \rho_i(R)\,dR = N_i \qquad \ldots\ldots\ldots\ldots \quad (A5)$$

The parameters a_i, b_i, c_i and d_i can be derived from the above equation:

(a) $c_i.(R_{i+1} - R_i) = N_i \Rightarrow c_i = N_i.(R_{i+1} - R_i)^{-1}$

(b) $a_i.(R_{i+1}^{\ 2} - R_i^{\ 2}) + b_i.(R_{i+1} - R_i) = N_i$.

This equation can only be solved if an extra condition is given. In this case the continuity of $\rho_i(R)$ over the zonal boundaries is stipulated: $\rho_i.(R_{i+1}) = \rho_{i+1}.(R_{i+1})$, from which it follows that

$$a_i.R_{i+1} + b_i = a_{i+1} + b_{i+1}.$$

To solve for all zones, $\rho(0)$ or $\rho(R_{ys})$, where R_{ys} is the radial position of the yarn surface, must be given.

(c) $\quad d_i.\ln(R_{i+1}.R_i^{-1}) = N_i \quad \Rightarrow \quad d_i = N_i.(\ln(R_{i+1}.R_i^{-1}))^{-1}.$

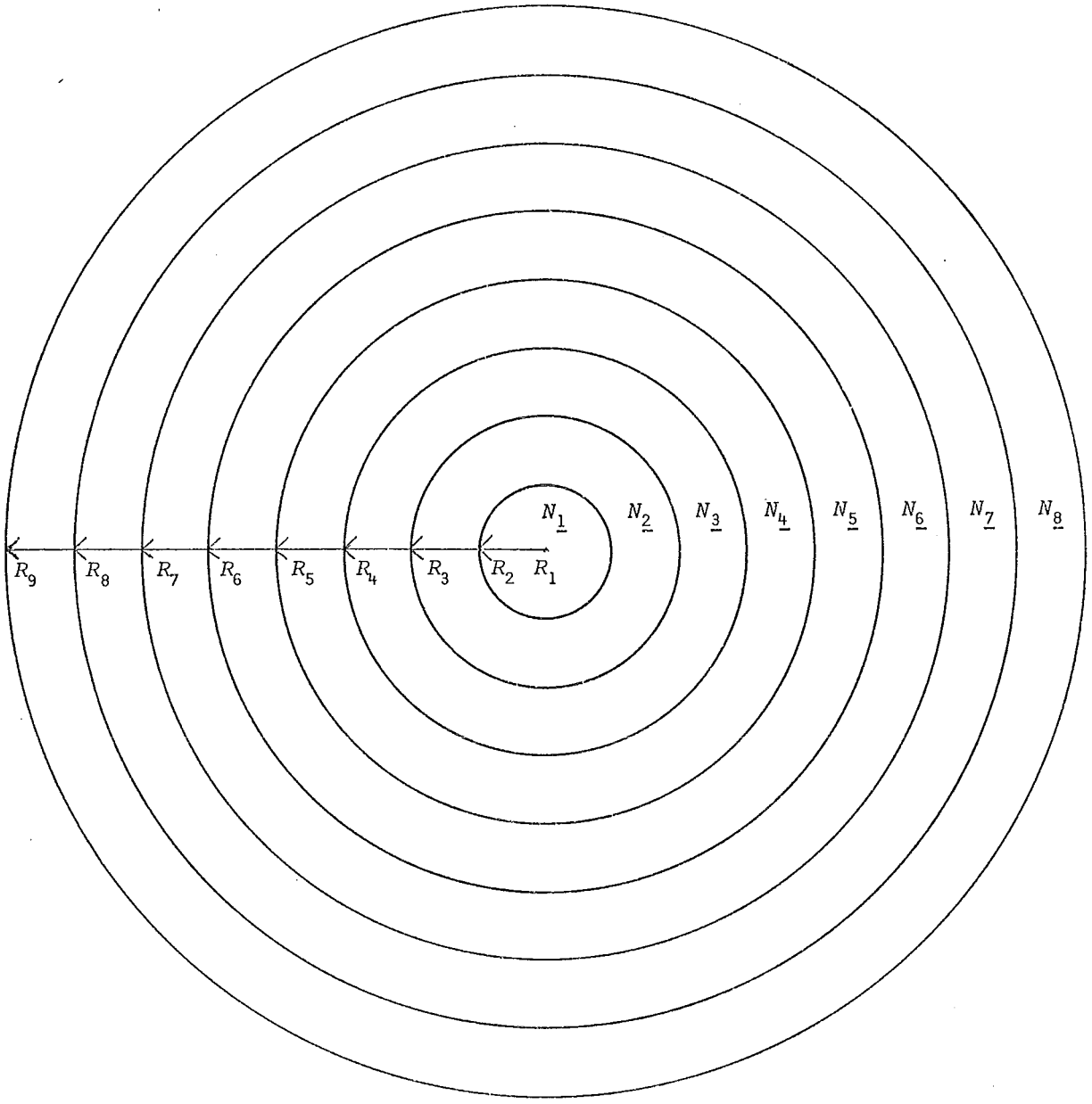

Fig. A1. Yarn cross-section density

APPENDIX B MIGRATION PATH

INTRODUCTION AND ASSUMPTIONS

In the migration yarn analysis the following assumptions are made about the paths of the individual fibres:

(a) each fibre path is identical except for a translation along and around the yarn axis, which implies that the fibres are of equal length;

(b) the twist of the path is constant: $\partial\theta/\partial Z = c$ . . . . (B1);

(c) the following is valid for any two points A and B on a fibre path with $R_A = R_B$: $\left|\partial R/\partial Z\right|_A = \left|\partial R/\partial Z\right|_B$ . . . . . (B2);

(d) the starting points of the fibre paths are evenly distributed along the yarn axis.

What is desired is an expression for the migrating-fibre path of the form: $Z = Z(R)$, which satisfies a certain yarn cross-section density and which follows a given elementary shape. Also the length of the path must be equal to L_f, the fibre length.

Furthermore two features are desirable for the migration-path function:

(a) continuity of the first derivative of the migration-path function to ensure a 'smooth'curve, and

(b) a closed analytical expression for the length along the path which is desirable for the analysis of the migration yarn.

The form of the migration-path function is dependent on the forms of the cross-section density function, $\rho(R)$, within each zone (see Appendix A). These are:

(a) $\rho(R) = c_i$ . . . . . (B3a)
constant within each zone and discontinuous over the yarn;

(b) $\rho(R) = a_i.R + b_i$ . . . . . (B3b)
linear function of R within each zone and piecewise continuous over the yarn; and

(c) $\rho(R) = d_i.R^{-1}$ . . . . . (B3c)
discontinuous over the yarn.

Unfortunately none of these three alternatives yields a function for the migration path which incorporates both of the desirable features stated above. Alternatives (a) and (b) yield expressions for the length along the path which can only be evaluated numerically and (c) and again (a) yield discontinuous first derivatives of the migration path.

The choice is clearly between alternatives (b) and (c) and here (c) is chosen because of its relative simplicity with regard to application in the migration-yarn analysis.

The elementary shape of the migration path is given by the radial positions of the fibre path ends and of the points where the fibre changes from inward migrating to outward migrating and vice versa. In Figure B1 a migration envelope is shown with the essential points encircled. It can be seen in the Figure that these points coincide with certain radii - these are the radii of the rings used in the cross-section density. This is not absolutely essential for the analysis of the migration path but it is very convenient and will be assumed to be valid here.

It is convenient to introduce the parameter n_i which is defined as the number of times a migration path traverses the concentric cylinder between R_i and R_{i+1}. For example, for the path illustrated in Figure B1 n is:

$$n_1 = n_2 = 2$$
$$n_3 = n_4 = n_5 = 3$$
$$n_6 = n_7 = 4.$$

MIGRATION-PATH ANALYSIS

A migration envelope of a typical fibre, A, is shown in Figure B2. Also shown are the radii of the inner and outer surfaces of a cylinder of infinitesimal width dR and the inner surface at radius R. The distance in the Z direction between an entry and an exit point of a segment of A passing through the cylinder is defined as dZ which is equal for all 'legs' of the migration path because of Equation (B2). A transverse cross-section, C, of the cylinder is taken at the point where A enters the cylinder from the inside with its third leg. To determine the number of fibres which pass through C the path of a second fibre, B, is drawn. Fibre B passes through C at the outer periphery just as A passes through at the inner periphery.

At radius $R + dR$ the distance in the Z direction between A and B is dZ and because all the fibre paths are identical except for a translation along (and around) the Z axis, the Z distance between the starting points of A and B must also be dZ. The number of fibres which pass through C with their third leg can now be determined by dividing dZ by dF, which is the Z distance between two consecutive fibres. Also the same number of fibres will pass through C with their second leg and fourth leg respectively. If the infinitesimal cylinder is located

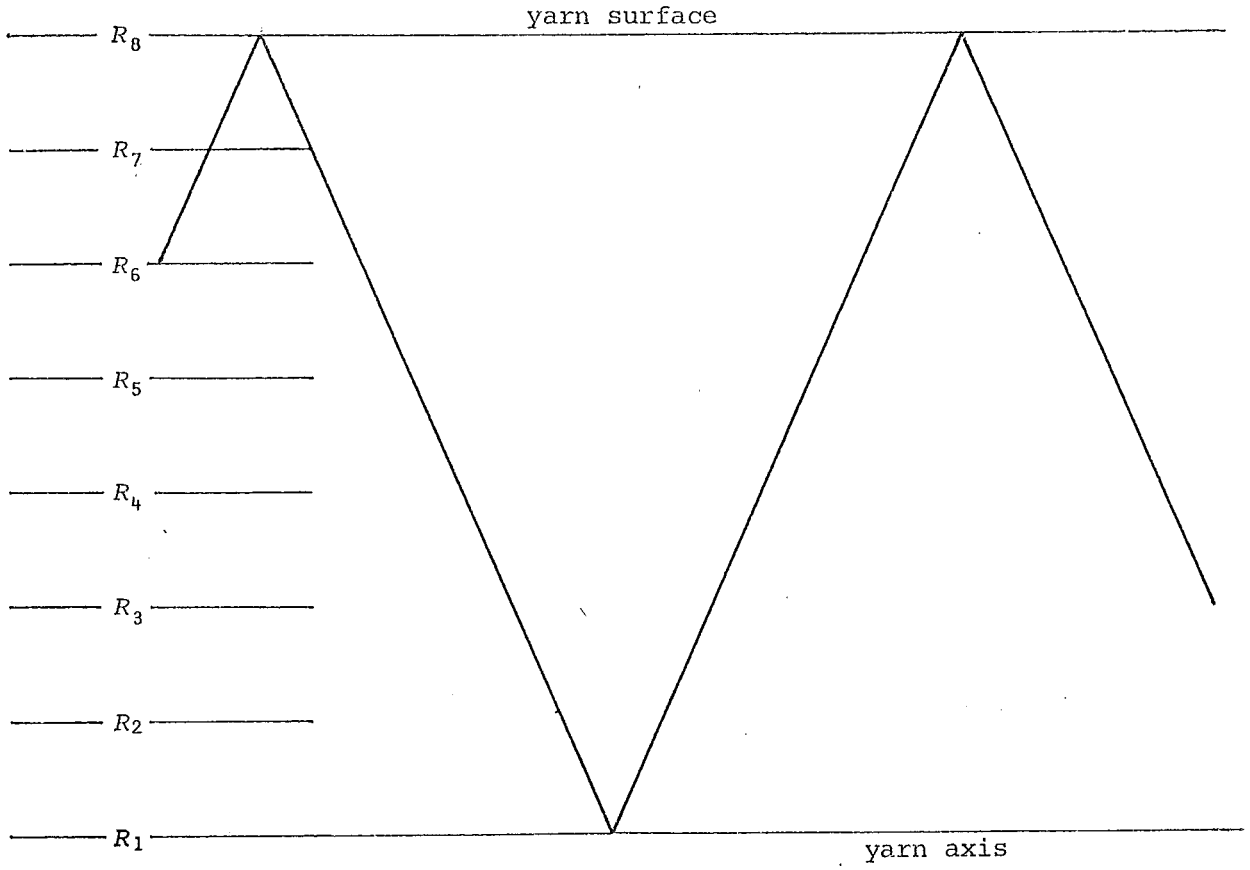

Fig. B1. Elementary shape of migration path

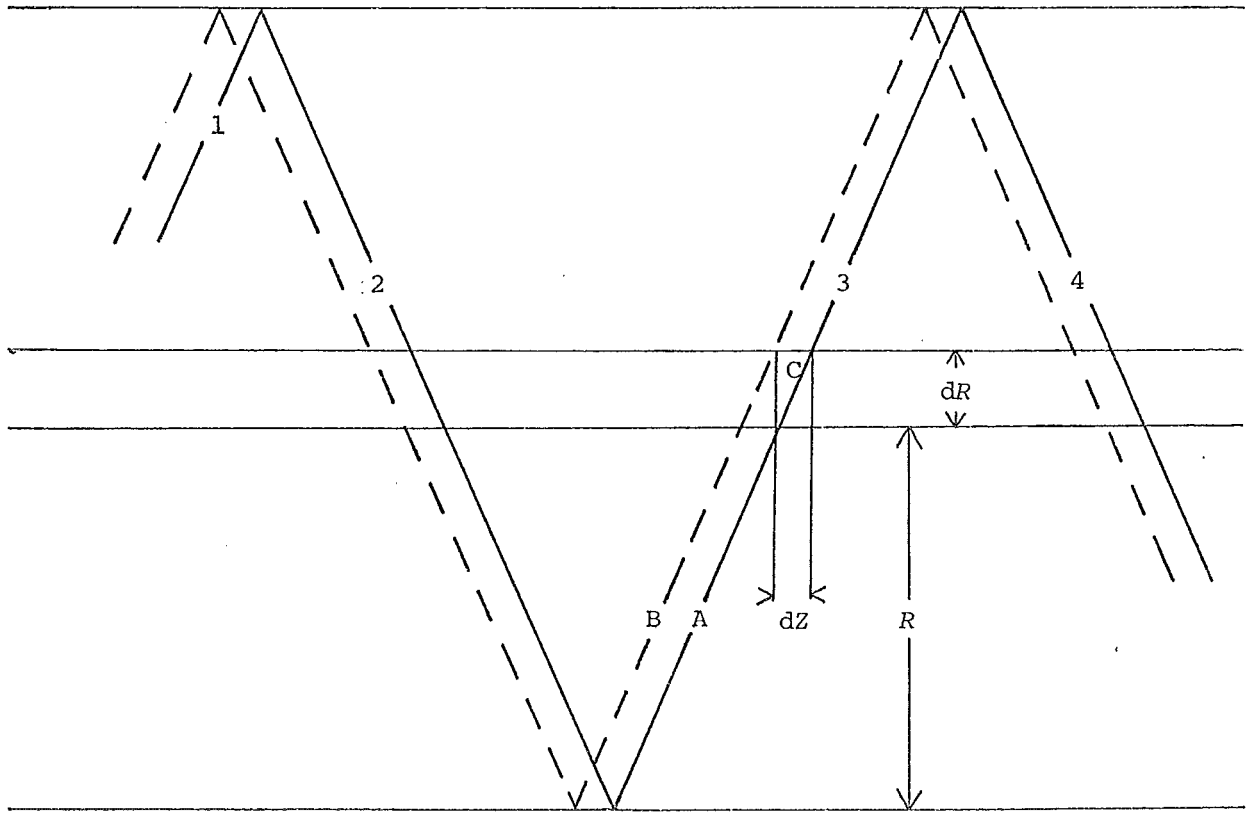

Fig. B2. Calculation of migration path from cross-section density

between R_i and R_{i+1} the total number of fibres which traverse C, which is defined as dN, will be equal to:

$$dN = n_i.dZ/dF \qquad \ldots\ldots\ldots\ldots\ldots\ldots \quad (B4)$$

From the given cross-sectional density of the yarn, $\rho_i(R)$, it follows that the number of fibres traversing C is:

$$dN = 2\pi.R.dR.\rho_i(R) \qquad \ldots\ldots\ldots\ldots\ldots\ldots \quad (B5)$$

On equating Equations (B4 and B5) an expression for dZ in terms of dR is found:

$$dZ = 2\pi.R.\rho_i(R).dF.dR/n_i \qquad \ldots\ldots\ldots\ldots\ldots\ldots \quad (B6)$$

There is still one unknown left in this equation, namely dF. To determine dF the total length of the fibre path is calculated with the aid of Equation (B6) and is then equated to the given length, L_f. From the resulting equation dF can be solved and resubstituted into Equation (B6), from which in turn the migration-path function, $Z = Z(R)$ can be determined.

The infinitesimal volume, dV, shown in Figure B3 is used to calculate the fibre length. The volume dV is taken out of the cylinder discussed before with the sides parallel with the co-ordinate axes and of such dimensions that a fibre traversing the cylinder will pass through diametrically opposed corner points.

The length of a side in the θ direction, $d\theta.R$, is related to dZ by the twist:

$$d\theta = 2\pi.dZ/TT \qquad \ldots\ldots\ldots\ldots\ldots\ldots \quad (B7)$$

where TT is the length along the Z axis of one turn of twist.

Because dV is infinitesimal the fibre segment of length dL can be considered to be straight and dL is defined as:

$$dL = (dR^2 + (d\theta.R)^2 + dZ^2)^{0,5} \qquad \ldots\ldots\ldots\ldots \quad (B8)$$

Substituting Equations (B6 and B7) into the above equation yields:

$$dL = dR.\left[1 + \left(\frac{(2\pi.R)^2.\rho_i(R).dF}{TT.n_i}\right)^2 + \left(\frac{2\pi.R.\rho_i(R).dF}{n_i}\right)^2\right]^{0,5} \quad (B9)$$

To find the total length this equation must be integrated with respect to dR over the total yarn radius. Because of the zonal dependence of N_i and n_i the integration must be done piece-wise over the zones. Also as the fibres traverse a certain zone n_i times the zonal contributions must also be multiplied by n_i. The total length of the fibre which is given by L_f is now defined as:

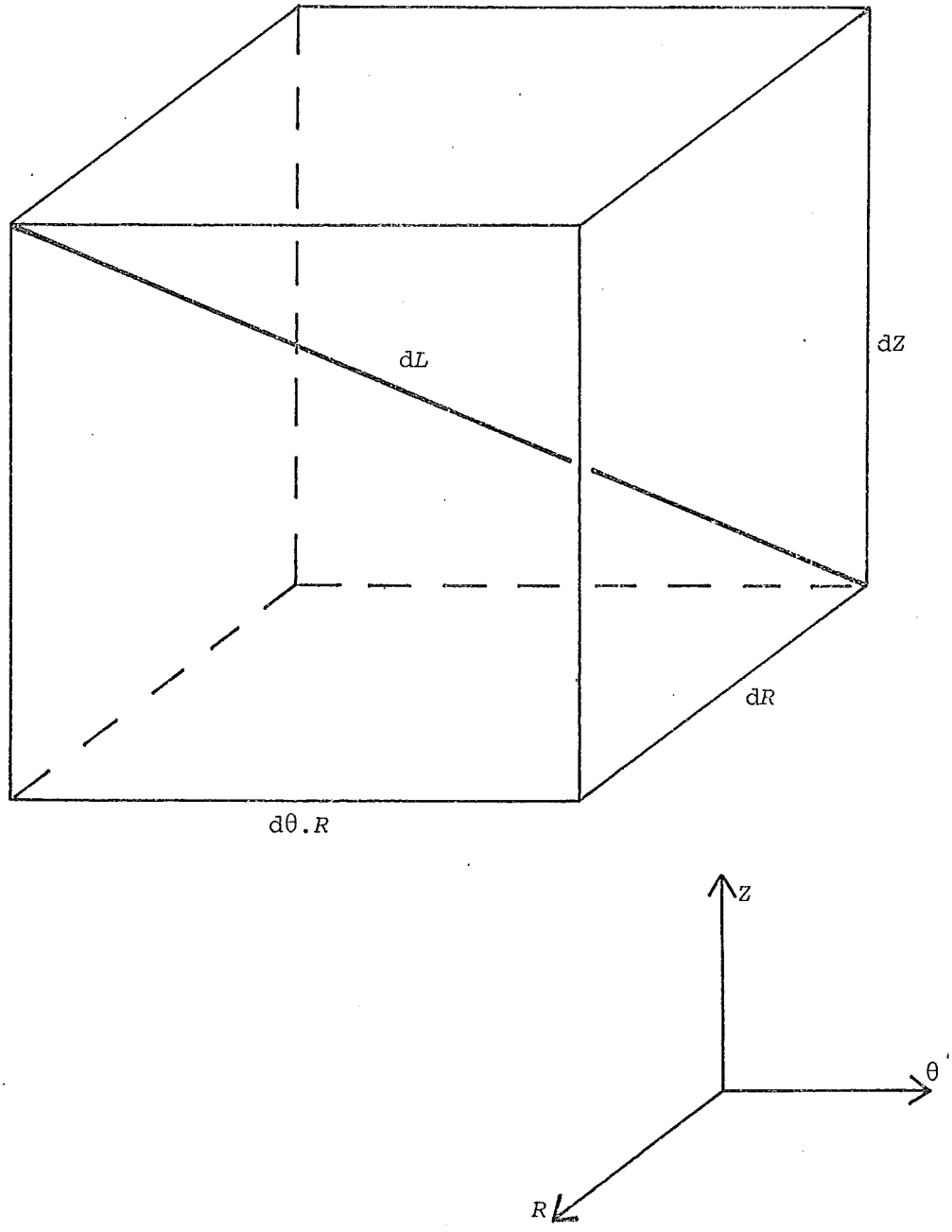

Fig. B3. Infinitesimal volume of a yarn

$$L_f = \sum_{i=1}^{m} n_i \int_{R_i}^{R_{i+1}} \left[1 + \left(\frac{(2\pi.R)^2.\rho_i(R).dF}{TT.n_i} \right)^2 + \left(\frac{2\pi.R.\rho_i(R).dF}{n_i} \right)^2 \right]^{0,5} dR \quad \text{(B10)}$$

where m is the total number of zones.

Numerical techniques must be used to determine dF from the above equation. A crude but simple and (in this case) effective procedure is the bisection method (59) using a numerical integration scheme to evaluate the integral. The integral can only be solved analytically for one particular form of $\rho_i(R)$ which will be discussed in the next section.

When a satisfactory value for dF is found this can be back-substituted into Equation (B6):

$$dZ = 2\pi.R.\rho_i(R).dF.dR/n_i \quad \text{(B11)}$$

Equation (B11) can be integrated to determine Z as a function of R:

$$\int dZ = \frac{2\pi.dF}{n_i} \int (\rho_i(R).R)\,dR \quad \text{(B12)}$$

The solution of Equation (B12) for the three alternative expressions for $\rho_i(R)$ in Equation (B3) becomes:

$$Z = \pi.dF.c_i.R^2/n_i + \text{constant} \quad \text{(B13a)}$$

$$Z = \frac{2\pi.dF}{n_i}.\left(\frac{a_i.R^3}{3} + \frac{b_i.R^2}{2} \right) + \text{constant} \quad \text{(B13b)}$$

$$Z = 2\pi.dF.R/d_i.n_i + \text{constant} \quad \text{(B13c)}$$

The constant can be evaluated at the appropriate places.

The path of the migrating fibre will be smooth if the first derivative of the path function, dZ/dR, is continuous throughout the yarn. This derivative can be determined from Equation (B11):

$$\frac{dZ}{dR} = \frac{2\pi.R.\rho_i(R).dF}{n_i}$$

It is clear that dZ/dR will only be continuous if $\rho_i(R)$ is continuous throughout the yarn as is the case for alternative (b) in the Equations (B3).

PATH LENGTH BEFORE AND AFTER YARN DEFORMATION

The path of the fibre between two radii R_{i+1} and R_i is shown in

Figure B4 in the undeformed yarn configuration. The radii R_{i+1} and R_i are the boundaries of zone i used in the determination of the cross-section density ρ_i. In the analysis performed here the finite element subdivision coincides with these zones which again is not absolutely essential but is very convenient.

The length of the fibre path per zone is derived from Equation (B10):

$$DL_i = \int_{R_i}^{R_{i+1}} \left(1 + \left(\frac{(2\pi.R)^2.\rho_i(R).dF}{TT.n_i} \right)^2 + \left(\frac{2\pi.R.\rho_i(R).dF}{n_i} \right)^2 \right)^{0,5} dR \qquad (B14)$$

This integral can only be solved analytically for one particular form of $\rho(R)$ which is case (c) (Equation (B3)):

$$\rho_i(R) = d_i.R^{-1} \qquad (B15)$$

Substituting Equation (B15) into Equation (B14) yields:

$$DL_i = \int_{R_i}^{R_{i+1}} \left(1 + \left(\frac{(2\pi.R)^2.d_i.dF}{TT.n_i.R} \right)^2 + \left(\frac{2\pi.R.d_i.dF}{n_i.R} \right)^2 \right)^{0,5} dR \qquad (B16)$$

This integral can be written as:

$$B.\int_{R_i}^{R_{i+1}} (A + R^2)^{0,5} dR \qquad (B17)$$

where $$A = \left(1 + \left(\frac{2\pi.d_i.dF}{n_i} \right)^2 \right).B^{-2} \qquad (B18)$$

and $$B = \frac{4\pi^2.d_i.dF}{TT.n_i} \qquad (B19)$$

The solution of Equation (B17) is (71):

$$DL_i = B \left| \left(\frac{R}{2}(A + R^2)^{0,5} + \frac{A}{2} \ln\left| R + (A + R^2)^{0,5} \right| \right) \right|_{R_i}^{R_{i+1}} \qquad (B20)$$

This can be evaluated by using Equations (B18) and (B19).

To determine the length of the fibre path within a zone after yarn deformation the type of deformation must be known. The axial

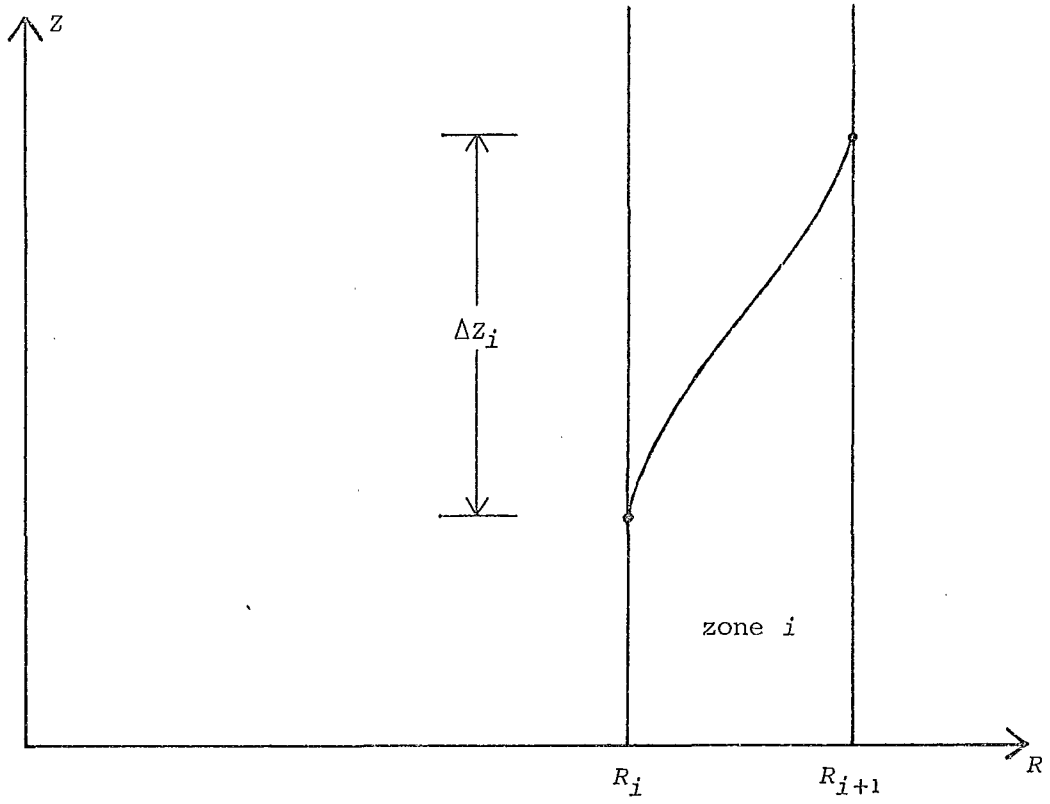

Fig. B4. Migration path in undeformed yarn

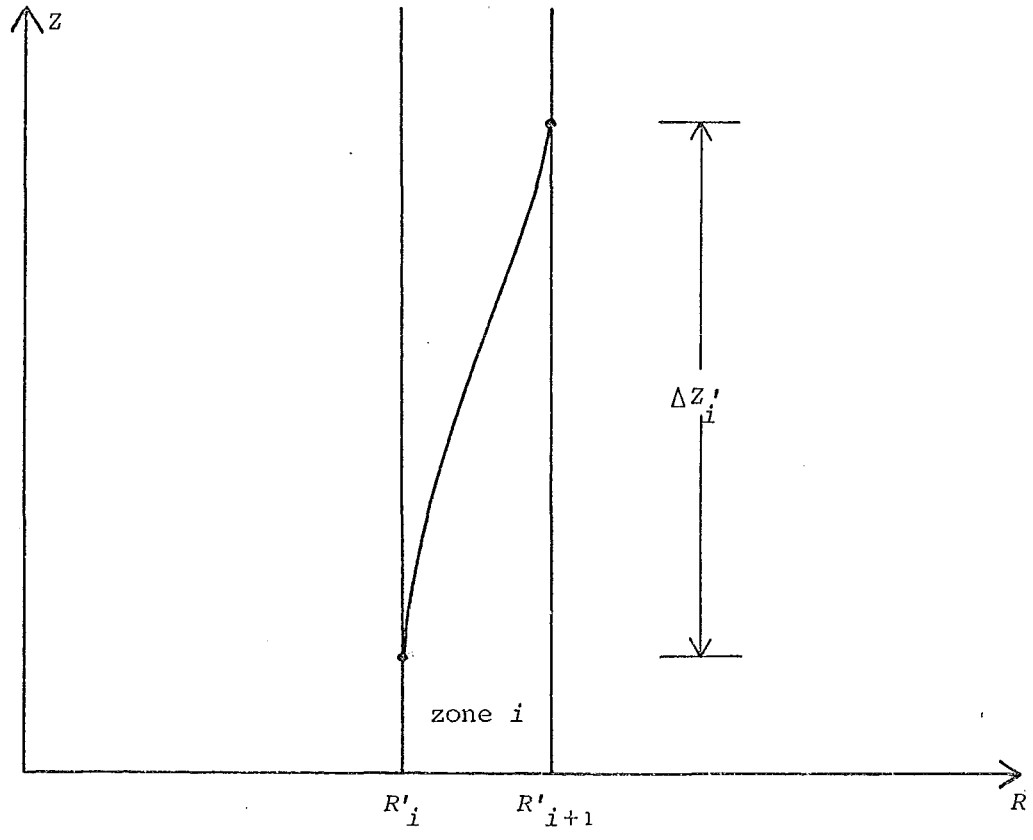

Fig. B5. Migration path in deformed yarn

elongation of the yarn is assumed to be uniform and for the radial deformation it is assumed that this is linear within each zone. In Figure B5 the deformed path of the fibre is shown. The distance in the Z-direction between the entry and exit points of a fibre in a zone is defined as ΔZ_i. In the undeformed configuration ΔZ_i for case (c) will be (Equations B3):

$$\Delta Z_i = \frac{2\pi . d_i . dF . (R_{i+1} - R_i)}{n_i} \qquad \ldots\ldots\ldots \text{(B21)}$$

Because of the uniform deformation in the axial direction, $\Delta Z'_i$, which is the distance between entry and exit points in the deformed yarn, becomes:

$$\Delta Z'_i = (1 + E_y) . \Delta Z_i \qquad \ldots\ldots\ldots \text{(B22)}$$

where E_y is the relative axial elongation of the yarn.

The length of the fibre path can be determined with the aid of Figure B3 where the original lengths of the sides dR and dZ are changed into dR' and dZ' respectively. These are:

$$dR' = dR . (R'_{i+1} - R'_i) . (R_{i+1} - R_i)^{-1} \qquad \ldots\ldots \text{(B23a)}$$

$$dZ' = (1 + E_y) dZ \qquad \ldots\ldots\ldots \text{(B23b)}$$

The expression for the length of the third side remains the same:

$$d\theta' . R = 2\pi . dZ . R/TT \qquad \ldots\ldots\ldots \text{(B23c)}$$

because dZ and TT deform the same amount.

After some manipulation of Equations (B23), Equations (B6 and B8) yield for the length of the fibre path in a deformed zone:

$$DL'_i = B' \int_{R'_i}^{R'_{i+1}} (A' + R^2) dR' \qquad \ldots\ldots\ldots \text{(B24)}$$

where $$A' = \left\{ 1 + \left[\frac{(1 + E_y) . 2\pi . R . \rho_i(R) . dF . (R_{i+1} - R_i)}{n_i . R'_i - R_i} \right]^2 \right\} B'^{-2}$$

and $$B' = \left[\frac{(2\pi . R)^2 . (1 + E_y) . \rho_i(R) . dF . (R_{i+1} - R_i)}{n_i . TT . (R'_{i+1} - R'_i)} \right] .$$

The solution of the above equation for case (c) is:

$$DL'_i = B' \Big|_{R'_i}^{R'_{i+1}} \left[\frac{R}{2} (A' + R^2)^{0,5} + \frac{A'}{2} \ln \left| R + (A' + R^2)^{0,5} \right| \right] \qquad \text{(B25)}$$

Equation (B24) cannot be solved explicitly for the other forms of $\rho_i(R)$.

APPENDIX C

APPROXIMATION OF FIBRE STRESS-STRAIN CURVE

A typical 'stress-strain' curve for a wool fibre is shown in Figure C1 in the form in which it is used in the analyses presented here, where F_A is the fibre axial force and E_f the relative elongation.

The curve must be approximated for use in calculations and in this case a piece-wise linear function is used, of the form:

$$F_A = a.E_f + b \qquad \ldots\ldots\ldots\ldots \quad (C1)$$

An example of this type of approximation is shown in Figure C1. The straight line through points i and $i+1$ is defined by:

$$F_A = \left(\frac{F_{A_{i+1}} - F_{A_i}}{E_{f_{i+1}} - E_{f_i}}\right).(E_f - E_{f_i}) + F_{A_i} \qquad \ldots\ldots\ldots \quad (C2)$$

Equating Equations (C1 and C2) yields:

$$a_i = (F_{A_{i+1}} - F_{A_i}).(E_{f_{i+1}} - E_{f_i})^{-1}$$

and $$b_i = -a_i.E_{f_i} + F_{A_i},$$

where a_i and b_i are valid between the points i and $i+1$.

The inverse function is:

$$E_f = a'_i.F_A + b'_i$$

where $$a'_i = a_i^{-1}$$

and $$b'_i = -b_i.a_i^{-1}.$$

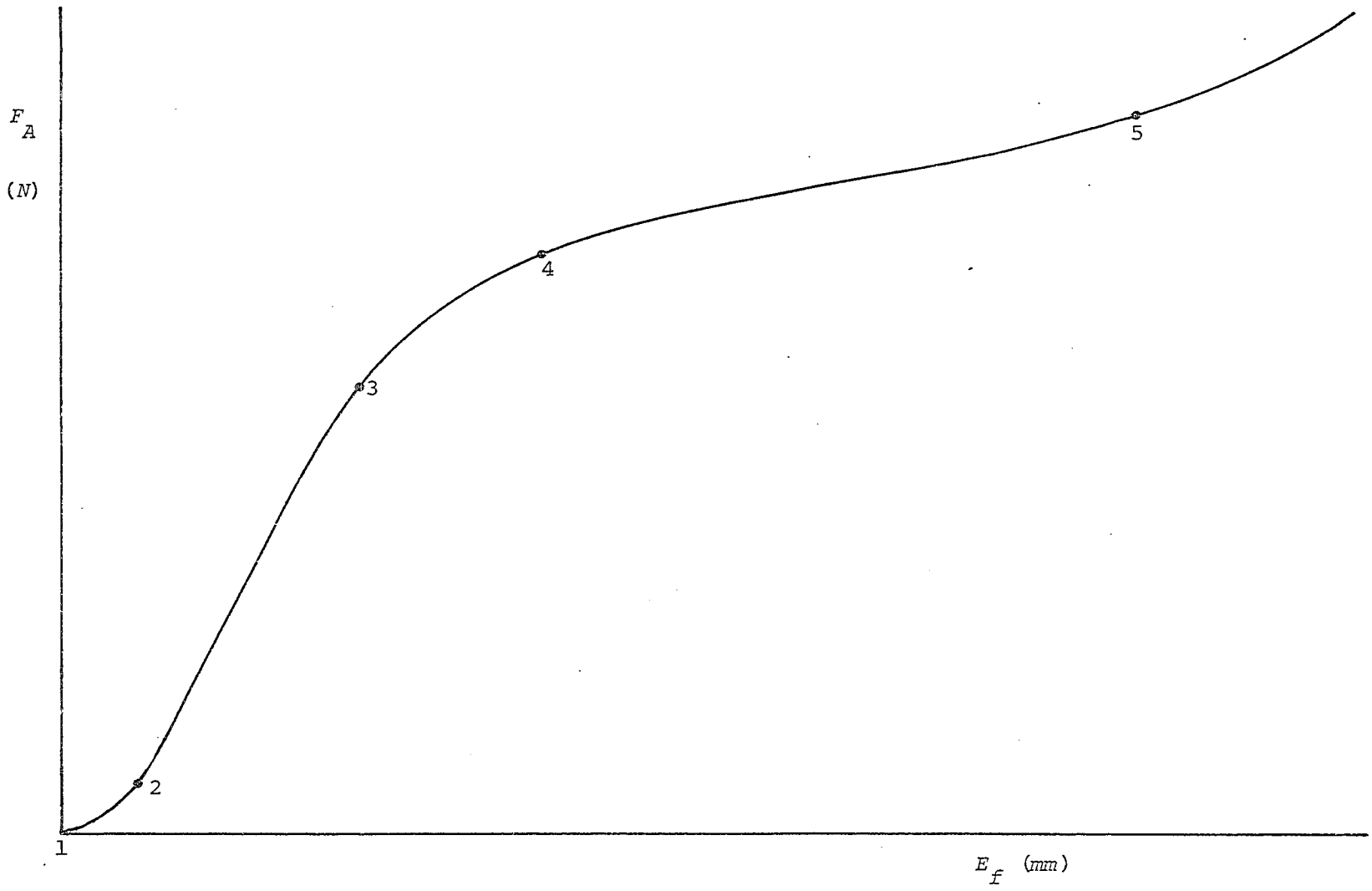

Fig. C1. Stress-strain curve of a wool fibre

APPENDIX D

CORRECTION FACTOR C FOR INTER-FIBRE FRICTION

INTRODUCTION

The axial force in a fibre in the staple-fibre model is caused by friction at the inter-fibre contact points. The individual contact frictional forces, F_c, are assembled into *FR*, the frictional force per unit length exerted on the fibre. The magnitude of F_c is known but not its direction. This is expressed in the equation for *FR* in Section 5.3.2, Equation (5.4), as the number of fibre contacts at which the frictional force, F_c, aids or opposes the slippage of a fibre. This is included in a correction factor, C, which is used to determine *FR* from the single-fibre withdrawal force, *WF*.

The correction factor, C, is given (Equation 5.6) as:

$$C = (1 - 2.n_{aid}.n_c^{-1}) \quad . . . . . \quad (D1)$$

where n_{aid} = the number of fibre contacts per unit length at which the frictional force aids the fibre in its movement, and

n_c = the total number of fibre contacts per unit length.

The ratio of n_{aid} to n_c, and therefore C, will be different for different migration paths and it can also vary along the path. Here this ratio is estimated for the two alternative migration paths used in the analysis described in Chapter 5.

V-SHAPED MIGRATION ENVELOPE

The V-shaped migration path as used here is symmetrical and has the fibre ends at the yarn surface as shown in Figure D1. Also shown is a small segment of a typical fibre, dA, which is situated in the outward migrating 'leg' ($\partial R/\partial Z > 0$). In the immediate vicinity of dA there are two groups of fibres, one migrating outwards like dA and one migrating inwards; these will be designated by an O and an I respectively.

Over the length of dA there will be n_c.dA contacts with neighbouring fibres. The parameter, n_c, is dependent on the local specific volume, V_{sp}, so it will be dependent on the radial location of dA, but over a small section of fibre it can be regarded as being constant. Because of the symmetry of the fibre paths in the model and the uniform distribution of fibres in the Z direction it can be assumed that on average the inter-fibre contacts along dA are equally divided between the inward and outward migrating fibres. If dA, which belongs to group

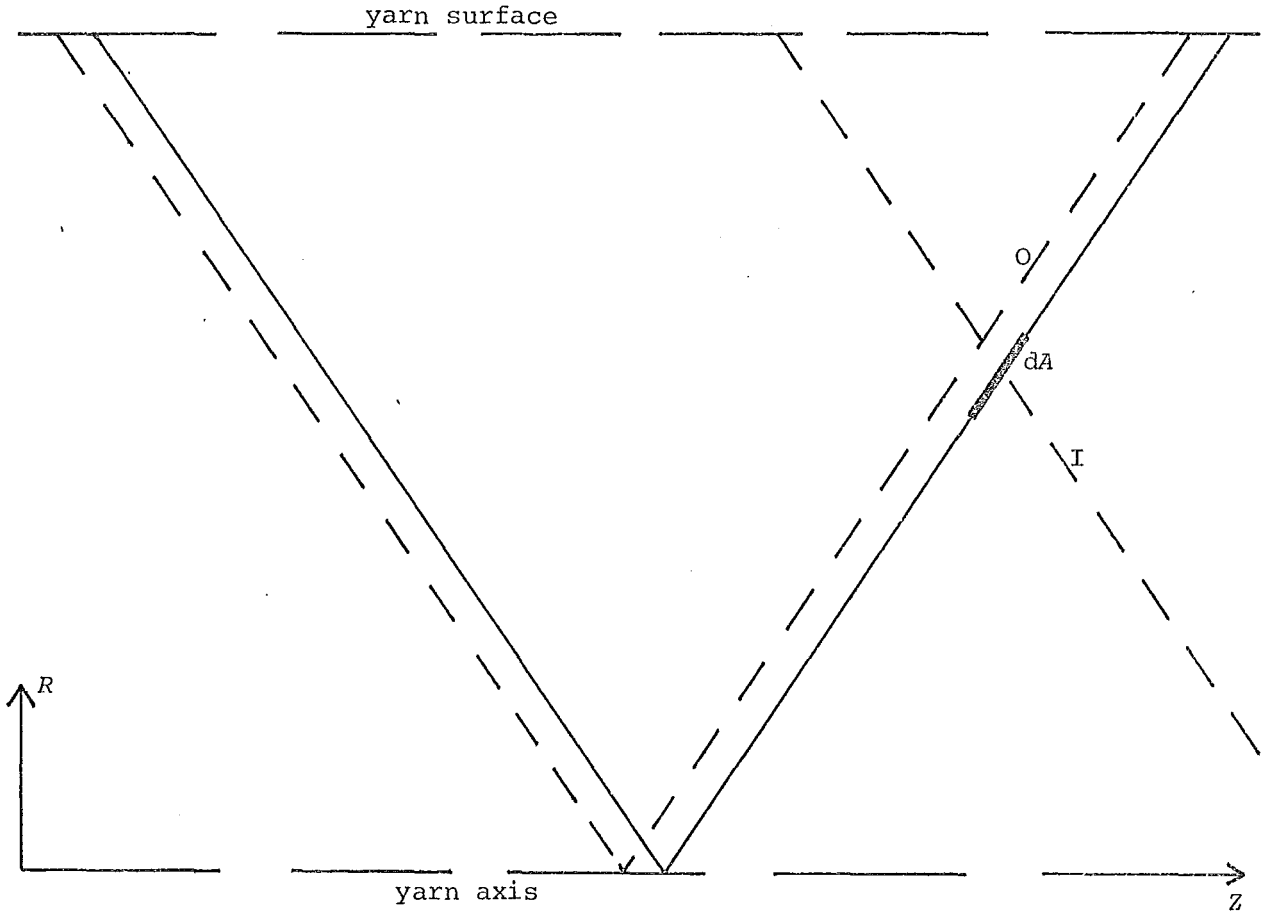

Fig. D1. V-shaped migration path

O, slips or tends to slip in a certain direction with respect to its tube all the neighbouring fibres of group I will slip (or tend to slip) approximately the same amount but in the opposite direction. The frictional forces, F_c, at the contacts between dA and neighbouring fibres of group I will therefore oppose the (potential) movement of dA in its tube. The neighbouring fibres of group O will (tend to) move approximately the same amount as dA and in the same direction. It must be noted that it will be very rare that a contacting fibre of group O will slip (or tend to slip) exactly the same amount as dA, therefore there will always be a slight difference in (potential) movement. From this it follows that the frictional forces at contacts between dA and fibres of group O will either aid or oppose dA in its movement; 'neutral' contacts can be neglected. The problem now is to quantify the portion of contacts which aid dA in its movement. As the neighbouring fibres of group O should show no bias towards slipping more or less than dA it is assumed here that half of the fibres of group O aid dA in its movement and the other half oppose it. As the fibres of group O make up half the contacts, as mentioned above, the proportion of contacts along dA at which frictional forces are exerted aiding dA in its movement will be approximately one-quarter of the total. This fraction is independent of the number of contacts per unit length so the correction factor for a V-shaped migration envelope is constant along the fibre and is (Equation D1):

$$C_V = (1 - 2 \times 0{,}25) = 0{,}5 \qquad \ldots\ldots\ldots \text{(D2)}$$

W-SHAPED MIGRATION ENVELOPE

A W-shaped migration envelope is shown in Figure D2 with the 'legs' numbered from 1 to 4. Because of the symmetrical behaviour of the fibre a certain relationship can be derived for the direction and amount of slipping of four fibre segments, each from a different leg of the W, located at the same radial position in the model. In Figure D3 a typical example is shown where the arrows indicate the direction and the amount of slipping and the figures designate the legs of the W to which the fibre segments belong. The amount of slipping of the fibre segments 1 and 4 is equal in magnitude but opposite in direction; the same holds for the pair of fibre segments, 2 and 3. The condition of symmetrical behaviour does not relate in any way to the amount or the direction of slipping between the pairs 1 and 4, and 2 and 3. However, the conditions set in Section 5.3.3 in order to use a simple method to determine the axial force imply that slipping is always towards the middle, M, and decreases with increasing distance from the fibre end.

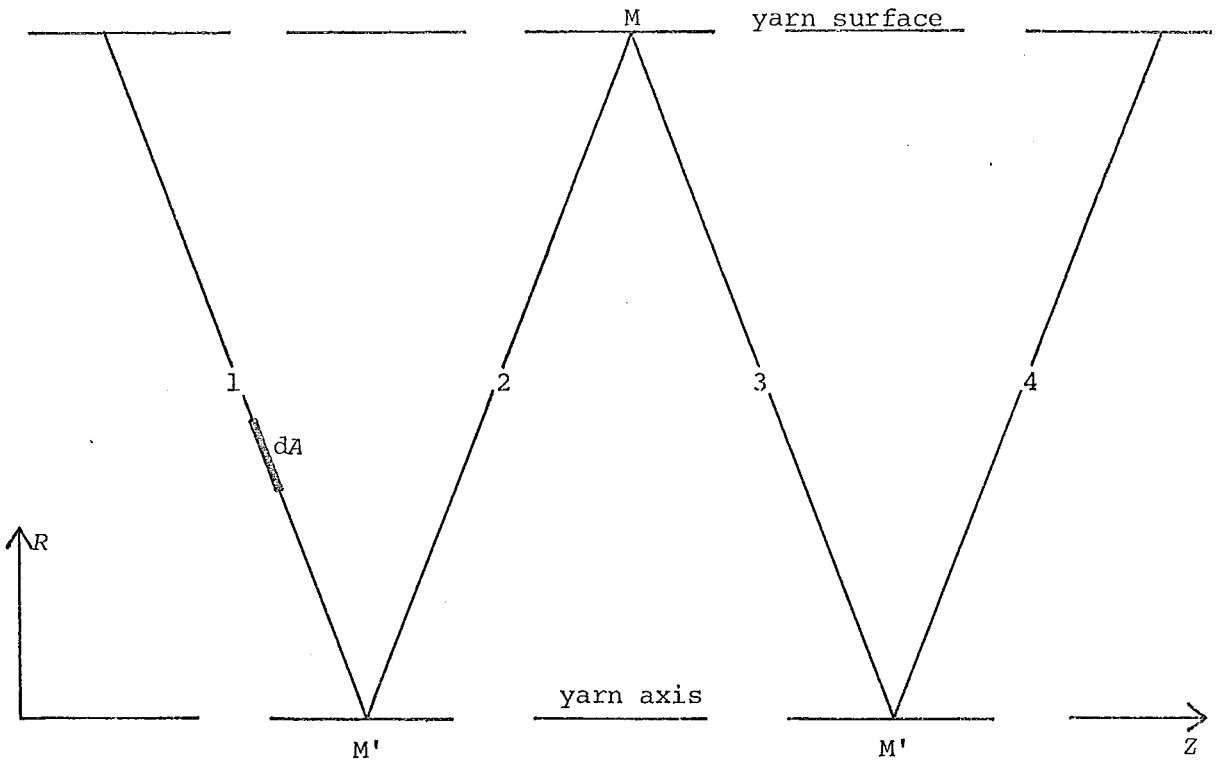

Fig. D2. W-shaped migration path

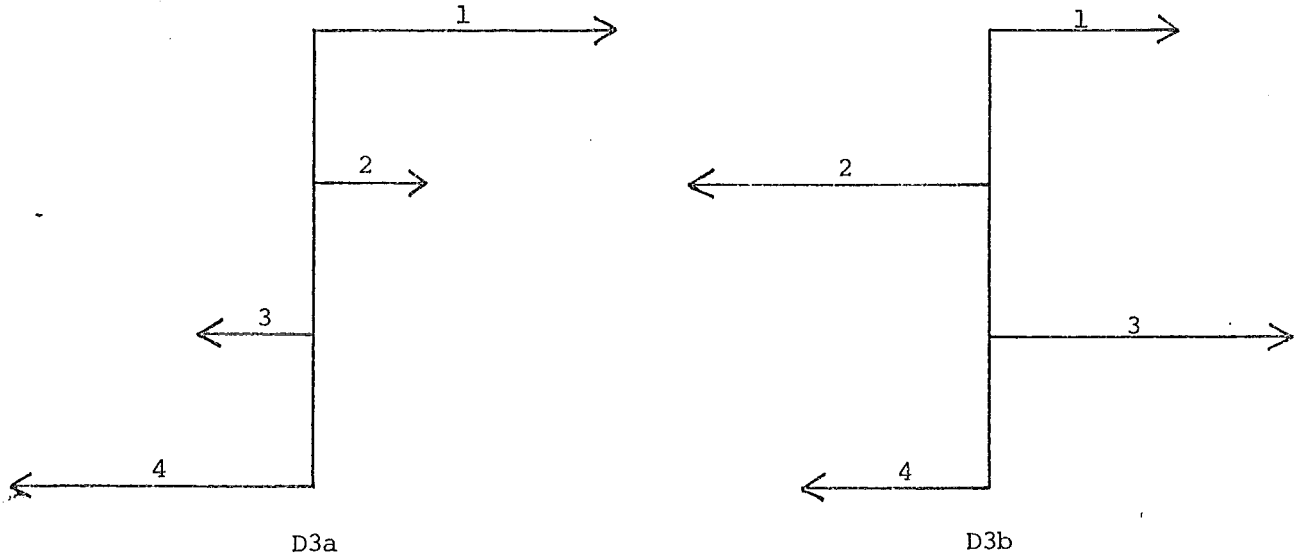

Fig. D3. Direction and amount of slippage of each leg of the W-shaped migration path

If that is the case there is no other possibility than indicated in Figure D3a, and the situation in Figure D3b could not arise.

A small fibre segment, dA, which is located in leg 1, will have a certain number of contacts along its length with other fibres. Because of the symmetry of the fibre paths and of the uniform distribution of fibres over the length of the yarn the contacts will, on average, be equally divided between the four legs, i.e., one-quarter of the contacts will be with leg 1 of other fibres and so on. It is evident from Figure D3a that fibres which contact dA, which belongs to leg 1, with their second, third or fourth legs will resist the slipping of dA. Using the same argument as in the previous section it follows that the fibres which contact dA with their first leg will be equally divided into aiding and opposing dA in its movement. From the above it follows that if dA is located in one of the outside legs of the W only one-eighth of the contact frictional forces will aid dA in its movement. Therefore:

$$^{O}C_{W} = (1 - 2 \times 0{,}125) = 0{,}75 \qquad \ldots\ldots\ldots \text{(D3)}$$

In the same way as above the correction factor for the inner leg follows:

$$^{I}C_{W} = (1 - 2 \times 0{,}375) = 0{,}25 \qquad \ldots\ldots\ldots \text{(D4)}$$

APPENDIX E

EXPERIMENTAL DETERMINATION OF FIBRE AND YARN STRENGTH

MEASUREMENT OF FIBRE AND YARN STRENGTH

The tensile properties of the wool fibres and yarns used in the evaluation of the analyses were measured on an Instron Tensile-testing machine. The specimens were elongated at a fixed rate and the resulting yarn forces were recorded on a chart against the elongation. For both short-gauge and long-gauge tests on the yarns they were simply clamped in the jaws of the testing machine, but a different method was used for the fibres which were difficult to manipulate because of their fineness. Fibres were first mounted with tape on a cardboard slide frame, as shown in Figure E1. The slide frames were easily mounted in the jaws of the testing machine, the sides of a frame being cut as illustrated in Figure E1 before starting the actual test.

INTERPRETATION AND AVERAGING OF RESULTS

Ideally the fibres and yarns were mounted in the jaws under a very low tension compared with their ultimate breaking tension, so that the specimen length at zero load can be taken as the gauge length, the distance between the tips of the jaws. However, especially in the case of fibres, this was impossible to do manually and therefore the fibres and yarns were always actually mounted with a certain amount of 'slack', i.e., slightly buckled. Some typical load-extension curves are shown in Figure E2; E2a concerns fibres with no crimp and E2b is typical of crimped fibres. Yarns manufactured from straight or crimped fibres showed a similar kind of behaviour in the initial range of elongation.

As can be seen in Figure E2a the load-extension curves were not necessarily 'lined up', i.e., their starting points did not coincide. This was due to the fibres (or yarns) being mounted slightly buckled in the testing machine, the exact amount of slack not being reproducible. When averaging the curves it was therefore necessary to have a reference point on each curve. In the case of uncrimped fibres this would be the starting point of each curve, A_1 and A_2. In the case of crimped fibres the usual procedure was to extend the linear part of the load-extension curve to the extension axis, giving the points A_3 and A_4 in Figure E2b. The straight length of a fibre (or yarn), SL, is then defined as

$$SL = GL + A \qquad \text{(E1)}$$

where GL is the gauge length between the jaws of the testing machine.

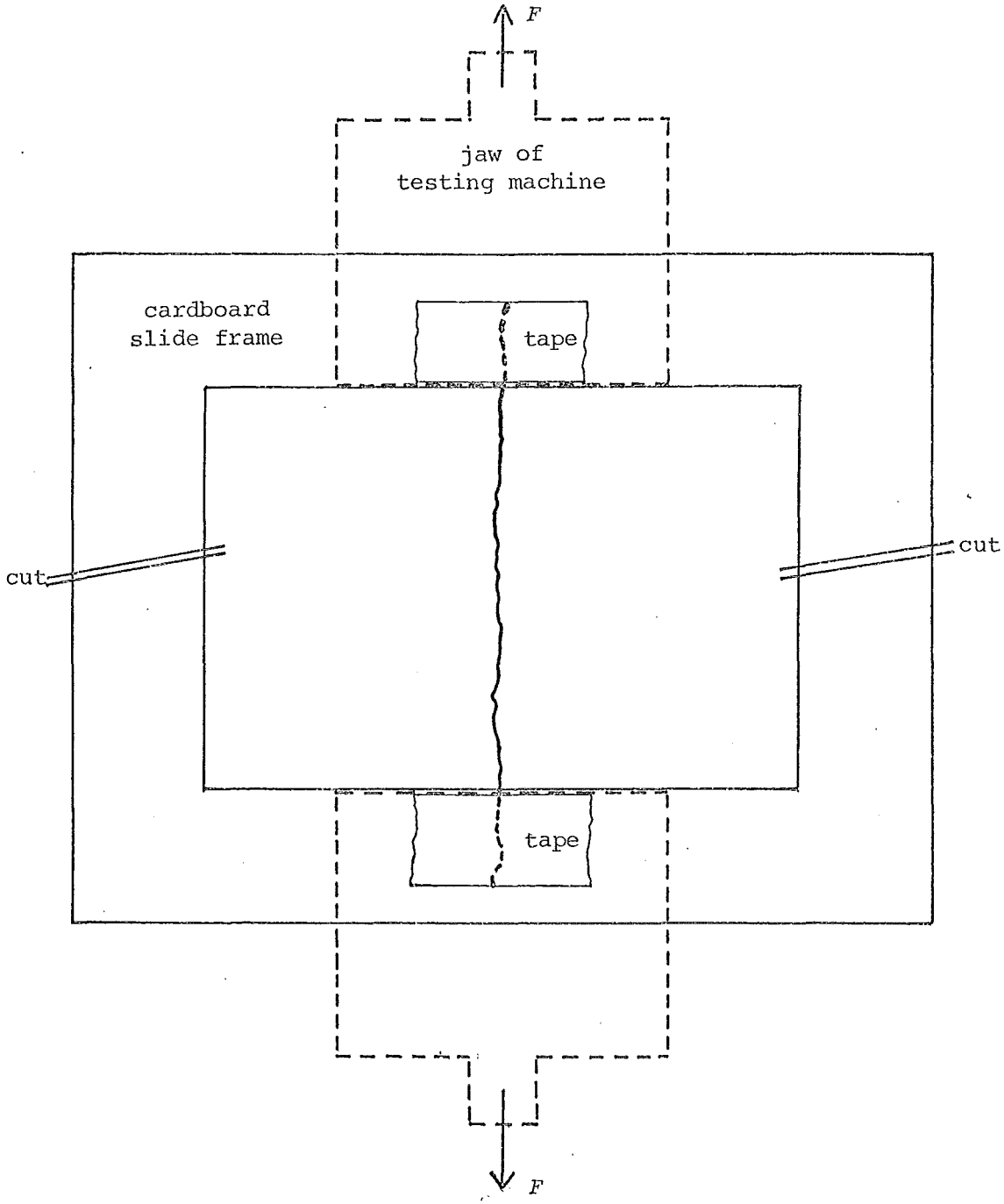

Fig. E1. Mounting of a fibre for testing its tensile strength

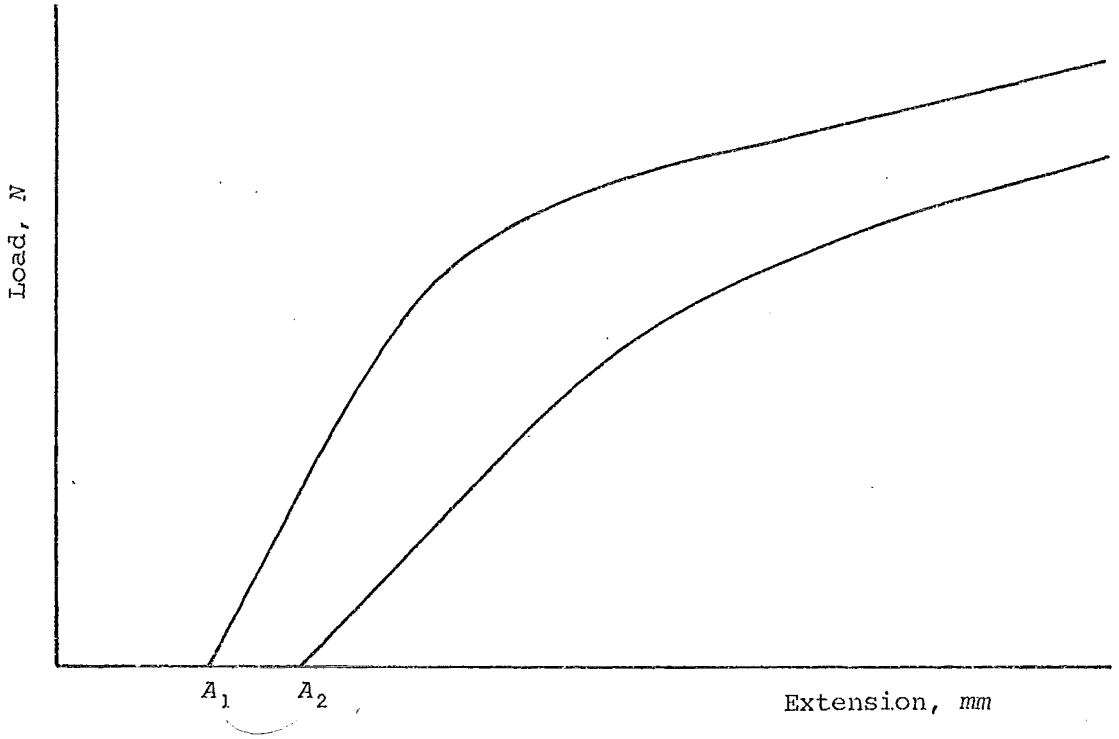

(a) without crimp

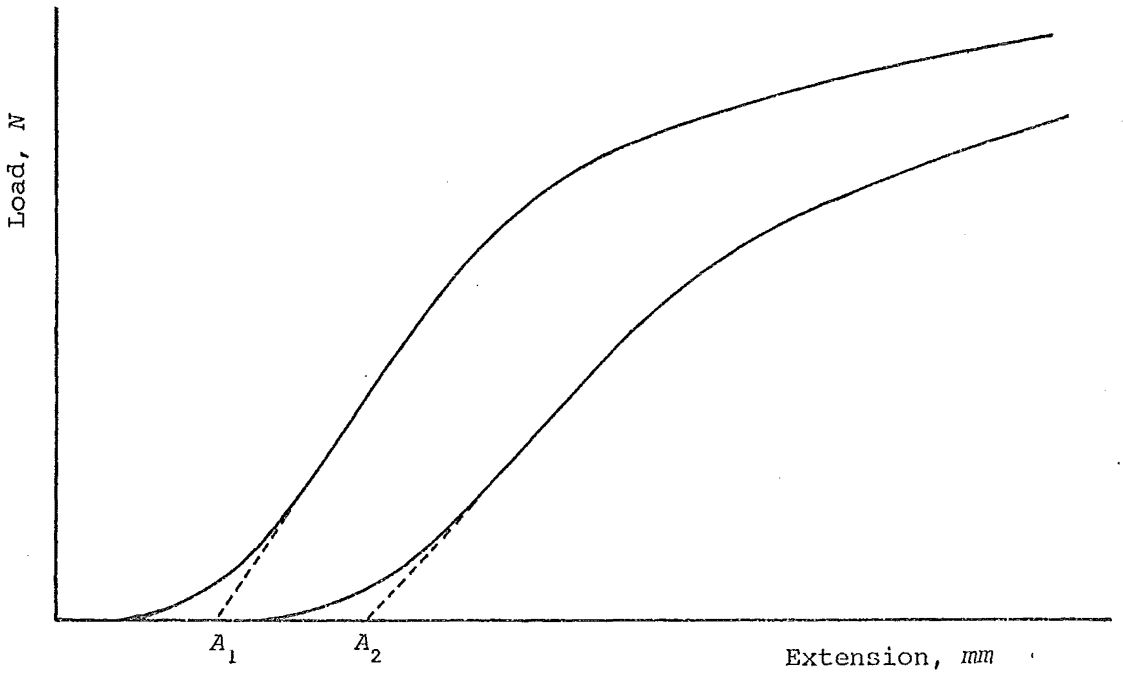

(b) with crimp

Fig. E2. Load-extension curves of wool fibres

The average value for SL was found in the usual way, i.e., by summing the values for each fibre and dividing by the number of specimens. The values of the extension for the reference point, $\bar{A}$, of the averaged curves is: $\bar{A} = \overline{SL} - GL$ . . . . . (E2)

Each load-extension curve was then converted so that the points A_i of each curve coincided with point A. These converted curves were then averaged in the usual way, the results being shown in Figure E3. The main problem was to define the point where the curve started. One fibre with a long uncrimping region would cause the average curve to also have a long uncrimping region. In this case commonsense was used and a reasonable point was chosen, designated by B in Figure E3. The average load-extension curve was then converted so that B coincided with the origin and so that the horizontal axis was expressed in relative elongation, %, rather than absolute extension.

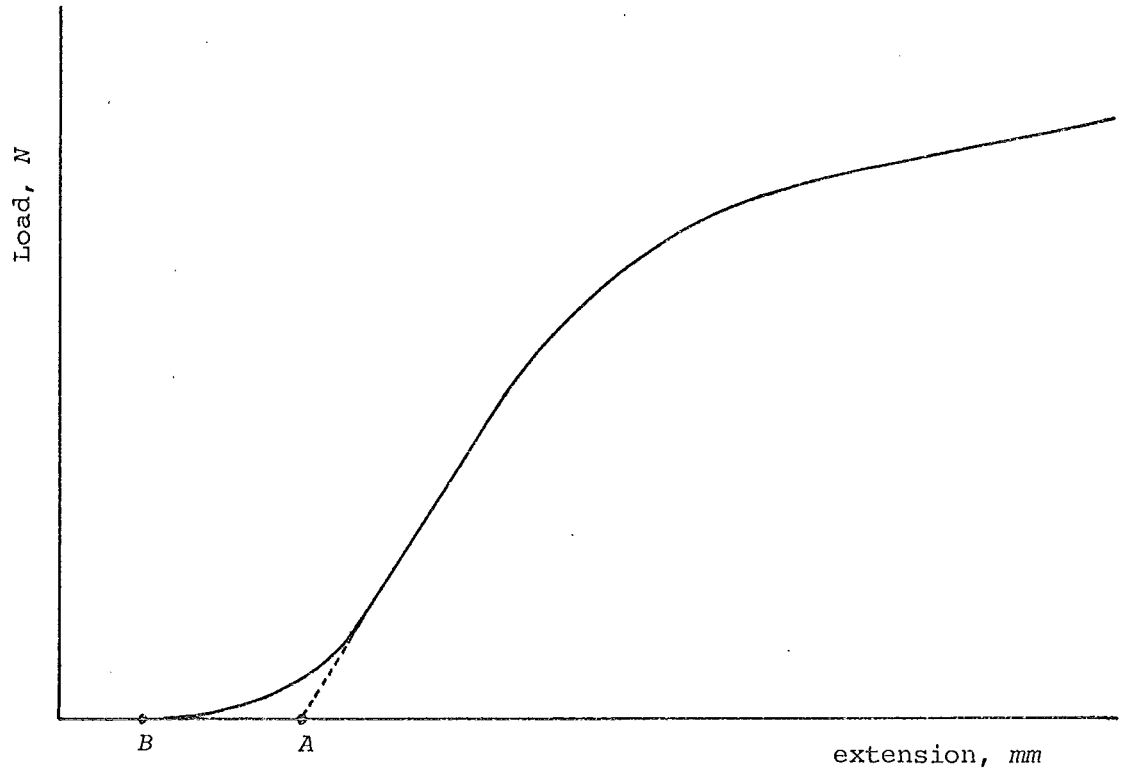

Fig. E3. Averaged fibre or yarn load-elongation curve

APPENDIX F

EXPERIMENTS ON THE COMPRESSIVE BEHAVIOUR OF WOOL SLIVERS

The aim of these experiments was to find a value for the constant, K, as used in the van Wyk relationship (Equation 2.1):

$$p = K\,(V_{sp}^{-3} - V_{sp_0}^{-3}) \qquad \ldots\ldots\ldots\ldots \quad (F1)$$

where p = lateral pressure exerted on the sliver

V_{sp} = current specific volume

V_{sp_0} = specific volume when $p = 0$.

The apparatus used in the experiments was very simple, namely a short U-shaped channel and a plunger which fitted into the channel as shown in Figure F1. The sliver was laid in the channel so that the general direction of the fibres in the sliver coincided with the x-axis as shown in Figure F1. The plunger was then placed on top of the sliver in the channel and a slowly increasing force, F, was exerted on the plunger in the Z direction. During the experiment two parameters were monitored, the force, F, and the height, h. At the end of the experiment, while the plunger was still at its lowest position, the ends of the sliver protruding from the channel were cut off with a razor blade; the plunger was then removed and the mass, M, of the remaining piece of sliver was determined.

The lateral pressure on the sliver is simply determined by:

$$p = F.(b.l)^{-1} \qquad \ldots\ldots\ldots\ldots \quad (F2)$$

and the specific volume, V_{sp}, by:

$$V_{sp} = h.b.l.(M)^{-1} \qquad \ldots\ldots\ldots\ldots \quad (F3)$$

The results are plotted with $(V_{sp}^{-3} - V_{sp_0}^{-3})$ on the horizontal axis and p on the vertical axis. A typical result is shown in Figure 2.2. The value of V_{sp_0} is usually found by setting out the values of p against V_{sp}^{-3} for the lower pressure range and extrapolating the curve to $p = 0$.

In this kind of graph a curve following the van Wyk relationship will be a straight line through the origin with tangent, K. From this it follows that an appropriate value for K can be found by fitting a straight line through the origin to the experimentally derived curve. In the large majority of experiments carried out by the author the shape of the experimental curve was such that there was no ambiguity about the best-fitting value for K. The deviation at the top of the curve in Figure 2.2, which is typical, is discussed in Section 2.4.1.

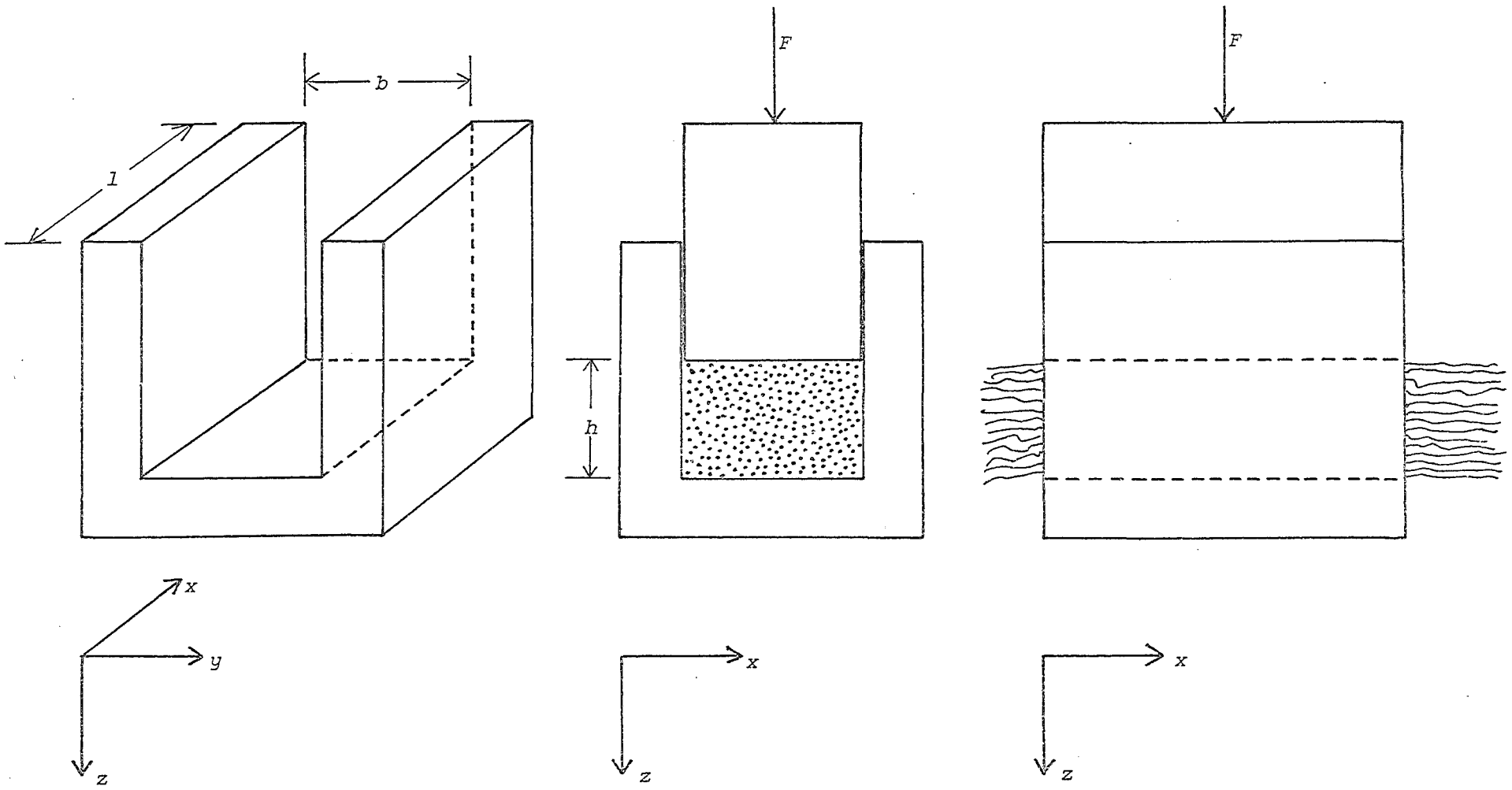

Fig. F1. Apparatus for testing lateral compressibility of a wool sliver

APPENDIX G

LATERAL PRESSURE DUE TO HELICALLY ORIENTED FIBRE TENSION

Given is a yarn with a co-ordinate system, (R,θ,Z). The principle stresses in the yarn are located in the fibre co-ordinate system, $(R_\alpha,\theta_\alpha,Z_\alpha)$, which is obtained by rotating the yarn co-ordinate system by an amount, α (helix angle), around the R axis.

The principle stresses are defined as:

$$\sigma_{RR\alpha} = \sigma_{\theta\theta\alpha} = T_L$$

$$\sigma_{ZZ\alpha} = T_A \ .$$

The problem is to determine the value of T_L if T_A is given.

The Cauchy equations of motion in the yarn co-ordinate system are defined as

$$\frac{\partial\sigma_{RR}}{\partial R} + \frac{1}{R}\cdot\frac{\partial\sigma_{R\theta}}{\partial\theta} + \frac{\partial\sigma_{RZ}}{\partial Z} + \frac{\sigma_{RR} - \sigma_{\theta\theta}}{R} = 0 \qquad \text{(G1a)}$$

$$\frac{\partial\sigma_{R\theta}}{\partial R} + \frac{1}{R}\cdot\frac{\partial\sigma_{\theta\theta}}{\partial\theta} + \frac{\partial\sigma_{\theta Z}}{\partial Z} + \frac{2\sigma_{R\theta}}{R} = 0 \qquad \text{(G1b)}$$

$$\frac{\partial\sigma_{RZ}}{\partial R} + \frac{1}{R}\cdot\frac{\partial\sigma_{\theta Z}}{\partial\theta} + \frac{\partial\sigma_{ZZ}}{\partial Z} + \frac{\sigma_{RZ}}{R} = 0 \qquad \text{(G1c)}$$

In the case where the yarn is uniform along the Z axis and is axisymmetric the following terms will be zero:

$$\frac{\partial\sigma_{ZZ}}{\partial Z} = \frac{\partial\sigma_{\theta\theta}}{\partial\theta} = \frac{\partial\sigma_{\theta Z}}{\partial Z} = \frac{\partial\sigma_{\theta Z}}{\partial\theta} = 0 \qquad \text{(G2)}$$

In order to describe the stresses in the yarn co-ordinate system in terms of T_A and T_L these are are transformed from $(R_\alpha,\theta_\alpha,Z_\alpha)$ to (R,θ,Z). This is done with the aid of a transformation matrix, $[TM]_\alpha$, which is described in Section 4.3.5.

$$\sigma_{RR} = T_L \qquad \text{(G3a)}$$

$$\sigma_{\theta\theta} = c^2.T_L + s^2.T_A \qquad \text{(G3b)}$$

$$\sigma_{ZZ} = s^2.T_L + c^2.T_A \qquad \text{(G3c)}$$

$$\sigma_{\theta Z} = c.s.T_L - c.s.T_A \qquad \text{(G3d)}$$

$$\sigma_{R\theta} = \sigma_{ZR} = 0 \qquad \text{(G3e)}$$

where $c = \cos\alpha$ and $s = \sin\alpha$.

Substituting Equations (G2 and G3) into Equations (G1) yields:

$$\frac{\partial T_L}{\partial R} + \frac{T_L - c^2 . T_L - s^2 . T_A}{R} = 0 \qquad \ldots\ldots\ldots \text{(G4)}$$

The other two equations vanish and Equation (G4) can be rewritten as:

$$\frac{\partial T_L}{\partial R} + \frac{\sin^2\alpha (T_L - T_A)}{R} = 0 \qquad \ldots\ldots\ldots \text{(G5)}$$

The unknown in the above equation is T_L which implies that Equation(G5) is a first-order linear differential equation of the form:

$$\frac{\partial T_L}{\partial R} + P(R) . T_L = Q(R) \qquad \ldots\ldots\ldots \text{(G6)}$$

where $P(R) = \sin^2\alpha / R$

$Q(R) = \sin^2\alpha . T_A / R$.

The general solution of Equation (G6) is (73):

$$T_L = e^{-\int P(R)\,dR} . \left(\int Q(R) . e^{\int P(R)\,dR} dR + C \right) \qquad \ldots\ldots \text{(G7)}$$

With $P(R)$ and $Q(R)$ defined as in Equation (G6) the solution will be impossible to obtain if α and T_A are determined by the Equations (4.6d and 4.15) in Sections 4.3.2 and 4.3.5 respectively. If, however, T_A and α are assumed to be constant within a series of small ranges of R, i.e., elements, a piecewise solution can be obtained relatively easily.

Using Equation (G6) the integral $\int P(R)$ becomes:

$$\int P(R)\,dR = \int \frac{s^2}{R} dR = s^2 \ln R$$

from which follows:

$$e^{\int P(R)\,dR} = e^{s^2 . \ln R} = R^{s^2} .$$

Equation (G7) now becomes:

$$T_L = R^{-s^2} . \left(\int \frac{s^2 . T_A}{R} . R^{s^2} dR + C \right)$$

$$= R^{-s^2} . \left(\int s^2 . T_A . R^{s^2 - 1} dR + C \right)$$

$$= R^{-s^2} \left(\frac{s^2 . T_A . R^{s^2}}{s} + C \right).$$

$$T_L = T_A + C . R^{-s^2} \qquad \ldots\ldots\ldots \text{(G8)}$$

To find C a boundary condition must be given. In this case the boundary condition is:

$$T_L(R_{ys}) = 0$$

where R_{ys} = the radial position of the yarn surface.

This implies that the solution has to be obtained by working from the outside of the yarn inwards through the elements. If the lateral pressure, T_L, has been determined at $R = R_2$ as T_{L_2} the constant, C, can be determined from Equation (G8):

$$T_{L_2} = T_A + C.R_2^{-s^2}$$

from which follows:

$$C = (T_{L_2} - T_A).R_2^{s^2} \qquad \ldots\ldots\ldots\ldots \quad (G9)$$

Substituting Equation (G9) into Equation (G8) yields for $R = R_1$ with $R_1 < R_2$:

$$T_{L_1} = T_A.\left(1 - \frac{R_2^{s^2}}{R_1^{s^2}}\right) + T_{L_2}.\left(\frac{R_2^{s^2}}{R_1^{s^2}}\right) \qquad \ldots\ldots\ldots \quad (G10)$$

where T_A and $s^2 = \sin^2\alpha$ are constant between R_2 and R_1.

For small values of α the variation with R can be incorporated into the solution. When α is small:

$$\alpha \simeq \sin\alpha \simeq \tan\alpha = 2\pi.R/TT \qquad \ldots\ldots\ldots \quad (G11)$$

This can be deduced from Figure 4.6. The term $\sin^2\alpha$ now becomes:

$$\sin^2\alpha = (2\pi.R/TT)^2 \qquad \ldots\ldots\ldots \quad (G12)$$

Substituting Equation (G12) into $P(R)$ and $Q(R)$ in Equation (G6) and in turn substituting the expressions obtained into Equation (G8) yields after the same procedure as followed before:

$$T_{L_1} = T_A.\left(1 - e^{2.\left(\frac{\pi}{TT}\right)^2.\left(R_2^2 - R_1^2\right)}\right) + T_{L_2}.\left(e^{2.\left(\frac{\pi}{TT}\right)^2.\left(R_2^2 - R_1^2\right)}\right)$$

$$\ldots\ldots \quad (G13)$$

APPENDIX H DATA USED FOR ANALYSES

CROSS-SECTION DENSITY OF YARNS

The number of fibres per zone of 0,0625 mm width is given below, starting at the yarn axis. The figures are the averages of four measurements per yarn.

Wool	Romney				Cheviot		Lincoln	
Tex	300		600		300		300	
Turns/m	100	180	80	130	100	180	100	180
Zone								
1	4	6,5	4	7,5	4	5	3	6,5
2	13	19	17	21,5	9	17	8	17
3	19,5	36,5	20	31,5	14	31	18	31
4	27	45,5	33	45,5	20	41	26	44
5	36	49	50	57,5	21	38	31	47
6	27,5	27	46	58	23,5	23	18	24
7	19	5	48	48,5	18,5	19	15	7
8	12,5	2	55	36,5	21	11	13	3
9	14	2	50	30	22	13	17	2
10	7	1	40	25	18	11	14	2
11	4	0	20	20	15	12	11	1
12	1		15	15	19	8	4	0
13	0		5	5	12	2	2	
14			2	3	7	2	2	
15			2	2	4	1	2	
16			2	1	0	1		
17			0	2		1		
18				2		0		
19				1				
20				0				

FIBRE AND SLIVER PROPERTIES

Wool	Romney	Cheviot	Lincoln
Mean fibre diameter, μm	36,9	34,1	37,4
Fibre linear density, *tex*	1,401	1,196	1,439
Average fibre length, *mm*	86,4	64,4	102,0
van Wyk's constant, $N.mm^{7}.mg^{-3}$	3,0	6,0	2,8

PARAMETERS FOR FIBRE STRESS-STRAIN CURVE (see Appendix C)

E is the range of elongations in percentages in which the values shown for a_i and b_i are valid. The parameters a_i and b_i are expressed in Newtons.

Romney			*Cheviot*			*Lincoln*		
E	a_i	b_i	E	a_i	b_i	E	a_i	b_i
0 - 0,5	0,4	0	0 - 0,5	1	0	0 - 2,4	3,13	0
0,5- 3,3	3,23	-0,014	0,5- 4,5	1,58	-0,003	2,4- 4	1,5	0,039
3,3- 4,5	1,54	0,042	4,5- 6,5	0,65	0,039	4 - 7,2	0,47	0,08
4,5- 7,7	0,44	0,091	6,5-14,6	0,21	0,067	7,2-14	0,19	0,1
7,7-34	0,16	0,11	14,6-34	-0,026	0,102	14 -39	0,20	0,1
34 -45	-0,045	0,18	34 -57	-0,38	0,207	38 -56	-0,73	0,46
45 -57	-1,31	0,75	57 -60	-0,47	0,28	56 -60	-1,3	0,78

Note that the values shown for a_i and b_i are used in Equation (C1) with E_f expressed as a fraction and not as a percentage.